

Motion Control Systems

For Offshore Lifting Operations

Koen Eerden



Delft University of Technology

Motion Control Systems

For Offshore Lifting Operations

by

Koen Eerden

to obtain the degree of Master of Science
at the Delft University of Technology,
to be defended publicly on Thursday October 12, 2023 at 1:00 PM.

Student number: 5406803
Project duration: September, 2022 – Oktober, 2023
Thesis committee: Prof. dr. Andrei Metrikine, TU Delft, chair
Dr. ir. Peter Meijers, TU Delft, supervisor
Ir. Edgar Steinebach, Heerema MC, supervisor
Ir. Alejandro Velez Isaza, Heerema MC, supervisor

Certain information within this thesis is confidential and has been censored.

An electronic version of this thesis is available at <http://repository.tudelft.nl/>.

Preface

In front of you is my master's thesis report, which is the final product of my educational journey. This journey started in 2015 in Eindhoven. After completing my bachelor's degree in Mechanical Engineering at Eindhoven University of Technology, I pursued a Master's in Offshore & Dredging Engineering at Delft University, finally leading me to Heerema Marine Contractors to write this master's thesis centered around motion control systems for offshore lifting operations.

I wish to express my gratitude to several individuals who helped me during this thesis project. First, I would like to thank Peter, my TU Delft supervisor, for his helpful inputs and inspirational insights as well as his enthusiastic and positive attitude during this project. I would like to express my appreciation to Alejandro and Edgar, my supervisors from Heerema Marine Contractors, for their insightful guidance and sharp criticism at the Leiden office.

I would like to thank Robin and Thijs, whose daily enthusiasm and strong lessons greatly enriched my time in Eindhoven and I want to thank Geer and Ruben for their passionate input and stimulating discussions in Delft, Leiden and in the cloud.

To my roommates Ruben, Yannick, Koen and Nathan, I extend my thanks for their daily support and their ability to expand perspectives, both within and beyond the context of this thesis. My sincere thanks go out to my family for their support throughout my entire period of study. Lastly, I am deeply grateful for amusement on the tracks to Leiden and the next door support.

I hope you enjoy reading this Master's Thesis report!

Koen Eerden
Rotterdam, October 2023

"You can't avoid The Circus. At some point we all make the list. Don't be afraid of The Circus."
– Admiral William H. McRaven

Abstract

This MSc thesis presents an investigation into motion control systems aimed at reducing swing motion of a lifting load during offshore heavy lifting operations. Two distinct models are developed for this objective. Subsequently, an analysis is done to assess the impact of various control aspects.

First, an assessment of the offshore heavy lifting market is performed. Following this, diverse motion control systems designed for offshore heavy lifting operations are examined. Special attention is given to the principle of the current damping tugger system used on vessels of Heerema Marine Contractors. Subsequent to this examination, multiple alternative aspects for this current damping tugger system are suggested.

Thereafter, a detailed model is developed, capable of simulating an offshore lifting operation with the use of a motion control system. For this model, the equations of motion are derived and used as the foundation for numerical MATLAB models. These MATLAB models are subsequently transformed into a Simulink model, which serves as the basis for designing the required controllers and setpoints. This model serves as a tool for investigation of the dynamics of offshore lifting operations when using a motion control system, but due to excessive computation time, it was not suitable for analyzing the effects of different control aspects of a motion control system.

Therefore, a simplified version of the model for offshore lifting operations with the use of a motion control system is developed, aiming to reduce the computation time of the model compared to the detailed model. This simplified model is called the analysis model. This analysis model is used for an analysis on the effects of different control aspects of a motion control system during an offshore lifting operation. These aspects comprise two different motion sensors are controller input along with three distinct control methods. The two sensors in question are one for measuring the motion of the winch and another for measuring the motion of the load. The first two control methodologies encompass two divergent setpoint calculation methods, one based on a linear equation and another founded upon a PID controller, both coupled with a winch controller. The third control method includes a controller that combines the setpoint and winch controller to one single, combined controller.

Throughout this analysis, the performance of each control aspect is evaluated across 24 unique scenarios. From these results it is concluded that the use of a load motion sensor result in superior system performance in comparison to employing a winch motion sensor in almost all scenarios. Furthermore, it was found that in combination with a load sensor, the setpoint calculation method based on a PID controller appeared to be the optimal choice in most scenarios, while, when using the winch sensor, both the linear setpoint calculation method and the combined controller method yield the best outcomes in most cases.

Contents

Preface	ii
Abstract	iv
List of abbreviations	xiv
List of symbols	xvi
1 Introduction	1
1.1 Offshore heavy lifting operations	1
1.1.1 Vessels of Heerema Marine Contractors	1
1.2 Problem statement	3
1.3 Research objective	3
1.4 Modeling approach and software	3
1.4.1 Analytically versus modeling software	3
1.4.2 Mathematical software	3
1.4.3 LiftDyn	4
1.5 Thesis outline	4
2 The offshore heavy-lifting market	5
2.1 Installation and decommissioning	5
2.1.1 Installation and decommissioning of offshore wind turbines	5
2.1.2 Installation and decommissioning of offshore platforms	5
2.2 The use of motion control systems in offshore operations	6
2.2.1 The use of Semi-Submersible Crane Vessels for Offshore Operations	6
2.2.2 The use of motion control systems	6
2.2.3 Weather impact on offshore operations	8
2.3 Conclusion	8
3 Motion control systems for offshore heavy lifting operations	9
3.1 Objective of a motion control system	9
3.1.1 Pay-in and pay-out motion	9
3.1.2 Motion damping	9
3.2 Current motion control system	10
3.2.1 The principle of the current damping tugger system	10
3.2.2 Slack and high tension cables	12
3.2.3 The control system of the damping tugger system	12
3.2.4 Conclusion	13
3.3 Alternatives within the current motion control system	13
3.3.1 Control goal	13
3.3.2 Alternative control setpoint	13
3.3.3 Alternative controller input	15
3.3.4 Conclusion	16
3.4 Motion sensors	16
3.4.1 Various types of motion sensors	17
3.4.2 Multiple sensors	18
3.4.3 Conclusion	18
3.5 Novel concepts for motion control systems	18
3.5.1 Multi-cable systems	18
3.5.2 Anti-swing slider systems	19
3.5.3 Tuned mass dampers	20
3.5.4 Electromagnetic interaction	21

3.5.5	Preventing motion of the load	21
3.5.6	Conclusion	21
3.6	Evaluation method of different control systems	22
3.6.1	Evaluation of effectiveness of control system	22
3.6.2	Similar study	23
3.6.3	Conclusion	24
3.7	Conclusion	24
4	Detailed model	25
4.1	Objective of the model	25
4.2	Method	25
4.2.1	Controlled lifting system	25
4.2.2	Lagrangian Method	25
4.2.3	Numerical model	26
4.2.4	Controller design	26
4.3	Modeling decisions of different elements of the systems	26
4.3.1	A two-dimensional or three-dimensional approach	26
4.3.2	Pendulum system	27
4.3.3	Modeling of the damping tugger system	28
4.3.4	Non-linear springs	28
4.3.5	Modeling of the control system	29
4.3.6	Vessel Motions	29
4.3.7	Standard parameters	30
4.4	Equations of motion	30
4.4.1	Free lifting system	30
4.4.2	The damping tugger system	33
4.4.3	Controlled lifting system	35
4.4.4	The static steady-state	36
4.5	Numerical model	37
4.5.1	MATLAB models	37
4.5.2	Verification of the MATLAB models	37
4.5.3	Purposes of the numerical models	38
4.6	Controller design	39
4.6.1	Simulink model	39
4.6.2	The PID controller of the damping tugger system	39
4.6.3	Identification of unstable response	40
4.6.4	Controller design for constant tension mode	41
4.6.5	Controller design for damping mode	45
4.7	Conclusion	48
5	Analysis model	49
5.1	Objective of the model	49
5.2	Method	49
5.2.1	Simplified lifting system	49
5.2.2	Numerical model	50
5.2.3	Controller design	50
5.3	Modeling decisions	50
5.3.1	Simplifications	50
5.3.2	Vessel motions	51
5.3.3	Standard parameters	51
5.4	Equations of motion	51
5.4.1	Simplified force system	52
5.4.2	Simplified lifting system	53
5.4.3	The static steady-state	54
5.5	Numerical model	55
5.5.1	MATLAB model	55
5.5.2	Purposes of the numerical models	55

5.6	Controller design	55
5.6.1	Simulink model	55
5.6.2	The maximum force setpoint	55
5.6.3	The motion control setpoint	58
5.6.4	The winch controller	60
5.6.5	The winch controller for the motion control setpoint	64
5.6.6	Combined controller	65
5.6.7	Constant tension mode	69
5.7	Conclusion	70
6	Results	71
6.1	Models	71
6.2	Analysis of the control methods and input	71
6.2.1	Analyzed aspects of the control system	71
6.2.2	Different analysis scenarios	72
6.2.3	Improvement factor	72
6.3	Effects of the control methods and input	73
6.3.1	Velocity of the load	73
6.3.2	Resulting root mean square of the velocity of the load	76
6.3.3	Resulting improvement factors	76
6.3.4	Effects of controller inputs	76
6.3.5	Effects of control methods	77
7	Discussion	80
7.1	Creation of the models	80
7.1.1	The detailed model	80
7.1.2	The analysis model	81
7.2	Analysis of the control methods and input	82
7.2.1	Comparison of the load and winch sensor	82
7.2.2	Comparison of motion control setpoint and maximum force setpoint	83
7.2.3	Comparison of motion control setpoint and combined controller	83
7.2.4	Comparison of maximum force setpoint and combined controller	84
7.2.5	Limitations of analysis	84
7.2.6	Evaluation of the results of the analysis	84
7.3	Evaluation of Heerema MC's damping tugger system	85
8	Conclusion	86
8.1	Models	86
8.2	Control methods and inputs	86
8.2.1	Control inputs	86
8.2.2	Control methods	87
9	Recommendations	88
9.1	Control inputs	88
9.2	Control method	88
	References	90
A	Detailed model	96
A.1	Standard parameters	96
A.2	Verification cases of the detailed model	96
A.2.1	Vessel motions and tip motions	96
A.2.2	Free lifting system	98
A.2.3	The damping tugger system	100
A.2.4	Controlled lifting system	101
A.3	Simulink ODE solver	103
B	Analysis model	105
B.1	Modeling the winch as translating mass	105
B.2	Deadband	106

- B.3 Limit values of motion control setpoint 106
- B.4 Verification of the analysis model 106
- C Results 109**
- D Equations of motion of detailed model 111**
- D.1 Free lifting system 111
- D.2 Damping tugging system 111
- D.3 Controller lifting system 115

List of Figures

1.1	Heerema MC' SSCV Sleipnir	2
1.2	The installation of the pylon of the Erasmusbridge by Heerema MC's SSCV Thialf in 1995	2
2.1	Three types of OWT foundations [19]	6
2.2	The process of mating [28]	7
2.3	Risk assessment on the different stages of blade-root installation [30]	7
3.1	View of damping tugger system on Heerema MC's Aegir [51]	10
3.2	Principle of winch and tugger cable	10
3.3	Force-velocity of a damping tugger system in damping mode [53]	11
3.4	A schematic overview of the control system and physical damping tugger system [50]	12
3.5	A analysis schematic illustration of the current control diagram of the damping tugger system	14
3.6	A analysis schematic illustration of the control diagram with the use of a load sensor	16
3.7	Wang Sun's multi-cable motion control system [76]	18
3.8	Ren Zhengru's multi-cable motion control system [33]	19
3.9	A schematic view of an anti-swing slider [77]	20
3.10	Principle of a TMD applied to a tower [85]	20
3.11	The system used by Zhang [98]	23
3.12	Input pitch vessel motion for Zhang's study [98]	23
3.13	The resulting rotation of the crane tip for Zhang's study [98]	23
4.1	A comparison of distinct load modeling methods [82]	27
4.2	Illustration of a spring pendulum [105]	28
4.3	The vessel displacement trajectory	29
4.4	A damped elastic pendulum	31
4.5	Visualization of wind force decomposition	32
4.6	The free lifting system	33
4.7	The physics of the damping tugger system	34
4.8	The controlled lifting system	35
4.9	Pitch vessel motion as input for the model	38
4.10	Simulink loop	39
4.11	Visualisation of winch limits	40
4.12	Unstable response due to an overly aggressive controller	41
4.13	Unstable response due to an overly conservative controller	41
4.14	Response with control gains of $P=0$, $I=0$ and $D=5$ and a tension setpoint of 130 kN	42
4.15	Response with PD controller for constant tension mode with gains of $k_p = 1$ and $K_d = 6$ in case 1	44
4.16	Response with PD controller for constant tension mode with gains of $k_p = 1$ and $K_d = 6$ in case 2	45
4.17	Response with PD controller for damping mode with gains of $k_p = 1$, $k_i = 1$ and $K_d = 1$	45
4.18	Response with PD controller for damping mode with gains of $k_p = 1$ and $K_d = 6$	46
4.19	Response with PD controller for damping mode with gains of $k_p = 10$ and $K_d = 100$	47
5.1	The x-displacement of suspension	52
5.2	The simplified force system	52
5.3	The simplified lifting system	54
5.4	The control loop of the simplified force system with maximum force setpoint	56
5.5	Visualisation of the maximum force setpoint including deadband	56

5.6	Comparison of the motion of the load	57
5.7	The damping force acting to the load	57
5.8	The damping force acting to the load over a time frame of [50 150] s	58
5.9	The control loop of the simplified force system with motion control setpoint	58
5.10	The displacement of the load with the chosen control parameters	59
5.11	The damping force action to the load	60
5.12	Comparison of the motion of the load	60
5.13	The control loop of the simplified lifting system with maximum force setpoint	61
5.14	The force in the cable compared to the force setpoint for a controller with gains $k_p = 1,000,000$ and $k_d = 1,000,000$ with time frame [650 950] seconds	62
5.15	The force in the cable compared to the force setpoint for a controller with gains $k_p = 100,000$ and $k_d = 100,000$ with time frame [650 950] seconds	63
5.16	The force in the cable compared to the force setpoint for a controller with gains $k_p = 300,000$ and $k_d = 100,000$	64
5.17	Comparison of the motion of the load	64
5.18	The control loop of the simplified lifting system with maximum force setpoint	65
5.19	The force in the cable compared to the setpoint	65
5.20	Comparison of the motion of the load	66
5.21	The control loop of the simplified lifting system with combined controller	66
5.22	The resulting force in the tugger cable due to the combined controller	67
5.23	Comparison of the motion of the load	68
5.24	Control diagram for constant tension mode	69
5.25	Constant tension mode	69
6.1	A situation where the motion of the load is reduced due to the presence of the control system	74
6.2	A second situation where the motion of the load is reduced due to the presence of the control system	74
6.3	A situation where the motion of the load is increased due to the presence of the control system	75
6.4	A situation where the presence of the controller does not reduce or increase the motion of the load	75
A.1	The input vessel motions in x - and y -direction	97
A.3	The input vessel rotation in θ_s -direction	97
A.2	The resulting motion of the crane tip, caused by both the horizontal vessel motion x_s and the vertical vessel motion y_s	98
A.4	The resulting motion of the crane tip, caused by both the horizontal vessel rotation θ_s	98
A.5	The amplitude and period of the vibrating mass compared to the calculated values	99
A.6	The behaviour of the pendulum with increased stiffness	99
A.7	The behaviour of the pendulum with decreased stiffness	100
A.8	The extension of springs 1 and 2 and the angle spring 1	101
A.9	The geometry of the springs	101
A.10	Damped motion of the system	102
A.11	The motion of the lifted load	103
A.12	The motion of the cable mass obtained from the model compared to the calculated period	103
A.13	ODE solver in simulink	104
B.1	Verification model of force system, case 1	107
B.2	Verification model of force system, case 1	107
B.3	Verification model of lifting system, case 2	108

List of Tables

4.1	Standardized parameters of the detailed model	30
4.2	Model parameter for comparison with the results of Zhang’s study	38
4.3	Outcomes of analysis 1 for the controller design of constant tension mode	42
4.4	Outcomes of analysis 2 for the controller design of constant tension mode	43
4.5	Outcomes of analysis 3 for the controller design of constant tension mode	44
4.6	Outcomes of analysis 1 the controller design of damping mode	47
5.1	Standard parameters of the simplified lifting system	51
5.2	Outcomes of analysis 1 for the controller design of the winch controller	62
5.3	Outcomes of analysis 2 for the controller design of the winch controller	63
5.4	Results of analysis 1 for the controller design of the combined controller	67
5.5	Results of analysis 2 for the controller design of the combined controller	68
6.1	Sample values for the explanation of the improvement factor	73
6.2	Sample improvement factors	73
6.3	Sample difference between improvement factors	73
6.4	The improvement factors of all executed scenarios	76
6.5	Colors indicating dominance dominance of a certain control aspect	77
6.6	Comparison of improvement factors of the winch sensor and the load sensor	77
6.7	Comparison of improvement factors of maximum force setpoint and the motion control setpoint when using the winch sensor	78
6.8	Comparison of improvement factors of motion control setpoint and the combined controller when using the winch sensor	78
6.9	Comparison of improvement factors of maximum force setpoint and combined controller	79
7.1	Comparison between the improvement factors when using the load sensor versus the winch sensor	82
7.2	Comparison between the improvement factors when using the motion control setpoint versus the maximum force setpoint	83
7.3	Comparison between the improvement factors when using the combined controller versus the motion control setpoint	84
C.1	RMS of the velocity of the load for all scenarios	110

List of abbreviations

Abbreviation	Definition
DOF	Degree of freedom
EOM	Equation of motion
GNSS	Global navigation satellite system
Heerema MC	Heerema Marine Contractors
LTMD	Liquid tuned mass damper
ODE	Ordinary differential equation
OWT	Offshore wind turbine
PD	Proportional-derivative
PI	Proportional-integral
PID	Proportional-integral-derivative
PTMD	Pendulum tuned mass damper
RFID	Radio-frequency identification
RMS	Root-mean-square
SSCV	Semi-submersible crane vessel
TMD	Tuned mass damper

List of symbols

Symbol	Definition	Unit
c	Damping constant	[Ns/m]
d	Deviation form setpoint	
e	Error	
E	Energy	[J]
F	Force	[N]
F_{max}	Maximum force limit in cable	[N]
F_{min}	Minimum force limit in cable	[N]
F_{pre}	Pre-tension	[N]
F_s	Force setpoint	[N]
g	Gravity constant	[Ns ² /m]
I	Inertia	[Nm/rad]
I_f	Improvement factor	[-]
k	Spring constant	[N/m]
k_d	Derivative control value	
k_i	Integral control value	
k_p	Proportional control value	
L	Lagrangian parameters	[J]
l	Length (initial)	[m]
m	Mass	[kg]
M	Moment	[Nm]
R	Rayleigh dissipation function	[Nsm]
r	Elongation of spring	[m]
\dot{r}	Velocity of elongation of spring	[m/s]
\ddot{r}	Acceleration of elongation of spring	[m/s ²]
r_w	Radius winch	[m]
RMS	Root mean square	
T	Kinetic energy	[J]
T_p	Time period	[s]
t	Time	[s]
U	Potential energy	[J]
u	controller output	
x	Horizontal displacement	[m]
\dot{x}	Horizontal velocity	[m/s]
\dot{x}_{lim}	Limiting horizontal velocity	[m/s]
\dot{x}_{sen}	Measured horizontal velocity by sensor	[m/s]
\dot{x}_{db}	Deadband velocity limit	[m/s]
\ddot{x}	Horizontal acceleration	[m/s ²]
θ	Rotation of crane cable	[rad]
$\dot{\theta}$	Rotational velocity of crane cable	[rad/s]
$\ddot{\theta}$	Rotational acceleration of crane cable	[rad/s ²]
ζ	Damping ratio	[Ns/m]

1

Introduction

This Master's thesis focuses on motion control systems for offshore heavy lifting operations. In this introduction, first, a general introduction to the topic of offshore heavy lifting operations is provided, then the problem statement and research objective are presented. Next, the modeling approach and the use of software are discussed. Lastly, the structure of this thesis is outlined.

1.1. Offshore heavy lifting operations

The offshore heavy lifting sector focuses on the installation and decommissioning of heavy structures, equipment or materials, mostly in a marine environment. These operations often pertain to offshore oil and gas platforms, wind turbine installations, bridge sections, and other marine infrastructure components.

Technological challenges in offshore lifting operations have always existed. The loads lifted during those heavy lifting operations are significant, resulting in critical operations. Environmental conditions, such as wave heights, currents, and winds are naturally changing. These conditions have a great impact on offshore lifting operations. As a result, detailed planning, accurate engineering computations, and extended risk evaluations are essential to guarantee the safety and effectiveness of these operations.

Over the years, technological advancements have significantly improved the efficiency and safety of these operations. Vessels and crew become more advanced every day and advancements in computer modeling allow for simulating operations on beforehand, optimizing strategies and minimizing risks. However, these technological advancements result in new operational demands, leading to new challenges, such as heavier loads or operating at heavier environmental conditions.

This Master's thesis aims to contribute to the technological advancements of the offshore lifting industry. It focuses on the use of motion control systems aiming to reduce the motion of the load during offshore lifting operations, especially those operations conducted by the vessels of Heerema Marine Contractors (Heerema MC).

1.1.1. Vessels of Heerema Marine Contractors

Several contractors operate in the offshore lifting sector. Heerema MC is one of those contractors. Heerema MC possesses multiple crane vessels, also known as heavy-lifting vessels. These vessels are specifically designed with large cranes capable of lifting heavy weights. Their substantial size ensures high vessel-stability, enhancing lifting operations. Figure 1.1 displays Heerema MC's semi-submersible crane vessel (SSCV) Sleipnir, built in 2019, that features two cranes, each with a capacity of 10,000 mT. This vessel is among the largest crane vessels of the world. Additionally, this vessel holds the record for the heaviest lift ever recorded, both offshore and onshore. This was a module with a weight of 17,000 mT [1].



Figure 1.1: Heerema MC' SSCV Sleipnir

Heerema MC actively participates in the installation and decommissioning of offshore structures. The company has installed and decommissioned numerous oil and gas platforms globally over the years and is recently active in installation of offshore wind turbines (OWTs) with crane vessels. Additionally, Heerema MC engages in unique heavy-lifting operations. For example, Heerema MC installed the pylon of the Erasmusbridge over the River Muse in Rotterdam in 1995 using the SSCV Thialf [2]. Figure 1.2 depicts an image of the installation of this pylon by the Thialf.



Figure 1.2: The installation of the pylon of the Erasmusbridge by Heerema MC's SSCV Thialf in 1995

1.2. Problem statement

In numerous offshore lifting operations, motion control systems are used. These systems aim to reduce the swing-motion of the lifted load. Various kinds of these motion control systems exist of which some are outlined in Section 3.5.

Vessels from Heerema MC are equipped with a motion control system, called the damping tugger system. This system applies a pulling force to the motion of the load. By actively adjusting this force, the goal is to dampen the load's motion. The principle of the damping tugger system is detailed in Section 3.2.1.

In some of Heerema MC's lifting projects, the damping tugger system remains unused. This choice is made because the system would not improve operational efficiency. In these cases the system does not always respond as it is expected to do. The pulling force in the tugger cable does not match expectations. The reason for this is not well understood yet [3]. Deeper understanding of the current damping system would possibly lead to the ability of improving the system. An improved performance of the system would result in a more efficient offshore lifting operation. This thesis aims to contribute to this understanding.

1.3. Research objective

In the problem statement, it is explained that a deeper understanding of the damping tugger system might lead to the ability of improving the system. Moreover, a better understanding of damping of the motion of the load, could be used for improving various motion control systems for offshore lifting operations. Therefore, the research objective focuses on contributing to the knowledge about motion control system for offshore heavy lifting operations in general. This research objective is defined as:

- Investigate how a motion control system for offshore heavy lifting operations can be improved.

To reach this objective, three main research questions will be answered in this thesis. These questions are provided below:

1. How can an offshore lifting operation with the use of a motion control system be modeled?
2. How can the use of a novel motion sensor improve efficiency of the current damping tugger system?
3. How can the use of a novel setpoint calculation method improve efficiency of the current damping tugger system?

1.4. Modeling approach and software

This section examines the use of different software tools. Firstly, the choice between analytic and numerical modeling approaches is discussed. Subsequently, various mathematical software packages are introduced, and the process of deriving vessel motions is explained.

1.4.1. Analytically versus modeling software

When considering modeling for this problem and its exploration, there are two main options: an analytic approach or the use of 3D numerical modeling software. 3D modeling software offers the advantage of rapidly creating models of intricate and extensive systems. OrcaFlex is particularly suitable for modeling offshore operations [4]. On the other hand, an analytical approach demands more time but ensures transparency and facilitates result validation in each step of modeling. Software tools can also be applied for mathematical aspects of the analytical approach. Given that the system is confined to 2D, it is chosen to use the analytical method due to its foundational insights.

1.4.2. Mathematical software

Maple software provides an ideal environment for algebraic operations, facilitating the derivation of equations of motion (EOMs) [5]. Additionally, MATLAB is a well-known software package for calculations, included with various ordinary differential equation (ODE) solver packages, with ODE45 being the most commonly used solver [6]. MATLAB's solver packages can be used to solve EOMs derived

within the Maple environment. Furthermore, Simulink, a block diagram environment within the MATLAB package, serves as a suitable tool for modeling control systems [6]. Both Maple and MATLAB will be used for mathematical computations in this thesis.

1.4.3. LiftDyn

As described in Section 4.3.6, the effect of load on vessel motion is disregarded. Consequently, the model's vessel motion is modeled as a predefined trajectory. This path may be derived analytically or through LiftDyn, a software package developed in-house by Heerema MC for hydrodynamic modeling. LiftDyn facilitates the generation of realistic vessel motions in both time and frequency domains, offering a quick and accurate means of producing realistic inputs [7].

1.5. Thesis outline

In this thesis, two main models are developed, with one specifically used for analyzing various control aspects of a motion control system. Initially, an assessment of the offshore heavy lifting market is presented in Chapter 2. Subsequent to this, Chapter 3 delves into different motion control systems for offshore heavy lifting operations, with a large focus on the principle of Heerema MC's existing damping tugger system, and also introduces alternative approaches for specific components of this system. Chapters 4 and 5 outline the development of the detailed and analysis models, respectively. The analysis model is used for the analysis of diverse control aspects, detailed in Chapter 6.2. Finally, the outcomes of the analysis together with the created models are presented, followed by a discussion of the results, which leads to several conclusions and recommendations.

2

The offshore heavy-lifting market

This chapter examines the offshore heavy lifting market. It evaluates the future of its various aspects, focusing on installation and decommissioning in the future and on the use of motion control systems during lifting operations.

2.1. Installation and decommissioning

The main focus of offshore heavy lifting operations is on the installation and decommissioning of offshore structures. This section highlights the market for installing and decommissioning OWTs and platforms.

2.1.1. Installation and decommissioning of offshore wind turbines

In response to the growing global demand for energy and the wish to reduce our reliance on fossil fuels, offshore wind power rose as a renewable energy source in the recent years [8]. Compared to onshore wind turbines, offshore wind farms do not affect land use and at sea, no physical obstacles disrupt wind flow. Moreover, offshore wind farms can be scaled up to generate greater energy output than their onshore counterparts [9] and OWTs produce more electricity per installed capacity unit due to the higher offshore wind velocities compared to onshore locations [8] [10]. Additionally, the larger size of OWTs compared to onshore counterparts contributes to increased energy production [11]. Given the benefits of offshore wind energy and the increasing demand for renewable sources, the profitability of the offshore wind market is promising for the upcoming decades.

While much research is being done on installation methods, decommissioning remains a largely overlooked aspect [12]. The transition of the offshore wind sector from experimental pilots to full projects occurred primarily in the early 2000s [13]. Given the operational lifespan of 20–25 years for OWTs [14], decommissioning of these turbines has only started recently and will follow the growth trajectory of installation over the past two decades. Topham's estimation indicates that approximately 20,000 OWTs will reach the end of their operational lifespan between 2030 and 2040 [15]. In essence, the decommissioning of OWTs promises to be a profitable market in the upcoming decades.

2.1.2. Installation and decommissioning of offshore platforms

Another significant segment within the offshore domain is the installation and decommissioning of offshore platforms. A literature review by Dan Cunha highlights the trend of decommissioning offshore platforms, particularly escalating since 2014. This is due to the increasing number of offshore platforms either undergoing decommissioning or being almost at the end of their lifespan [16]. As of 2022, the global count of offshore platforms exceeds 12,000 [17]. Hence, the decommissioning of offshore platforms currently represents a profitable market.

2.2. The use of motion control systems in offshore operations

This section examines the improvement of offshore operations with the implementation of motion control systems. First, the suitability of a floating vessel, such as a SSCV, for the offshore operations is assessed. Subsequently, an analysis of the use of motion control systems is done, followed by a review of the impact of weather conditions on these operations.

2.2.1. The use of Semi-Submersible Crane Vessels for Offshore Operations

The current OWT market consists primarily of bottom-founded structures [18]. Three examples of these support structures are a monopile, gravity-based structure and jacket structure, which are illustrated in Figure 2.1 [19].

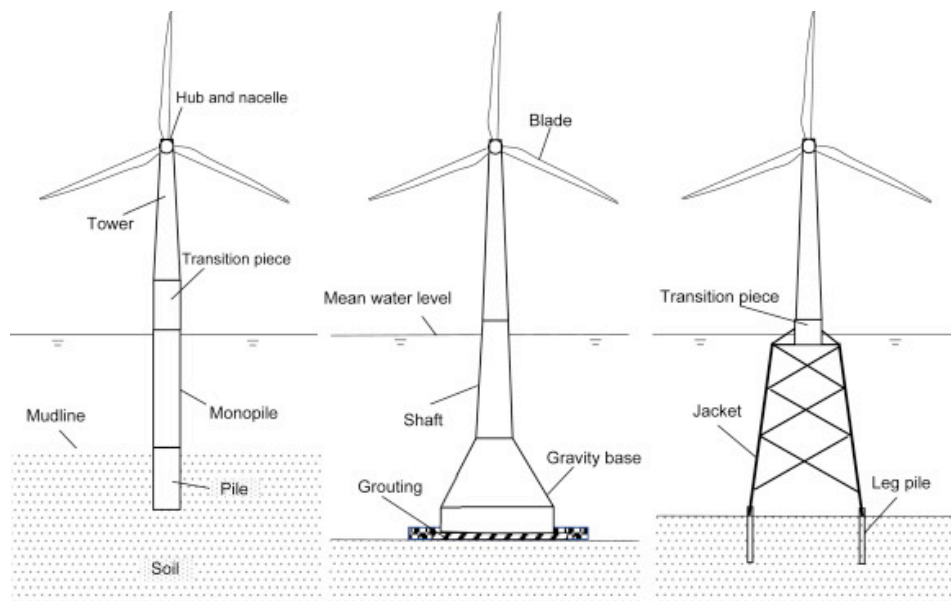


Figure 2.1: Three types of OWT foundations [19]

The SSCVs is well suitable for offshore operation, due to its outstanding motion response [19]. Heerema MC has successfully demonstrated the capability of installing OWTs using SSCVs by means of the rotor nacelle assembly method [20]. While alternative vessel types, typically jack-up vessels have historically been used for installation [21], SSCVs have advantages like easier relocation and a wider range of applicable water depths [22]. In contrast, jack-up vessels are able to eliminate hydrodynamic instability by rising above sea level [23] [24]. However, the large size of SSCVs provides outstanding stability as well [19]. A study by Lin and Berlin revealed that SSCVs with a lifting capacity of 10,000 tons exhibited lower motion responses during wind turbine installation compared to mono-hull vessels, leading to higher allowable sea states and improved operability [25]. Ultimately, the suitability of vessel choice for wind turbine installation depends on factors such as costs and operability, with SSCVs being a viable option.

During wind turbine installation projects, Heerema MC's uses their vessels for installation only [20] [26], while literature suggests that crane vessels with large deck space could both install and transport turbines [23]. However, due to the slow and heavy nature of SSCVs, using them for transportation would likely results in higher expenses [9] [27] and cannot enter most ports [3]. Thus, it is recommended that SSCV's are employed exclusively for turbine installation. Furthermore, while SSCVs have been historically used for decommissioning offshore platforms, research is needed to determine the challenges for decommissioning OWTs.

2.2.2. The use of motion control systems

Accurate positioning of the load, particularly during mating between the load e.g., blades or a platform and the structure, is crucial. During installation of OWTs, several mating processes occur. One of these mating processes is assembling the turbine to the support structure, as depicted in Figure 2.2 [28].

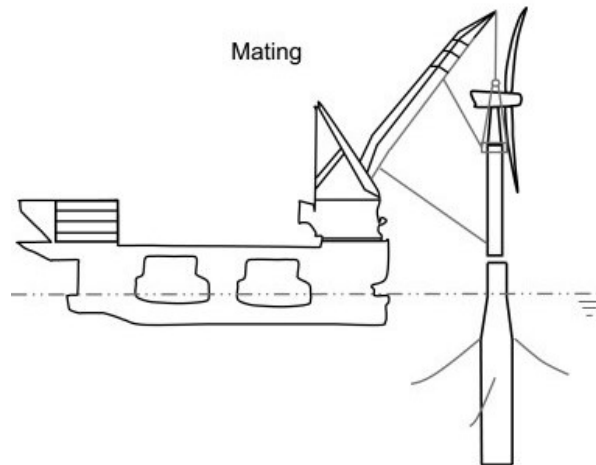


Figure 2.2: The process of mating [28]

The motion of the vessel can impact load stability, potentially hindering successful assembly [28]. Blade-root mating, a critical stage of installation, has been identified as particularly risky [29]. Jiang and Verma (2023) provide a risk assessment on the different stages of installation, depicted in Figure 2.3, identifying blade-root mating as the most critical stage. Verma's research indicates a high chance of impact-induced damage to blade roots during mating, with significant negative consequences for the structure [28] [30]. Studies by Vagnes et al. (2020), Xu (2020) suggest a motion control system comparable to Heerema MC's damping tugger system [31] [32], and Zhengru Ren (2021) suggests a motion control system with wires from different directions. Both methods can reduce structural impact and improve operability and safety during installation. Notably, these systems have demonstrated substantial reductions in payload motion [31] [32] [33], thereby contributing to successful wind turbine assembly.

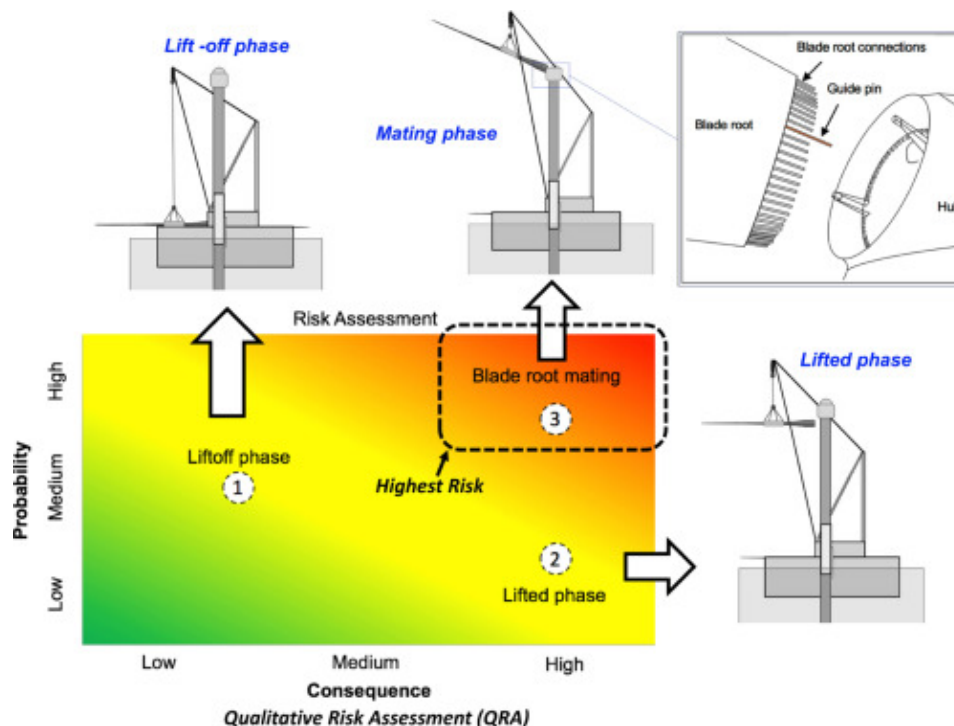


Figure 2.3: Risk assessment on the different stages of blade-root installation [30]

Also, Jacobs states in his MSc thesis that the use of tugger cables improves the mating process during installation of a platform, increasing operability of platform installations [34]. During decommissioning, motion control systems can contribute to smoother operations, potentially leading to less damage and high chance of recycling possibilities [35]. Stabilization of loads during platform decommissioning could also minimize disturbance to marine life [36]. As environmental considerations gain importance, these factors are expected to play a significant role in the decommissioning sector in the coming decades.

Motion control systems also offer benefits for on-deck operations, a substantial part of offshore operations. Challenges, such as the transfer of foundations between barges, basket transfer and crew or on-deck component relocated can be improved with motion control systems [9] [23] [37]. Also, for projects like Heerema MC's rotor nacelle assembly method, on-deck assembly plays an important role. Due to the use motion control systems these projects are more cost-effective and operationally efficient [20] [26].

2.2.3. Weather impact on offshore operations

Weather conditions highly influence offshore operations, with adverse weather leading to increased vessel motion and operational difficulties or delays. Several studies emphasize weather as a main factor affecting offshore operations [38] [39] [40]. Operations are constrained to specific periods of favorable weather, known as weather windows, affecting vessel operability. Accurate forecasts are crucial, yet limited by data availability [41]. Uncertainties and limitations persist in weather predictions [42] [43], necessitating the reliance on error statistics to quantify forecast uncertainty.

Proposed solutions, such as predictive models for short-term wind and wave conditions [22] [44], aim to improve operability decisions. Hamedani challenges the conservative approach to allowable weather limits, while Wu Gao highlights the tendency for weather uncertainty to result in overestimation of limits [45]. The severity of accidents during offshore operations underscores the importance of minimizing risk [46] [47] [48]. Increasingly large OWTs may heighten weather sensitivity in the sector [49].

While further research on weather forecasts may reduce uncertainties, mitigating the impact of weather is preferred. A motion control system is one of the options to mitigate weather impact.

2.3. Conclusion

Heerema Heerema MC is active in both offshore installation and decommissioning. A review of the profitability of this sectors is done, leading to the conclusion that this industry will be profitable in the upcoming years. Furthermore, the use of the motion control system during offshore lifting operations is discussed. Correct use of motion control systems in OWT operations demonstrates improved efficiency, safety, and operability. SSCV's offer advantages in wind turbine installation due to their substantial stability. Weather's significant impact on offshore operations necessitates the development of reliable forecasts and strategies to reduce weather sensitivity. Motion control systems can mitigate challenges with load motion during installation, decommissioning and on-deck operations. Further research about motion control systems is essential to refine these systems.

3

Motion control systems for offshore heavy lifting operations

This chapter provides an exploration of various concepts of motion control systems for offshore heavy lifting operation, particularly emphasizing the system implemented by Heerema MC. The discussion of the latter leads to questioning certain elements and suggesting alternative solutions. Furthermore, various types of motion sensors are discussed in this chapter.

3.1. Objective of a motion control system

The primary aim of a control system is to damp the swing motion of the lifted load. This section elaborates on such damping and explores the two reference systems that are being employed.

3.1.1. Pay-in and pay-out motion

In a two-dimensional setting, a swinging load attached to a crane can move either towards or away from the crane. Movement towards the crane is called 'pay-in' motion, while movement away from the crane is called 'pay-out' motion.

3.1.2. Motion damping

The primary objective of the motion control system is to maintain the position of the elevated load at a desired point. Consequently, the system aims to mitigate any externally induced oscillations affecting the load. Furthermore, the motion control system is frequently used for rotational control of the load, but this is not covered in this thesis.

In the context of a motion control system, damping refers to the dissipation of kinetic energy. A decrease in kinetic energy results in a reduction of the load's motion. In the case of the existing damping tugger system, this energy dissipation is created by the tension exerted on the tugger cable. Due to the tension of in the cable being high during pay-out motion compared to pay-in motion, damping is created.

In the end, the primary objective of the motion control system is to minimize the motion of the load relative to a predefined reference value, commonly referred to as the setpoint. In scenarios where a single disturbance gives rise to oscillatory movement, the ensuing oscillations are attenuated over a temporal duration due to the inherent damping mechanisms. It is important to note that the process of damping needs a finite period of time for completion. In circumstances with a continuous disturbance, damping leads to reduction of the amplitude of the motion but may not lead toward a complete equilibrium. Achieving such a state is only feasible under conditions of critical damping, a scenario that is not attainable with the existing damping tugger system, because this would lead to exertion of prohibitively high forces on the tugger cable. Given these constraints, the complete reduction of motion of the load is considered to be unachievable with the current system in almost all cases.

In the majority of operational scenarios, the total minimization of load movement is not needed, as a specific degree of motion is allowed. Consequently, the system functions effectively when the movement is reduced and maintained below a desired threshold.

3.2. Current motion control system

This section reviews the principle of the current motion control system used by Heerema MC, which is referred to as the damping system. First, the components of the system are reviewed. Subsequently, three distinct modes are outlined, with the third mode being the actual damping mode, which is the main subject of this thesis.

3.2.1. The principle of the current damping tugger system

The current damping system comprises of four primary components: a winch, an electromotor, a tugger cable, and a control system. The control system controls the load [50]. Typically, tugger systems are configured with pairs of two or four winches and corresponding tugger cables. Figure 3.1 depicts a damping tugger system with two tugger cables onboard Heerema MC's Aegir [51]. Utilizing a pair of tugger cables enables the rotation of the load within the horizontal plane. However, this thesis focuses specifically on the operation of a single winch and its tugger cable in a two-dimensional plane.

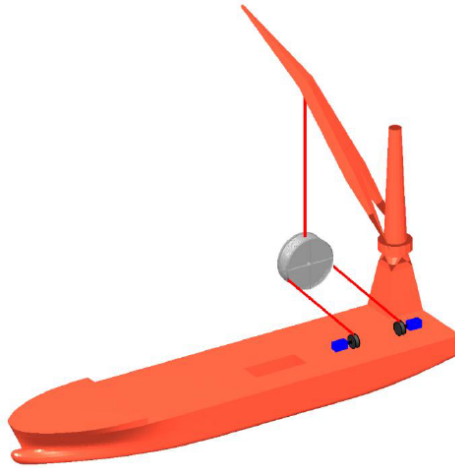


Figure 3.1: View of damping tugger system on Heerema MC's Aegir [51]

The fundamental principle of the tugger system involves the use of the winch to apply a specific tension to the tugger cable, thus initiating a pulling force on the load. This pulling force is altered by the rotation of the winch as depicted in Figure 3.2. Various methods of using this force to improve offshore operations are available. Below, three distinct modes are described.

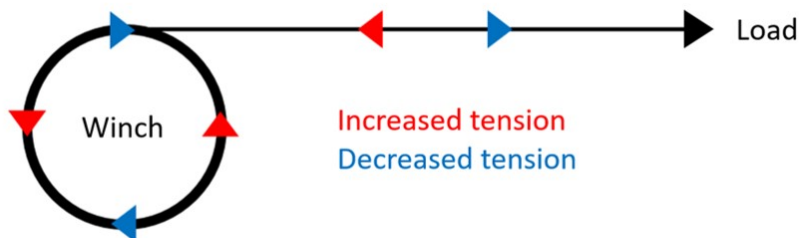


Figure 3.2: Principle of winch and tugger cable

Fixed length mode

When in fixed length mode, the winch initially tightens the tugger cable to a predetermined tension level and maintains this cable length, e.i. the winch keeps its position and does not rotate after reaching the predetermined tension level. This setup essentially functions as a spring. While suitable for handling lighter loads, it becomes a critical limiting factor for heavier loads [51] [52]. This is attributed to the fact that the load aligns with the horizontal movement of the vessel due to the tugger cables. The tugger cables accelerate the load, and heavier loads result in increased forces. To overcome the risk of slack cables, a high pre-tension is essential.

Constant tension mode

The constant tension mode involves the winch rotating to sustain a consistent tension level in the tugger cables. A constant tension would lead to a constant force applied to the load, which has no significant impact on the dynamics of the load, because a constant force does not damp motion. In practical scenarios, the force is not constant, because it is affected by factors like the winch's inertia, interaction with the controller and motion of the load in other directions than the plane of operation. These factors lead to fluctuations around the constant tension setpoint, leading often to a bit of damping [51] [52]. In essence, when analyzed theoretically, the constant tension mode should not result in damping. However, a practical implementation of the constant tension can lead to damping due to interaction with external factors.

An alternative method to use constant tension mode (or fixed length mode) for damping motion of the load, involves manually adjusting the tension setpoint. Crane operators adjust the setpoint for the constant tension to create a difference in force during a cycle, leading to damping of load's motion [51].

Damping mode

During damping mode, the rotation of the winch modifies the tension in the cable. When the load pays out, the tension is set high, whereas during load pay-in, the tension is set low. The tension during pay-in motion adds kinetic energy to the system, while tension during pay-out motion absorbs kinetic energy. Due to the higher tension during pay-out, the net added kinetic energy is negative, resulting in a net damping effect on the system [51].

An illustration of this principle can be found in a playground scenario involving a swing. Consider a girl named Alice, who is actively swinging back and forth. Now, suppose a boy called Bob intends to stop Alice's swinging motion (with the intention of switching turns). To achieve this, Bob pulls on the swing precisely when Alice is moving away from Bob. This reduces the kinetic energy of Alice on the swing, reducing its motion. However, when the swing is moving back towards Bob, he stops pulling, otherwise he will add kinetic energy and the motion of the swing increases again. In this scenario, Alice on the swing represents the swing load, and Bob pulling on the swing represents the damping tugger system.

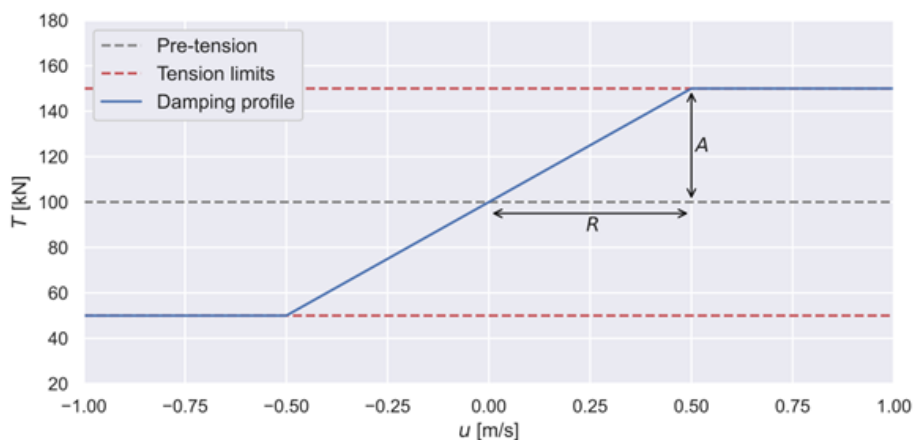


Figure 3.3: Force-velocity of a damping tugger system in damping mode [53]

The larger the difference between the energy extraction and energy addition, the larger the net damping. As a result, the difference between the maximum and minimum tensions within the tugger cable, i.e., the variation between the highest and lowest forces in the cable, significantly impacts the damping rate of the system [54] [55]. An additional factor that contributes to the damping rate is the speed of tension switching in the cable. A faster switch means the tension remains longer at its extreme values, improving overall efficiency [54].

A force-velocity relationship shows the effect of the factors described above. As illustrated in Figure 3.3, this relationship describes the interaction between tension T (or force) within the cable and the horizontal speed of the load u , based on a certain simulation [53], where A is the change in tension and R is the change in speed. The damping profile signifies the force-velocity relationship. A steeper slope in this line means a higher damping ratio. Determining the ideal damping ratio depends on various conditions and is a complex challenge. Presently, crane operators typically find the appropriate damping ratio by a trial-and-error approach [3].

3.2.2. Slack and high tension cables

The movement of the load, triggered by the motion of the vessel or crane, is a swinging motion. As the tugger cable is horizontally fixed to the load, it is elongated due to the load's motion. This causes the tension in the tugger cable to constantly increase and decrease. It is important to ensure that the tension in the tugger cable remains between the safe limits, as too high tension could result in cable breakage. Consequently, the tension must stay below a predefined threshold.

On the other hand, allowing the tension to drop below zero, i.e. indicating a slack cable, should be prevented at all times, because retensioning of the cable leads to high impact forces on the winch. Thus, the tension in the cable must balance between avoiding excessive tension and preventing a catenary.

3.2.3. The control system of the damping tugger system

Figure 3.4 depicts a schematic overview of the control system and physical damping tugger system. The velocity of the cable is assumed equivalent to that of the load and winch [50]. The control's setpoint value is derived from the force-velocity relationships explained in Section 3.2.1.

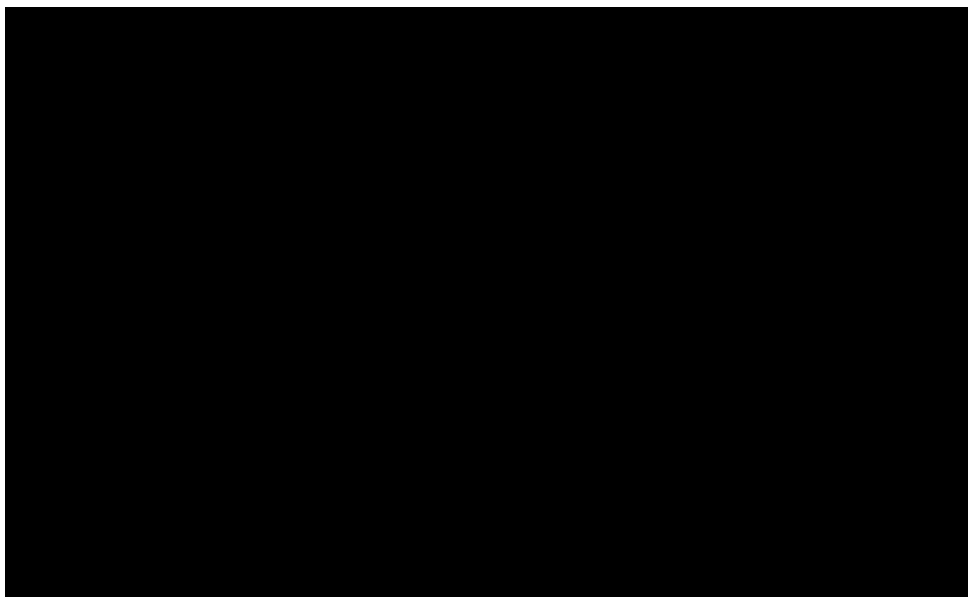


Figure 3.4: A schematic overview of the control system and physical damping tugger system [50]

This control setup gives rise to two main questions. Firstly, the assumption of identical velocities for the winch, cable, and load is brought into question. Variability could arise due to cable elongation or catenary, resulting in potentially divergent velocities for the winch, cable, and load. Additionally, high tension in the cable might introduce high-frequency vibrations that could impact velocity measurements. If such deviations in velocities occur, the controller might receive inaccurate inputs, potentially resulting in issues like unintended motion or instability.

Secondly, the method behind deriving the setpoint is brought into question. The current setpoint calculation relies on a linear relationship with input velocity. However, this approach may not sufficiently account for factors influencing the winch response, for instance, the inertia of the winch, thereby leading to unintended response of the controller. Given these considerations, further research is necessary to validate the effectiveness of these two aspects within the current system. Consequently, these two topics emerge as interesting research questions for the scope of this thesis.

3.2.4. Conclusion

This section reviewed the principle behind Heerema MC's existing motion control system. Two aspects of the current system are questioned: (1) the validity of the assumption that the velocity of the winch, cable, and load are equal and (2) the method behind deriving the setpoint. These aspects form the base for two out of three research questions, which are described in Section 1.3.

3.3. Alternatives within the current motion control system

Alternatives for the questioned aspects of the current system, described in Section 3.2, are discussed in this section.

3.3.1. Control goal

The motion of the load is a relative motion compared to certain reference systems. In the case of the damping tugger system, it should be able to damp motion compared to two distinct reference systems: the global reference system and the on-deck reference system. The global reference system corresponds to the fixed world's reference system. It may be necessary to dampen motion relative to a fixed point in the world during specific scenarios, such as the installation of a topside on a bottom-founded structure. In different situations, an object like a turbine could be positioned on the vessel's deck. In this operation, motion should be damped relative to the vessel's motion, utilizing the vessel's reference system for damping purposes. It is worth noting that certain operations require damping relative to both reference systems in quick succession, for instance during the Arcadis Ost project [3], where the nacelle and blades were assembled onto the tower on the vessel's deck, necessitating motion damping relative to the vessel's reference system. Subsequently, the tower was installed on top of the earth-fixed monopile, requiring motion damping relative to the global reference system.

The horizontal origin of the global reference system consistently aligns with the predetermined location where the object is intended to be placed. Conversely, the on-deck reference system is related to the global reference system through the incorporation of the vessel's motion dynamics. The horizontal origin of the on-deck reference system is precisely aligned with the crane tip's centerline. Given that the on-deck reference system is dynamic, moving synchronously with the vessel, its horizontal origin remains steadfastly aligned with the centerline of the crane tip.

3.3.2. Alternative control setpoint

In Figure 3.5 a simplified version of the control diagram of the current damping tugger system is depicted. The control setpoint, or setpoint calculation method, is the input to the winch controller and is indicated by a red block. The setpoint of the damping mode of the currently used damping tugger system is formulated as a mathematical equation, as described in Section 3.2.1. In this thesis, this setpoint method is called the maximum force setpoint. This setpoint fluctuates between the upper and lower force limits, adhering to a linear relationship characterized by a maximum and minimum limit. This

particular relationship is identified as the force-velocity relation and is mathematically expressed as:

$$F_s = \begin{cases} F_{max} & \dot{x}_{sen} \geq \dot{x}_{lim-upper} \\ \zeta \cdot \dot{x}_{sen} + F_{pre} & \dot{x}_{lim-lower} < \dot{x}_{sen} < \dot{x}_{lim-upper} \\ F_{min} & \dot{x}_{sen} \leq \dot{x}_{lim-lower} \end{cases} \quad (3.1)$$

Here, F_s denotes the force setpoint within the cable system, while F_{max} and F_{min} represent the established upper and lower force limits, respectively. The force setpoint attains these specified limits when the measured velocity of the load x_{sen} exceeds the limit velocity x_{lim} in either a positive or negative direction. Additionally, F_{pre} denotes the pre-tension, and ζ symbolizes the damping ratio.

It is noteworthy that a higher damping ratio facilitates a more rapid transition of the setpoint between the maximum and minimum force limits. Faster switching results in the setpoint remaining at its extreme values for extended duration, thereby contributing to a net increase in the system's damping within a cycle. A graphical representation of the force-velocity relationship is provided in Figure 3.3.

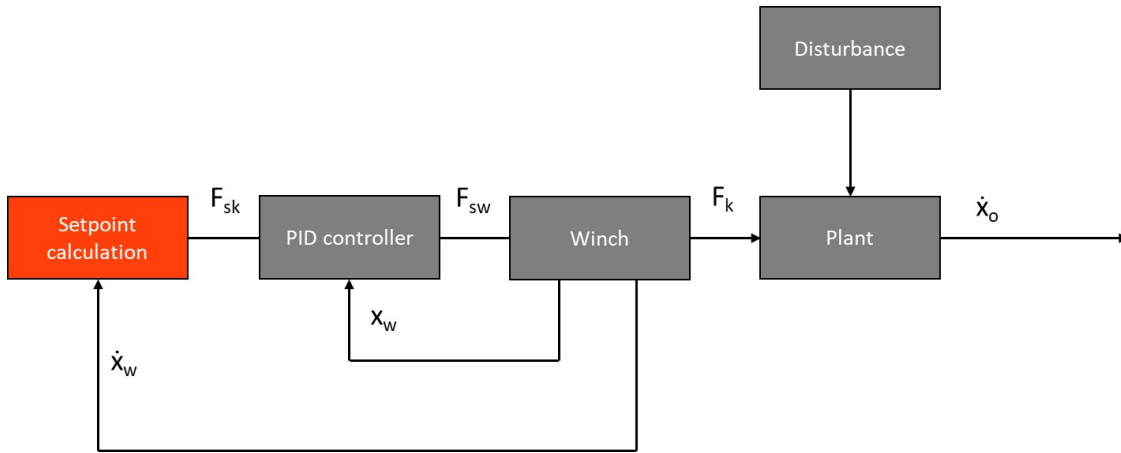


Figure 3.5: A analysis schematic illustration of the current control diagram of the damping tugger system

When using this particular setpoint, the primary objective is to oscillate between the upper and lower bounds of tension, with a short transition time. The linear part in the force-velocity relationship accounts for the system's physical constraints. This linear section starts a transition to the opposite force limit before the load's velocity approaches zero, thereby affording a period for transition. If this transitional duration is sufficiently long, the physical system is capable of following the setpoint, thereby improving the system's robustness.

Nonetheless, because the movement of the load is a pendulum motion, the velocity of the load is subject to continuous variation. Because the maximum force setpoint is defined by a linear relationship, it does not respond to the rate of change of the error.

Furthermore, the shift from the linear portion of the force-velocity curve to the limit values of force, at the moment when the velocity reaches its limiting value \dot{x}_{lim} , constitutes an abrupt transition. As illustrated in Figure 3.3, this relationship exhibits bifurcations at both the positive and negative limit values of the load's velocity. Such abrupt transitions or discontinuities in the setpoint calculation could impact the controller's performance, potentially leading to system instabilities or overcompensation [3]. Due to these limitations associated with the maximum force setpoint method, this thesis explores an innovative approach for setpoint calculation, termed as the motion control setpoint.

The motion control setpoint is an alternative setpoint calculation method for the maximum force setpoint. The motion control setpoint uses the same mathematical framework as a proportional-derivative (PD) controller, leading the relation:

$$F_s = \bar{k}_p \cdot e_o + \bar{k}_i \cdot \int e_o + \bar{k}_d \cdot \dot{e}_o \quad (3.2)$$

In this context, F_s represents the tension setpoint, while \bar{k}_p , \bar{k}_i and \bar{k}_d correspond to the proportional, integral and derivative control gains, respectively. It is crucial to calibrate these control parameters such that the tension setpoint F_s remains within its predefined upper and lower bounds. This calibration is facilitated through the prediction of the maximum and minimum load velocity \dot{x}_{lim} and the maximum load acceleration \ddot{x}_{lim} . In the case of pendulum motion, both the maximum velocity and acceleration are correlated with the system's maximum displacement and oscillation frequency. The variable e_o denotes the velocity error of the load, which is defined as follows:

$$e_o = \dot{x}_s - \dot{x}_{sen} \quad (3.3)$$

Here, the setpoint velocity of the load can be either zero or identical to the velocity of the vessel, contingent upon the reference system utilized for the operation.

The setpoint method provides a control input without sudden discontinuities. In contrast to the maximum force setpoint, the motion control setpoint yields a more continuous input function for the control algorithm, thereby potentially improving the robustness of the overall system. The latter is investigated. Both setpoint strategies will be implemented under identical scenarios, followed by an analysis of their performance.

3.3.3. Alternative controller input

The computation of the setpoint is done with the input provided to the controller, derived from sensor measurements. A variety of input parameters may be employed, of which the displacement, velocity and acceleration of the winch, tugger cable and load are discussed.

In an ideal scenario, the load would exhibit pendulum-like motion and eventually reach an equilibrium state, due to the presence of the motion control system. In this case, the pendulum is in its static equilibrium state, the load would be motionless, precisely below the point of suspension. Mathematically, this is represented as $x_0 = 0$. When the pendulum is in a state of oscillation, the velocity of the load at $x_0 = 0$ will reach either its maximum or minimum value within a cycle. This is because at the lowest point of oscillation, the potential energy is equal to zero, while the kinetic energy reaches its peak. Correspondingly, the acceleration of the load is zero at $x_0 = 0$ due to the load having achieved its maximum (or minimum) velocity before reverting to zero. Therefore, at the equilibrium point, the equations $x_0 = \dot{x}_0 = 0$ and $|\dot{x}_0| = \dot{x}_{max}$ hold true. This describes the phase difference among displacement, velocity, and acceleration.

The current damping tugger system uses velocity as input for the control system. The phase of the velocity is equal to the phase of the desired force in the cable. It is possible to take displacement or acceleration as input. However, the displacement or acceleration is out of phase with the desired force in the cable, so this would lead to a less straight forward input. Hence, it is chosen to maintain velocity as the primary input variable for the controller for the alternatives explored within this thesis.

As elaborated in Section 3.1.2, motion reduction is accomplished through energy dissipation. The energy dissipated over a single cycle is defined as follows:

$$E_{dis} = \int_{t=0}^{t=T_p} (F \cdot x_o) dt \cdot \frac{1}{T_p} \quad (3.4)$$

where E_{dis} is the dissipated energy during the cycle, F denotes the force in the cable and T_p is the time period of the cycle. From this equation it is concluded that the dissipated energy is highest when the force F is at its maximum.

The input parameter used for the controller serves to establish the controller setpoint, which is ideally the load's velocity. A direct approach for obtaining the load's velocity involves its direct measurement. To obtain velocity data of the load, motion sensors must be used. The feasibility of using such sensors is discussed in Section 3.4.

Easier alternatives for obtaining motion data includes the measurements of the winch or the tigger cable. This is done with Heerema MC's damping tigger system, as described in Section 3.2.3. In this system, the velocity of the winch is measured, and it is assumed that this velocity is equal to that of the load. The assumption rests on the argument that the elongation of the tigger cable is negligibly small, thereby causing a neglectable difference in the motion of the load, the tigger cable, and the winch.

However, the validity of such an assumption within this specific system is questioned. Due to the different natural frequencies of the winch, the tigger cable and to the load, different vibrations may arise. Additionally, periods of cable slack introduce temporal uncertainties in the load's motion. In the case that this assumption is invalid, incorrect input data for the controller is used. This could adversely affect the performance of the damping system, potentially inducing system instabilities or even counterproductive damping effects e.i. increasing the load's motion. The use of the load sensor would eliminate any uncertainties about the motion of the load.

Figure 3.5 presents the control diagram of the current system that uses the winch sensor. It is evident from the diagram that this is not an actual feedback loop for the load velocity. Using a load sensor would result in a control diagram as displayed in Figure 3.6. This second diagram depicts an actual feedback loop for the load velocity.

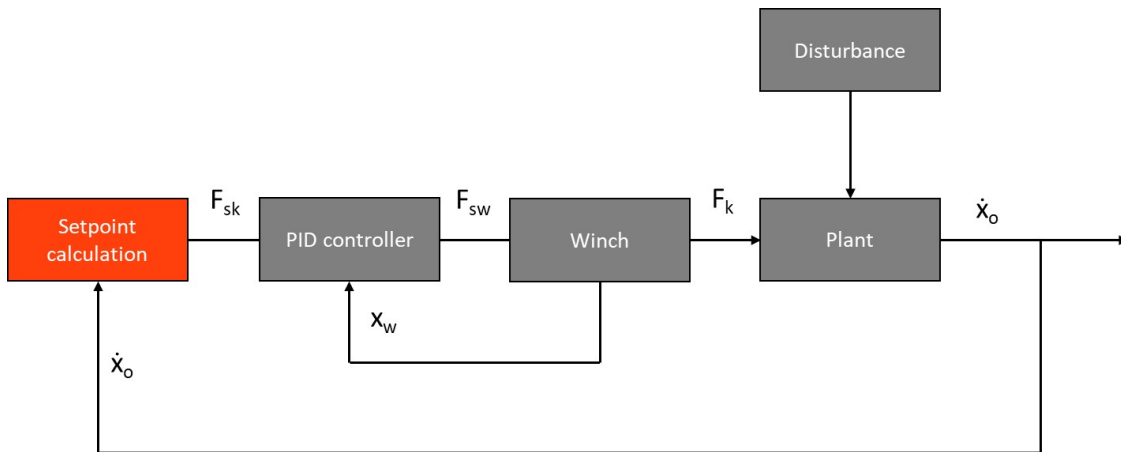


Figure 3.6: A analysis schematic illustration of the control diagram with the use of a load sensor

In this thesis, both methods for velocity measurement are examined. These methods will be implemented in the computational model under identical experimental conditions. Subsequently, differences in motion measurement, as well as difference in the performance of the damping system, will be analyzed.

3.3.4. Conclusion

In Section 3.2, two aspects of the current motion control system are questioned. This section provides alternatives to the questioned aspects of the current system. These alternatives are considered as potential improvements. In this thesis, models will be created and used to evaluate these alternatives. A comparison will be done between the performance of the existing system and a system that includes these alternatives under identical conditions. Finally, an analysis of both performances will be done.

3.4. Motion sensors

This thesis examines the use of the motion of the load instead of the motion of the tigger cable or winch as an input parameter for the controller, what is suggested in Section 3.3. If this was applied, this motion must be measured by new sensors. Before investigating the effect of a different input parameter for the controller, it is imperative to explore potential constraints within sensor technologies prior to implementation. In this section, the viability of employing sensors for this purpose is assessed. The focus here is on establishing the feasibility of sensor deployment, by an evaluation of multiple sensors in terms of their feasibility, measurement range, and accuracy.

3.4.1. Various types of motion sensors

Motion sensors come in several categories. Zhu Zhang has categorized them and assessed their prevalence based on a review of research papers. Visual sensors emerge as the most widely used, constituting roughly 30% of all papers, followed by inertial measurement (14%), laser detection (13%), radio-frequency identification (10%), global navigation satellite system (8%), and ultrasonic ranging (6%) [56]. The subsequent sections elaborate on each distinct sensor category.

Visual sensors

Visual sensors, such as camera sensors, are widely used for motion tracking. Studies by Kawai demonstrate the use of a camera embedded in a crane to calculate swing angles [57]. Similarly, Wang and Tan showcase the potential of tracking moving loads using visual sensors [58]. The underlying principle involves imaging the target through high-frequency photography. Each pixel in the image is scanned, and algorithms translate this into distance data. This technique ensures rapid and precise data capture, resulting in high accuracy, a wide measurement range, and near-real-time information [59] [60].

Nonetheless, visual sensors require an unobstructed line of sight to the measured object, limiting operational space. Furthermore, they are sensitive to sunlight interference, sometimes reducing their range to 3-10 meters and making them less reliable during daylight hours [61] [62]. To that extent, the question arises if heavy rain pollutes the line of sight. The impact of sunlight, artificial construction lighting, heavy rain, and other visual distractions necessitates further investigation before considering visual sensors as a robust option for motion measurement during offshore heavy-lift operations.

Inertial sensors

Inertial sensors measure an object's acceleration. They encompass accelerometers for linear acceleration and gyroscopes for angular motion. By integrating these measurements over time, velocity and position can be estimated. However, integration introduces error accumulation, affecting accuracy when using inertial sensors for velocity or position measurement [59] [63] [64]. The advantage of inertial sensors is the single-device attachment to the measured object, eliminating the need for a line of sight. However, such a sensor must be installed on the load. Moreover, the simple principle leads to rapid processing times, enabling nearly real-time measurements.

Laser detection

Laser detection relies on emitting a laser toward an object and measuring the travel time of the reflected light to determine distance. Due to time measurement being exceptionally accurate, high distance accuracy, in the order of micrometers, is achieved [65] [66] [67]. The technique's extensive measurement range, in the order of kilometers, surpasses offshore operational requirements [66] [67]. However, the sensor is restricted to a direct line of sight between sender and receiver, limiting operational space. Moreover, it only measures the distance to the first object in the line of sight, making it blind to possible obstructions such as rain or cables [59] [68]. Combining laser and camera techniques could lead to a solution for the blindness for obstructions. Nevertheless, challenges remain, including the impact of load geometry on accurate motion measurement. Despite these challenges, laser measurement remains an attractive option for offshore motion measurement due to its simplicity, robustness, and extended range.

Radio-frequency identification

Radio-Frequency Identification (RFID) is a system comprising tags and readers. While initially designed for data transmission, it has been applied to motion measurement, such as fall detection [69]. However, using RFID as a motion sensor for heavy industry is not recommended [70]. Thus, RFID is excluded from further consideration in this thesis.

Global navigation satellite system

Global Navigation Satellite System (GNSS) determines location by combining signals from multiple satellites, typically requiring at least four satellites for accuracy [71]. While a standalone GNSS receiver achieves positioning accuracy of around five meters [59], enhanced accuracy in the millimeter range can be attained using a network of ground-based base stations [72] [73]. However, reliance on ground stations limits offshore applicability and makes GNSS unsuitable for motion measurement during offshore operations.

Ultrasonic ranging

The principle of ultrasonic ranging is comparable to the laser sensor technique. Sound waves are emitted and reflected. The traveling time of the waves is used to measure distance. It is suited for short-range measurements between 5 to 15 meters [59], making it unsuitable for offshore operations.

3.4.2. Multiple sensors

To ensure accurate measurements, multiple sensors should be used to mitigate errors. While Osumi found challenges in implementing two sensors for swing motion measurement [74], McKenzie successfully employed three uncoupled sensors to achieve accurate motion results [75]. The optimal number or combination of sensors depends on the sensor type and the specific offshore heavy lift operation. Further research must be done making any assertions regarding the needed number of sensors.

3.4.3. Conclusion

In this section various sensors were examined in terms of feasibility, accuracy, and range. Visual and laser sensor techniques demonstrate potential for load motion measurement. Inertial sensors also offer promise, despite integration challenges. In summary, despite challenges, several sensors show potential suitability for motion measurement during offshore operations. Based on the knowledge gained in this section, the assumption is made that the implementation of sensors for load motion measurement is feasible throughout the rest of this thesis.

3.5. Novel concepts for motion control systems

In this section, various motion control system concepts are discussed in terms of their feasibility and potential. The current motion control system has been elaborated upon in Section 3.2.

3.5.1. Multi-cable systems

The current damping system configuration involves pairs of either two or four winches along with their corresponding tigger cables. These winches are positioned on a single side of the load, allowing force application solely in one direction. An alternative approach suggests incorporating cables from different directions to create an interplay of forces. Wang Sun presents a motion control system utilizing three tigger cables arranged in three directions, as depicted in Figure 3.7 [76]. To accommodate these cables, the crane boom features two perpendicular beams and a longitudinal beam extension. Anti-swing winches regulate the tension in the tigger cables, situated at the end of the three beams. This configuration substantially reduces load motion by up to 80% [76].

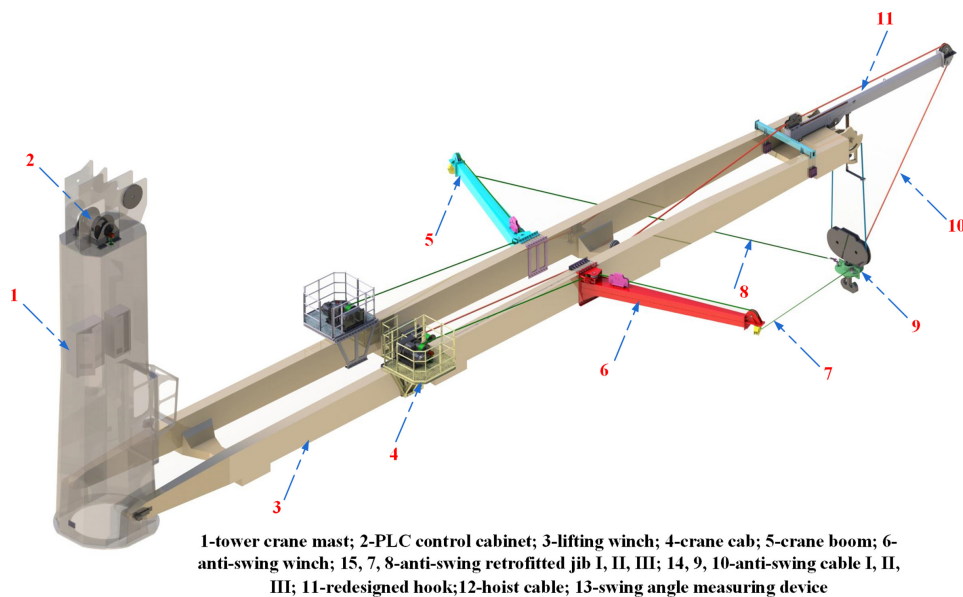


Figure 3.7: Wang Sun's multi-cable motion control system [76]

While Wang Sun's concept demonstrates viability, its practicality for incorporation on vessel poses challenges. The onboard cranes have different geometries, notably a steeper height inclination, leading to difficulties with the boom extension. Furthermore, the considerable forces associated with heavy-lifting might be too large for anti-swing booms. An alternative arrangement involves positioning winches on the deck at considerable distances from one another. However, deck space is limited. Nevertheless, this concept proves effective within its specific parameters, so future research into its applicability could be interesting.

Another multi-cable concept is presented by Ren Zhengru, incorporating two sets of four cables to damp swinging motion, as illustrated in Figure 3.8 [33]. These tugger cables are attached at different heights to two points on the load, enabling motion reduction in all directions. A dedicated winch controls tension in each tugger cable. Ren Zhengru's analysis indicates a potential 70% reduction in load motion using this setup [33]. An interesting facet of this design is the placement of two high and two low cables from the sides, eliminating the need for cables attached beyond the vessel's deck limits. On the other hand, a drawback of this approach is the number of cables, reducing the operational space. Despite this drawback, the concept holds promise for future exploration in motion control systems research.

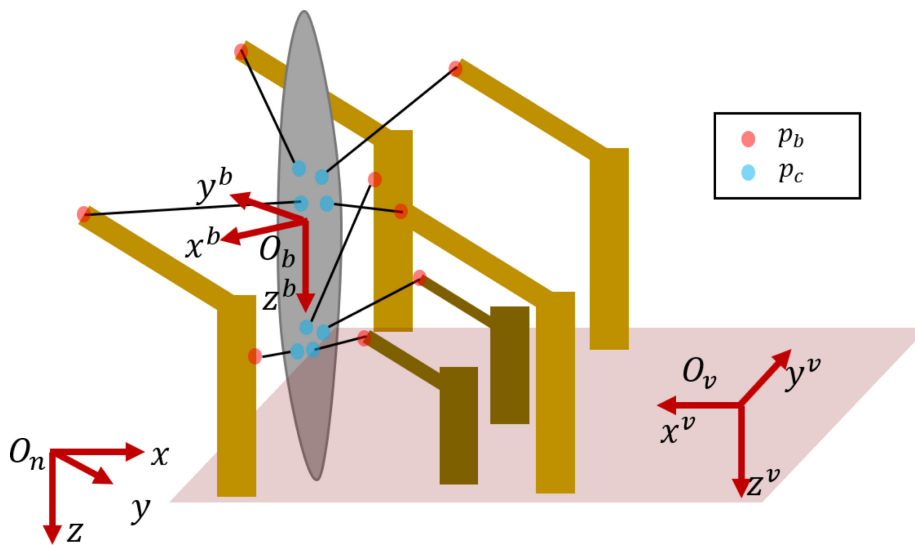


Figure 3.8: Ren Zhengru's multi-cable motion control system [33]

3.5.2. Anti-swing slider systems

A completely different approach to motion control systems is the anti-swing slider system. This concept involves suspending the load from a slider on the crane's tip. This slider possesses sideways mobility, intended to compensate the pendulum motion exhibited by the load. The slider's movement is controlled by a dedicated controller. The anti-swing slider principle is visually depicted in Figure 3.9 [77]. This principle is widely employed in bridge cranes, but application to boom cranes is also observed [77] [78].

Studies conducted on anti-swing sliders indicate the potential to mitigate the resonant motion of the load [77] [79] [80] [81] [82]. However, these results primarily focus on relatively light loads. When considering heavier loads, certain complexities emerge. The mass of the load affects the slider's inertia, necessitating high actuator forces. On the other hand, heavy loads often hang from relatively lengthy crane cables, resulting in a low oscillation frequency of the load. This low frequency may mitigate the issue by allowing for reduced slider speeds. Furthermore, the dynamic movement of the slider introduces varying gravitational forces upon the crane. These varying forces affect the dynamics of the crane, resulting in a potential risk of significant reduction in the crane's maximum lifting capacity, which is untenable. Consequently, prior to considering the application of an anti-swing slider system for offshore heavy-lifting, further research must be conducted. However, this concept will not be further explored in this thesis.

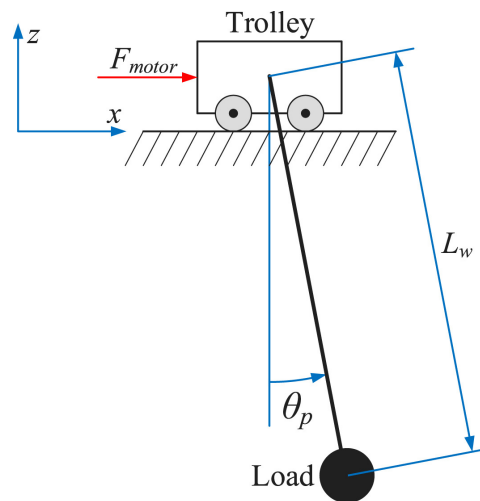


Figure 3.9: A schematic view of an anti-swing slider [77]

3.5.3. Tuned mass dampers

Tuned mass dampers (TMDs) are widely used damping systems in various engineering applications. A TMD comprises two masses with different weights, connected mostly by springs and dampers. When something causes the primary, heavier, mass to vibrate, like an earthquake shaking a building, the TMD comes into action. Energy from the primary mass is moved to the secondary, smaller, mass, which starts to vibrate. This energy transfer between the masses helps to reduce the vibration of the primary mass. Eventually, both masses slow down and stop moving because of external damping, like friction. The selection of the secondary mass weight tunes the system's natural frequency to a desirable range [83].

TMDs are widely applied in structures susceptible to seismic forces, such as towers [84]. In this context, towers are engineered with a secondary mass capable of vibration to a certain extent. During earthquakes, the tower's vibrational energy is transmitted to the secondary mass, mitigating the tower's vibration. The design of the secondary mass ensures it can vibrate effectively without issue. Figure 3.10 depicts the principle of TMD applied to a tower [85].

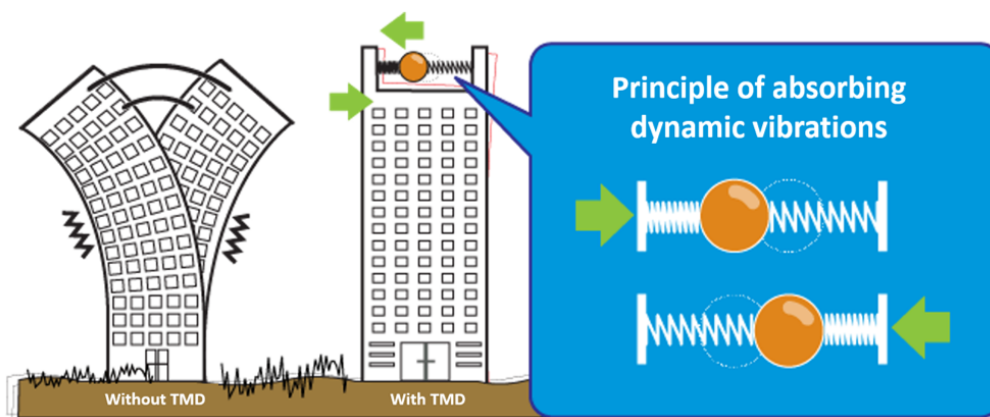


Figure 3.10: Principle of a TMD applied to a tower [85]

Although TMDs originated as earthquake mitigation, their use extends to various other domains. Carlot describes their implementation near their origin to mitigate vibrations caused by wind forces in buildings [86]. Additionally, TMDs are used in bridges [87], machinery [88] [89], and the OWT sector [90] [91].

Despite their proven results, TMDs possess certain drawbacks. A TMD is tuned to a single frequency, posing challenges when the frequency changes. Furthermore, their installation necessitates extra

weight and space, introducing design constraints [92]. Moreover, the addition of a secondary mass introduces new degrees of freedom (DOF) for control, resulting in a more complex system that can be challenging to manage.

Over time, innovative TMD variants have been developed to address specific issues. The pendulum TMD (PTMD) and liquid TMD (LTMD) are interesting solutions. In PTMD, the secondary mass is suspended like a pendulum from the primary mass, following the same principles as the original TMD but with potential design benefits. The LTMD also retains the original TMD's principles but substitutes the solid mass with a liquid, what could be beneficial when a range of frequencies of sea waves must be covered [91]. However, the complexity of a liquid mass, especially its modeling and control during vibration, poses challenges. Furthermore, an interesting variation involves energy recovery from the vibrating secondary mass, proposed by Kecik, using electromagnetics [93]. While this concept aligns with sustainability goals, energy recovery can dampen the TMD's motion and potentially reduce performance.

TMDs come in diverse types and sizes and have demonstrated their effectiveness in mitigating undesired motions. The main drawback is the additional weight they introduce, particularly concerning heavy loads encountered in offshore heavy-lifting. Nevertheless, history showed that solutions to heavy force issues are attainable. As such, TMDs hold potential for enhancing efficiency and operability in offshore operations, making it an interesting subject for further research.

3.5.4. Electromagnetic interaction

Another concept for motion control involves the use of electromagnetic interaction. This concept offers the advantage of applying both pulling and pushing forces to the load, in contrast to cables which are limited to pulling forces only [94]. However, a limitation is that the load must possess magnetic properties, and there exists a possibility of undesirable interactions between the electromagnetic waves and objects other than the intended load. Currently, research on this topic is being done at Delft University of Technology.

3.5.5. Preventing motion of the load

Another method of ensuring minimal load movement involves preventing the initiation of load motion. One strategy for mitigating load vibrations is by counteracting the oscillations induced by vessel motions. A technique used for this purpose is known as heave compensation. Heave motion can be classified into two distinct categories: earth-fixed heave compensation, which aims to restrain the vessel's vertical movement, and heave motion compensation, which aims to compensate the vertical motion of the vessel [95] [96]. However, since the focus of this research lies beyond heave motion, it remains beyond the scope of this thesis.

An alternative and innovative approach to prevent load excitation involves the utilization of wind absorbers, as suggested by Beller. Beller's research presents various wind absorbers and demonstrates their potential to absorb up to 80% of wind-induced forces, consequently reducing load motion due to wind forces [97]. Nonetheless, due to the typically minor impact of wind forces when compared to the dominant gravitational forces experienced during heavy-lifting operations [3], wind absorbers will not receive further examination within the context of this thesis.

3.5.6. Conclusion

Several new ideas are explored, and upon examination, three systems exhibit promise: the multi-cable system, the anti-swing slider system, and the implementation of a TMD. However, despite their potential, these options bring feasibility challenges. It is worth noting that an installation need not be confined to a single concept; multiple concepts could be integrated. In this regard, the prevention of motion of the load could be incorporated into a motion control system. Nevertheless, this area needs further research, which could have been an interesting topic for this thesis, however it is chosen to focus on investigate possible improvements of Heerema MC's currently used motion control system e.i. the damping tugger system.

3.6. Evaluation method of different control systems

Distinct motion control systems, or different versions of the same system, are evaluated. When comparing the effectiveness of these systems, a compare value must be established. Various potential compare values are discussed in this section. Furthermore, a study that used a system similar in physics and a modeling approach similar to that of this thesis is discussed.

3.6.1. Evaluation of effectiveness of control system

Distinct motion control systems can be evaluated by comparing the amount of energy extracted by the system from the load. However, the primary objective of the motion control system is to minimize the motion of the load, which is achieved by extracting energy. Therefore, it is more appropriate to compare motion control systems based on their main goal, namely, the reduction of load motion, rather than on energy extraction.

When a setpoint is established, the error is determined by the difference between the actual value and the setpoint value. Let q represent a sample value. The setpoint for this value is q_s . Therefore, the error for q is:

$$e_q = q - q_s \quad (3.5)$$

where e_q is the error of q . The deviation of the setpoint is the absolute value of the error. This deviation defines how far the actual value is away from the error. The average deviation over a time frame T_p is then defined as:

$$d_{q-av} = \int_0^{T_p} |q - q_s| dt \cdot \frac{1}{T_p} \quad (3.6)$$

The average deviation of the setpoint $d_{q_{av}}$ can also be used to compare model outcomes of different situations. In this thesis the average deviation from the velocity setpoint of the load is used as compare value.

The kinetic energy within a system leads to motion. The kinetic energy of a sample mass m is expressed as:

$$T = \frac{1}{2} m \dot{x}^2 \quad (3.7)$$

where T denotes the kinetic energy and \dot{x} is the velocity of the mass. The average kinetic energy over a time frame t is then expressed as:

$$T_{av} = \frac{1}{2} \int_0^{T_p} (m \dot{x}^2) dt \cdot \frac{1}{T_p} \quad (3.8)$$

The average kinetic energy of the load can be used to compare model outcomes of different situations.

When a generalized mean from a series of outputs is required, the root mean square (RMS) can be applied. The RMS represents the square root of the mean of all squared values in the series. The RMS can be used for comparing different series of values, such as the motion of a load over a time frame. In this thesis, the RMS of the velocity of the load of the motion is used to compare the effects of different control aspects. The RMS of the velocity of the load is expressed as:

$$RMS = \int_0^{T_p} (\dot{x}^2) dt \cdot \frac{1}{T_p} \quad (3.9)$$

where \dot{x} is the velocity of the load or mass. When comparing equations 3.8 and 3.9, it becomes evident that the average kinetic energy of the load and the RMS of the velocity of the load are proportional to each other, since the mass m is constant. Hence, the RMS of the load's velocity conveys information regarding the kinetic energy of the load. In this thesis, RMS will be used to compare velocity of the load over a time frame.

In summary, the three suitable parameters that are suitable for comparison are: the average deviation from the setpoint of the velocity of the load, the average kinetic energy of the load, and the RMS of the velocity of the load.

3.6.2. Similar study

Following a literature review, a study was identified that used a system similar in physics and a modeling approach similar to that of this thesis [98]. Figure 3.11 depicts the system used by Zhang. The vessel motions serve as the input for Zhang’s model, producing multiple output variables. Notably, one output variable is the rotation of the crane cable θ .

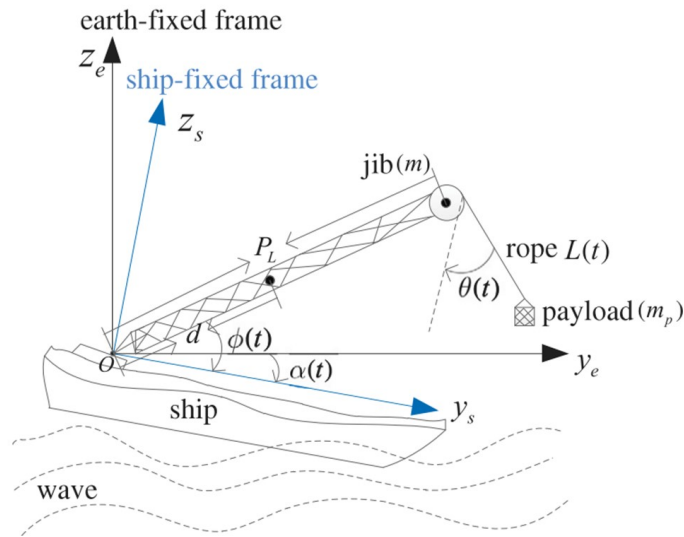


Figure 3.11: The system used by Zhang [98]

Zhang’s study focuses on developing an adaptive tracking approach for an anti-swing system. This objective slightly varies from the objective of this thesis. Nevertheless, the outcomes of Zhang’s research might be comparable to the findings of this study. The input vessel motion used in Zhang’s research is a pitch vessel motion, depicted in Figure 3.12.

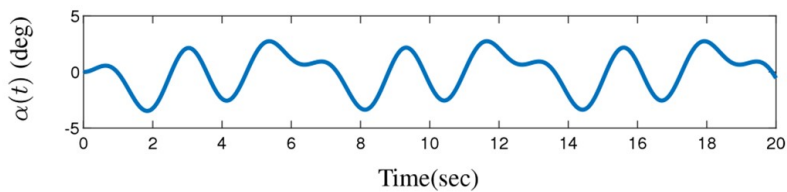


Figure 3.12: Input pitch vessel motion for Zhang’s study [98]

The vessel movement results in a crane cable rotation, as depicted in Figure 3.13. In Section 4.5.2, the outcomes of the detailed model will be compared to the outcomes of Zhang’s study.

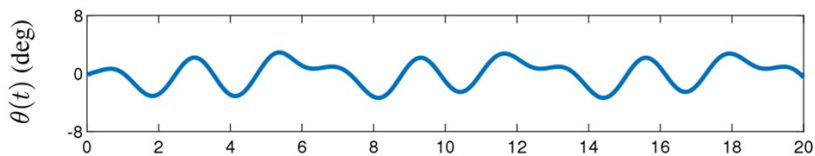


Figure 3.13: The resulting rotation of the crane tip for Zhang’s study [98]

3.6.3. Conclusion

The objective of the motion control system is to reduce the motion of the load. Three suitable parameters for comparison are: the average deviation from the setpoint of the load's velocity, the average kinetic energy of the load, and the RMS of the load's velocity. The choice of comparison value depends on the specific situation. Furthermore, a study that used a system similar in physics and a modeling approach similar to that of this thesis is discussed.

3.7. Conclusion

This chapter examines various motion control systems for offshore heavy lifting operations, with a focus on the system used by Heerema MC. The discussion on Heerema MC's system raises two questions, serving as the base for two of the three research questions addressed in this thesis. These research questions appear in Section 1.3. After this discussion, two alternative approaches are proposed: one for the control setpoint and another for the control input. The efficacy of these proposed alternatives within the motion control system will be analyzed in this thesis. Implementation of the alternative control input comes with the use of new sensors. An assessment on various sensor techniques confirms the feasibility of incorporating these new sensors into the system.

4

Detailed model

This chapter describes the development of a model for simulating a lifting operation while using a motion control system. Initially, the objectives of the model development are described, followed by explanations of modeling methods, modeling decisions and standard parameters. Next, three systems are introduced, and their EOMs are derived. Thereafter, numerical MATLAB models are developed and assessed through verification cases. These numerical models are subsequently converted to Simulink models, serving as the foundation for the controller design phase. In this stage, a controller for the constant tension mode is successfully designed. An attempt is then made to design a controller for the damping mode, encountering issues such as prolonged computation time. Consequently, a decision is made to simplify the model to mitigate these issues. This process is described in Chapter 5.

4.1. Objective of the model

The objective is to develop a model that is suitable for the analysis of the effects of the controller setpoints and inputs outlined in Section 3.3. This model should simulate the motion of the load excited by vessel motion and controlled by the current motion control system e.i. the damping tugger system. The simulation model will incorporate both the crane vessel responsible for lifting the load and the damping tugger system connected to it.

4.2. Method

The approach for constructing the detailed model is outlined in this section. Initially, multiple systems will be constructed to describe the physics of a lifting operation. Subsequently, a numerical model will be developed, and a controller will be designed. This is intended to provide a foundational model for the analysis of the distinct controller setpoints and inputs of Section 3.3.

4.2.1. Controlled lifting system

The created system that describes the physics of the lifting operation is called the controlled lifting system. Certain modeling decisions are required, as outlined in Section 4.3. After making these decisions, a schematic diagram is generated to serve as the foundation for deriving the EOMs for the system. To simplify the derivation process, the detailed controlled lifting system is divided into two less complex systems: one representing free lifting operation and another representing the damping tugger system. The EOMs are then derived for these smaller systems. The knowledge gained from these derivations are used for the formulation of the EOMs for the complete controlled lifting system.

4.2.2. Lagrangian Method

The EOMs are derived by means of the Lagrangian method [99]. Initially, it is essential to identify the DOFs of the system. The number of DOFs corresponds with the number of resulting EOMs. Subsequently, the kinetic and potential energies of the system are defined, which are used to formulate the Lagrangian parameter. Using both the Lagrangian parameter and the Euler-Lagrange equation leads to the derivation of the EOMs.

In cases where the system incorporates dampers or other elements that cause energy dissipation, the Lagrangian method should also include Rayleigh's dissipation function [100]. This function accounts for any defined dissipation terms within the system.

4.2.3. Numerical model

After deriving the EOMs, the next step is creating a numerical model. Initially, a MATLAB model is created, employing the ODE45 numerical solver to solve the EOMs. This solver provides a dynamic response, specifying the DOFs along with their first time-derivatives. Verification relies on the responses generated by these MATLAB models.

4.2.4. Controller design

The objective of the model is to simulate how the damping tugger system behaves during its damping mode. To achieve this, a controller for this mode needs to be developed. This controller is designed within the Simulink environment, because of Simulink's suitability for controller design. Conversion from the MATLAB script to the Simulink environment will be done by integrating a MATLAB Function Block. Additionally, the MATLAB ODE solver is replaced with a Simulink ODE solver. Appendix A.3 elaborates on the Simulink ODE solver.

The control system for damping mode is, in fact, an extension of a control system for the constant tension mode. For the constant tension mode, the setpoint remains a single constant value. In contrast, the setpoint for the damping mode takes the form of a mathematical expression that includes the winch's measured velocity, as described in Section 3.3.2. Designing the damping mode's controller can start by adapting a functional controller from the constant tension mode and adjusting for the damping mode setpoint. Initially, design efforts focus on the constant tension mode controller, followed by testing. Once confirmed functional, adjustments are made to implement the damping mode setpoint.

As discussed in Section 3.2.1, the controller used for the damping tugger system is a standard PID controller. It takes the tension setpoint as its input. The aim is not to design an optimum controller, but rather to identify one that works effectively for system analysis. The design methodology follows a trial and error process. Various sets of proportional, integral, and derivative gains will be tested. An evaluation will be done to select the optimal controller. Given that the two modes possess distinct objectives, the evaluation of the controller relies on a distinct parameter for each mode. For constant tension mode, the control that forces the setpoint to deviate least from the desired setpoint is chosen. In the context of damping mode, the control response that minimizes load motion will be selected. Due to the extensive time required for simulations, tests will focus on broad parameter ranges.

After designing functional controllers for both constant tension and damping modes, it will be implemented into the Simulink model. This Simulink model will be used to explore the motion of the load excited by vessel motion and controlled by the damping tugger system.

4.3. Modeling decisions of different elements of the systems

This section provides explanations on the decisions made regarding the construction of the lifting system. These decisions are about the system's dimensions, vessel movements as well as the modeling approaches of the motion of the load, the damping tugger system, the control system and certain cables. Furthermore, standardized values for specific parameters are discussed in this section.

4.3.1. A two-dimensional or three-dimensional approach

The controlled lifting system can be either in a two-dimensional (2D) or three-dimensional (3D) environment. While calculations based on a 3D model are more complex, they provide greater information. The choice between them depends on the research goal. For this thesis, which focuses on investigating a damping system, a single damping system's response can serve as a suitable test. Previous studies with similar research objectives have demonstrated the competence of a 2D model, such as investigations into single anti-swing slider controller systems [77] [79] [80] and crane dynamics of offshore crane vessels [37] [82] [101] [98]. Therefore, it is suspected that a 2D model will suffice for this research.

4.3.2. Pendulum system

The swing motion of a suspended load on a crane resembles the swinging motion of a pendulum system. Consequently, the crane can be modeled as a pendulum system comprising three main components: the load, the crane cable, and the crane tip, assuming a frictionless pivot point. The manner in which these components are modeled must be determined.

A straightforward approach to modeling the load involves representing it as a point mass, assuming that factors like geometry or additional components e.g., the hook have no impact on motion, as seen in comparable studies [77] [80] [102] [37]. An alternative is to model the load as a double pendulum, as Moradi did [79], accounting for other moving parts like the hook. More complex load models exist, such as Wu and Wang's use of a double pendulum with distributed mass beam [82]. They demonstrate the difference between the motion of a single pendulum with a point mass and the double pendulum with a distributed mass beam. Figure 4.1 [82] illustrates these various pendulum configurations: the single pendulum, the quasi-periodic single pendulum, which is a single pendulum attached to a laterally moving trolley resulting in two frequencies, and the second-mode pendulum, representing the double pendulum with a distributed mass beam suspended from the trolley. Notably, the difference between these configurations primarily involves the presence of additional frequencies, while the core motion remains consistent. The goal of this research is to analyze an improved motion control system, which can be achieved adequately with a point mass, as demonstrated by Wu and Wang.

A crane cable is comprised of a set of cables; Heerema MC's crane cables typically consist of 64 cables [103]. A common simplification in crane modeling is to treat the set of cables as a single cable with high stiffness [103], as normally done within Heerema MC and seen in various studies [77] [80] [104] [37][79]. Additionally, a high-stiffness cable can be approximated as a rigid bar, assuming negligible elongation, as done as well in those studies [77] [80] [104] [37]. Another option is to model the crane cable as a dissipative spring, incorporating both spring and damping elements, similar to Jutten's approach [101]. Given the potential weight of the load, assuming negligible elongation for a high-stiffness cable may not hold true, thus the option of a dissipative spring is a more accurate manner to model the cable.

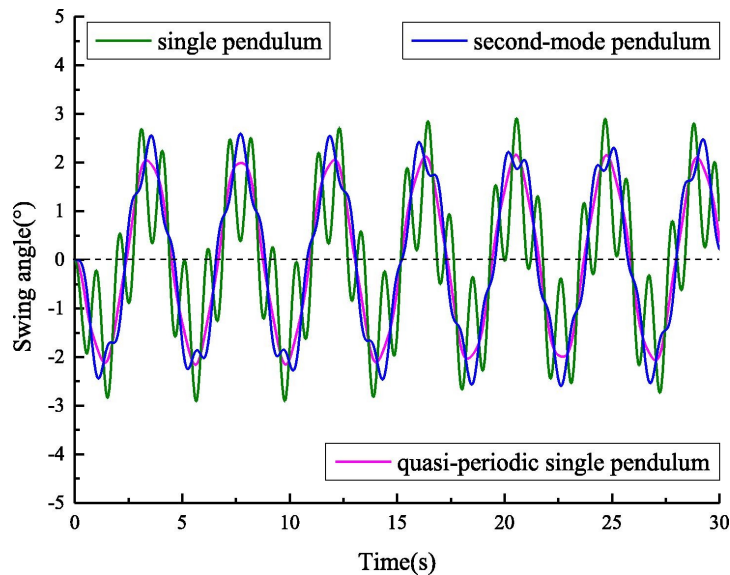


Figure 4.1: A comparison of distinct load modeling methods [82]

The distinction in complexity between the option of a rigid bar or a damping spring as cable is demonstrated through the two EOMs. The EOM for a basic pendulum system is given by:

$$\ddot{\theta} + \frac{g}{r} \sin(\theta) = 0 \quad (4.1)$$

Here, θ signifies the angle of the pendulum, r is the length of the cable and g denotes the gravity constant. If the crane cable is characterized as a damping spring, the pendulum system would transform into a spring pendulum. Figure 4.2 provides a visual representation of this spring pendulum setup [105]. The system of equations governing the motion would then appear as follows [106] [107]:

$$m\ddot{x} - m(x+r)\dot{\theta}^2 + c\dot{x}kx - gm \cos(\theta) = 0 \quad (4.2)$$

$$m(x+r)^2\ddot{\theta} + 2m(x+r)\dot{x}\dot{\theta} + gm(x+r) \sin(\theta) = 0 \quad (4.3)$$

Here, x denotes the extension of the spring (with length r), m signifies the mass of the load, and c and k the damping and spring coefficients of the dissipating spring, respectively. This introduces heightened mathematical complexity in contrast to the simple pendulum equation of 4.1. Nevertheless, this study opts for a detailed simulation of the system, therefore the crane cable is modeled as a dissipative spring.

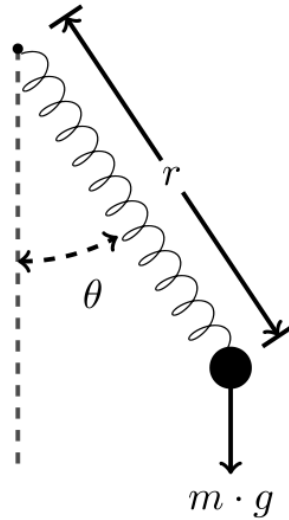


Figure 4.2: Illustration of a spring pendulum [105]

In the context of this thesis, the crane is to be modeled as a rigid beam, eliminating the influence of any potential crane deformation. This simplified approach was used in several prior studies [77] [80] [104] [37].

4.3.3. Modeling of the damping tugger system

The motion control system comprises four primary components: a winch, an electromotor, a tugger cable, and a control system, with the modeling of the latter covered in Section 4.3.5. If the electromotor is considered as an ideal system, always delivering the desired output, it can be left out, as seen in Bron's MSc thesis [53]. This simplification ensures that the focus remains on the winch and cable motion, which are the main points of interest. Similarly to the crane cable, the same reasoning applies: modeling the tugger cable as dissipative springs is necessary for accurate modeling. Hence, the tugger cable is modeled as a dissipating spring.

Additionally, the mass of the tugger cable could be important, especially given the horizontal orientation of the cable. The presence of mass would result in a catenary geometry for the cable. Therefore, this mass is represented in the system as a point mass situated at the center of two dissipating springs.

4.3.4. Non-linear springs

In this study, cables function as dissipative springs. However, a cable behaviour can be modeled as a spring only when it is tensioned. If not tensioned, these cables become slack. Unlike typical springs, slack cables display no axial stiffness, resulting in completely different behaviour. Therefore, cables are

modeled as non-linear springs. In this particular system, the non-linear springs have uniform stiffness in the tension state, while they possess no stiffness ($k = 0$) in the compression state.

4.3.5. Modeling of the control system

The field of control technology is extensive, bringing various types of controllers. Within damping technology for pendulum-like movements, different forms of intelligent controllers are applied. For example, adaptive control is used by Qian et al. when facing uncertain weather conditions during installation [102], while Zhai et al. apply fuzzy control during transitions between decks [37]. Currently, the damping tugger systems utilize a proportional-integral (PI) controller, which is essentially a PID controller with no derivative gain. This study aims to explore the impact of modifying the control input and altering the control setpoint calculation under identical conditions. Notably, the intention is not to switch to a different controller type, hence no additional investigation is conducted on controllers other than the PID controller.

4.3.6. Vessel Motions

The vessel motion is affected by wave elevation and water currents. Additionally, the load can influence the vessel motion during a lifting operation. Due to the substantial weight of the load, it could potentially impact the vessel's motion, which, in turn, influences the load's motion. This dynamic leads to a coupling between the motions of the vessel and the load. However, this study concentrates solely on dampening the load's motion, excluding an examination of this interplay. Consequently, the impact of the motion of the load on the motion of the vessel is not considered in this thesis and the motion of the vessel is given by a prescribed trajectory.

The motion trajectories of the vessel is created using the LiftDyn software package, adhering to realistic vessel behaviors of Heerema MC's vessels. As a 2D space is used, it generates vessel movements in three specific directions: the translational surge (x_s), translational heave (y_s) and rotational pitch (θ_s) direction. LiftDyn is used for generating the surge, heave and pitch trajectories. Subsequently, the corresponding velocity and acceleration trajectories in these three directions are derived. Figure 4.3 illustrates the displacement and rotation trajectories. The motion trajectories have a length of 1200 seconds. Therefore, every run done for this model has a maximum length of 1200 s. As can be observed, the trajectories provide no motion before $t = 50$ s. This absence of movement is intentional. The initial 50 seconds serve to test the system in static steady-state, ensuring no initial kinetic energy exists.

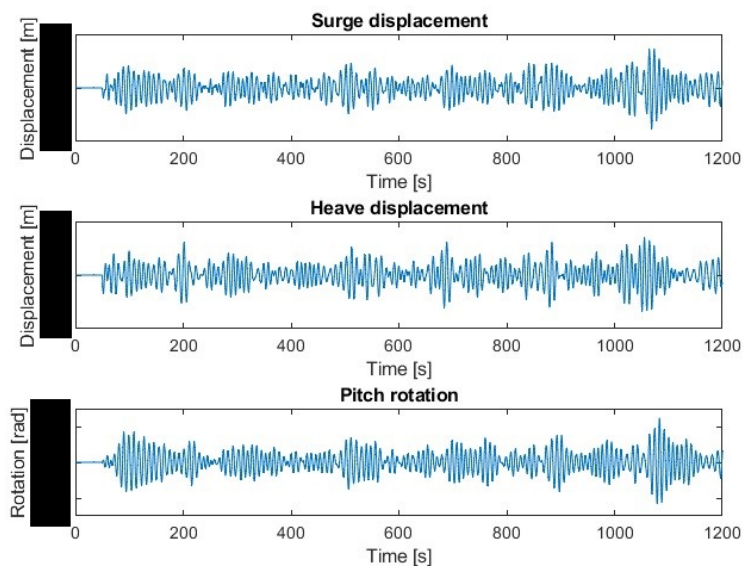


Figure 4.3: The vessel displacement trajectory (*magnitude of displacement and angles is confidential information*)

4.3.7. Standard parameters

In this model multiple parameters are standardized, which are listed in Table 4.1. Appendix A.1 provides explanations for selecting these specific values.

Element	Parameter	Symbol	Value	Unit
General	Gravity constant	g	9.81	m/s ²
Crane cable	Stiffness	k_{tm}	4.85	MN/m
Crane cable	Damping constant	c_{tm}	10	kNs/m
Crane tip	X-coordinate	l_{tx}	40	m
Crane tip	Y-coordinate	l_{ty}	100	m
Load	Weight	m_o	500	mT
Tugger cable	Half the initial length	l_{0t}	60	m
Tugger cable	Stiffness	k_c	2	kN/m
Tugger cable	Damping constant	c_c	10	kNs/m
Tugger cable	Mass per length	m_c	73	kg/m
Winch	Radius	r_w	1.5	m
Winch	X-coordinate	l_{wx}	0	m
Winch	Y-coordinate	l_{wy}	30	m

Table 4.1: Standardized parameters of the detailed model

4.4. Equations of motion

The sets of EOMs for the distinct systems are derived in this section. First, the derivation of the EOMs for the free lifting system occurs in steps. Thereafter, the EOMs for the damping tugger system are derived. Following this, these two systems are merged to formulate the controlled lifting system and its EOMs are derived. Finally, the steady-state is discussed.

4.4.1. Free lifting system

The lifting crane cable of the vessel possesses elastic and damping properties that affect the motion of the object suspended on the cable. Hence, the vessel's crane cable is modeled as a damped elastic pendulum, a type of pendulum that incorporates both damping and elastic behavior of the suspension. In other words, the cable of the pendulum is represented as a spring and damper, resulting in an oscillating pendulum with amplitude decreasing over time. However, this could be false in the presence of an excitation force. Figure 4.4 depicts the damped elastic pendulum system. For this scenario, the tip of the crane is fixed, resulting in a 2DOF system consisting of the rotation at the crane tip θ_t and the translation of the spring r_t . The initial length of the spring is l_s , so the time-dependent length of the spring is:

$$l_t(t) = l_s + r_t(t) \quad (4.4)$$

Moreover, the horizontal and vertical motion of the object are denoted by x_o and y_o , respectively. It is assumed that the dissipating spring is subjected to loading only in the longitudinal direction, so no perpendicular forces to the spring are considered. Furthermore, it is assumed that if the spring is elongated, its damping and restoring characteristics are linear.

When deriving the EOMs for a damped elastic pendulum, the relevant coordinates must be determined first. The time-dependent horizontal and vertical displacement of the crane tip, defined as x_t and y_t , respectively, have its origin in the global axis system with coordinates X and Y . To that extend, the time-dependent coordinates of the load are defined as:

$$x_o = x_t + l_t(t) \cdot \sin(\theta_t(t)) \quad (4.5)$$

$$y_o = y_t - l_t(t) \cdot \cos(\theta_t(t)) \quad (4.6)$$

In the present scenario, the coordinates of the crane tip are fixed at the center of the coordinate system. In a later stage, the system will be extended to include vessel motions, and the coordinates of the crane

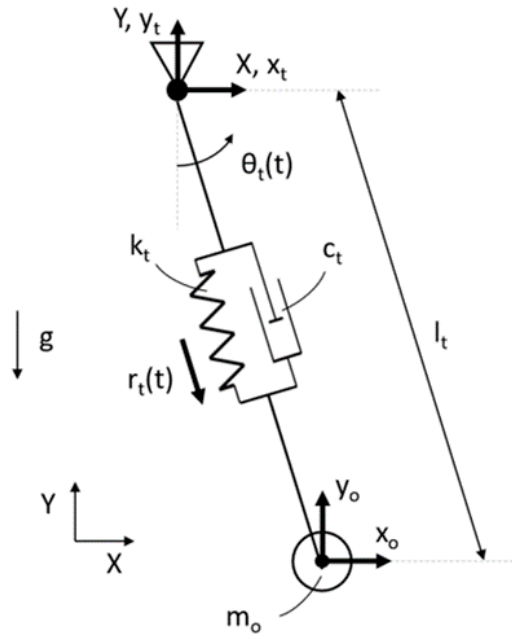


Figure 4.4: A damped elastic pendulum

tip will be updated accordingly. The coordinate descriptions are used to describe the kinetic energy T and potential energy U of the system, as:

$$T = \frac{1}{2} m_o (\dot{x}_o^2 + \dot{y}_o^2) \quad (4.7)$$

$$U = m_o g (y_{oi} - y_o) + \frac{1}{2} k_{tm} r_t(t)^2 \quad (4.8)$$

The initial vertical coordinate of the object is denoted as y_{oi} and is defined as y_o when $\theta_t(t) = 0$ and $r_t(t) = 0$. The Lagrangian of the system can then be expressed as $L = T - U$. Additionally, the Rayleigh dissipation R is described as [100] [108]:

$$R = \frac{1}{2} c_{tm} \dot{r}_t(t)^2 \quad (4.9)$$

By means of the Euler-Lagrangian equation, the EOMs for the damped elastic pendulum system are derived and look like:

$$\frac{d}{dt} \frac{\partial L}{\partial \dot{\theta}_t} - \frac{\partial L}{\partial \theta_t} + \frac{\partial R}{\partial \dot{\theta}_t} = 0 \quad (4.10)$$

$$\frac{d}{dt} \frac{\partial L}{\partial \dot{r}_t} - \frac{\partial L}{\partial r_t} + \frac{\partial R}{\partial \dot{r}_t} = 0 \quad (4.11)$$

Since this system has two DOFs, two EOMs are obtained using the Lagrangian method. Isolating the two DOFs result in:

$$\ddot{\theta}_t(t) = \frac{-\sin(\theta_t(t)) \cdot g + 2\dot{r}_t(t)\dot{\theta}_t(t)}{-(l + r_t(t))} \quad (4.12)$$

$$\ddot{r}_t(t) = \frac{m_o(l + r_t(t))\dot{\theta}_t(t)^2 - m_o g \cos(\theta_t(t)) - c_{tm}\dot{r}_t(t) - k_{tm}r_t(t)}{m_o} \quad (4.13)$$

Now, wind force will be integrated to the EOMs. It is assumed that these forces act as horizontal point forces exclusively on the load, with the presumption that they exert no influence on any other

component of the system. This assumption is done, because the area of the crane cable exposed to wind is neglectable compared to the area of the load.

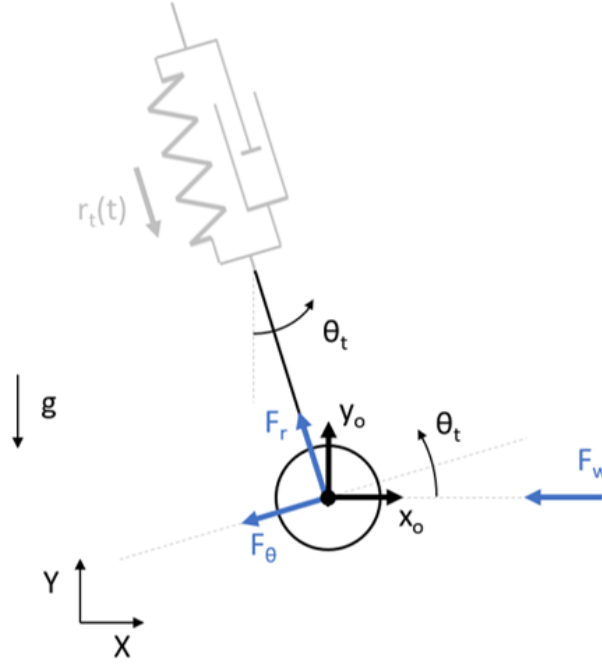


Figure 4.5: Visualization of wind force decomposition

Figure 4.5 illustrates the inclusion of the winch force to the free lifting system. Given the rotation at the crane tip, denoted as θ_t , the wind force acting on the load can be decomposed into a tangential force, F_r , and an angular force, F_θ . Both these forces are changing due to the variable angle θ_t . The tangential force results in a force in the longitudinal direction of the spring, while the angular force results in a moment exerted on the crane tip, oriented in the direction of θ_t . These are defined as:

$$F_{wr} = -F_w \sin(\theta_t) \quad (4.14)$$

$$M_{w\theta} = F_\theta l_t = -F_w \cos(\theta_t) l_t \quad (4.15)$$

The Euler-Lagrange equations visible in equations 4.10 and 4.11 are extended with the tangential wind force and the wind moment resulting in equations:

$$\frac{d}{dt} \frac{\partial L}{\partial \dot{\theta}_t} - \frac{\partial L}{\partial \theta_t} + \frac{\partial R}{\partial \dot{\theta}_t} = M_{w\theta} \quad (4.16)$$

$$\frac{d}{dt} \frac{\partial L}{\partial \dot{r}_t} - \frac{\partial L}{\partial r_t} + \frac{\partial R}{\partial \dot{r}_t} = F_{wr} \quad (4.17)$$

Leading to a new set of EOMs:

$$\ddot{\theta}_t(t) = \frac{\cos(\theta_t(t)) \cdot \frac{F_w}{m_o} - \sin(\theta_t(t)) \cdot g + 2\dot{r}_t(t)\dot{\theta}_t(t)}{-(l + r_t(t))} \quad (4.18)$$

$$\ddot{r}_t(t) = \frac{-\sin(\theta_t(t)) \cdot F_w + m_o(l + r_t(t))\dot{\theta}_t(t)^2 - m_o \cdot g \cdot \cos(\theta_t(t)) - c_{tm}\dot{r}_t(t) - k_{tm}r_t(t)}{m_o} \quad (4.19)$$

Lastly, the set of EOMs is extended with the vessel motions. As depicted in Figure 4.6, the motion of the crane tip is influenced by the vessel's movement because of the rigid connection, subsequently impacting the motion of the suspended object. The extended system is 2D in nature, including three predetermined vessel motions: surge translation $x_s(t)$, heave translation $y_s(t)$, and pitch rotation $\theta_s(t)$.

The horizontal length L_{tx} and vertical length L_{ty} , are the distances between the center of gravity of the vessel and the crane tip.

The impact of the vessel motion is implemented into the system by motion of the crane tip. The moving coordinates of the crane tip are expressed as:

$$x_t = x_s + L_{tx} \cos(\theta_s) + L_{ty} \sin(\theta_s) \quad (4.20)$$

$$y_t = y_s + L_{tx} \sin(\theta_s) + L_{ty} \cos(\theta_s) \quad (4.21)$$

Coordinates x_t and y_t are now time-dependent coordinates. Despite these changes, equations 4.5 and 4.6 remain applicable to this system since the time-dependent coordinates of the lifted object depend on the tip coordinates. The frictionless nature of the tip rotation implies that the rotation of the vessel θ_s , does not directly affect the rotation of the pendulum θ_t . Instead, it indirectly impacts the object's motion by influencing the motion of the tip.

The equations for kinetic energy, the potential energy and the Rayleigh dissipation are unaffected by the extension of the vessel motions. Therefore, the kinetic energy T of equation 4.34, the potential energy U of equation 4.35 and the Rayleigh dissipation R of equation 4.9 hold true for this system. However, the initial vertical displacement of the load y_{oi} is now defined by the vertical coordinate of the load y_o when $\theta_t(t) = 0$, $r_t(t) = 0$, $y_s(t) = 0$ and $\theta_s(t) = 0$.

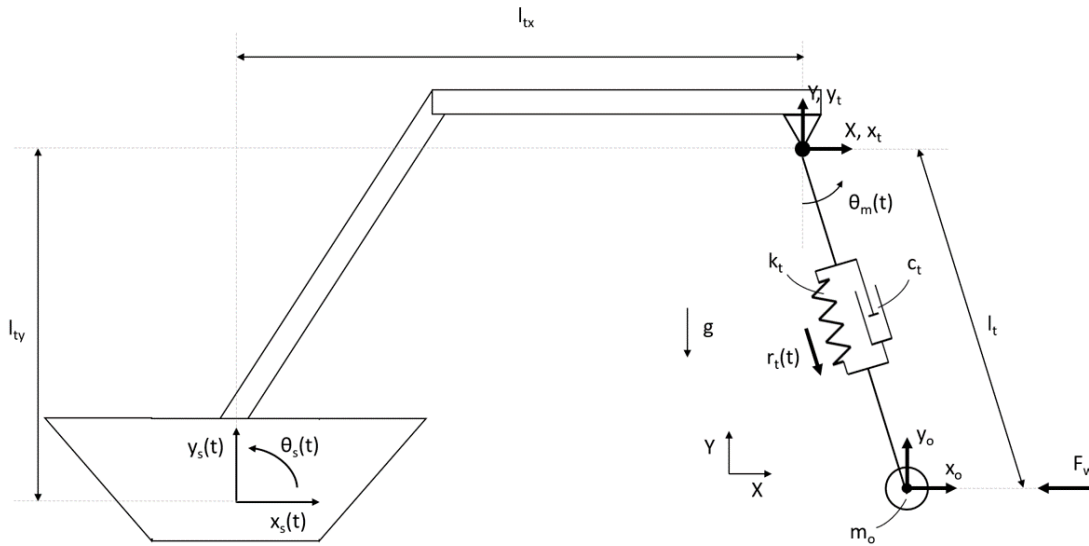


Figure 4.6: The free lifting system

Once again, the EOMs for this system are derived using the Lagrangian method. Due to the length of the equation it is given in appendix D. This set of EOMs represents the motion of the free lifting system.

4.4.2. The damping tigger system

In this section, the EOMs for the physics of damping tigger system are derived. Initially, the EOMs for the tigger cable alone are derived, followed by the addition of the winch to the system, resulting in the final set of EOMs for the damping tigger system.

The tigger cable, which connects the winch to the lifted object, is modeled as a point mass inclined between two non-linear dissipating springs in series. This non-linearity is described in Section 4.3.4. The point mass accounts for the weight of the tigger cable, which has a notable impact on the bend of the cable and must, therefore, be included in the system. The series of dissipating springs represents

both the damping and restoring characteristics of the tugger cable. Due to the vessel motions, both the winch and the load are moving with respect to the global axis system. Given that this section focuses only on modeling the tugger cable, the winch and object are modeled as two moving ends of the cable. Figure 4.7 provides a visualization of the damping tugger system.

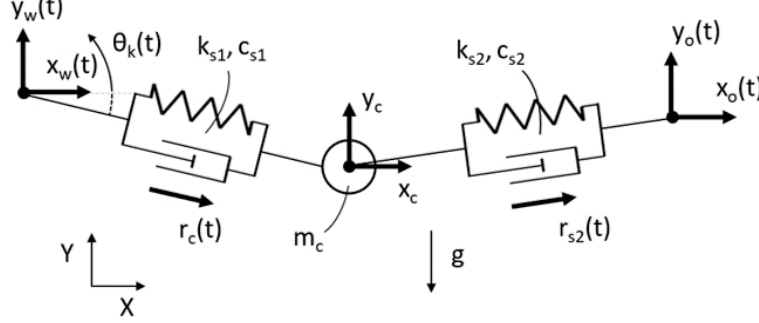


Figure 4.7: The physics of the damping tugger system

In this scenario, the motions of the winch $x_w(t)$ and $y_w(t)$ and the motions of the object $x_o(t)$ and $y_o(t)$ are prescribed. The initial coordinates of the winch $x_w(t=0)$ and $y_w(t=0)$ corresponds to those of the global coordinate system X and Y . The two DOFs are the rotation $\theta_k(t)$ and elongation $r_c(t)$ of spring 1. The latter leads to the time-dependent length of spring 1, defined as:

$$l_{s1}(t) = l_{ns1} + r_c(t) \quad (4.22)$$

Where l_{s1} is the length of spring 1 and l_{ns1} is the nominal length of spring 1. The function of the winch is modifying the tension in the tugger cable, which is achieved by adjusting the cable's length through the winch's rotation. In essence, the winch's rotation elongates the cable, thus alters the length of spring 1. This phenomenon is modeled by rewriting the rotation of the winch to a change of the nominal length of spring 1 as:

$$l_{ns1-new}(t) = l_{ns1-old}(t) - \theta_w(t)r_w \quad (4.23)$$

Leading to a new equation for the time-dependent length of spring 1:

$$l_{s1} = l_{ns1} + r_c(t) - \theta_w(t)r_w \quad (4.24)$$

The time-dependent length of the spring and the time-dependent coordinates of the mass are described as:

$$x_c = w_x(t) + \cos(\theta_k(t)) * l_{s1} \quad (4.25)$$

$$y_c = y_x(t) + \sin(\theta_k(t)) * l_{s1} \quad (4.26)$$

The motions of the mass of the tugger cable is utilized to describe the time-dependent length of spring 2 as:

$$l_{s2} = \sqrt{(x_o(t) - x_c(t))^2 + (y_o(t) - y_c(t))^2} = l_{ns2} + r_{s2}(t) \quad (4.27)$$

Where l_{ns2} and $r_{s2}(t)$ represent the nominal length and elongation of spring 2, respectively. Rewriting equation 4.27 leads to the elongation of spring 2:

$$r_{s2} = l_{s2}(t) - l_{ns2} \quad (4.28)$$

By means of equations 4.22, 4.25, 4.26 and 4.28, the expressions for the kinetic energy T and potential energy U of the system are defined as:

$$T = \frac{1}{2} m_c (\dot{x}_c^2 + \dot{y}_c^2) \quad (4.29)$$

The Rayleigh dissipation function R of this system is also a summation of the Rayleigh dissipation functions of the free lifting system (e.g. equation 4.9) and the damping tigger system (e.g. equation 4.31), leading to:

$$R = \frac{1}{2}c_{tm}\dot{r}_t(t)^2 + \frac{1}{2}c_{s1}\dot{r}_c(t)^2 + \frac{1}{2}c_{s2}\dot{r}_{s2}^2 \quad (4.36)$$

The Lagrangian Methods leads to the four Euler-Lagrange expressions:

$$\frac{d}{dt} \frac{\partial L}{\partial \dot{\theta}_t} - \frac{\partial L}{\partial \theta_t} + \frac{\partial R}{\partial \dot{\theta}_t} = M_{w\theta} \quad (4.37)$$

$$\frac{d}{dt} \frac{\partial L}{\partial \dot{r}_t} - \frac{\partial L}{\partial r_t} + \frac{\partial R}{\partial \dot{r}_t} = F_{wr} \quad (4.38)$$

$$\frac{d}{dt} \frac{\partial L}{\partial \dot{\theta}_k} - \frac{\partial L}{\partial \theta_k} + \frac{\partial R}{\partial \dot{\theta}_k} = 0 \quad (4.39)$$

$$\frac{d}{dt} \frac{\partial L}{\partial \dot{r}_c} - \frac{\partial L}{\partial r_c} + \frac{\partial R}{\partial \dot{r}_c} = 0 \quad (4.40)$$

The evaluation of these expressions leads to the EOMs for the controller lifting model. These EOMs are presented in appendix D.

4.4.4. The static steady-state

A system achieves a steady state when the energy it contains remains constant over time. This can occur either due to the system exhibiting repetitive motion, such as harmonic oscillations, or due to the absence of motion. The latter condition is referred to as the static steady state. When a system is in a static steady-state, motion is absent, indicating that the system is at rest. In this thesis, the static steady-state is the initial state for every system analyzed over a time period, eliminating any initial energy. All energy appearing during the simulation is attributed to vessel movements or the control system for motion.

Steady-state values represent the DOFs at when the system is in a steady-state, whether it is a static steady-state or a steady-state with repetitive motion. When the system is in a static steady-state, the absence of motion ensures that all time derivatives equal zero. Consequently, only the displacement values, which are non-derivative functions, could have non-zero values. These values serve as the starting point for the ODE-solver, as discussed in Section 4.5.1.

It should be noted that a system could have multiple steady-state positions. If the system in this thesis exhibits more than one static steady-state position, each will be assessed. The most suitable static steady-state position will then be chosen for further study.

The steady-state values derive from a specific equation for static steady-state conditions. Replacing all time derivatives with zero in the EOMs results in the static steady-state equation. Isolating the DOF leads to the static steady-state value for the DOF. This becomes clear in the following example. Equations 4.12 and 4.13 present the set of EOMs for the free lifting system derived in Section 4.4.1, displayed once more:

$$\ddot{\theta}_t(t) = \frac{-\sin(\theta_t(t)) \cdot g + 2\dot{r}_t(t)\dot{\theta}_t(t)}{-(l + r_t(t))} \quad (4.41)$$

$$\ddot{r}_t(t) = \frac{m_o(l + r_t(t))\dot{\theta}_t(t)^2 - m_o g \cos(\theta_t(t)) - c_{tm}\dot{r}_t(t) - k_{tm}r_t(t)}{m_o} \quad (4.42)$$

Substituting all derivatives with zero in equation 4.41 leads to:

$$\frac{-\sin(\theta_t) \cdot g + 2 \cdot 0 \cdot 0}{-(l + r_t)} = \frac{-\sin(\theta_t) \cdot g}{-(l + r_t)} = 0 \quad (4.43)$$

Rewriting the equation yields $\sin(\theta_t) = 0$, leading to $\theta_t = q \cdot 2\pi$. This indicates that the system achieves a static steady-state at $\theta_t = 0, \pi, 2\pi, 3\pi$ etc. This means the system reaches its static steady-state

when the load is either at its lowest position, directly below the suspension, or at its highest position, directly above the load. The latter scenario is not feasible in offshore lifting operations. Consequently, the static steady-state value for θ_t is established as $\theta_t = 0$.

Setting all derivatives to zero in equation 4.42 leads to:

$$\frac{m_o(l + r_t \cdot 0)^2 - m_o g \cos(\theta_t) - c_{tm} \cdot 0 - k_{tm} r_t}{m_o} = \frac{-m_o g \cos(\theta_t) - k_{tm} r_t}{m_o} = 0 \quad (4.44)$$

Given that $\theta_t = 0$, equation 4.44 could be rewritten to:

$$r_t = \frac{-m_o g \cos(\theta_t)}{k_{tm}} = \frac{-m_o g}{k_{tm}} \quad (4.45)$$

So, the static steady-state values for the DOFs of the free lifting system are given by $\theta_t = 0$ and $r_t = \frac{-m_o g}{k_{tm}}$. These values can be verified through arguments. A value of θ_t equal to zero indicates the load occupies the lowest possible point, a typical position for the pendulum in its static steady-state. Moreover, $F_{r_t} = m_o g$ denotes the gravitational force acting on the load. The relationship $r_t = \frac{-m_o g}{k_{tm}}$ can be expressed in the form of Hooke's law, as:

$$F_{r_t} = k_{tm} \cdot r_t \quad (4.46)$$

Where r_t denotes the elongation of the spring due to gravitational force. This elongation corresponds to the elongation of the crane cable in the absence of axial oscillations or swing motion, being the static steady-state elongation.

In summary, the static steady-state values are derived by replacing all time-derivatives with zero. This approach is demonstrated with the set of EOMs of the free lifting system, but could be applied for every set of EOMs.

4.5. Numerical model

The EOMs are derived for three systems: the free lifting system, the damping tugger system, and the controlled lifting system. These EOMs are the foundation for the numerical models detailed in this section. Three MATLAB models, corresponding to the three sets of EOMs, are created, which could be used for multiple research goals.

4.5.1. MATLAB models

Three MATLAB models are created, corresponding to the three sets of EOMs derived for the free lifting system, the damping tugger system and the controlled lifting system. Each model shares a similar structure and objective. Inputs include the EOMs, a specified time frame, values for parameters such as mass weights and spring stiffness, and the vessel motions. The numerical ODE solver ODE45 is used to solve the EOMs. The initial conditions of the ODE solver are the static steady-state values of the DOFs, derived following the method explained in Section 4.4.4.

The non-linear dissipative springs are implemented using an if-loop that examines whether the spring is in a state of compression or tension. When the spring is tensioned, the standard stiffness and damping coefficient are applied. However, when the spring is compressed, the stiffness and damping coefficient are set to zero.

The output of the ODE solver consists of the DOFs and the corresponding first time-derivatives. This output, combined with input parameters, is used for the calculation of various translational and rotational displacements and velocities, and forces within the model.

4.5.2. Verification of the MATLAB models

In Section 3.6.2, a study is discussed that used a system with similar physics and a modeling approach similar to the one used for the development of the numerical MATLAB model for the free lifting system. Zhang [98] conducted this study. The outcomes of Zhang's research are compared with those of the

MATLAB model for the free lifting system. Initially, parameters from the similar study are incorporated into the MATLAB model, resulting in the new model parameters shown in Table 4.2. Subsequently, the input pitch motion for the free lifting system model is adjusted to align with the input of Zhang's model, as illustrated in Figure 3.12. Additionally, both surge and heave motion are set to zero, mirroring Zhang's model settings. Finally, the model is executed to generate the resulting rotation of the crane cable.

Figure 4.9 displays the input pitch vessel motion θ_s and the resulting rotation of the crane cable θ_t . When comparing Figure 4.9 with Figure 3.13, it is observed that the crane cable rotation in both models has a similar order of magnitude [98], demonstrating that the modeling approach of the detailed lifting model results in valid outcomes within this specific case. Additionally, multiple other verification cases are employed to assess the validity of the results from all three models. These cases are provided in Appendix A.2.

Element	Parameter	Symbol	Value	Unit
Crane cable	Length	l	0.35	m
Load	Mass	m_o	1	kg
Crane tip	Horizontal coordinate	l_{tx}	1	m
Crane tip	Horizontal coordinate	l_{tx}	1	m

Table 4.2: Model parameter for comparison with the results of Zhang's study

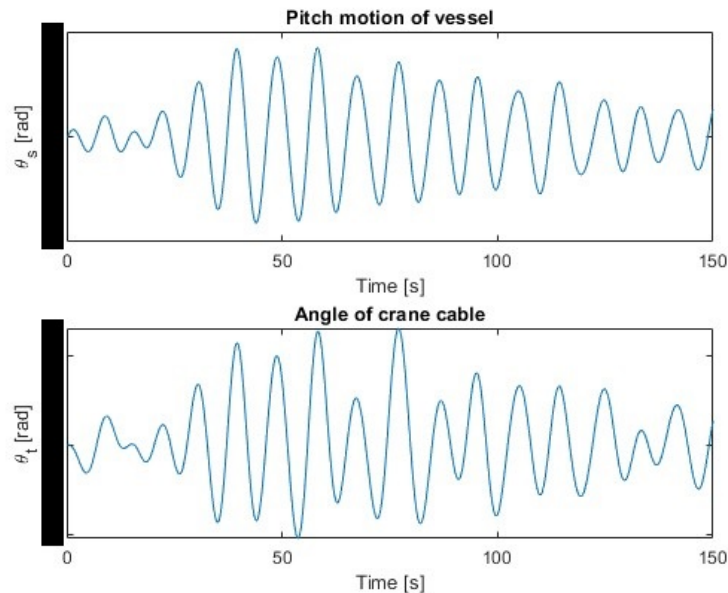


Figure 4.9: Pitch vessel motion as input for the model (*magnitude of angles is confidential information*)

4.5.3. Purposes of the numerical models

The three created models can be used to gain more understanding of the physics of a lifting operation and of the damping tigger system. For example, the free lifting system can be used for investigating the motion of the load during free lifting under different environmental conditions, or for studying the effect of the load on the crane cable. Moreover, the model of the damping tigger system can be used to study vibrations within the damping tigger system or the impact of the load's motion on the system, which is less commonly done. Finally, the controlled lifting system can be used to examine vibrations within the entire system or the effects of movement of specific elements on other elements. When the winch is kept motionless, this model can also be used to study the motion of a load connected to a tigger cable to a fixed point.

4.6. Controller design

The goal for the detailed model is to function both in constant tension model and in damping mode. First, a Simulink model is created and the controller is designed in this environment. As outlined in Section 4.2.4, two distinct controllers are created, each corresponding to one of these modes. The aim of this design process is not to create the perfect controller, but to develop one that performs effectively during system analysis. A trial and error method is used for this purpose. Given the substantial amount of time required for running simulations, the tests will prioritize a wide scope of parameters. The discussion starts with an examination of the PID controller used in the damping tugger system, followed by the design processes for the controllers corresponding to one of the two modes.

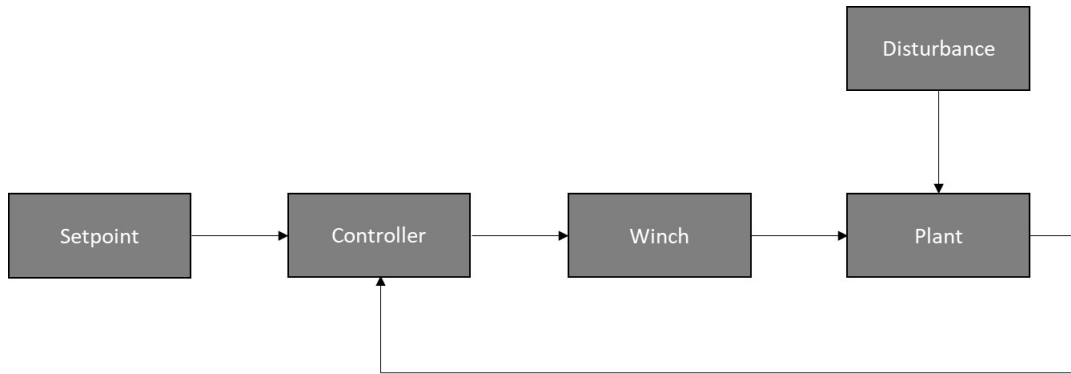


Figure 4.10: Simulink loop

4.6.1. Simulink model

A Simulink model was created to investigate the controller of the damping tugger system. This model contains four main elements: the setpoint calculation, controller, plant and disturbance. The latter is the vessel motion. Figure 4.10 depicts the control loop of the Simulink model. The plant comprises the MATLAB script that defines the system's physics as described in Section 4.5.1, and a block that outlines the winch limitations. The Simulink approach retains identical input and output values to the MATLAB method detailed in Section 4.5.1.

Physical aspects, like the electromotor power and winch inertia, limit the winch's rotation. This is modeled incorporating velocity and acceleration boundaries. Within these boundaries, the rotation velocity of the winch aligns with the controller output. If the controller output surpasses a boundary, the winch output retains that boundary value until the controller output returns within the limits. For example, with a maximum winch velocity of 1 rad/s and a controller output of 1.5 rad/s, the winch output stays at 1 rad/s until the controller output drops below 1 rad/s again. Figure 4.11 illustrates this scenario. In essence, the controller output is cut-off when exceeding limits.

4.6.2. The PID controller of the damping tugger system

The control system comprises a controller responsible for winch acceleration. This controller is a typical PID controller. In mathematical terms, a PID controller can be represented as:

$$u = k_p \cdot e + k_i \cdot \int e + k_d \cdot \dot{e} \quad (4.47)$$

where u is the controller output and k_p , k_i and k_d denote the proportional, integral and derivative control value, respectively, and e is the error input of the controller. This error is defined as a measured parameter minus the setpoint. Mathematically, this error is expressed as:

$$e = q_{sen} - q_s \quad (4.48)$$

where e is the error, q_{sen} is the measured parameter and q_s is the setpoint.

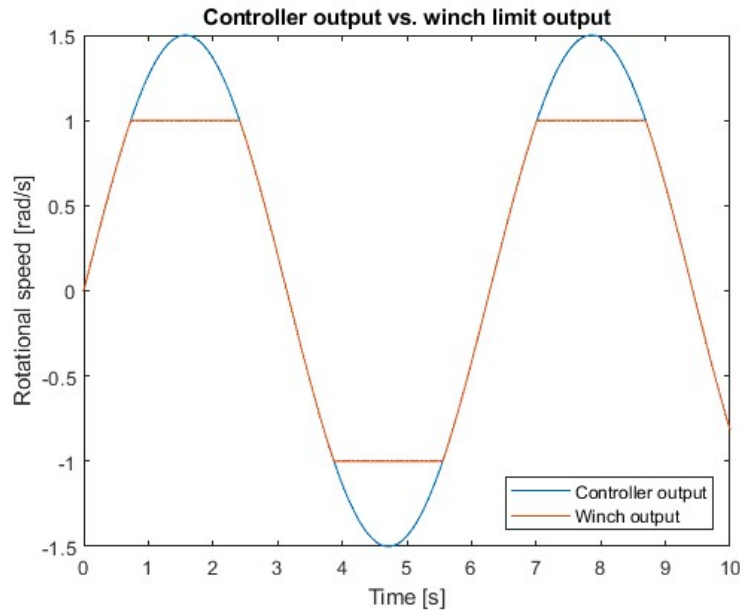


Figure 4.11: Visualisation of winch limits

In the case of the damping tugger system, the error is defined as the difference between the measured tension in the tugger cable and the tension setpoint. The cable tension is continuously measured by a motion sensor. The measured data is compared to the tension setpoint, leading to the tension error:

$$e_t = T_{sen} - T_s \quad (4.49)$$

where T_{sen} is the measured tension, while T_s denotes the tension setpoint. The error serves as the controller's input. In that extend, the expression for the controller used in the damping tugger system is:

$$u = k_p \cdot e_t + k_i \cdot \int e_t + k_d \cdot \dot{e}_t \quad (4.50)$$

This controller will be tuned to an effective controller for the objective of the model. The tuning of the controller includes choosing values for the proportional, integral and derivative gain of the controller.

4.6.3. Identification of unstable response

In applying a controller to a damping system, the goal is to reduce the motion of the load. However, an inappropriate controller may produce an undesired response. Such an undesired response could result in exceeding maximum cable tension, the cable falling slack, or even increase of load motion. This undesirable behavior often arise from instabilities in the controller's performance.

These instabilities may originate from multiple factors. Two common causes involve either an overly aggressive or an overly conservative controller. The aggressive controller can result in overshooting and exceeding system limits, while the latter may lead to an inadequate influence on the system. Figure 4.12 illustrates a scenario with an overly aggressive controller. Such a controller is highly sensitive to small errors, responding significantly to small vibrations in the tugger cable or small changes in the load's motion. This can potentially result in exceeding limits. One specific limit is the lower tension threshold of the cable. When this tension drops below zero, the cable becomes slack, leading to unpredictable behavior and resulting instabilities. As the controller continues to operate, these instabilities typically make the situation worse, as observed in Figure 4.12.

An overly conservative controller inadequately responds to changes in the load's motion. When the load switches from pay-in to pay-out motion, a quick reaction from the controller is essential to prevent excessive tension. A controller lacking sufficient response fails to adjust in time, causing a significant increase in tension. Figure 4.13 demonstrates this phenomenon. As observed, the winch speed re-

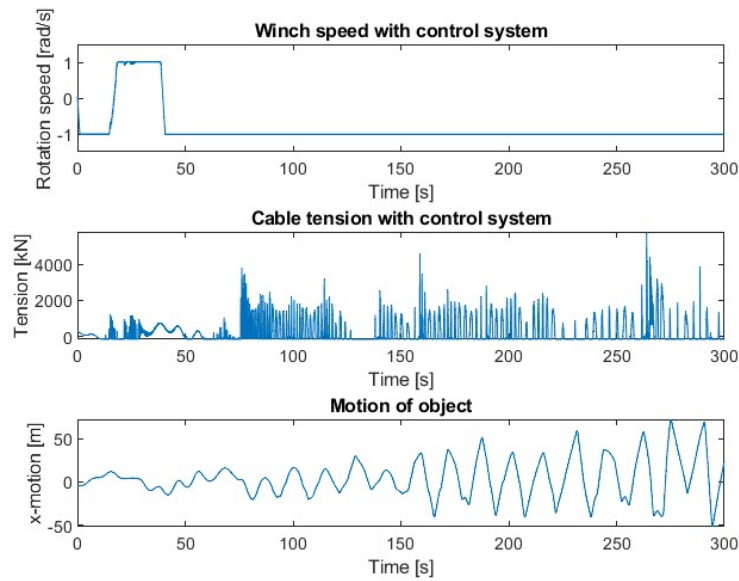


Figure 4.12: Unstable response due to an overly aggressive controller

mains at its minimum or maximum levels during tension peaks. This indicates that the winch rotation cannot follow the load's motion due to a delayed start.

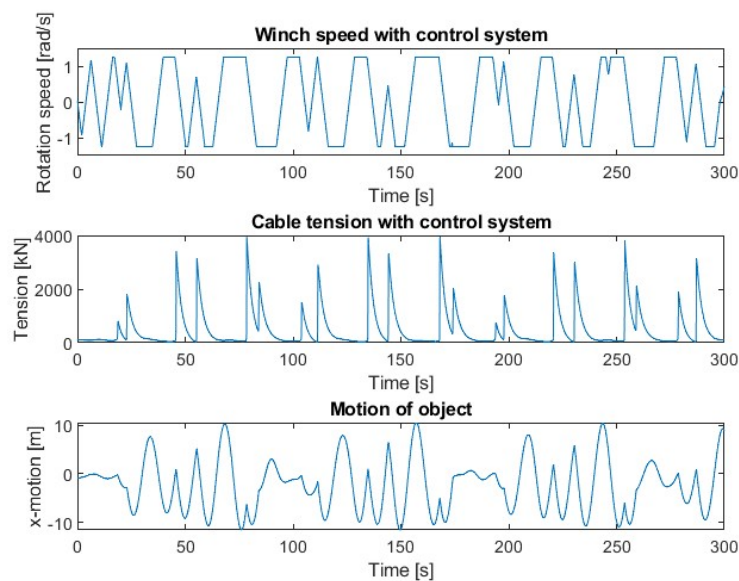


Figure 4.13: Unstable response due to an overly conservative controller

4.6.4. Controller design for constant tension mode

For the constant tension mode, the integral term k_i of the PID controller is set to zero, converting it to a PD controller. This is done because the integral term results in an unstable response for this specific controller. Several cases with a non-zero value for the integral term were executed, all leading to tension falling slack. This instability likely arises from the continuously varying input accumulated by the integral term. Setting both proportional and derivative gains, k_p and k_d , to zero is also examined. When the proportional gain is set to zero, the cable tension converges to the pre-tension value rather than stabilizing around the tension setpoint. Figure 4.14 illustrates the winch movement, cable tension,

and load motion when the controller gains are $k_p = 0$, $k_i = 0$ and $k_d = 5$ with a tension setpoint of $F_s = 130$ kN. Similar outcomes occur with different derivative gains. Setting the derivative gain at zero and retaining only the proportional term results in overshoot, which in turn causes unstable response.

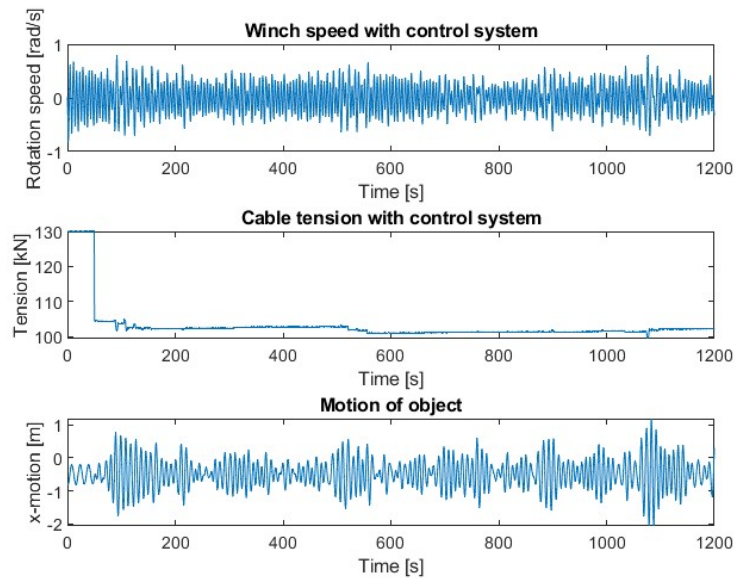


Figure 4.14: Response with control gains of $P=0$, $I=0$ and $D=5$ and a tension setpoint of 130 kN

The PD controller's response is analyzed for multiple proportional and derivative gain combinations. First, an analysis is done with a tension setpoint of $F_s = 100$ kN, corresponding to a tension of 10 mT. The analysis is done with proportional and derivative gains within the range [1 4 7 10 13 16], all with a tension setpoint of 100 kN. The results are presented in Table 4.3. In the observed results, run 10 delivers optimal outcomes. This run uses a proportional value of 4 and a derivative value of 10, resulting in an average tension deviation of 59.8 N. This outcome indicates effective maintenance of constant tension by the controller. High outcomes suggest an unstable response, leading to exagger-

Run	k_p	k_d	Average deviation [N]	Run	k_p	k_d	Average deviation [N]
1	1	1	1644.2	19	1	1	19700.4
2	1	4	63.8	20	10	4	3162.7
3	1	7	81.4	21	10	7	2129.8
4	1	10	104.0	22	10	10	1929.6
5	1	13	128.5	23	10	13	72.6
6	1	16	150.1	24	10	16	285.5
7	4	1	9821.8	25	13	1	55088.1
8	4	4	1922.8	26	13	4	9379.3
9	4	7	118.7	27	13	7	5483.8
10	4	10	59.8	28	13	10	2562.4
11	4	13	60.8	29	13	13	1764.8
12	4	16	65.7	30	13	16	470.9
13	7	1	10039.6	31	16	1	34923.6
14	7	4	5731.0	32	16	4	10344.6
15	7	7	1887.4	33	16	7	3573.8
16	7	10	81.4	34	16	10	3340.3
17	7	13	93.2	35	16	13	2519.2
18	7	16	69.7	36	16	16	1872.7

Table 4.3: Outcomes of analysis 1 for the controller design of constant tension mode

ated tension deviation values. Analysis also reveals that proportional values of [1 4 7] yield much better outcomes compared to [10 13 16]. Consequently, the latter range is disregarded as a viable option for the proportional value.

A second analysis is done, this time for two cases. The setpoints are $F_s = 100$ kN for case 1 and $F_s = 130$ kN for case 2, corresponding to 13 mT of tension. Tested values for the proportional value include [1 4 7], while derivative values comprise [1 4 7 10 13 16]. The resulting data appear in Table 4.4. In the second case with tension at $F_s = 130$ kN, a combination of a proportional value of $k_p = 4$ and derivative value of $k_d = 10$ yields an average outcome. Run 3, combining a proportional value of 1 with a derivative value of $k_p = 7$, produces the optimal result for this case. Given the proper performance of run 3 in both cases, this is a potential proper controller.

Run	k_p	k_d	Average deviation [kN]	
			$F_s = 100$ kN	$F_s = 130$ kN
1	1	1	1644.2	761143.2
2	1	4	63.8	408.1
3	1	7	81.4	164.8
4	1	10	104.0	185.4
5	1	13	128.5	184.4
6	1	16	150.1	209.9
7	4	1	9821.8	89486.8
8	4	4	1922.8	61040.8
9	4	7	118.7	2025.8
10	4	10	59.8	797.6
11	4	13	60.8	595.5
12	4	16	65.7	445.4
13	7	1	10039.6	334293.4
14	7	4	5731.0	1546508.2
15	7	7	1887.4	51588.8
16	7	10	81.4	4324.2
17	7	13	93.2	1601.0
18	7	16	69.7	726.9

Table 4.4: Outcomes of analysis 2 for the controller design of constant tension mode

In the second analysis, a wide range was used. Subsequent refinement focuses on control gains representing the optimal controller identified in this earlier analysis, specifically, the controller from run 3 with $k_p = 1$ and $k_d = 7$. For the third analysis, the range for proportional gain includes [1, 2, 3], and for the derivative gain, [5, 6, 7, 8, 9]. It is worth noting that a proportional gain of $k_p = 0$ results in unstable behavior, and thus is excluded from this analysis. Data from this third analysis appear in Table 4.5. These results indicate that the controller from run 1 has optimized performance at a tension setpoint of $F_s = 100$ kN, while the controller from run 2 is best for a setpoint of $F_s = 130$ kN. The controller from run 2 provides the most effective overall performance for both cases and is therefore selected for further efficiency analysis.

The controller of run 2 undergoes further evaluation. The control gains of this controller are $k_p = 1$, $k_i = 0$ and $k_d = 6$. Figure 4.15 presents the motion of the winch, the tension in the cable, and the motion of the load for case 1, with a tension setpoint of $F_s = 100$ kN. The tension remains close to the setpoint value.

Figure 4.16 illustrates the same controller for case 2, with a tension setpoint of $F_s = 130$ kN. Compared to case 1, tension displays slightly more fluctuation, yet remains close to the setpoint. Next, the controller is also tested in cases with tension setpoints of $F_s = 90$ kN, $F_s = 110$ kN, $F_s = 120$ kN and $F_s = 140$ kN. In each case, the output remains close to the designated setpoint. Based on these observations, it is concluded that the controller meets the requirements. Thus, selection of this controller for subsequent use is confirmed, resulting in a PID controller with gains of $k_p = 1$, $k_i = 0$ and $k_d = 6$.

Run	k_p	k_d	Average deviation [kN]	
			$F_s = 100$ kN	$F_s = 130$ kN
1	1	5	62.1	139.3
2	1	6	96.4	46.3
3	1	7	81.4	164.8
4	1	8	220.6	108.2
5	1	9	469.3	125.8
6	2	5	8404.6	196740.5
7	2	6	3645.6	13758.0
8	2	7	301.9	7189.4
9	2	8	156.5	7513.7
10	2	9	266.2	9142.8
11	3	5	318154.4	31965.4
12	3	6	311945.9	94776.0
13	3	7	369749.1	136100.1
14	3	8	7253.9	69586.7
15	3	9	588.6	55995.7

Table 4.5: Outcomes of analysis 3 for the controller design of constant tension mode

In this section, a notable aspect is that changing the tension setpoint impacts the performance of a controller. As concluded from Table 4.4, different tension setpoints have different optimized settings for the controller. During damping mode, the tension setpoint is constantly changing. Therefore, a controller may need to continuously adapt its settings for optimal performance in damping mode. This is further discussed in Section 4.6.5.

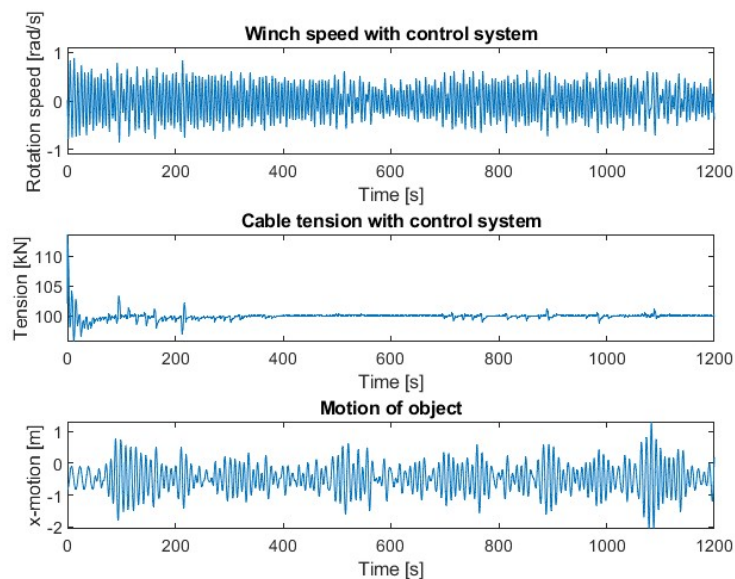


Figure 4.15: Response with PD controller for constant tension mode with gains of $k_p = 1$ and $K_d = 6$ in case 1

Incorporation of this controller into the Simulink model results in a system suitable for analysis of lifting operations using the damping tugger system in constant tension mode. A limitation of this model is the large computational time. Although computational time varies with different model configurations, it often surpasses 15 minutes for simulating an operation with a virtual duration of 1200 s.

Despite the computational duration, the model could be used effectively for examining lifting operations using the damping tugger system in constant tension mode with various tension setpoints. Efficacy of the model gets verified for tension setpoints ranging between $F_s = 90$ kN and $F_s = 140$ kN.

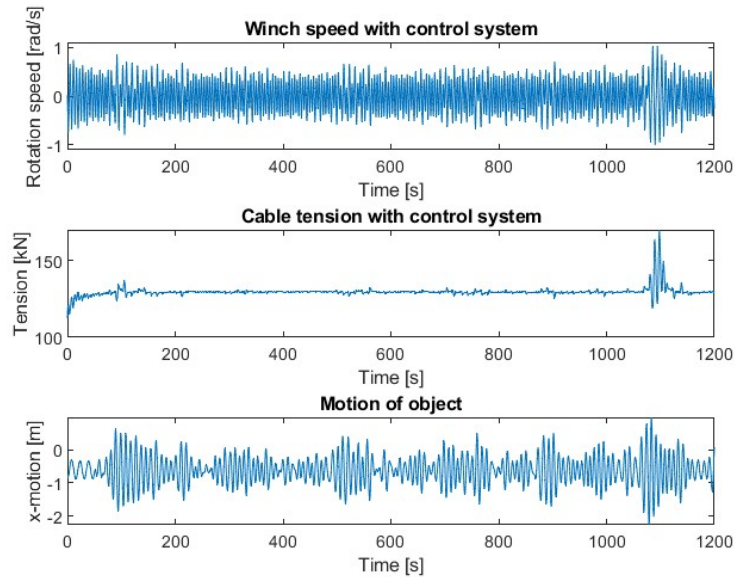


Figure 4.16: Response with PD controller for constant tension mode with gains of $k_p = 1$ and $K_d = 6$ in case 2

4.6.5. Controller design for damping mode

The design of the controller for the damping mode follows the same approach as the design of the controller for the constant tension mode. Notably, the setpoint for the damping mode is different from the setpoint of the constant tension mode. The setpoint of the damping mode has a maximum and minimum tension as input and calculates the desired tension based on this maximum and minimum tension and the measured velocity. This maximum and minimum tension is set to 180 kN and 20 kN, respectively. The comparison of different controller settings is based on the average kinetic energy of the load. The controller implying the lowest average kinetic energy of the load is considered as the most effective one.

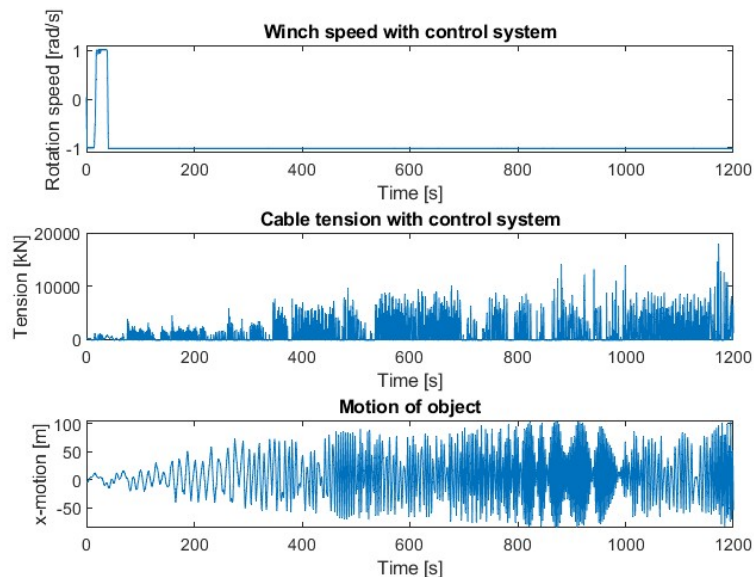


Figure 4.17: Response with PD controller for damping mode with gains of $k_p = 1$, $k_i = 1$ and $K_d = 1$

It is important to highlight that the computational time for executing these models can be large. The computation time varies depending on the settings of the model. In some cases, settings can lead to a computational time exceeding an hour for a simulated time span of 1200 seconds. This results in time-consuming analyses of controller settings.

As elaborated in Section 4.6.4, varying the setpoint for constant tension mode leads to different optimized controller configurations. This is particularly noteworthy because, in damping mode, the tension setpoint is not static but continuously changes. This suggests that an optimal controller for damping mode may need to be adaptive. However, it is chosen to keep a simple PID controller and not explore the effects of an adaptive controller.

First, A PID controller with gains $k_p = 1$, $k_i = 1$ and $k_d = 1$ is tested. Figure 4.17 displays the system response. This response is unstable, similar to controllers in constant tension mode with a non-zero integral term. Additional experiments with non-zero integral gain also yield unstable behavior, leading to the conclusion that a PD controller should also be used for the damping mode.

Now, the PD controller that is designed for the constant tension mode is applied to the damping mode. Figure 4.18 illustrates the controller's performance. The frequency of the winch is much higher compared to the frequency of the load. Such difference occur due to the control system reacting to small vibrations in the tensioned cable. This reactivity prevents the system from stabilizing around the setpoint of $x_s = 0$. Observations indicate that the mass oscillates around $x_o = 2.5$ m at $t = 600$. The winch consistently operates at its maximum and minimum velocities throughout the cycle, indicating system operation at the winch's performance limits.

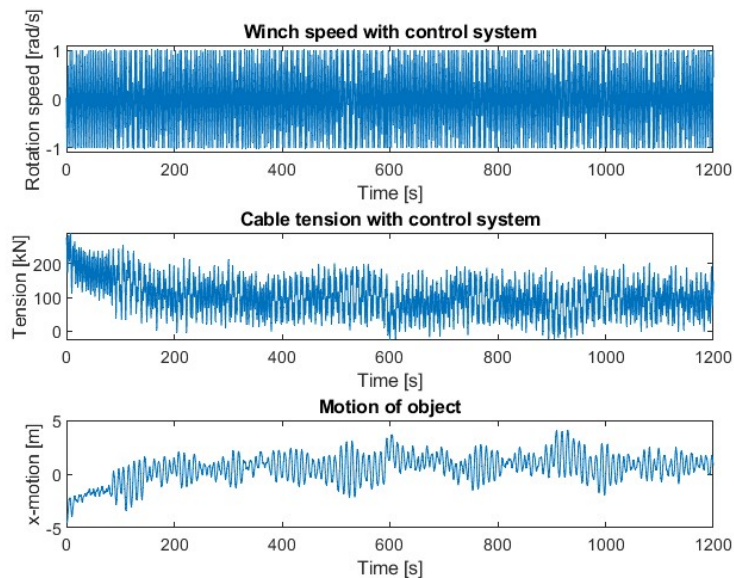


Figure 4.18: Response with PD controller for damping mode with gains of $k_p = 1$ and $K_d = 6$

To explore further the performance of the PD controller in maintaining constant tension, multiple PD controllers are tested. Controllers with settings for proportional and derivative gains within the range of [1, 4, 7, 10] are tested. The results are either closely those of Figure 4.18 or yield unstable outcomes. From this, the hypothesis is derived that a controller in the order of these gains has no major impact on the motion of the load. Therefore, higher gains are tested. The range of proportional and derivative gains tested are [1 10 100], except for the controller with gains $k_p = 1$ and $k_d = 1$ since these settings are already examined.

The results for these controller settings are presented in Table 4.6. The optimal controller appears to be from run 5, characterized by gains $k_p = 10$ and $k_d = 100$, which yielded an average kinetic energy of 2920.4 J. This controller is the only controller that provided stable, unlike other controllers that all produce unstable outcomes. A detailed analysis of run 5, illustrated in Figure 4.19, reveals that its response closely aligns with that in Figure 4.18. Similar to previously designed controllers, this controller also has no significant impact on motion.

Run	k_p	k_d	Average kinetic energy [J]
1	1	10	55187.5
2	1	100	54634.6
3	10	1	117283.1
4	10	10	56834.4
5	10	100	2920.4
6	100	1	78094.0
7	100	10	210076.3
8	100	100	56773.5

Table 4.6: Outcomes of analysis 1 the controller design of damping mode

Up to this point, an effective controller for the damping mode has not been created. Numerous gain combinations were evaluated, ranging from high gains in the order of 1,000 and 10,000 to low gains in the range of 0.1 to 0.001. Additionally, variations in the maximum and minimum tension did not enhance controller performance. Eliminating the winch limitations slightly improved the outcomes; a controller with gains $k_p = 10$ and $k_d = 100$ leads to an average kinetic energy of 1176.9 J. However, this was achieved at the expense of heavily exceeding winch acceleration and velocity limits. In summary, no suitable controller has been identified for the damping mode in this Simulink model.

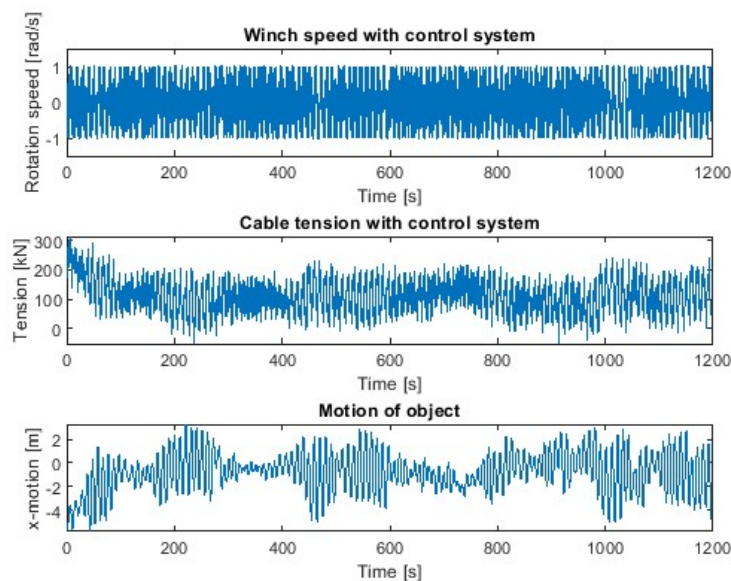


Figure 4.19: Response with PD controller for damping mode with gains of $k_p = 10$ and $K_d = 100$

Several factors could contribute to the difficulty of identifying an appropriate controller for the system. First, it may be that a PID controller is not the optimal choice for this objective. As concluded in Section 4.6.4, varying setpoints result in different optimized controller settings for constant tension modes. While PID controllers are suitable to many control systems, they may not be for this particular application. As mentioned earlier in this section, an adaptive controller might yield better performance, but this is not further investigated.

Even if a PID controller is considered appropriate, multiple factors could compromise its performance. Firstly, the truncation of the controller's output, implemented to model winch limits, may result in an unstable response. Essentially, the controller may overcompensate for this truncated output. Another issue could arise if the controller reacts to small vibrations in the system, such as the axial vibrations of the inclined mass of the tugger cable. While this mass does not exist in this form in reality, its modeled presence could induce axial vibrations. Additionally, due to the complexity of the model various simplifications are done, such as the elimination of the effect of the load on the motion of the winch. These factors, among others, could adversely affect the controller design process.

Nevertheless, a suitable controller for the damping mode is not found after several approaches. Given the extensive time required for controller testing and the unsuccessful attempts, a decision has been made to explore an alternative approach, as described in Chapter 5. While creating the detailed model, various new perspectives emerged which will be used in the alternative approach. Among these perspectives are potential simplifications that could be applied to the system without adversely impacting the results. These potential simplifications are described Section 5.3.1.

4.7. Conclusion

A representation of the physics of a lifting operation with the use of a motion control system is created in this chapter, referred to as the lifting system. Initially, the lifting system is split into a free lifting system and the damping tugger system. The EOMs for these systems are derived by means of the Lagrangian method. The knowledge obtained from these derivations is used for the derivation of the EOMs for the controlled lifting system. Thereafter, three MATLAB models are created, each corresponding to a derived set of EOMs. The numerical solver ODE45 serves for solving the EOMs in these MATLAB models. Verification across multiple cases confirms the reliability of all three MATLAB models, enabling their usage for gaining more understanding of the physics of a lifting operation and of the damping tugger system.

The MATLAB model for the controlled lifting operation serves as the foundation for the Simulink model. This Simulink model aims to gain more understanding of the system's controller component. Both the constant tension mode and the damping mode are incorporated into the Simulink model, resulting in a model suitable for examining both modes.

The objective of the controller design is not to design an optimized controller but to develop one that performs effectively during system analysis. The controller that is designed for the constant tension mode is a controller of PID form with the proportional, integral and derivative settings being $k_p = 1$, $k_i = 0$ and $k_d = 6$, respectively. Since the integral gain is zero, the controller is, in fact, a PD controller. Implementation of this controller into the Simulink model leads to a model that is suitable for running simulations of the damping tugger system in constant tension mode during a lifting operation, for various setpoints within the range of $F_s = 90$ kN to $F_s = 140$ kN. Despite the often large running time, the model serves as an effective tool for examining the damping tugger system in constant tension mode.

For the damping mode, no effective controller was designed. Several controller settings with proportional and derivative gains ranging from the order of 0.011 to 10,000 were tried, but did not lead to a suitable controller. Furthermore, different minimum and maximum tension setpoint were tried as well as eliminating the winch limitations, but this did not lead to a suitable controller. Several possible causes of the difficulties with the control design are discussed. First, it could be that a PID controller could not be the right controller for this objective because of the varying setpoint during damping mode. An adaptive controller could be more suitable but this is not further investigated. Other causes could be the truncation of the controller output as result of modeling the winch limitations, possible small vibrations or modeling simplifications that affect the controllers response.

Given the extensive time required for controller testing and the unsuccessful attempts, a decision has been made to develop a new, simplified model for further research. This simplified model is called the analysis model and is elaborated upon in Chapter 5. Multiple new insights derived from the creation of the detailed model are use for the analysis model.

5

Analysis model

In this section, a simplified version of the model from Chapter 4 is developed, called the analysis model. While this model shares the primary objective with the detailed model, it also aims to mitigate the issues encountered during the development of the detailed model. This chapter starts with the model development objective and the explanation of various simplifications, model decisions and standard parameters. Subsequently, two systems are introduced, and their EOMs are derived. Numerical MATLAB models are then created, and the results are evaluated with verification cases. These numerical models are, thereafter, converted into Simulink models, where both the maximum force setpoint and the motion control setpoint are implemented. Following this, the winch controller is developed and implemented, resulting in a model ready for analyzing the impacts of various controller setpoints and inputs of Section 3.3. Finally, a simpler control method is introduced as a third control option.

5.1. Objective of the model

Consistent with the objective of the detailed model presented in Section 4, the aim of the development of the analysis model is to facilitate the analysis of the effects of the different controller setpoints and inputs, which are outlined in Section 3.3. Similar to the detailed model, this simplified version is designed to simulate the motion of the load influenced by vessel motion and controlled by the motion control system. Given that the excessive computation time of the detailed model was a main problem within Chapter 4, this analysis model aims to reduce computational time by implementing several simplifications.

5.2. Method

The method used for developing the analysis model is outlined in this section. This approach is partly equal to the method used for the detailed model, as described in Section 4.2, while also introducing some new methodology elements.

5.2.1. Simplified lifting system

The system developed in this chapter is called the simplified lifting system. It is derived from several simplifications applied to the detailed model, which is discussed in Chapter 4. These simplifications are outlined in Section 5.3.1. Prior to developing the simplified lifting system, an intermediate system, called the force system, is constructed. This model consists solely of the crane, the load, and the damping force acting upon the load, leaving out the tugger cable and winch. The force system is used for two primary functions: to assess the required damping force in the load i.e., determining the force in the tugger cable needed to damp the load's motion and to act as a preliminary step in creating the complete Simplified lifting system.

The EOMs for both systems are derived using the same approach used for the derivation within the detailed model, which is described in Section 4.2.2. Specifically, the Lagrangian method is used for these derivations. Additionally, the Rayleigh Dissipation Function is used to account for any elements of the system that dissipate energy.

5.2.2. Numerical model

After deriving the EOMs, two numerical MATLAB models are created, each corresponding to a specific set of EOMs. Similar to the detailed model, the ODE45 numerical solver is used to solve these EOMs, yielding a dynamic response that specifies the DOFs and their corresponding first time-derivatives. The numerical models are subsequently verified using specific verification cases.

5.2.3. Controller design

The design phase for the controller of the analysis model differs from that of the detailed model. Initially, Simulink models for both the force system and the lifting system are constructed. The conversion from the MATLAB script to the Simulink environment follows the same approach used for the detailed model, using the Simulink ODE solver as described in appendix A.3. Thereafter, two setpoints, maximum force setpoint and the motion control setpoint, are integrated into the Simulink model of the force system. For the motion control setpoint, the control parameters are determined within the Simulink model. After implementation of these setpoints, the resulting damping forces acting in the load is examined. A positive outcome of this examination leads to a feasible setpoint for the winch controller. Following this, the winch controller is developed within the Simulink model for the lifting system. It is designed based in the maximum force setpoint. Once a suitable winch controller has been developed for this setpoint, its suitability for the motion control setpoint are assessed. Thereafter, a simpler control method is designed. In this method, the winch controller and setpoint calculation are integrated into a single controller. This controller controls the winch using the motion of the load as input, eliminating the need for a feedback loop for the motion of the winch.

Lastly, the constant tension mode is implemented to the system and the results of this mode are compared to the results of the detailed model. Subsequently, the designed setpoints and controllers are incorporated into the Simulink model, resulting in a complete model of the lifting system. This model serves as a basis for the analysis of the two controller setpoints and inputs, which are outlined in Section 3.3. The results of this analysis are presented in Chapter 6.

5.3. Modeling decisions

This section provides details in the design choices made for the construction of the simplified lifting system. The system is developed after implementing several simplifications to the detailed lifting system. This section outlines these simplifications, as well as the vessel motion and standard parameters.

5.3.1. Simplifications

Five key simplifications distinguish the simplified lifting system from the detailed system. Firstly, in the detailed model, the tugger cable is represented as two dissipation springs with a point mass positioned between them. The longitudinal and transversal frequencies of this point mass are significantly higher than the frequencies of the winch and load motion, and thus, they do not interfere with these components. Consequently, the point mass can be eliminated, and the tugger cable can be simplified as a single dissipating spring.

Secondly, the crane cable exhibits a large stiffness due to its strength. This large stiffness results in a natural frequency for this cable that far exceeds the frequencies of vessel motion, winch motion, and even the natural frequency of the tugger cable. Hence, the spring representing the crane cable does not disrupt the dynamics of the overall system. Consequently, the crane cable is represented as a rigid bar.

The elimination of the point mass in the tugger cable and the modeling of the crane cable as a rigid bar can substantially reduce the computational time required for the model, since these elements are sensitive for high-frequency vibrations with small amplitude. This high-frequency vibrations drastically increase computation time.

The third simplification pertains to the winch. Unlike the detailed model, where the winch is treated as a rotational mass, the analysis model represents it as a translational mass. However, the rotational motion of the winch is translated into translational motion for the tugger cable. Consequently, the ro-

tational motion of the winch results in a translational motion of the tugger cable in the analysis model. Thus, the winch is portrayed as a mass capable of solely translational motion in the analysis model. Mathematical details regarding the relationship between a rotating mass and a translating mass are elaborated in Appendix B.1.

Furthermore, the input motion is simplified. In the detailed model, the vessel motion consists of surge, heave, and pitch rotation of the vessel, which are converted into x- and y-motions of the crane tip. However, the primary motion of the crane tip is along the x-axis, and the y-motion has a negligible impact on system dynamics. Consequently, the analysis model exclusively considers the x-motion of the tip. This simplification is achieved by eliminating the vessel and crane in the analysis model, restricting the motion of the crane tip to a single horizontal direction.

Lastly, the purpose of the model is to analyze the impact of various controller aspects. The controller responds to the load's motion. In the detailed model, the winch's position is influenced by the vessel's motion. So both the winch and the load are affected by the vessel motions. However, the objective is to analyze the system's response when the load's motion differs from that of the winch. If the winch remains stationary, the load will experience motion due to the input motion at the crane tip. Consequently, the location of the winch is considered stationary and unaffected by the vessel's motion to isolate the analysis of load and winch motion responses.

These five simplifications result in a new version of the model, called the simplified lifting system, which is discussed in greater detail in Section 5.4. It should be noted that the non-linearity of the springs, described in Section 4.3.4, is not applicable to this chapter. This is because it is manually ensured that the springs are always in tension.

5.3.2. Vessel motions

As outlined in Section 5.3.1, the motion of the suspension is reduced to a single direction. Figure 5.1 depicts the horizontal motion of the suspension over time, induced by vessel motions. Similar to the vessel motion in the detailed model discussed in Section 4.3.6, there is no motion during the initial 50 seconds to examine the system's static steady-state behaviour. Unlike the detailed model, this trajectory spans 1500 seconds, with the final 250 seconds also being motionless. This extension aims to demonstrate the behaviour of the system as the motion eventually dampens out.

5.3.3. Standard parameters

The simplified lifting system comprises five parameters that maintain constant values throughout each run of the model. These parameters are presented in Table 5.1. These constant values will be applied up to and including the control design phase. After the control design phase, multiple scenarios will be executed in which two specific parameters, the mass of the load m_o and the mass of the winch m_w , will be varied within certain ranges.

Element	Parameter	Symbol	Value	Unit
General	Gravity constant	g	9.81	m/s ²
Crane cable	Length	l	50	m
Load	Mass	m_o	1,000	mT
Tugger cable	Stiffness	k_c	1	MN/m
Tugger cable	Max. allowed force	F_{max}	-50	kN
Tugger cable	Min. allowed force	F_{min}	-250	kN
Winch	Mass	m_w	5	mT

Table 5.1: Standard parameters of the simplified lifting system

5.4. Equations of motion

In this section, the EOMs for both the simplified force system and the simplified lifting system are derived. The method employed for this derivation is equal to the one used for the derivation of the EOMs for the detailed lifting system. The latter derivation is outlined in Section 4.4.

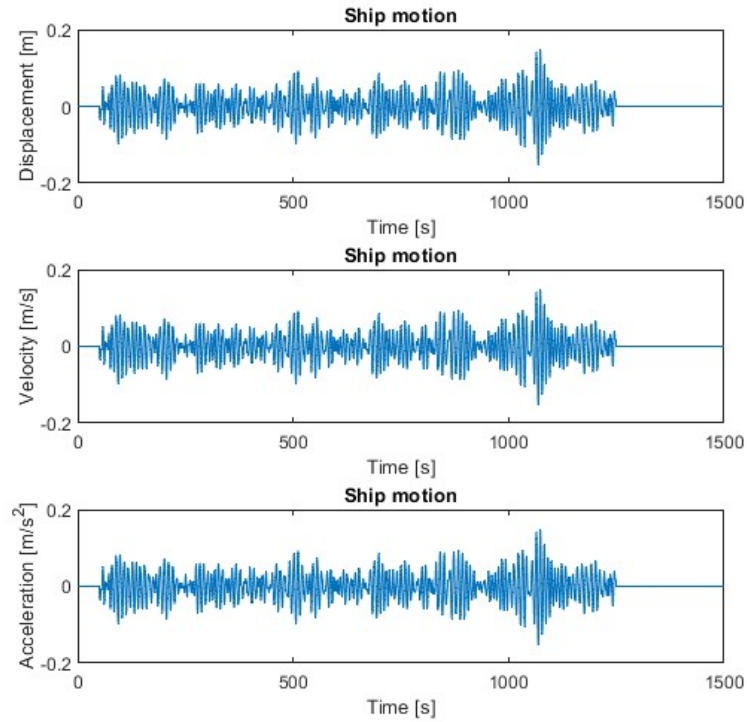


Figure 5.1: The x-displacement of suspension

5.4.1. Simplified force system

The simplified force system consists of the pendulum system with a moving suspension. The system is depicted in Figure 5.2. This system is a 1DOF system with $\theta(t)$ as the DOF, representing the time-dependent angle of the suspended crane cable. Notably, the x-motion of the suspension x_t is prescribed, so this is not a DOF. Being a 1DOF system, it yields only one EOM.

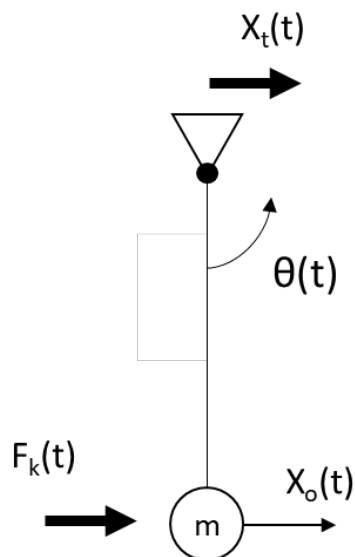


Figure 5.2: The simplified force system

The time-dependent horizontal displacement of the crane tip is denoted by x_t and is referenced to the global coordinate system with axes X and Y . In this context, the time-dependent coordinates of the load are defined as follows:

$$x_o = x_t(t) + \theta(t)l \quad (5.1)$$

$$y_o = l - l \left(1 - \frac{\theta(t)^2}{2} \right) = \frac{l\theta(t)^2}{2} \quad (5.2)$$

Here, x_t is the time-dependent coordinate of the moving suspension, and l represents the length of the crane cable. The angles are simplified using the small angle theory, which is justified by the fact that the crane cable angle will always remain small during a lifting operation. In the event that the crane cable angle exceeds the threshold for the small angle theory, it indicates an unsafe condition, and such an operation will not be undertaken. Next, the kinetic and potential energy equations are derived:

$$T = \frac{1}{2}m (\dot{x}_o^2 + \dot{y}_o^2) \quad (5.3)$$

$$U = mg (y_o - y_{o-in}) \quad (5.4)$$

where m is the weight of the load, and y_{o-in} denotes the y_o coordinate of the load when the system is in initial position, i.e., the y_o coordinate when $\theta = 0$ and $x_t = 0$, which leads to $y_{o-in} = 0$. These energy equations lead to the Lagrangian:

$$L = T - U \quad (5.5)$$

No damping element, such as a cable with damping properties, is present in this system, so the Euler-Lagrange equation does not imply Rayleigh's law. The Euler-Lagrange equation, without Rayleigh's law, for this system is:

$$\frac{d}{dt} \frac{\partial L}{\partial \dot{\theta}} - \frac{\partial L}{\partial \theta} = F_k(t)l \quad (5.6)$$

where F_k is the time-dependent horizontal force acting in the load, intended to dampen its motion. The damping force F_k is multiplied by the length because the DOF θ represents an angle, and thus, the damping force acts as a damping moment. Rewriting this equation and isolating the acceleration term leads to the following EOM:

$$\ddot{\theta} = \frac{-\theta(t)gm - \ddot{x}_t m + F_k(t)}{lm} \quad (5.7)$$

This is the EOM for the simplified force system. Section 5.5 describes the implementation of this EOM into a numerical model.

5.4.2. Simplified lifting system

The simplified lifting system, illustrated in Figure 5.3, is an extension of the simplified force system of Section 5.4.1. This extension includes the addition of a winch and a tugger cable, represented as a point mass, capable of translational motion, and a non-linear spring, as Section 5.3 describes.

Due to the presence of the winch, this system becomes a 2DOF-system. Therefore, two EOMs will be derived for the DOFs $\theta(t)$ and $x_w(t)$, representing the rotation of the crane cable and the translation of the winch, respectively. The coordinates of the load x_o and y_o remain identical to those in the simplified force system, indicated in equations 5.1 and 5.1.

Again, the small angle theory is applied. The presence of the winch and the tugger cable affects the kinetic and potential energy equations. The equations defining the kinetic and potential energy in this system are:

$$T = \frac{1}{2}m (\dot{x}_o^2 + \dot{y}_o^2) + \frac{1}{2}m_w (\dot{x}_w^2) \quad (5.8)$$

$$U = mg (y_o - y_{o-in}) + \frac{1}{2}k (x_w(t) - x_o(t))^2 \quad (5.9)$$

where m is the weight of the load, m_w is the weight of the winch, k is the stiffness of the spring and again, y_{o-in} denotes the y_o coordinate of the load in a initial position which is also in this case $y_{o-in} = 0$. These energy equations lead to the Lagrangian:

$$L = T - U \quad (5.10)$$

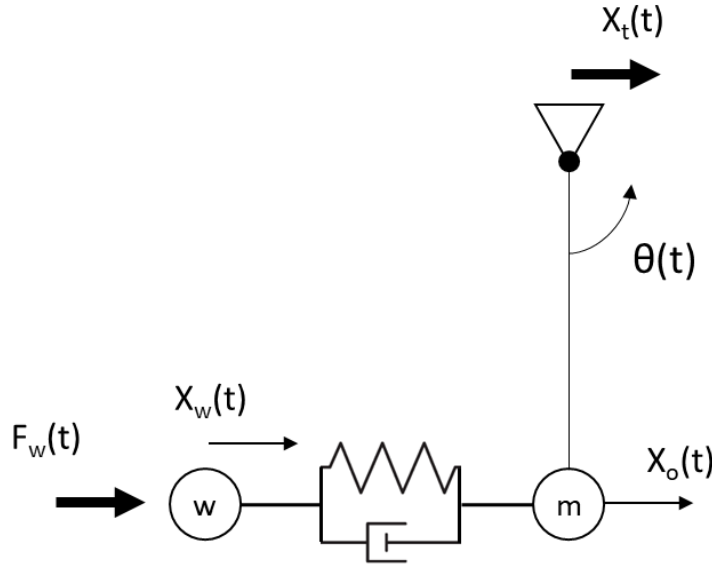


Figure 5.3: The simplified lifting system

Thereafter, the Rayleigh dissipating function, elaborated on in Section 4.2.2, is derived as:

$$R = \frac{1}{2}c(\dot{x}_w - \dot{x}_o)^2 \quad (5.11)$$

The Euler-Lagrange equation, including the term for the Rayleigh dissipation functions are:

$$\frac{d}{dt} \frac{\partial L}{\partial \dot{\theta}} - \frac{\partial L}{\partial \theta} + \frac{\partial R}{\partial \dot{\theta}} = 0 \quad (5.12)$$

$$\frac{d}{dt} \frac{\partial L}{\partial \dot{x}_w} - \frac{\partial L}{\partial x_w} + \frac{\partial R}{\partial \dot{x}_w} = F_w(t) \quad (5.13)$$

where F_w is the time-dependent horizontal force acting in the winch. Solving this equation and isolating the acceleration terms, leads to the following EOMs:

$$\ddot{\theta} = \frac{-mg\theta(t) - m\ddot{x}_t - k(x_t(t) + \theta(t)l - x_w(t)) - c(\dot{x}_t + \dot{\theta}l - \dot{x}_w)}{ml} \quad (5.14)$$

$$\ddot{x}_w = \frac{F_w(t) + k(x_t(t) + \theta(t)l - x_w(t)) + c(\dot{x}_t + \dot{\theta}l - \dot{x}_w)}{m_w} \quad (5.15)$$

These are the EOMs for the simplified lifting system, which will be incorporated in a numerical model, elaborated on in Section 5.5.

5.4.3. The static steady-state

The static steady-state equations for the simplified force and lifting systems are derived using the approach as outlined in Section 4.4.4. This results in the static steady-state equation for the simplified force system as follows:

$$\theta = \frac{F_k(t)}{gm} \quad (5.16)$$

Similarly, for the simplified lifting system, the static steady-state equations are:

$$\theta = \frac{k \cdot (x_w - x_t)}{mg + kl} \quad (5.17)$$

$$x_w = \frac{F_w(t)}{k} + x_t + \theta l \quad (5.18)$$

These equations are employed to calculate the static steady-state values of the DOFs, which then serve as the initial conditions for the ODE solver.

5.5. Numerical model

The EOMs derived in Section 5.4 are the foundation for the created numerical MATLAB models. These models are described in this section along with the purpose of the models.

5.5.1. MATLAB model

Two numerical MATLAB models have been developed corresponding to the two sets of EOMs derived in Section 5.4. These numerical models are created in consistent manner with the MATLAB models for the detailed model, as explained in Section 4.5.1. Thus, the ODE45 numerical solver is used for solving the EOMs and initial conditions are ascertained through static steady-state equations. The validity of the outcomes of these models is assessed through verification cases, which are provided in appendix B.4.

5.5.2. Purposes of the numerical models

The numerical model corresponding to the simplified force system could be used to investigate the required force in the load to damp its motion. This increases understanding of the optimal tension for the tugger cable during a lifting operation. Moreover, this model is the basis for the Simulink model used for controller design.

The second numerical model is designed to explore the influence of the winch and tugger cable in the load's motion. This leads to a better understanding of damped lifting operations. Additionally, this model could be used for an analysis of the relation between the load's motion, the winch's motion and the tension in the tugger cable. Similar to the first model, this numerical model also serves as the basis for a Simulink model for controller design.

5.6. Controller design

This section outlines the design phase for the controllers and setpoints. Initially, the numerical MATLAB models described in Section 5.5 will be transformed into Simulink models. Subsequently, parameters for the maximum force setpoint and the motion control setpoint will be established. Following this, the winch controller is designed. Thereafter, both the setpoint and controller are integrated into the created Simulink model for the lifting system, resulting in a complete model of the lifting operation. Lastly, the constant tension mode is implemented to the system and the results of this mode are compared to the results of the detailed model.

5.6.1. Simulink model

Two Simulink models were created during the controller design phase: one for designing the controller for the maximum force setpoint and another for the controller for the motion control setpoint. Both models can be integrated with the two sets of EOMs. In the design approach for both controllers, the EOM for the force system is initially applied to determine the required force in the load. Subsequently, the EOMs for the lifting system are used to design the controllers for the entire system.

5.6.2. The maximum force setpoint

First, the maximum force setpoint is integrated into the Simulink model of the simplified force system. Figure 5.4 illustrates the control loop for this configuration, where $F_s k$ represents the setpoint for the force in the load. This setup has no PID controller because the force setpoint is calculated based in the measured velocity, denoted as \dot{x}_{sen} . The calculated force is directly applied to the load. Additionally, a velocity deadband is implemented to mitigate fluctuations around zero with small amplitudes. This deadband is active within the velocity range of $\dot{x}_{sen} = 0.05$ m/s to $\dot{x}_{sen} = -0.05$ m/s and significantly reduces computational time. Further details on this deadband are provided in Appendix B.2.

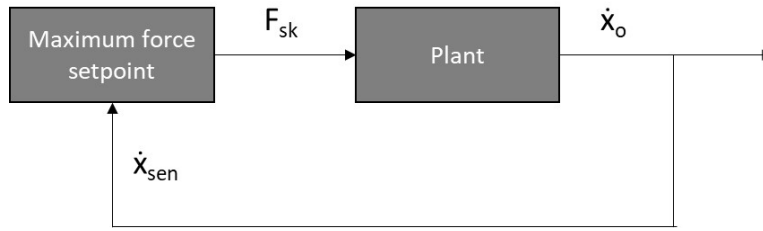


Figure 5.4: The control loop of the simplified force system with maximum force setpoint

The implementation of the deadband into the maximum force setpoint determined by equation 3.1 leads to an updated mathematical expression for the maximum force setpoint:

$$F_s = \begin{cases} F_{max} & \dot{x}_{sen} \geq \dot{x}_{lim-upper} \\ \zeta \cdot \dot{x}_{sen} + F_{pre} & \dot{x}_{db-lower} < \dot{x}_{sen} < \dot{x}_{lim-upper} \\ 0 & \dot{x}_{db-lower} \geq \dot{x}_{sen} \leq \dot{x}_{lim-upper} \\ \zeta \cdot \dot{x}_{sen} + F_{pre} & \dot{x}_{lim-lower} < \dot{x}_{sen} < \dot{x}_{db-upper} \\ F_{min} & \dot{x}_{sen} \leq \dot{x}_{lim-lower} \end{cases} \quad (5.19)$$

Here, F_s denotes the force setpoint within the cable system, while F_{max} and F_{min} represent the established upper and lower force limits, respectively. The force setpoint attains these specified limits when the measured velocity of the load x_{sen} exceeds the limit velocity x_{lim} in either a positive or negative direction. The damping ratio is represented by ζ and the upper and lower value of the deadband is denoted as $\dot{x}_{db-upper}$ and $\dot{x}_{db-lower}$. When the measured velocity of the load is within the deadband limits $\dot{x}_{db-upper}$ and $\dot{x}_{db-lower}$, the force setpoint is 0. Additionally, F_{pre} denotes the pre-tension, and ζ symbolizes the damping ratio. Figure 5.5 includes a visualisation of this maximum force setpoint.

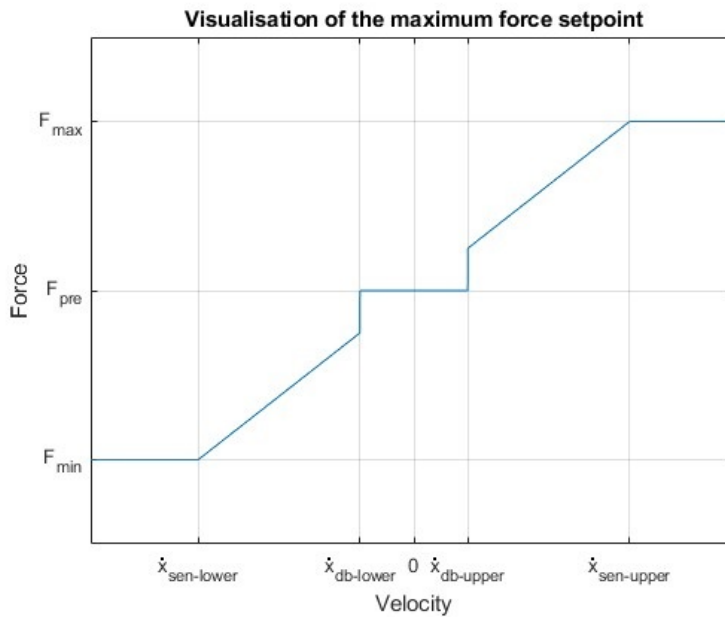


Figure 5.5: Visualisation of the maximum force setpoint including deadband

Within this thesis, the damping ratio ζ is set to 1,000 kNs/m. The force limits are $F_{max} = -50$ kN and $F_{min} = -250$. Given that the measured velocity is approximately 0.1 m/s, this particular damping ratio results in a force magnitude in the order of 100 kN. The force acting in the load influences the load's motion, leading to a reduction. This is observed when comparing Figure 5.6a and Figure 5.6b, which show the response of the load without the application of any damping force and with the application of the design maximum force setpoint, respectively. The force applied to the load over time is illustrated

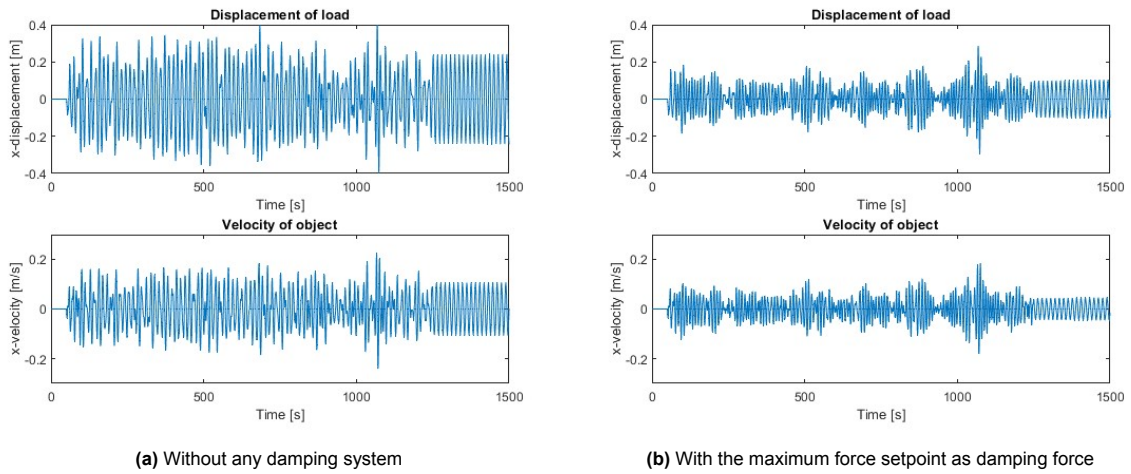


Figure 5.6: Comparison of the motion of the load

in Figure 5.7. The force remains within the boundaries of $F_{max} = -50$ kN and $F_{min} = -250$. A visualisation of the same force, within the time interval [50, 150] seconds, is presented in Figure 5.8. In this figure, the impact of the deadband, linear setpoint calculation, and truncation at the force limits can be observed. The deadband ensures that the force immediately drops to zero when the velocity falls within the deadband values, corresponding to force values $F = -100$ kN and $F = -200$ kN.

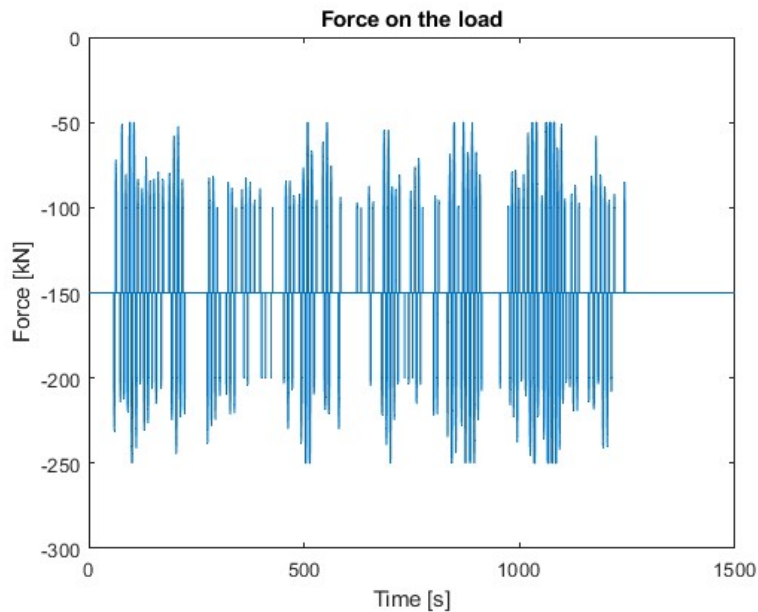


Figure 5.7: The damping force acting to the load

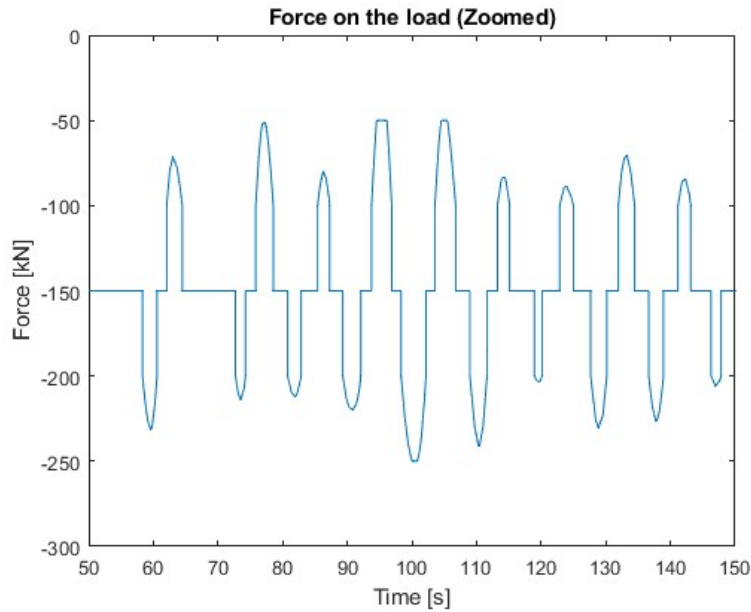


Figure 5.8: The damping force acting to the load over a time frame of [50 150] s

5.6.3. The motion control setpoint

Now, the motion control setpoint is intergrated into the force system. The motion control setpoint is a setpoint calculation method is the form of a standard PD controller, which is described in equation 3.2. The parameters for this setpoint will be determined in this section. To do so, the motion control setpoint is implemented into the force system, leading to the control loop of Figure 5.9.

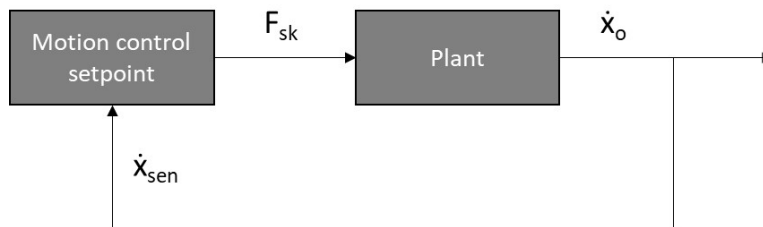


Figure 5.9: The control loop of the simplified force system with motion control setpoint

The input for the controller is the error of the velocity of the load e_o . This error is defined as:

$$e_o = \dot{x}_{so} - \dot{x}_{sen} \quad (5.20)$$

where e_o is the error of the load velocity, \dot{x}_{so} denotes the setpoint for the velocity of the load and \dot{x}_{sen} represents the measured velocity of the load. The measured error is continuously changing due to the changing disturbance. An integral term would sum this continuously changing error, what would lead to unstable response of the controller. Therefore a PD-controller form is most appropriate for the purpose of a motion control setpoint. This is essentially a PID-controller with an integral controller gain set to zero. The mathematical expression for a PD-controller is as follows:

$$F_{sk} = \bar{k}_p \cdot e_o + \bar{k}_d \cdot \dot{e}_o \quad (5.21)$$

Here, \bar{k}_p and \bar{k}_d represent the proportional, integral and derivative gains of the PID-controller, respectively. Notably, the difference of equation 5.21 and equation 3.2, which describes the mathematical expression of a PID-controller, is the integral term.

The objective is to design a setpoint that ensures the force in the cable effectively reducing the motion of the load without exceeding maximum and minimum force limits in the cable, $F_{max} = -50$ kN and $F_{min} = -250$ kN. Since truncation of the output of the controller should be avoided as much as possible, the controller must be tuned in such a way that the setpoint will not exceed the limits of the force in the cable. Therefore, first, the maximum gains for the controller are determined. This maximum is set to 450,000, as appendix B.3 describes.

These earlier described limits for the proportional and derivative terms are used to verify if the controller parameters come close to the limits. It is important to consider that both the proportional and derivative terms in the control equation add up, leading to a lower actual limit, as shown in equation 3.2. If the control parameters approach the limit, an additional check is performed in the setpoint for the force in the cable, F_{sk} , to ensure it does not exceed the cable force limit. Conversely, if the control parameters are far from the limit, it is assumed that the controller will be sufficient.

The design of the controller is accomplished via a case. In this case the load initiates with a displacement of 0.50 m, and there is no wave excitation present. The objective is to dampen the load's displacement to 0.01 m after 15 seconds. The controller is deemed successful if it achieves this goal.

Following a trial and error process, the control parameters are found to be $\bar{k}_p = 95,000$ and $\bar{k}_d = 70,000$. Figure 5.10 depicts a zoomed-in view around 15 seconds of the response to the specified case. As demonstrated, the displacement of the load is less than 0.01 m at 15 seconds, confirming that these controller parameters are satisfactory. It is assumed that this is not a problem. Since the controller satisfies the objective and the gains do not approach the limits of 450,000, it is selected for testing it as the motion control setpoint.

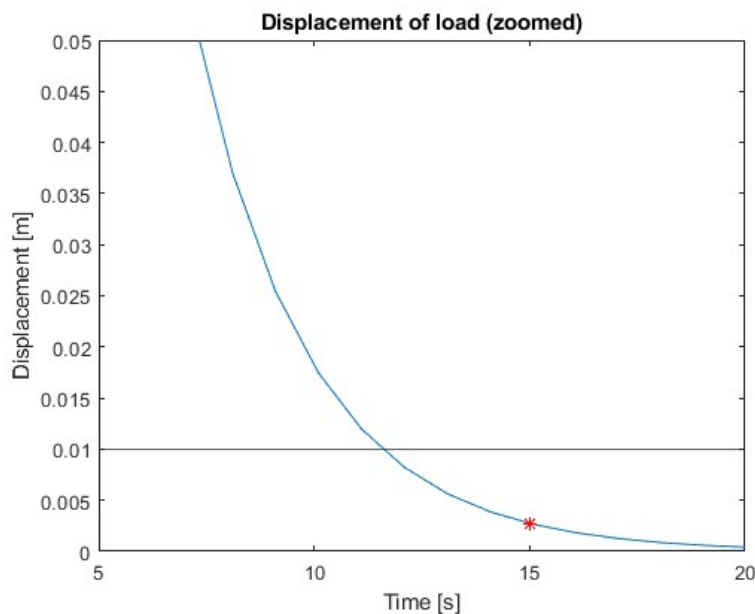


Figure 5.10: The displacement of the load with the chosen control parameters

The selected controller parameters are incorporated into the force system for testing it as the motion control setpoint. This is done by testing the load's response to vessel motion. The force acting in the load, induced by the motion control setpoint is shown in Figure 5.11 and the resulting motion of the load is shown in Figure 5.12b. Figure 5.12a shows the motion of the load with only the pre-tension and damping force applied, which was also shown in Figure 5.6a. When comparing Figure 5.12a to Figure 5.12b, a significant reduction of the load is observed.

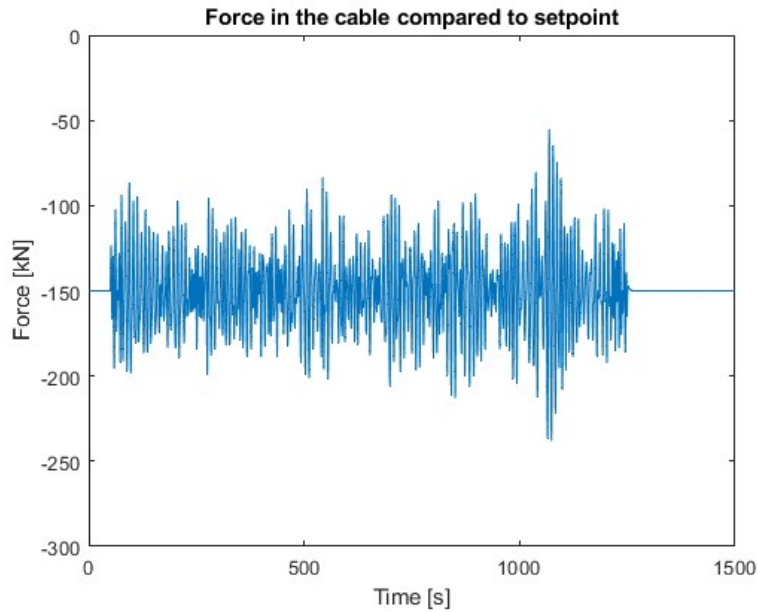


Figure 5.11: The damping force action to the load

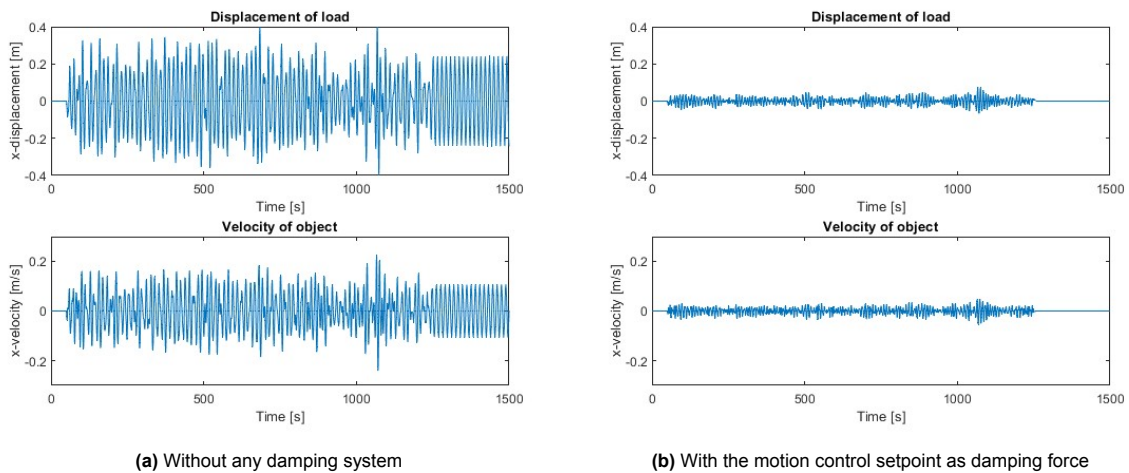


Figure 5.12: Comparison of the motion of the load

5.6.4. The winch controller

Next, the Simulink model is extended to the lifting system, so the winch and tigger cable are now included. A PID controller is also integrated, which controls the motion of the winch. The winch controller is designed upon the maximum force setpoint. After a winch controller is designed that works properly for the maximum force setpoint, it is checked if it works properly for the motion control setpoint as well. This is done in Section 5.6.5. The updated control loop is illustrated in Figure 5.13. In this figure, F_{sk} denotes the setpoint for the force in the spring, while F_{sw} and F_k represent the forces in the winch. It is important to note that when no controller is applied, the winch exhibits unrestricted motion, resulting in oscillations.

The PID controller, which controls the motion of the winch, aims that the force exerted by the cable aligns with the force setpoint. In other words, the objective is to minimize the deviation between the actual cable force and the setpoint. This controller functions under a primary constraint: the force in the cable must not exceed its limits. As outlined in Section 5.2, the focus is on developing an adequate controller for research analysis, rather than an optimized one.

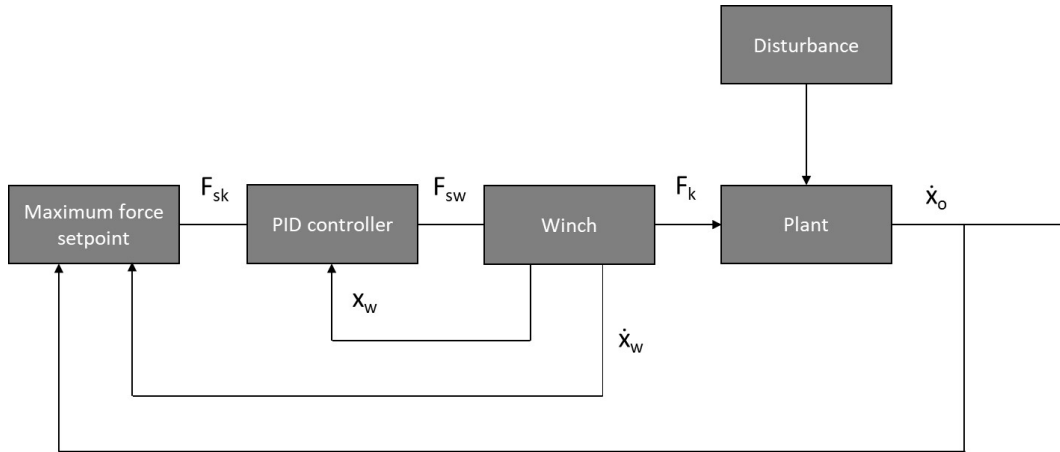


Figure 5.13: The control loop of the simplified lifting system with maximum force setpoint

First, the setpoint for the winch displacement x_{sw} is calculated using Hooke's law as follows:

$$x_{sw} = \frac{F_{sk}}{k} + x_o \quad (5.22)$$

Here, x_{sw} represents the displacement of the left side of the spring, and x_o denotes the displacement of the right side of the spring. The position error of the winch e_w is then calculated as:

$$e_w = x_{sw} - x_w \quad (5.23)$$

Where x_w represents the measured position of the winch, and x_{sw} is the setpoint for the position of the winch. Subsequently, this error serves as the input for a PD controller that regulates the setpoint for the force in the winch. The setpoint of the force of the winch is defined as:

$$F_{sw} = k_p \cdot e_w + k_i \cdot \int e_w + k_d \cdot \dot{e}_w \quad (5.24)$$

Here, k_p , k_i and k_d represent the proportional, integral and derivative gains of the PID controller, respectively. It is important to note that this model assumes the winch actuator works ideally, meaning that the force in the winch is always equal to the system's setpoint. In real-world scenarios, factors such as inertia, control system delays, may cause the force to deviate from the setpoint. However, this research does not consider these real-world effects, as its primary focus is on determining the desired setpoint for the force in the winch.

In the process of designing the controller for the detailed model, it was concluded that a non-zero integral gain resulted in unstable controller behaviour. After testing, the same was concluded for the winch controller in the analysis model. Consequently, the integral gain of the PID controller is set to zero, effectively converting it into a PD controller.

The displacement error for the load is in the order of 0.1, whereas the force is in the order of 100,000. Therefore, it is hypothesised that a winch controller with parameters in the order of 1,000,000 should function properly. This hypothesis is tested by evaluating PD controllers with gains ranging from 1 to 1,000,000, based in the deviation of the cable force from the setpoint, as elaborated in Section 3.6.1. The results are presented in Table 5.2. Run 21 yields the smallest deviation from the setpoint, contrary to the initial hypothesis. However, the cable force significantly overshoots the setpoint, as is observed in Figure 5.14. In this specific case, the force limits of $F_{max} = -50$ kN and $F_{min} = -250$ kN are not exceeded. However, this is due to the low velocity of the load, not to the controller's efficacy. If the load were to move at higher velocity, this controller would likely cause the force limits to be exceeded. Thus, this controller is considered overly aggressive and unsuitable for the application.

Run	k_p	k_d	Average deviation [kN]	Run	k_p	k_d	Average deviation [kN]
1	10	1	43.2	22	10,000	1	14.6
2	10	10	43.6	23	10,000	10	14.5
3	10	100	43.8	24	10,000	100	14.6
4	10	1,000	40.7	25	10,000	1,000	14.2
5	10	10,000	21.7	26	10,000	10,000	12.3
6	10	100,000	6.9	27	10,000	100,000	6.6
7	10	1,000,000	2.0	28	10,000	1,000,000	2.0
8	100	1	43.0	29	100,000	1	7.7
9	100	10	41.7	30	100,000	10	7.7
10	100	100	42.4	31	100,000	100	7.7
11	100	1,000	39.8	32	100,000	1,000	7.4
12	100	10,000	21.4	33	100,000	10,000	6.1
13	100	100,000	6.9	34	100,000	100,000	4.5
14	100	1,000,000	2.0	35	100,000	1,000,000	1.9
15	1000	1	33.9	36	1,000,000	1	12.2
16	1000	10	34.0	37	1,000,000	10	12.2
17	1000	100	33.9	38	1,000,000	100	12.0
18	1000	1,000	31.7	39	1,000,000	1,000	11.2
19	1000	10,000	19.1	40	1,000,000	10,000	7.1
20	1000	100,000	6.8	41	1,000,000	100,000	2.7
21	1000	1,000,000	2.0	42	1,000,000	1,000,000	1.4

Table 5.2: Outcomes of analysis 1 for the controller design of the winch controller

The controllers that were tested and showing a significant deviation from the setpoint were identified as overly conservative, concluding that there is a trade-off between being too conservative, which results in large deviations from the setpoint, and being too aggressive, leading to overshooting the setpoint. Consequently, the focus is shifted towards identifying a controller that closely adheres to the setpoint without large exceedance.

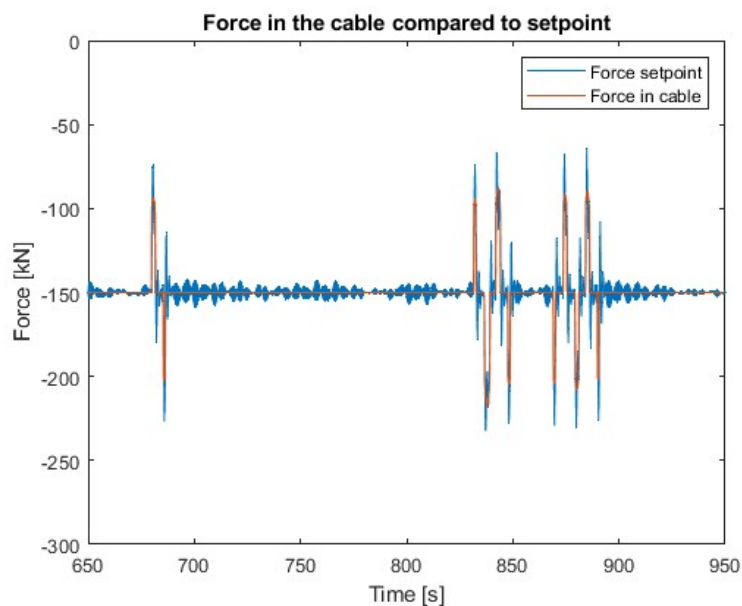


Figure 5.14: The force in the cable compared to the force setpoint for a controller with gains $k_p = 1,000,000$ and $k_d = 1,000,000$ with time frame [650 950] seconds

An examination was done on a winch controller with proportional and derivative gains set at $k_p = 100,000$ and $k_d = 100,000$. Figure 5.15 illustrates the force in the cable relative to the force setpoint within the time frame [650, 950] seconds. The Figure shows that the force in the tugger cable generated by this controller adheres well to the setpoint. Therefore, it is concluded that a controller with gains in the order of 100,000 is suitable for this system.

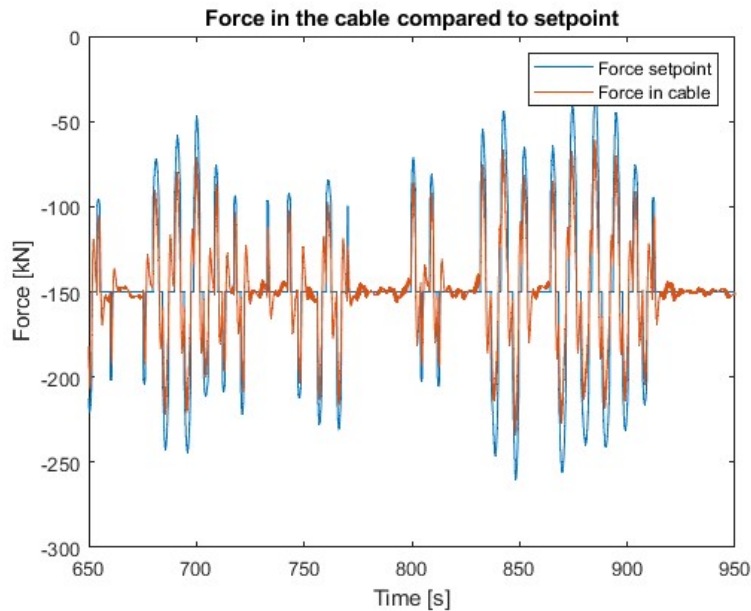


Figure 5.15: The force in the cable compared to the force setpoint for a controller with gains $k_p = 100,000$ and $k_d = 100,000$ with time frame [650 950] seconds

Due to the promising results obtained with a controller with gains of $k_p = 100,000$ and $k_d = 100,000$, it was decided to design controllers with gains within this order of magnitude. Various controllers were tested within this range. The results are shown in Table 5.3. Notably, the controller with gains $k_p = 300,000$ and $k_d = 150,000$ result in the best performance.

Run	k_p	k_d	Average deviation [kN]	Run	k_p	k_d	Average deviation [kN]
1	50,000	50,000	6.25	9	150,000	50,000	4.16
2	50,000	100,000	5.47	10	150,000	100,000	3.86
3	50,000	150,000	4.83	11	150,000	150,000	3.63
4	50,000	300,000	3.56	12	150,000	300,000	3.08
5	100,000	50,000	4.92	13	300,000	50,000	3.58
6	100,000	100,000	4.49	14	300,000	100,000	3.05
7	100,000	150,000	4.15	15	300,000	150,000	2.88
8	100,000	300,000	3.31	16	300,000	300,000	2.91

Table 5.3: Outcomes of analysis 2 for the controller design of the winch controller

The performance is depicted in Figure 5.16. As observed, the cable force closely aligns with the force setpoint. Although it exceeds the force limits at certain moments, for example around 1100 seconds, this slight exceeding is not considered problematic.

Figure 5.17b illustrates the load's motion when the selected controller is applied. An improvement is observed when comparing this to Figure 5.17a, which shows the motion of the load without any damping force. It should be noted that Figure 5.12a is not equal to Figure 5.17a, because the first is the motion of the load without damping force for the force system and the latter is the motion of the load without damping force for the lifting system. The motion of the load is not completely damped after 1250 seconds, which marks the end of the vessel's trajectory, because the load's velocity remains

within the deadband. Employing a controller with gains $k_p = 300,000$ and $k_d = 150,000$ ensures that the actual force in the cable closely remains to the force setpoint, exceeding it only marginally. This slight exceeding is considered unproblematic, making this controller well-suited for this application.

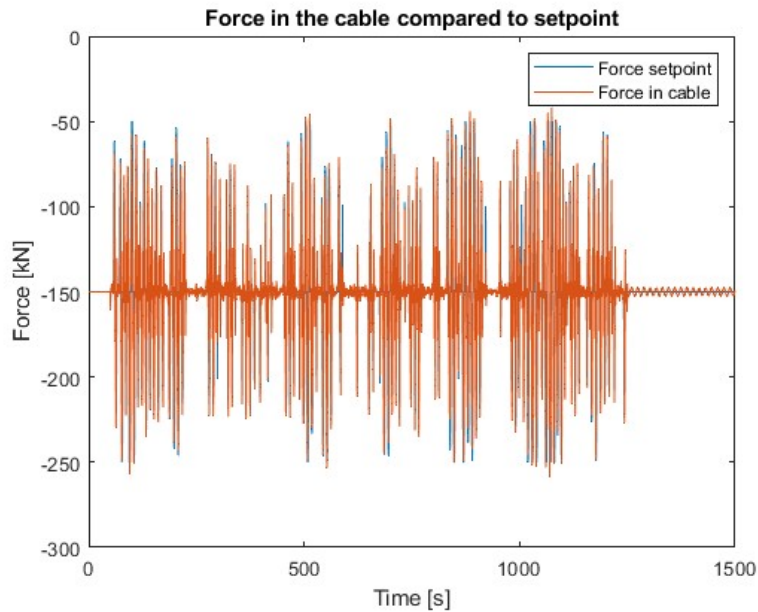


Figure 5.16: The force in the cable compared to the force setpoint for a controller with gains $k_p = 300,000$ and $k_d = 100,000$

In summary, the designed controller effectively ensures that the force in the cable closely aligns with the force setpoint. Moreover, it significantly mitigates load motion compared to scenarios without a control system. Consequently, a PD controller with a proportional gain of $k_p = 300,000$ and a derivative gain of $k_d = 150,000$ is chosen as winch controller.

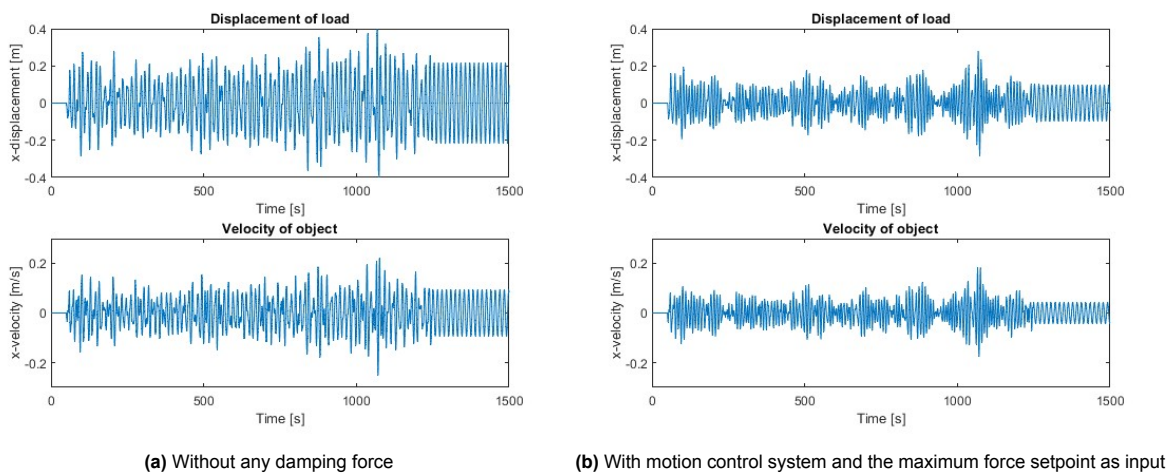


Figure 5.17: Comparison of the motion of the load

5.6.5. The winch controller for the motion control setpoint

Lastly, the motion control setpoint is integrated with the lifting system to evaluate whether the winch controller, designed in Section 5.6.4, is also effective for this setpoint. The resulting control loop is depicted in Figure 5.18.

The model is executed, and the actual force in the cable is compared with the force setpoint, as illustrated in Figure 5.19. The force in the cable closely aligns with the setpoint. Additionally, the resulting

motion of the load is presented in figure 5.20b. When this motion is compared to the load movement without the implementation of a controller, shown in Figure 5.20a, it is observed that the motion of the load is reduced when the motion control setpoint is employed in combination with the winch controller, which is designed in Section 5.6.4. Given that the cable force remains close to the setpoint and the resultant load motion is reduced in comparison to the scenario without a controller, it can be concluded that the derived motion control setpoint functions effectively in combination with the winch controller.

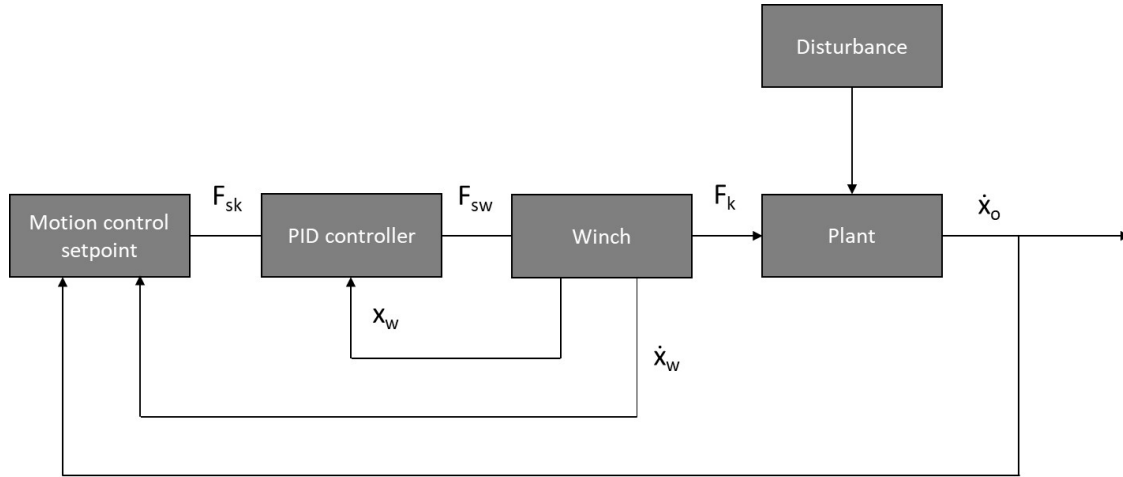


Figure 5.18: The control loop of the simplified lifting system with maximum force setpoint

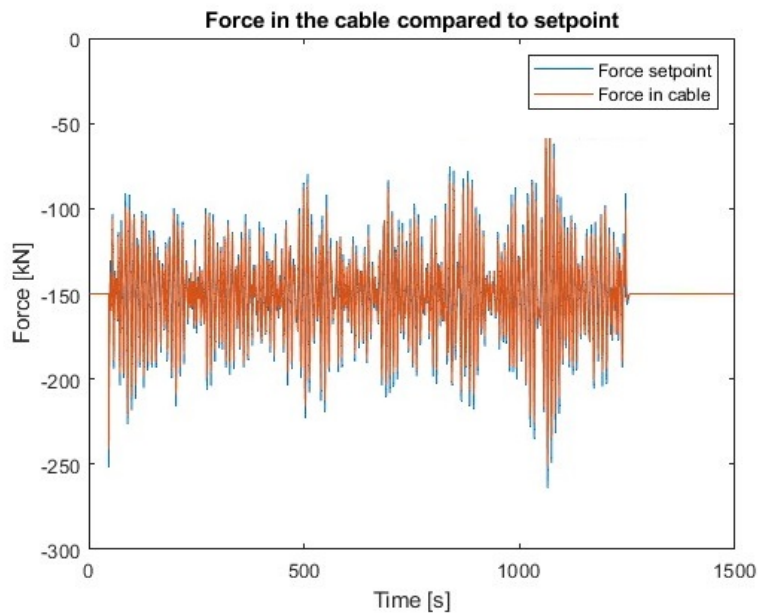


Figure 5.19: The force in the cable compared to the setpoint

5.6.6. Combined controller

Now, the setpoint calculation and winch controller have been integrated into a single controller, as well as the combined controller. This method enables the controller to control the winch's motion, which in turn results in a specific force in the cable, exerting force in the load. The load error, represented as e_o , as defined in equation 5.20, serves as the controller's input. This is illustrated in the control loop depicted in Figure 5.21. In this setup, only one feedback loop is used: the feedback loop for the motion of the load. The motion of the winch is not monitored, making this a more straightforward system.

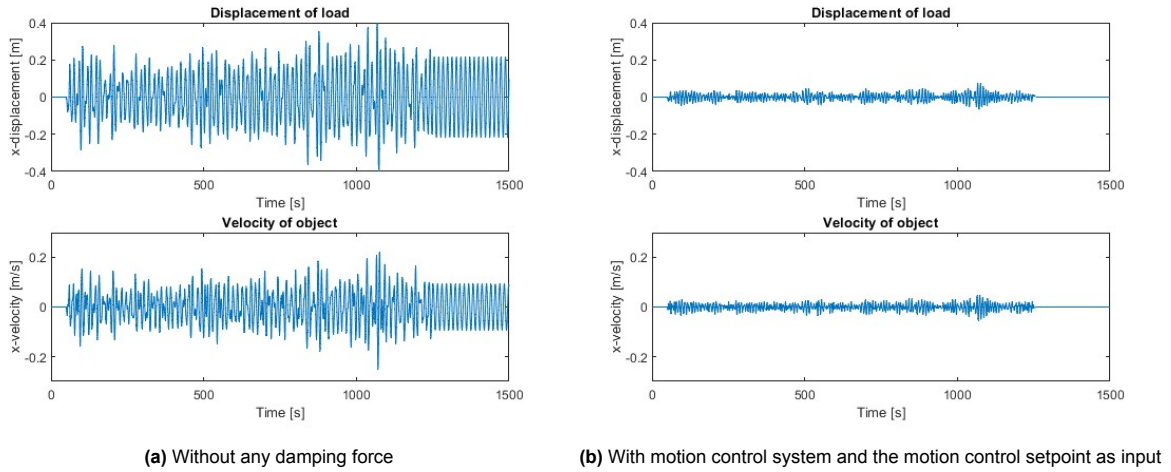


Figure 5.20: Comparison of the motion of the load

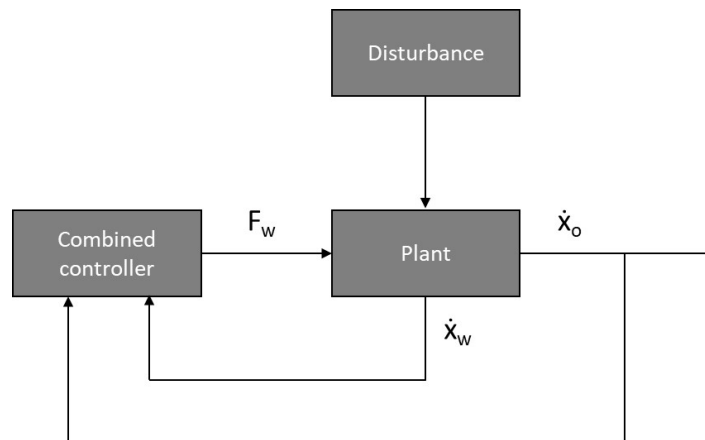


Figure 5.21: The control loop of the simplified lifting system with combined controller

However, with less motion data captured, the system might be more sensitive to instabilities. Nevertheless, a controller is developed for this approach. The objective is to design a controller to assess the system's impact in the load, rather than to create an optimized controller.

The mathematical expression for the PID-controller in this system is:

$$F_w = \bar{k}_p \cdot e_o + \bar{k}_i \cdot \int e_o + \bar{k}_d \cdot \dot{e}_o \quad (5.25)$$

Here, F_w represents the force in the winch, while \bar{k}_p , \bar{k}_i , and \bar{k}_d denote the proportional, integral, and derivative gains of the PID controller, respectively. As in the previous controller design approaches, the integral term was tested to check whether it induces instability in the response. This was indeed found to be the case, so the integral term was set to zero, converting the controller to a PD-controller.

As outlined in Section 5.6.4, the displacement error for the load is in the order of 0.1, while the force is in the order of 100,000. It is hypothesized that a winch controller with parameters in the order of 1,000,000 would be effective. Hence, controller gains of [10, 100, 1,000, 10,000, 100,000, 1,000,000] are examined. Their effectiveness is evaluated based in the average kinetic energy of the load, and the outcomes are presented in Table 5.4. Several controller settings result in an infinite average kinetic energy, which is not feasible in practice. This indicates that the system becomes unstable. In this context, the motion control system begins to add energy, resulting in an infinite response in this theoretical model. Thus, controller settings that lead to an infinite response are considered unsuitable.

Run	k_p	k_d	Average kinetic energy [J]	Run	k_p	k_d	Average kinetic energy [J]
1	10	10	16748.2	19	10,000	10	12205.1
2	10	100	16293.6	20	10,000	100	11292.9
3	10	1,000	10058.1	21	10,000	1,000	7534.1
4	10	10,000	2194.4	22	10,000	10,000	2556.0
5	10	100,000	881.3	23	10,000	100,000	973.0
6	10	1,000,000	Unstable	24	10,000	1,000,000	Unstable
7	100	10	16963.8	25	100,000	10	409566.0
8	100	100	16064.6	26	100,000	100	380643.9
9	100	1,000	9852.1	27	100,000	1,000	195177.3
10	100	10,000	2202.2	28	100,000	10,000	22009.7
11	100	100,000	880.8	29	100,000	100,000	2813.6
12	100	1,000,000	Unstable	30	100,000	1,000,000	Unstable
13	1,000	10	16270.3	31	1,000,000	10	Unstable
14	1,000	100	15640.5	32	1,000,000	100	Unstable
15	1,000	1,000	9728.7	33	1,000,000	1,000	Unstable
16	1,000	10,000	2213.5	34	1,000,000	10,000	Unstable
17	1,000	100,000	889.4	35	1,000,000	100,000	Unstable
18	1,000	1,000,000	Unstable	36	1,000,000	1,000,000	Unstable

Table 5.4: Results of analysis 1 for the controller design of the combined controller

Nevertheless, two conclusions are drawn from the results of Table 5.4. Firstly, both proportional and derivative gains of 1,000,000 result in an unstable response. This instability may come from exceeding limits due to too high controller outcome due to the sum of the gains, though this is not tested in this thesis. Secondly, a derivative gain of 100,000 yields optimal results, evident from the top performances in runs 11, 5, 17, and 23. Notably, combining this derivative gain with a proportional gain of 100,000 does not yield as good outcomes, potentially due to the sum of the gains as well.

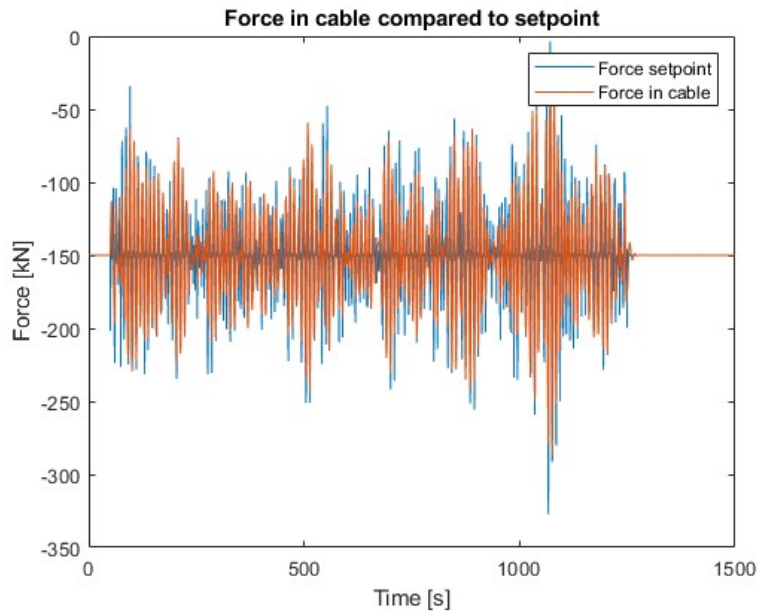


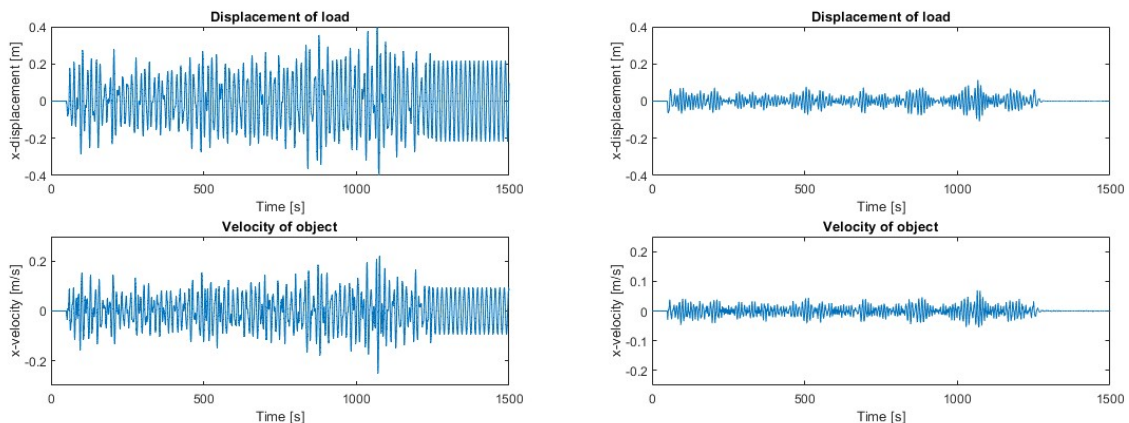
Figure 5.22: The resulting force in the tugger cable due to the combined controller

Subsequently, runs 11, 5, 17, and 23 are further analyzed. These controllers demonstrate similar responses, except for run 23 which excessive overshoots the force limits of $F_{max} = -50$ kN and $F_{min} = -250$ kN. Among the top three controllers, the one yielding the lowest average kinetic energy is chosen for future controller design. This is the controller with gains of $\bar{k}_p = 100$ and $\bar{k}_d = 100,000$.

Run	k_p	k_d	Average kinetic energy [J]	Run	k_p	k_d	Average kinetic energy [J]
1	50	50,000	1114.9	19	300	50,000	1118.1
2	50	100,000	880.5	20	300	100,000	884.0
3	50	200,000	615.4	21	300	200,000	615.7
4	50	300,000	Unstable	22	300	300,000	Unstable
5	50	400,000	Unstable	23	300	400,000	Unstable
6	50	500,000	Unstable	24	300	500,000	Unstable
7	100	50,000	1113.1	25	400	50,000	1116.7
8	100	100,000	880.8	26	400	100,000	884.3
9	100	200,000	615.1	27	400	200,000	616.8
10	100	300,000	Unstable	28	400	300,000	Unstable
11	100	400,000	Unstable	29	400	400,000	Unstable
12	100	500,000	Unstable	30	400	500,000	Unstable
13	200	50,000	1116.4	31	500	50,000	1118.4
14	200	100,000	883.2	32	500	100,000	886.2
15	200	200,000	616.1	33	500	200,000	617.1
16	200	300,000	Unstable	34	500	300,000	Unstable
17	200	400,000	Unstable	35	500	400,000	Unstable
18	200	500,000	Unstable	36	500	500,000	Unstable

Table 5.5: Results of analysis 2 for the controller design of the combined controller

A more refined analysis is conducted around the settings of run 11. Proportional gains of [50, 100, 200, 300, 400, 500] and derivative gains of [50,000, 100,000, 200,000, 300,000, 400,000, 500,000] are tested. The outcomes are listed in Table 5.5, leading to three observations. Firstly, derivative gains of 300,000 or above lead to instability, and secondly, a derivative gain of 200,000 delivers the most favorable results and thirdly, the value of the proportional gain has minimal impact in the average kinetic energy. Nevertheless, the most efficient controller of this analysis is from run 9, with gains $\bar{k}_p = 100$ and $\bar{k}_d = 200,000$.



(a) Without any damping force

(b) The motion of the load with implication of the combined controller

Figure 5.23: Comparison of the motion of the load

Additional assessment of this controller is positive. As seen in Figure 5.22, the force in the cable slightly exceeds the limits. However, as with the design phase of the winch control, executed in Section 5.6.4, this slight exceeding is considered acceptable. The resulting motion of the load, illustrated in Figure 5.23b, highlights a reduction in load motion due to the controller when compared to Figure 5.23a. Hence, the PD-controller, with settings $\bar{k}_p = 100$ and $\bar{k}_d = 200,000$, is selected as the combined controller.

5.6.7. Constant tension mode

Now, constant tension mode is created. As explained in section 4.2.4, the constant tension mode's reference value is a predefined fixed value. This results in the control diagram depicted in figure 5.24. As depicted, there exists a singular controller within this system, namely, the winch controller. The parameters deduced in section 5.6.4 are used for this controller as well.

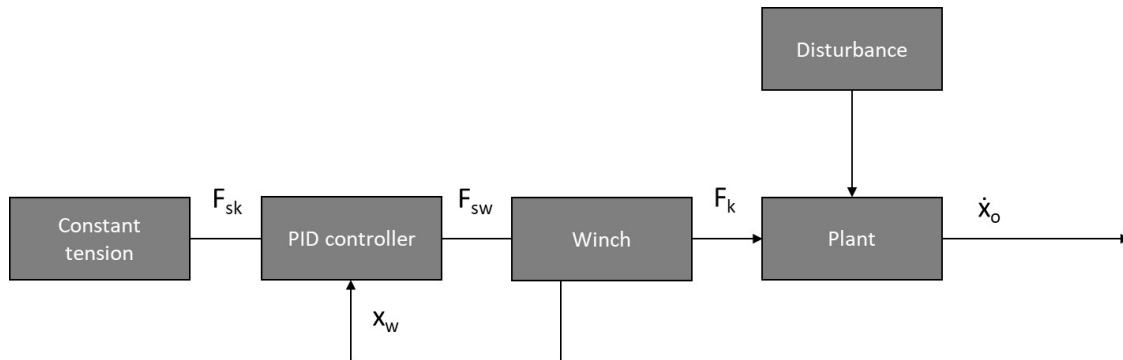


Figure 5.24: Control diagram for constant tension mode

The results of this constant tension mode are compared to the results of the constant tension mode created with the detailed model of section 4.6.4. The conditions for both models are set equal, so the constant tension reference point is established at $F_s = -100$ kN and both models only have a surge vessel motion as input motion. Figure 5.25a displays the cable force and load displacement produced by the analysis model, whereas Figure 5.25b exhibits the cable force and load displacement yielded by the detailed model.

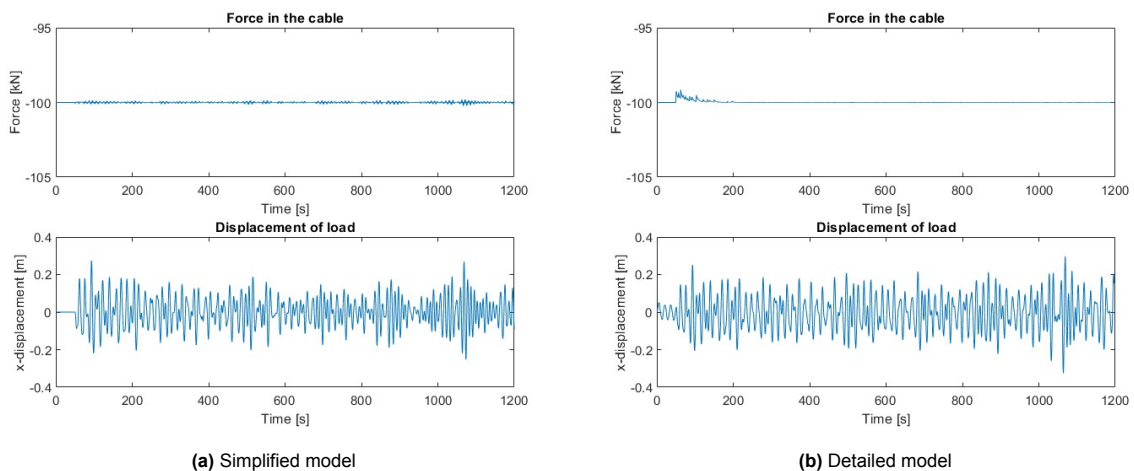


Figure 5.25: Constant tension mode

Upon examination of Figures 5.25a and 5.25b, it becomes evident that both models effectively maintain a constant tension. In the analysis model, there are minimal fluctuations in the cable's force around the setpoint, with their magnitude being negligible small. The detailed model exhibits even smaller force fluctuations, except for a notable peak in force occurring between $t = 50$ s and $t = 200$ s. This peak arises because vessel motion is present only after 50 seconds. Consequently, it impacts the cable's force at $t = 50$ s, momentarily disrupting equilibrium, and gradually returns to equilibrium by $t = 200$ s. Nevertheless, both models demonstrate a functioning constant tension mode.

Although, the behaviour of the load is not exactly equal for the two models, several similarities in the load displacement are observed. Notably, both displacements share a similar order of magnitude, approximately 0.3 m. Moreover, both models exhibit peaks in load displacement at synchronized in-

tervals. For instance, peaks occur around $t = 150$ s, $t = 500$ s, $t = 850$ s, and $t = 1050$ s in both models.

Despite inherent differences between the models, the analysis model's load displacement is comparable to that of the detailed model in this specific scenario. Consequently, the analysis model can serve as a viable alternative to the detailed model. Using the analysis model significantly reduces computation time, making it a more efficient tool for analyzing the control aspects of the motion control system.

5.7. Conclusion

Two systems are developed in this chapter: the force system and the lifting system. The force system focuses solely in the cranetip, the motion of the load, and the damping force exerted in the load. It is designed to explore the impact of the damping force in the load. The lifting system represents a simplified version of the detailed lifting system discussed in Chapter 4. The lifting system extends the force system with the winch and tigger system and serves as the foundational model for analyzing the two controller setpoints and inputs of Section 3.3.

The EOMs for these systems are derived using the Lagrange method and form the basis for two numerical MATLAB models. The numerical solver ODE45 is used to solve these EOMs. Multiple verification cases confirm the reliability of these MATLAB models, enabling their usage for gaining more understanding of the physics of a lifting operation and of the damping tigger system.

Subsequently, these MATLAB models are converted into Simulink models. Both the maximum force setpoints and motion control setpoints are incorporated into these Simulink models. Parameter selection for the motion control setpoint is conducted via a trial-and-error approach within the Simulink framework. Eventually, a PD-controller with a proportional gain of $\bar{k}_p = 95,000$ and a derivative gain of $\bar{k}_d = 70,000$ is selected.

Thereafter, a winch controller is designed based in the maximum force setpoint. After multiple analyses, a PD-controller featuring a proportional gain of $k_p = 300,000$ and a derivative gain of $k_d = 150,000$ yields the best winch response. This controller is then tested in combination with the motion control setpoint to whether it functions with this setpoint. The controller's performance proves to be satisfactory, confirming its suitability with both the maximum force and motion control setpoints.

Consequently, a new control system, namely the combined controller, is introduced. This system directly controls the motion of the winch based in the error in the load's motion, eliminating the feedback loop from the winch motion. This controller is a PD-controller with a proportional gain of $\bar{k}_p = 100$ and a derivative gain of $\bar{k}_d = 200,000$.

Lastly, the constant tension mode is integrated into the analysis model, and a comparison is made with the detailed model, revealing similar results. Thus, the analysis model can be considered a practical substitute for the detailed model. The use of the analysis model considerably decreases computational time, making it a more efficient tool for analyzing the control aspects of the motion control system.

Finally, the designed setpoints and controllers are integrated into the Simulink model, resulting in a complete model of the lifting system. This integrated model is used for the analysis the controller setpoints and inputs, described in Chapter 6.2. The results of this analysis are presented in Chapter 6.

6

Results

In this chapter, the results obtained in this thesis are presented. First, the methodology for the creation of the models is presented. Thereafter, an analysis of the control aspects, described in section 3.3, is provided. Lastly, the results obtained in this analysis are presented. The results are discussed in Chapter 7.

6.1. Models

Initially, a detailed model was developed and evaluated through verification cases. Subsequently, the constant tension mode was successfully designed and incorporated into this model, resulting in a model suitable for simulating offshore lifting operations utilizing a motion control system in constant tension mode.

Following this, the model was simplified to the analysis model, to enhance its efficiency in analyzing control system aspects. This analysis model significantly reduced computational time compared to the detailed model. Controllers and setpoints were derived successfully, making the analysis model suitable for simulating offshore lifting operations with a motion control system in damping mode across various control inputs and methods.

Subsequently, the constant tension mode was integrated into the analysis model, and a comparative analysis was conducted against the detailed model, which yielded similar outcomes. Hence, the analysis model can be regarded as a pragmatic alternative to the detailed model. Its utilization substantially reduces computational time, rendering it a more efficient instrument for scrutinizing motion control system's control aspects.

6.2. Analysis of the control methods and input

An analysis of various control methods and inputs is conducted. The evaluation involves analyzing the resulting motion of the load when these control methods and inputs are implemented. For this analysis, the analysis model described in Chapter 6.2 is used. This model is capable of simulating a lifting operation using a motion control system.

6.2.1. Analyzed aspects of the control system

Two aspects of the control system will be analyzed: the control methods and the control inputs. In Section 3.3, two distinct setpoints for the winch controller are discussed: the maximum force setpoint and the motion control setpoint. These represent two separate control methods. A third control method, known as the combined control method, is introduced in Section 5.2.3. The impacts of all three control methods on the motion of the load are analyzed in this evaluation.

Section 3.3.3 describes two distinct controller inputs. The first controller input measures the motion of the tugger cable close to the winch, assuming that the motion of the winch, the tugger cable, and

the load are identical. Because of this assumption, the measured motion of the tugger cable serves as the control input. The second controller input examined is the motion of the load, which is directly measured and sent as feedback to the controller. These controller inputs are termed the winch sensor and the load sensor in the analysis, respectively.

A control method only functions with an input. Therefore, during the analysis, the control methods and inputs are integrated, resulting in $3 \times 2 = 6$ possible combinations. For the sake of completeness, all 6 combinations of control methods and inputs are analyzed.

6.2.2. Different analysis scenarios

The analysis involves multiple scenarios. These scenarios arise from varying certain parameters. The parameters are: the mass of the load, the mass of the winch, and the reference system for the setpoint. These parameters are elaborated upon below. The variations in the parameters result in $4 \times 3 \times 2 = 24$ scenarios. Each combination of control method and input is run once for every scenario. With 24 scenarios and 6 combinations of control methods and inputs, this amounts to $24 \times 6 = 144$ distinct model executions.

Mass of the load

Four distinct mass values for the load are considered. The masses range from the estimated weight of a relatively small object transfer to the maximum lifting capacity of a crane on Heerema MC's SSCV Sleipnir. The small object's mass is estimated at 10 mT, while the maximum capacity of a Sleipnir crane is 10,000 mT [109]. Steps of $\times 10$ between the minimum and maximum values are selected, resulting in the use of four masses: [10, 100, 1,000, 10,000] mT.

Mass of the Winch

Three different values are selected for the mass of the winch. The middle value represents a realistic winch mass. This mass is set at 5 mT, corresponding to a rotational winch with a diameter of 1 meter. Based on equation B.10, the translational winch also has a mass of 5 mT. The other two masses, values five times smaller and five times larger than the middle value. Hence, the chosen mass values for the winch are [1, 5, 25] mT.

Reference systems

The motion control system is evaluated using two distinct reference systems for determining the setpoint of load movement. These systems are the global reference system and the on-deck reference system, as detailed in Section 3.3.1.

Vessel motions

The vessel motion trajectory remains consistent throughout this analysis. This choice was made because varying the mass of the load, the mass of the winch, and the use of two reference systems provided sufficient scenarios.

6.2.3. Improvement factor

The impact of various control methods on the motion control system will be assessed. The different control methods and inputs lead to different motion of the load. This difference is indicated by the RMS of the velocity of the load, as described in Section 3.6.1. The evaluation is based on the RMS of the velocity of the load, because the ultimate objective of the motion control system is to damp the velocity of the load.

First, the RMS of the velocity of the load without a control system for the specific scenario is calculated; this serves as the base value. Subsequently, the RMS of the velocity of the load, resulting from the various control methods and inputs for this scenario, is determined. These RMS values are then compared to the base value, and the percentage improvement (or deterioration) is computed as:

$$I_f = \frac{RMS_{com} - RMS_{base}}{RMS_{base}} \cdot 100\% \quad (6.1)$$

where I is the improvement value, RMS_{com} represents the RMS of the velocity of a certain combination and RMS_{base} denotes the RMS of the velocity of the base value. This results in a percentage improvement for each combination of methods and inputs for every scenario.

Case	1	2	3
Base	10	8	4
Sensor A	8	4	6
Sensor B	2	4	3

Table 6.1: Sample values for the explanation of the improvement factor

The aforementioned is further explained using an example. Table 6.1 displays sample values that could be the outcomes from a certain model. Applying equation 6.2.3 to sensor A for scenario 1 yields:

$$I_f = -\frac{RMS_{com} - RMS_{base}}{RMS_{base}} \cdot 100\% = -\frac{8 - 10}{10} \cdot 100\% = 20\%$$

The improvement of a control system using sensor A in scenario 1 is 20%. Table 6.2 displays all computed improvements. A deterioration is also possible, as demonstrated by the system with sensor B in scenario 3, denoted by a minus sign.

Case	1	2	3
Sensor A	20%	50%	25%
Sensor B	80%	50%	-50%

Table 6.2: Sample improvement factors

After deriving all improvement factors, a comparison of various control aspects will be done based on these factors. This is done by subtracting one improvement factor from another, resulting in the difference denoted as ΔI_f . Taking Case 1 from Table 6.2 as an illustration, the difference in improvement factors between sensor A and sensor B is then calculated as follows:

$$\Delta I_f = I_{fA} - I_{fB} = 20\% - 80\% = -60\% \quad (6.2)$$

This indicates that the improvement when using sensor B is 60% higher than when using sensor A. This comparative approach is employed across all control aspects. To enhance legibility, the cell colors in the result-containing tables signify the superior improvement factor. Table 6.3 illustrates the distinction in improvement factors between sensor A and sensor B across the three exemplary cases. Sensor A's superiority is denoted by dark grey, while sensor B's superiority is represented by light grey.

Case	1	2	3
ΔI_f	-60%	0%	75%

Table 6.3: Sample difference between improvement factors

6.3. Effects of the control methods and input

An analysis was done on the impact of the various control methods and inputs. In total, all 6 combinations of the control methods and inputs are tested within 24 unique scenarios.

6.3.1. Velocity of the load

The results from the model execution provide a time frame for the displacement and velocity of the load. Different combinations of control methods and inputs are compared with the base motion of the scenarios, that is, the motion of the load when no control system is active. Figures 6.1 and 6.2 depict a result where the implementation of a control system reduces the motion of the load compared to the

same situation with no active controller. The control method implemented in Figure 6.1 is the winch controller in combination with the maximum force setpoint, in a scenario that includes a winch of 1 mT and a load of 1000 mT, referenced to a global system.

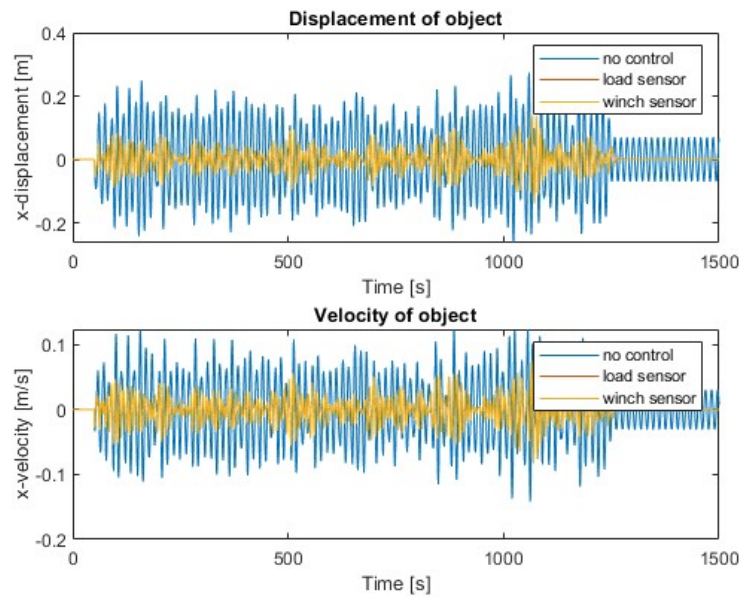


Figure 6.1: A situation where the motion of the load is reduced due to the presence of the control system

The control method implemented in Figure 6.2 is the winch controller in combination with the motion control setpoint, in a scenario that includes a winch of 1 mT and a load of 10 mT, referenced to a global system.

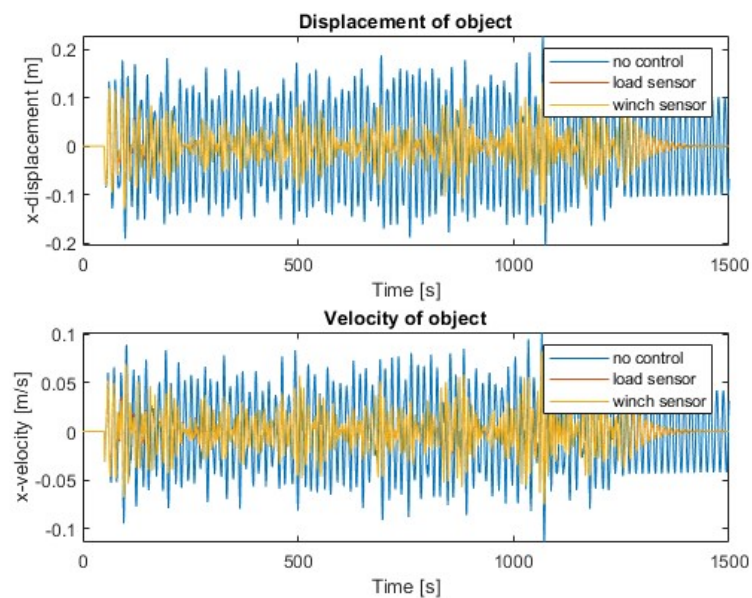


Figure 6.2: A second situation where the motion of the load is reduced due to the presence of the control system

In contrast, certain controllers result in an increased motion of the load under specific scenarios because of a counteractive response. Figure 6.3 illustrates such a situation. It is evident that the move-

ment of the load increases significantly when the load sensor is used. The control method employed is the winch controller combined with the maximum force setpoint. This scenario involves a winch of 25 mT and a load of 1,000 mT, using an on-deck reference system.

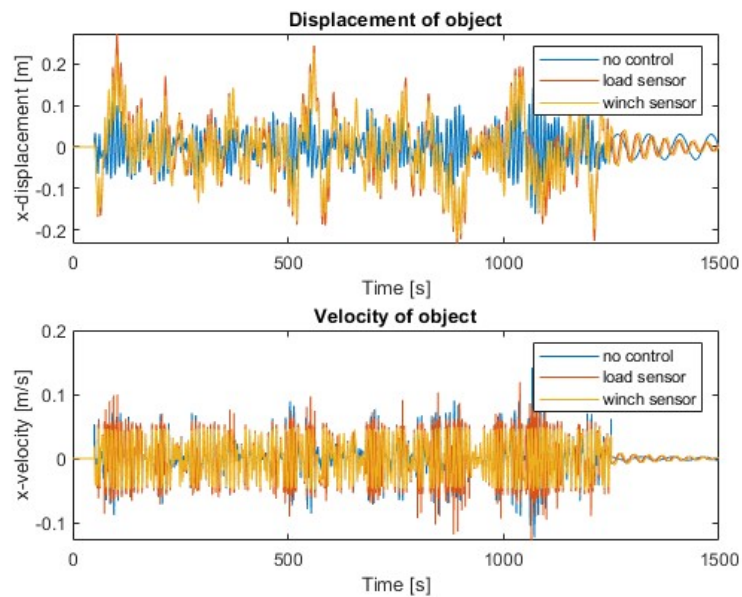


Figure 6.3: A situation where the motion of the load is increased due to the presence of the control system

Lastly, Figure 6.4 illustrates a situation where the controller's presence neither significantly reduces nor increases the motion of the load. This observation is made using the combined controller method in a scenario with a winch of 25 mT and a load of 10 mT, employing an on-deck reference system. The motion of the load with a control system differs from the motion without a control system, showing variations that are sometimes larger and sometimes smaller, indicating that the control system affects the load's motion. However, from this figure, it is not evident whether the controller's response significantly reduces or increases the motion of the load.

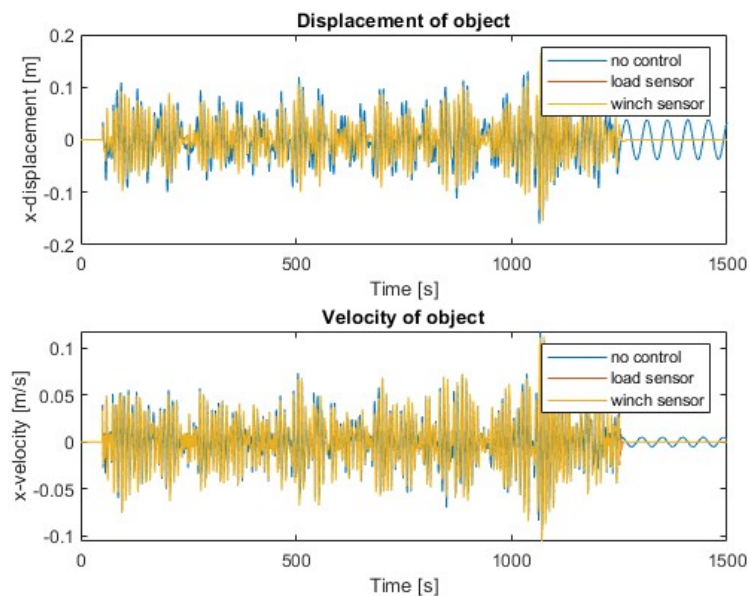


Figure 6.4: A situation where the presence of the controller does not reduce or increase the motion of the load

6.3.2. Resulting root mean square of the velocity of the load

The RMS of the velocity of the load was calculated for each combination of control methods and inputs across different scenarios. These are then compared to the RMS of the velocity of the load without the use of any control system for the corresponding scenarios. Appendix C provides the specific values of the RMS of the velocity for all scenarios.

6.3.3. Resulting improvement factors

The specific values of the RMS of the velocity of all scenarios are presented in appendix C. The corresponding improvement factors are provided in this section. The derivation method of the improvement factor is provided in Section 6.2.3. Table 6.4 provides the improvement factors for all scenarios. Some scenarios result in notably high, negative improvement factors. The highest value observed is an improvement factor of -492% , as shown in Table 6.4. This situation is demonstrated in Figure 6.3. These high negative improvement factors arises from system instability, causing significant motion of the load. Such motion results in a high RMS of the velocity of the load.

Reference system \Rightarrow		On-deck			Global		
m_o [mT] \downarrow	m_w [mT] \Rightarrow	1	5	25	1	5	25
Maximum force setpoint							
10	Load	31%	3%	-9%	29%	19%	16%
	Winch	41%	4%	-12%	33%	19%	16%
100	Load	48%	37%	21%	57%	28%	29%
	Winch	37%	25%	8%	56%	27%	26%
1000	Load	41%	51%	35%	59%	64%	53%
	Winch	34%	46%	28%	45%	54%	44%
10000	Load	32%	34%	43%	59%	64%	53%
	Winch	23%	26%	39%	45%	54%	44%
Motion control setpoint							
10	Load	90%	84%	84%	93%	85%	79%
	Winch	47%	19%	11%	95%	89%	85%
100	Load	97%	95%	94%	95%	92%	89%
	Winch	51%	20%	2%	86%	76%	67%
1000	Load	75%	79%	71%	82%	85%	78%
	Winch	-52%	-35%	-87%	-15%	3%	-43%
10000	Load	42%	37%	41%	82%	85%	78%
	Winch	1%	-8%	-1%	-15%	3%	-43%
Combined controller							
10	Load	83%	33%	9%	93%	89%	86%
	Winch	81%	28%	4%	92%	87%	86%
100	Load	56%	36%	-30%	77%	74%	-492%
	Winch	41%	23%	17%	71%	68%	73%
1000	Load	39%	49%	37%	61%	70%	63%
	Winch	35%	46%	32%	58%	68%	60%
10000	Load	26%	24%	32%	33%	34%	45%
	Winch	21%	20%	30%	28%	30%	42%

Table 6.4: The improvement factors of all executed scenarios

6.3.4. Effects of controller inputs

The study compares various control aspects in pairs. In this section, cell colors are used for readability. Table 6.5 presents control aspects and their associated colors indicating dominance. For instance, in a scenario comparing the load and winch sensors, if the load sensor performs better, the cell is colored red. If the winch sensor performs better, the cell is colored blue.

The two distinct controller inputs are the winch motion and the load motion. These inputs are compared by subtracting the improvement factor of the winch sensor from that of the load sensor for each case. The resultant factor indicates the difference in the RMS of the velocity of the load ΔI_f between the use of the load sensor and the use of the winch sensor. A positive difference, depicted in red, suggests that the winch sensor is more effective than the load sensor. Conversely, a negative difference in the improvement factor, shown in blue, signifies that the load sensor results in decreased load motion.

Control aspect	Color
Load sensor	Red
Winch sensor	Blue
Maximum force setpoint	Yellow
Motion control setpoint	Green
Combined controller	Purple

Table 6.5: Colors indicating dominance dominance of a certain control aspect

Table 6.6 provides the differences in improvement factors for the maximum force setpoint. The load sensor yields better results in 61 scenarios, while the winch sensor is superior in 8 scenarios. In 3 scenarios, the difference is negligible.

Reference system \Rightarrow	On-deck			Global		
m_w [mT] \Rightarrow	1	5	25	1	5	25
m_o [mT] \Downarrow	Maximum force setpoint					
10	-10%	-1%	3%	-4%	0%	0%
100	11%	12%	13%	1%	1%	3%
1000	7%	2%	6%	14%	10%	9%
10000	10%	8%	5%	14%	10%	9%
	Motion control setpoint					
10	43%	65%	72%	-2%	-4%	-5%
100	46%	75%	92%	9%	16%	22%
1000	126%	114%	158%	96%	82%	121%
10000	40%	45%	42%	96%	82%	121%
	Combined controller					
10	2%	6%	4%	1%	2%	0%
100	14%	13%	-47%	6%	6%	-564%
1000	4%	3%	5%	2%	2%	3%
10000	5%	4%	2%	5%	4%	2%

Table 6.6: Comparison of improvement factors of the winch sensor and the load sensor

6.3.5. Effects of control methods

The control methods are now assessed. Firstly, the maximum force setpoint and the motion control setpoint are evaluated. The improvement factor for the maximum force setpoint is subtracted from the improvement factor for the motion control setpoint in each scenario. This provides a factor indicating the difference in the RMS of the velocity of the load ΔI_f , when using the motion control setpoint instead of the maximum force setpoint. A positive difference in the improvement factor, displayed in green, implies that the motion control setpoint outperforms the maximum setpoint method. Conversely, a negative difference in the improvement factor is shown in yellow, indicating that the maximum setpoint leads to more reduction of the motion of the load.

Table 6.7 illustrates the difference in improvement factors for the winch sensor. Clearly, in 10 scenarios, the motion control setpoint produces better results, while in 14 scenarios, the maximum force setpoint is superior.

Reference system \Rightarrow	On-deck			Global		
m_w [mT] \Rightarrow	1	5	25	1	5	25
m_o [mT] \Downarrow	winch sensor					
10	5%	15%	23%	62%	70%	69%
100	14%	-4%	-6%	29%	50%	40%
1000	-85%	-81%	-115%	-60%	-51%	-87%
10000	-21%	-34%	-40%	-60%	-51%	-87%
	Load sensor					
10	59%	82%	93%	64%	66%	64%
100	49%	59%	73%	38%	64%	59%
1000	34%	28%	626%	22%	21%	25%
10000	-21%	-34%	-40%	-60%	-51%	-87%

Table 6.7: Comparison of improvement factors of maximum force setpoint and the motion control setpoint when using the winch sensor

Consider the motion control setpoint and the combined controller. The improvement factor of the motion control setpoint is subtracted from the improvement factor of the combined controller in every instance. This difference yields a factor that indicates the reduction in the RMS of the velocity of the load ΔI_f , when using the combined controller instead of the motion control setpoint. A positive difference, displayed in purple, suggests that the combined controller performs better than the motion control setpoint. Conversely, a negative difference in the improvement factor, shown in green, indicates that the motion control setpoint results in decreased motion of the load.

Table 6.8 presents the differences in improvement factors when employing the winch sensor. The data shows that in 20 scenarios, the combined controller provides superior outcomes, while in 27 scenarios, the motion control setpoint is more effective. In 1 scenario no superior control method is identified.

Reference system \Rightarrow	On-deck			Global		
m_w [mT] \Rightarrow	1	5	25	1	5	25
m_o [mT] \Downarrow	Winch sensor					
10	34%	9%	-7%	-3%	-2%	1%
100	-10%	3%	15%	-15%	-8%	6%
1000	87%	81%	119%	73%	65%	103%
10000	20%	28%	31%	43%	28%	85%
	Load sensor					
10	-7%	-51%	-75%	0%	4%	6%
100	-41%	-60%	-124%	-18%	-18%	-581%
1000	-35%	-30%	-34%	-21%	-15%	-15%
10000	-15%	-13%	-9%	-48%	-51%	-33%

Table 6.8: Comparison of improvement factors of motion control setpoint and the combined controller when using the winch sensor

Consider the maximum force setpoint and the combined controller. The improvement factor of the maximum force setpoint is subtracted from the improvement factor of the combined controller in every instance. This difference yields a factor that indicates the difference in the RMS of the velocity of the load ΔI_f , when using the combined controller instead of the motion control setpoint. A positive difference, shown in purple, indicates that combined controller leads to better results. Conversely, a negative difference in that the improvement factor, shown in yellow, indicates that the maximum force setpoint results in decreased motion of the load.

Table 6.9 presents the differences in improvement factors when employing the winch sensor. The data shows that in 30 scenarios, the maximum force setpoint provides superior outcomes, while in 7 scenarios, the combined controller is more effective. In 11 scenarios, no clear difference is seen.

Reference system \Rightarrow	On-deck			Global		
m_w [mT] \Rightarrow	1	5	25	1	5	25
m_o [mT] \Downarrow	Winch sensor					
10	-3%	-1%	-1%	-3%	-2%	-1%
100	1%	0%	0%	-2%	-2%	-2%
1000	0%	0%	-1%	-2%	-2%	-2%
10000	-20%	-19%	-18%	-15%	-13%	-12%
	Load sensor					
10	-4%	-2%	-1%	-3%	-2%	-1%
100	0%	0%	3%	-2%	-3%	22%
1000	0%	0%	-1%	0%	-1%	-1%
10000	1%	0%	0%	3%	2%	2%

Table 6.9: Comparison of improvement factors of maximum force setpoint and combined controller

7

Discussion

In this chapter, the results described in Chapter 6 are discussed. To obtain these results, two models are created and the outcomes are compared. Following this, an analysis of the impacts of various control aspects is conducted. The choices made during the development of the models, the execution of the analysis, and the assessment of the outcomes are discussed below.

7.1. Creation of the models

This discussion covers the results, purposes, and limitations of the developed numerical models. Following, the Simulink model and the controller design phase are discussed.

7.1.1. The detailed model

Three numerical MATLAB models were developed, based on the corresponding sets of EOMs. These EOMs were derived using the Lagrange method. The derivation was executed in steps to reduce complexity, resulting in a robust method for deriving the EOMs.

After the creation of the numerical models in MATLAB, the validity of the model's results was evaluated through several verification cases. For the detailed model, this included a comparison to the results of a study by Zhang, which employed a similar modelling approach [98]. All results within the verification cases, including the comparison with Zhang's study, were demonstrated to be valid, suggesting the model is likely accurate. However, the outcomes are not compared to data, due to the current lack of data for this specific case. Conducting such a comparison would enhance the verification of the model.

The three developed models can be used to increase understanding of the physics of lifting operations and the damping tigger system, like investigation of load motion, force and vibration during offshore lifting operations. Despite the multiple purposes of the numerical models, both models are bound to several limitations. First, investigation could only done with passive motion control systems, because there is no control system integrated into the MATLAB models. However, this is present in the Simulink model. Additionally, the effects of gravitational force of the load on the vessel are not incorporated into the model, hence it cannot be studied using these numerical models. Finally, the model includes only a single vessel motion trajectory. While it is possible to integrate a different vessel motion trajectory, the model does not currently provide other vessel motion trajectories.

Furthermore, the derivation of the EOMs for both the damping tigger system and the controlled lifting system results in extensive equations. Even though the derivation of these EOMs was done in steps, yielding a robust method, the resulting equations are complex. Consequently, research using models based on these complex EOMs might pose challenges with understanding the physics within the model due to their complexity. However, the issue is addressed with the introduction of the analysis model. The analysis model resulted in more straightforward EOMs that are easier to understand, making analysis more straightforward.

Thereafter, the MATLAB model for the controller lifting operation was converted into a Simulink model. This model contains both the constant tension mode and damping mode. A PD-controller was developed demonstrated effectiveness for simulations in the tension setpoint range of $F_s = 90$ kN to $F_s = 140$ kN. The implementation of the controller into the Simulink model resulted in a model suitable for examining lifting operations using the damping tugger system in constant tension mode.

For the damping mode, the different controller design approaches and the different controller settings appeared to be ineffective. Several reasons might make it challenging to select a suitable controller for the system. One reason is that a PID controller might not be the best option for these objectives. As concluded from the design phase of the controller for the constant tension mode, changing setpoints lead to different optimized controller settings for constant tension modes. While PID controllers work well for many control systems, it might not be an ideal controller for changing setpoints. A suggestion for a better controller is an adaptive controller, potentially offering better results to a changing setpoint. However, this hypothesis has not been further explored.

Even when a PID controller seems suitable, various factors could reduce its performance. One such factor is the truncation of the controller's output, which is done to model the winch limits. This truncation could lead to instability. In essence, the controller might adjust too much for this truncated output. Another potential problem is that the controller responds to minor system vibrations, like the axial vibrations from the tugger cable's inclined mass. Even though this mass does not truly exist in this manner, its modeled existence might cause axial vibrations.

Due to the complexity of the model, it was not well understood why the different controller design approaches and the different controller settings for the damping mode were ineffective. An examination of the effects on the controller of the above mentioned factors would provide a deeper understanding of the issues in the controller design for damping mode. This understanding might lead to a successful design strategy. However, the objective is to analyse the different control aspects. Due to the extensive computational time of the model, this analysis would be time-consuming. Hence, the decision was made to develop a new, simpler model, called the analysis model.

7.1.2. The analysis model

Two simplified systems have been developed. Simplifications are done based on new insights that were obtained during the creation of the detailed model. These simplifications imply several elements that has small effect on the dynamics of the system, when using it for the analysis of the control aspects. Important simplifications are the reduction of crane tip motion to a single direction, the elimination of the mass of the tugger cable and the decision to model the winch as a translation in stead of a rotating mass. These simplifications affect the accuracy of the outcomes of the model.

The EOMs for these newly created systems are derived using the Lagrange method. Again, the derivation was executed in steps to reduce complexity, resulting in a robust method for deriving the EOMs. The derivation results in much simpler EOMs compared to the EOMs derived during the development of the detailed model.

Subsequently, two numerical MATLAB models suitable for analyzing the physics of offshore lifting operations and the motion control system for the load are developed. After the creation of the numerical model in MATLAB, the validity of the model's results was evaluated through several verification cases. All results within the verification cases, were demonstrated to be valid, suggesting the model is likely accurate. Compared to the MATLAB models created for the detailed model, the MATLAB models of the analysis model are simpler and therefore understanding what happens during a simulation is easier. This results in more straightforward analyses.

The numerical MATLAB models are converted into Simulink models. Within the Simulink environment, parameters for the motion control system are chosen and a PD-controller for the winch is designed. This winch controller demonstrated effectiveness for both setpoints. Additionally, a novel control system is developed that uses the motion of the load as input and directly manages the winch motion without measuring the motion of the winch.

In the section detailing controller design phases, it is highlighted that the controllers are designed to function properly but are not optimized. The controllers and setpoints are designed within specific scenarios. These facts imply that the controllers might perform differently across scenarios. In some situations, certain controllers might not function effectively, indicating that controller performance can vary due to the controller being not designed for the specific scenario. This variability can influence the results when comparing different scenarios. The effect of this on the analysis is discussed in Section 7.2.5.

The Simulink model serves as a tool for analyzing offshore lifting operations, either with or without a motion control system. For example, by changing the weight of the winch or the load, as done in Chapter 6.2, multiple outcomes can be observed. Additionally, factors such as the stiffness and damping ratio of the tugger cable, as well as different control methods, inputs and parameters, can be adjusted. While the model serves various purposes, some limitations exist. The current assumption is that the control loop comprises only a setpoint, a controller, and the physics of the winch and load. This overlooks other potential influences, such as a motor for the winch. This assumption may affect the accuracy of the model when comparing its results to real-world situations. Additionally, high-frequency vibrations might increase simulation time, but this issue is infrequently encountered during model execution.

The computation time of the analysis model is significantly reduced when comparing with the detailed model, making it a more efficient means for scrutinizing control facets. The comparison between both models was conducted under constant tension mode, yielding comparable outcomes. Consequently, it is inferred that the analysis model serves as a more efficient substitute for the detailed model concerning the objectives of this thesis. Employing the analysis model substantially reduces the required time for analysis. As the results align within the same magnitude, they may be used for assessing control aspects. However, the models were exclusively evaluated under constant tension mode only. When using the analysis model for different objectives it would be wise to investigate the accuracy of its results compared to those of the detailed model.

7.2. Analysis of the control methods and input

The results of the comparison of control methods and inputs are summarized and discussed in this section. Thereafter, the effect of the controllers and the different scenarios on the outcomes of this analysis is discussed.

7.2.1. Comparison of the load and winch sensor

Table 7.1 presents the comparison between the improvement factors when using the load sensor versus the winch sensor. Out of 72 scenarios, 61 favored the load sensor, 8 favored the winch sensor, and in 3 scenarios, neither sensor showed superiority.

Control method	Load sensor	No difference	Winch sensor	Number of scenarios
Maximum force setpoint	19	2	3	24
Motion control setpoint	21	0	3	24
Combined controller	21	1	2	24
Total	61	3	8	72

Table 7.1: Comparison between the improvement factors when using the load sensor versus the winch sensor

When assessing Table 6.6, it is seen that the load sensor enhances the motion control system's performance in the majority of scenarios. However, in a significant number of the scenarios, the difference in the improvement factors between the load sensor and the winch sensor never exceeds 15%. This implies that the choice of sensor slightly improves the system when the maximum force setpoint is applied. In contrast, the motion control setpoint shows that the improvement factor difference between the two sensors can be substantial, with several cases surpassing 100%. In two scenarios, the load sensor results in an undesirable response, making the winch sensor the more favorable choice.

To summarize, the results show that the load sensor generally provides a better response than the winch sensor across multiple scenarios. In most cases, the improvement factor differences between the two sensors remain within 15%. Occasionally, there are significant differences, favoring either sensor. Based on the presented results, the load sensor appears more likely to be the optimal choice in the scenarios addressed in this thesis.

The difference in performance of the system arises from difference inputs when either the winch or load sensor is used. As explained in section 3.3.3, the use of the winch sensor comes with the assumption that the winch's motion is directly proportional to that of the load, which is not necessarily true. One reason for this, is the existence of dissimilar natural frequencies within the winch, the tugger cable, and the load, resulting in different longitudinal oscillations. Moreover, intervals of cable slack cause temporal uncertainties in the motion of the load. In contrast, the use of the load sensor eliminates any uncertainties about the motion of the load, leading to a more precise measurement. This explains the superiority of the results when using the load sensor.

7.2.2. Comparison of motion control setpoint and maximum force setpoint

Table 7.2 presents the comparison between the improvement factors when using the motion control setpoint versus the maximum force setpoint. The findings suggest that the motion control setpoint generally performs better than the maximum force setpoint when utilizing the load sensor. However, with the winch sensor, the maximum force setpoint often outperforms the motion control system, though the margin of superiority is less pronounced than of the motion control sensor in combination with the load sensor. In 48 scenarios, 28 favored the motion control setpoint, while 20 favored the maximum force setpoint. This indicates a slight advantage for the motion control setpoint.

Sensor	Motion control setpoint	No difference	Maximum force setpoint	Number of scenarios
Winch	10	0	14	24
Load	18	0	6	24
Total	28	0	20	48

Table 7.2: Comparison between the improvement factors when using the motion control setpoint versus the maximum force setpoint

When examining Table 6.7, significant differences in the improvement factor among various control methods are observed. These differences exceed 20% in most scenarios and even go beyond 50% in several cases. In some situations, these larger differences favor the maximum force setpoint, while in others, they favor the motion control setpoint. As a result, no clear dominance appears in the magnitude of these improvement factor differences.

In conclusion, the motion control setpoint offers superior performance with the load sensor. Conversely, the maximum force setpoint performs better with the winch sensor. The latter combination describes actually the current damping tugger system. However, the latter's advantage is less pronounced than the former's. Nevertheless, the motion control system shows dominance in combination with the load sensor and the maximum force setpoint shows superiority in combination with the winch sensor. The overall assessment leans towards the motion control setpoint.

7.2.3. Comparison of motion control setpoint and combined controller

Table 7.3 presents the comparison between the improvement factors when using the combined controller versus the motion control setpoint. It is clearly visible that the motion control setpoint outperforms the combined controller when the load sensor is applied, while the combined controller shows superiority when the winch sensor is applied. Out of 48 scenarios, 20 favored the combined controller and 27 favored the motion control setpoint, and in 1 scenario, neither control method showed superiority.

When examining Table 6.8, it becomes evident that the choice of the sensor has large impact on the performance of the distinct control methods. When using the winch sensor, the combined controller outperforms the motion control setpoint in many instances. The improvement factors for the motion con-

control setpoint are substantial, often surpassing 20% in numerous scenarios. However, when using the load sensor, significant differences in improvement factors towards the motion control setpoint are seen. Consequently, there is no evident superiority in the magnitude of these improvement factor differences.

In conclusion, the motion control setpoint offers superior performance with the load sensor. Conversely, the combined controller performs better with the winch sensor. The overall assessment leans slightly towards the motion control setpoint.

Sensor	Combined controller	No difference	Motion control setpoint	Number of scenarios
Winch	18	0	6	24
Load	2	1	21	24
Total	20	1	27	48

Table 7.3: Comparison between the improvement factors when using the combined controller versus the motion control setpoint

7.2.4. Comparison of maximum force setpoint and combined controller

When examining Table 6.9, it is evident that the majority of differences in improvement factors are below 5%, with 11 scenarios indicating no difference in improvement factors. The exception is for scenarios with a winch sensor and a load weighing 10,000 mT. As the majority of the improvement factor differences approach zero, this comparison does not clearly show a superior control method.

7.2.5. Limitations of analysis

In Section 7.1.2, the effect of controllers being designed for a single scenario is discussed. To minimize this effect during the analysis of different controller methods and inputs the ranges of varying parameters are centred around values for which the controllers are designed. Additionally, the analysis is done within a wide range of scenarios and the performance is checked for every scenario, leading to counting only one unstable response. Given these measures, the controllers are deemed suitable for this analysis and used for this analysis.

Furthermore, the scenarios examined during the analysis are fictional. In numerous cases, certain control aspects showed superiority. However, before confirming that one control aspect is genuinely better than another, further research is necessary, for instance simulating the effects of control aspects in real-world scenarios and testing them in actual operations.

Lastly, during the creation of the alternative controller inputs, described in section 3.3.3, the decision has been made to retain velocity as the primary unit for the controller input. This choice has been made due to the alignment between the current system's use of velocity as a control input and the velocity being in phase with the desired force in the cable. An in-phase input facilitates a more direct setpoint calculation in contrast to the utilization of out-of-phase units such as displacement or acceleration. However, an exploration of the effects of using displacement or acceleration as controller inputs has not been conducted. It is advisable to do an investigation into the consequences of employing these parameters as controller input variables. Furthermore, an exploration of the impact of employing higher-order derivatives, such as jerk or snap, could also be done. To that extend, it should be noted that each second successive derivative of velocity, is in phase with the desired force in the load.

7.2.6. Evaluation of the results of the analysis

The load sensor provides a better response than the winch sensor in most scenarios. In most situations, the improvement factors between the two sensors differ by less than 15%. Occasionally, there is a significant difference, which can favor either sensor. Nevertheless, it is evident that the use of the load sensor leads to a better performance of the motion control.

When the load sensor was incorporated, the motion control setpoint, combined with the winch sensor, the performance of the motion control system was superior. However, using the winch sensor,

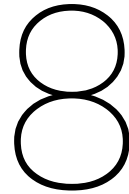
both the maximum force setpoint and the combined controller yielded a better performance of the motion control system than the motion control setpoint did. No distinct advantage was observed between the maximum force setpoint and the combined controller.

In conclusion, the motion control system performed better with the load sensor than with the winch sensor. When examining the control method, the motion control setpoint in combination with the winch controller demonstrated the best performance with the load sensor. Conversely, the results for both the maximum force setpoint and the combined controller were generally superior to the motion control system when the winch sensor was used.

7.3. Evaluation of Heerema MC's damping tigger system

Regarding Heerema MC's damping tigger system, it is assumed that the motions of the load and the winch are identical, as described in Section 3.2.1. However, in the investigated scenarios within this thesis, these motions differ. From this, it is concluded that incorporating a different sensor could potentially improve the performance of the currently used damping tigger system. Therefore, it is recommended to do more research on the incorporation of a load sensor within the damping tigger system.

This currently used damping tigger system incorporates a setpoint calculation in the form of the maximum force setpoint, as described in Section 3.2.1. The scenarios assessed in this thesis indicate that this calculation method is effective in combination with the winch sensor. However, when integrating the load sensor, the motion control setpoint calculation demonstrates superior performance of the damping tigger system. In conclusion, the selection of the control method depends on the sensor choice. If the load sensor is incorporated, it is recommended to conduct further exploration on the use of alternative control methods, especially on a control method incorporating a setpoint calculation with the form of a motion control setpoint.



Conclusion

In this thesis, a model suitable for analysing multiple control aspects, is developed successfully. This analysis model was subsequently used for an analysis on various control methods and input methods. The conclusions drawn in this thesis are outlined below.

8.1. Models

Initially, a model was created that is suitable for the analysis of different control aspects. This was done by first creating a detailed model that represents the physics within an offshore lifting operation. The outcomes of this detailed model were subsequently evaluated with verification cases. However, the computation time of the detailed model turned out to be excessive, making the detailed model unsuitable for an analysis of the different control aspects. Therefore, a new model was created, called the analysis model.

Consequently, a second model, denoted as the analysis model, was created. In its creation, several insights obtained during the development of the detailed model were used. These insights encompassed various simplifications that could be applied without significantly altering the system's dynamics.

Thanks to these simplifications, the computation time of the analysis model is significantly reduced, making it a much more efficient tool for analyzing the impacts of the various controller aspects. A comparative evaluation of the outcomes produced by the analysis model and the detailed model was executed under constant tension conditions. Remarkably, both outcomes show comparable results. From this, it was concluded that the complexity of the detailed model could be reduced effectively for the objective of this thesis, leading to a much more effective model for the analysis of the control aspects.

8.2. Control methods and inputs

The analysis examined different control methods and control inputs. The specific control methods investigated include the maximum force setpoint and the motion control setpoint, both in combination with the winch controller, and a combined controller, which uses the motion of the load as input and directly controls the motion of the winch. The analysis was based on multiple hypothetical scenarios and led to an overview of the difference in performance when using different control aspects within various scenarios. To validate the performance of the motion control system with the use of the different control aspects outside these scenarios, additional research is required.

8.2.1. Control inputs

The use of the winch motion sensor comes with the assumption that the motion of the winch maintains a direct correlation with that of both the tugger cable and the lifted load. In contrast, when using the load motion sensor, any uncertainties within the relation between the load's motion and the winch or tugger cable are eliminated, as the output from the load motion sensors precisely tracks the dynamics of the load's motion.

When interpreting the outcomes derived from the analysis of control aspects, the use of the load motion sensor often yields a more favorable response than the winch motion sensor. Although the improvement rates between the two sensors are less than 15% in many situations, it is evident that use of the load sensor improves the performance of the motion control system in the scenarios analyzed within this thesis.

Consequently, it is concluded that the motion of the load and the motion of the winch are not directly proportional. In this specific scenario, relying only on the winch's motion to accurately track the load's motion is not accurate enough. Hence, it is recommended to incorporate a load motion sensor capable of tracking the load's motion. By using this load motion sensor, the controller's input becomes more accurate, thereby leading to an improved system performance.

8.2.2. Control methods

Three different control methods are tested: the maximum force setpoint, the motion control setpoint and the combined controller. The first two are used in combination with a winch controller, while the latter method merges the setpoint calculation with the winch controller to one single controller. It should be noted that the current damping tugger system functions with a control method in the form of the maximum force setpoint and the winch motion is the controller input.

The incorporation of the load motion sensor lead to superior performance of the motion control system when the motion control setpoint was used. In contrary, both the use of the maximum force setpoint and the combined controller showed better performance of the motion control system compared to the use of the motion control setpoint, when the winch sensor was used. There was no clear advantage between the maximum force setpoint and the combined controller.

9

Recommendations

In this thesis, the effects of various control methods and controller inputs on a motion control system were examined and the results were assessed. Based on the evaluation of these results, two primary recommendations are provided. The provided recommendations could lead to an improved performance of Heerema MC's currently used damping tigger system. This improvement would imply a decrease of the undesired motions of the lifted loads during offshore operations, ensuring safer and more efficient offshore lifting operations.

9.1. Control inputs

The first recommendation regards the motion sensor of a motion control system. Within Heerema MC's currently used damping tigger system, the motion of the winch is measured and converted to the motion of the load, under the assumption that it is directly proportional to that of the load. After evaluating various control methods and controller inputs, it became evident that in the assessed scenarios, the motion of the winch and the load were not consistently proportional. Notably, the motion control system exhibited superior performance in nearly all assessed scenarios when the load motion sensor was used. The use of the load sensor eliminates possible uncertainties about the motion of the load. Consequently, this leads to a more accurate control input, what improves the performance of the motion control system. Hence, it is recommended to use a sensor that measures the motion of the load instead of the motion of the winch.

When deciding to implement the load motion sensor, it is recommended to conduct further research concerning its performance in scenarios beyond those examined in this thesis. Moreover, additional investigation is recommended about the sensor type and the implementation method. For instance, displacement sensors and acceleration sensors may yield favorable outcomes, which were not evaluated in this thesis. Therefore, it is recommended to investigate the effects of these sensor types as well.

Conversely, the current motion control system used by Heerema MC relies on a winch motion sensor, as measuring the winch's motion is mostly more easier than measuring the motion of the load. This could be an argument for retaining the winch motion sensor. In that case, it must be accepted that the controller input is less accurate in comparison to the implementation of the load motion controller.

In summary, it is advised to use load motion sensor instead of a winch motion sensor. The use of the load motion sensor reduces uncertainties concerning the motion of the load, resulting in a more accurate control system input.

9.2. Control method

The second recommendation regards the control method of the motion control system. The analysed scenarios in this thesis indicate that the motion control setpoint calculation demonstrates superior performance when the load motion sensor is used. On the other hand, when the winch sensor is used, the maximum force setpoint and the combined controller method show superior results compared to when

the motion control setpoint is used. In conclusion, the selection of a control method relies, among other factors, on the selection of the sensor in use.

In the previous section, it is argued that the use of the load motion sensor yields better performance of the motion control system. When using this sensor, it is the motion control setpoint method that demonstrates the most promising results and is thus recommended for controller design. Conversely, when deciding to retain with the winch motion sensor, for the sake of simplicity, the use of the maximum force setpoint or the combined controller method is recommended.

Moreover, this thesis examines only three control methods, whereas alternative methods, such as adaptive control, may also prove to be effective. Nevertheless, this thesis showed that different control methods yield varying performance outcomes, depending on control input values and control parameters. Consequently, an investigation into the performance of other control methods is recommended, along with the comparison of different control strategies across various situations and objectives.

In conclusion, the choice of the control method depends on the selection of the sensor in use. Should the load motion sensor be implemented, as suggested in section 9.1, it is recommended to design a control system based upon the motion control setpoint method. However, should the decision be made to stay with the winch sensor, the use of a control method in the form of the maximum force setpoint or the combined controller is recommended. In both scenarios, further exploration of alternative control methods is recommended to ultimately determine the optimal approach.

References

- [1] *Heerema breaks lifting record with 17,000 metric ton TotalEnergies' Tyra TEG module*. 2023. URL: <https://www.heerema.com/news/heerema-breaks-lifting-record-with-17000-metric-ton-totalenergies-tyra-teg-module> (visited on 05/09/2023).
- [2] *Bijzondere gevaartes zij aan zij in de Rotterdamse haven*. 2020. URL: <https://www.ad.nl/rotterdam/bijzondere-gevaartes-zij-aan-zij-in-de-rotterdamse-haven-af074fee/> (visited on 05/09/2023).
- [3] Heerema Marine Contractors. In-house knowledge. 2023.
- [4] Orcina. *OrcaFlex Help*. 2023.
- [5] Waterloo Maple Inc. *Maple User manual*. 2014.
- [6] The MathWorks Inc. *Matlab & Simulink Support*. 2023.
- [7] Heerema Marine Contractors. "LiftDyn Manual". 2018.
- [8] Peter Enevoldsen and Mark Z Jacobson. "Data investigation of installed and output power densities of onshore and offshore wind turbines worldwide". In: *Energy for Sustainable Development* 60 (2020).
- [9] Taha Aborgela et al. "Heavy lift semi-submersible ships utilization in offshore wind turbines industry". In: *Energy Reports* 8 (2022).
- [10] Bo Yang et al. "A feasibility study of reducing scour around monopile foundation using a tidal current turbine". In: *Ocean Engineering* 220 (2021).
- [11] Alessandro Singlitico, Jacob Østergaard, and Spyros Chatzivasileiadis. "Onshore, offshore or in-turbine electrolysis? Techno-economic overview of alternative integration designs for green hydrogen production into Offshore Wind Power Hubs". In: *Renewable and Sustainable Energy Transition* 1 (2021).
- [12] Eva Topham and David Mcmillan. "Sustainable decommissioning of an offshore wind farm". In: *Renewable Energy* 255 (2016).
- [13] Iván Pineda and Kristian Ruby. *The European offshore wind industry - key trends and statistics 2015*. Tech. rep. 2016.
- [14] Jonas Pagh Jensen. "Evaluating the environmental impacts of recycling wind turbines". In: *Wind Energy* 22 (2 Feb. 2019), pp. 316–326.
- [15] Eva Topham et al. "Challenges of decommissioning offshore wind farms: Overview of the European experience". In: *Journal of Physics: Conference Series* 1222 (1 May 2019).
- [16] Priscila Da Cunha et al. "Decommissioning of offshore oil and gas platforms: A systematic literature review of factors involved in the process". In: *Ocean Engineering* 255 (2022).
- [17] Dianne L. McLean et al. "Influence of offshore oil and gas structures on seascape ecological connectivity". In: *Global Change Biology* 28 (11 June 2022).
- [18] IRENA. "Renewable power generation costs in 2018". In: (2019).
- [19] Zhiyu Jiang. "Installation of offshore wind turbines: A technical review". In: *Renewable and Sustainable Energy Reviews* (2021).
- [20] *History made by Heerema with offshore testing campaign*. 2023. URL: <https://www.heerema.com/insights/history-made-by-heerema-with-offshore-testing-campaign> (visited on 05/03/2023).
- [21] Michiel A J Uit Het Broek et al. "Evaluating resource sharing for offshore wind farm maintenance: The case of jack-up vessels". In: *Renewable and Sustainable Energy Reviews* 109 (2020).

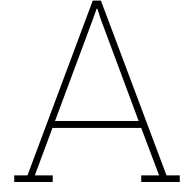
- [22] Mengning Wu et al. "Prediction of short-term wind and wave conditions for marine operations using a multi-step-ahead decomposition-ANFIS model and quantification of its uncertainty". In: *Ocean Engineering* 188 (Sept. 2019).
- [23] Kurt Thompsen. *Offshore Wind: A Comprehensive Guide to Successful Offshore Wind Farm Installation*. Academic Press Inc, 2014, pp. 203–217.
- [24] I A A Smith et al. "Limiting Motions for Jack-Ups Moving onto Location". In: *Marine Structures* (1995).
- [25] Yuna Zhao et al. "Numerical study on the feasibility of offshore single blade installation by floating crane vessels". In: *Marine Structures* 64 (2018).
- [26] *Heerema installs DOT wind turbine*. 2018. URL: <https://www.heavyliftnews.com/heerema-installs-dot-wind-turbine/> (visited on 05/04/2023).
- [27] Yaohua Guo, Haijun Wang, and Jijan Lian. "Review of integrated installation technologies for offshore wind turbines: Current progress and future development trends". In: *Review of integrated installation technologies for offshore wind turbines: Current progress and future development trends* 267 (2022).
- [28] Amrit Shankar Verma et al. "Impact assessment of a wind turbine blade root during an offshore mating process". In: *Engineering Structures* 180 (Feb. 2019), pp. 205–222.
- [29] "Numerical modeling and analysis of the dynamic motion response of an offshore wind turbine blade during installation by a jack-up crane vessel". In: *Ocean Engineering* 165 (Oct. 2018), pp. 353–364.
- [30] Amrit Shankar Verma et al. "A review of impact loads on composite wind turbine blades: Impact threats and classification". In: *Renewable and Sustainable Energy Reviews* 178 (May 2023).
- [31] David Vågnes et al. "Low-Height Lifting System for Offshore Wind Turbine Installation: Modelling and Hydrodynamic Response Analysis Using the Commercial Simulation Tool SIMA". In: *Proceedings of the International Conference on Offshore Mechanics and Arctic Engineering - OMAE* 1 (Dec. 2020).
- [32] Jiafeng Xu et al. "Virtual Prototyping of a Low-Height Lifting System for Offshore Wind Turbine Installation". In: *Proceedings of the International Conference on Offshore Mechanics and Arctic Engineering - OMAE* 9 (Dec. 2020).
- [33] Zhengru Ren et al. "Model-free anti-swing control of complex-shaped payload with offshore floating cranes and a large number of lift wires". In: *Ocean Engineering* 228 (May 2021).
- [34] Peter Jacobs. *Evaluation of transient lift loads during a decommissioning operation with a crane vessel*. 2017.
- [35] Nur Dalila Alias and Yun li Go. "Decommissioning platforms to offshore solar system: Road to green hydrogen production from seawater". In: (2023).
- [36] Ann Scarborough Bull and Milton S. Love. "Worldwide oil and gas platform decommissioning: A review of practices and reefing options". In: *Ocean Coastal Management* 168 (Feb. 2019), pp. 274–306.
- [37] Meng Zhai et al. "Observer-based adaptive fuzzy control of underactuated offshore cranes for cargo stabilization with respect to ship decks". In: *Mechanism and Machine Theory* (175).
- [38] Floris Goerlandt and Jakub Montewka. "Maritime transportation risk analysis: Review and analysis in light of some foundational issues". In: *Reliability Engineering System Safety* 138 (June 2015), pp. 115–134.
- [39] Shahrzad Faghih-Roohi, Min Xie, and Kien Ming Ng. "Accident risk assessment in marine transportation via Markov modelling and Markov Chain Monte Carlo simulation". In: *Ocean Engineering* 91 (Nov. 2014), pp. 363–370.
- [40] Thomas Poulsen and Rasmus Lema. "Is the supply chain ready for the green transformation? The case of offshore wind logistics". In: *Renewable and Sustainable Energy Reviews* (2017).
- [41] Ravi Kumar Pandit, David Infield, and James Carroll. "Incorporating air density into a Gaussian process wind turbine power curve model for improving fitting accuracy". In: *Wind Energy* 22 (2 Feb. 2019), pp. 302–315.

- [42] Ricardo Martins Campos et al. "Global assessments of the NCEP Ensemble Forecast System using altimeter data". In: *Ocean Dynamics* 70 (3 Mar. 2020), pp. 405–419.
- [43] Quillon Harpham et al. "A Bayesian method for improving probabilistic wave forecasts by weighting ensemble members". In: *Environmental Modelling Software* (2016).
- [44] James W. Taylor and Jooyoung Jeon. "Probabilistic forecasting of wave height for offshore wind turbine maintenance". In: *European Journal of Operational Research* 267 (3 June 2018), pp. 877–890.
- [45] Mengning Wu, Zhen Gao, and Yuna Zhao. "Assessment of allowable sea states for offshore wind turbine blade installation using time-domain numerical models and considering weather forecast uncertainty". In: *Ocean Engineering* 260 (Sept. 2022).
- [46] Qing Yu et al. "Geometrical risk evaluation of the collisions between ships and offshore installations using rule-based Bayesian reasoning". In: *Reliability Engineering System Safety* 210 (2021).
- [47] Adrian Stetco et al. "Machine learning methods for wind turbine condition monitoring: A review". In: *Renewable Energy* 133 (Apr. 2019), pp. 620–635.
- [48] D. Cevalco, S. Koukoura, and A. J. Kolios. "Reliability, availability, maintainability data review for the identification of trends in offshore wind energy applications". In: *Renewable and Sustainable Energy Reviews* 136 (Feb. 2021).
- [49] Koch, baluku, and Habakurama. "The challenges of building inner sea offshore wind farms-the cases of Lillgrund and Anholt". In: *Proceedings of the 9th Nordic Conference on Construction Economics and Organization* (2017).
- [50] *Control of reel handling winches*. Tech. rep. order of damping tuggers by Heerema. Huisman Equipment B.V., May 2011.
- [51] Geert Meskers and Radboud van Dijk. *A damping tugger system for offshore heavy lifts*. Tech. rep. Heerema Marine Contractors, 2012.
- [52] Nick Sanders. "Work-ability increase using tugger control". MA thesis. Delft University of Technology, 2019.
- [53] Thijs Bron. *Model-free Positioning Control of a Payload by use of Wires Thesis report*. 2022.
- [54] Heerema Engineering Solutions. In-house knowledge. 2023.
- [55] Henk Lageveen. "Modelling and Steering of Tuggerwinch". MA thesis. Delft University of Technology, Apr. 2014.
- [56] "Technologies, levels and directions of crane-lift automation in construction". In: *Automation in Construction* 153 (Sept. 2023).
- [57] "Measurement system design for sway motion based on image sensor". In: *Proceedings of the 2009 IEEE International Conference on Networking, Sensing and Control, ICNSC 2009* (2009), pp. 185–188.
- [58] Tianlei Wang et al. "Visual Tracking of Dynamic Overhead Cranes via Sparse Representation". In: *Procedia Computer Science* 131 (2018).
- [59] Aravinda S. Rao et al. "Real-time monitoring of construction sites: Sensors, methods, and applications". In: *Automation in Construction* 136 (Apr. 2022).
- [60] Patrick Hübner et al. "Evaluation of HoloLens Tracking and Depth Sensing for Indoor Mapping Applications". In: *Sensors 2020, Vol. 20, Page 1021* 20 (4 Feb. 2020).
- [61] Tarek Omar and Moncef L. Nehdi. "Data acquisition technologies for construction progress tracking". In: *Automation in Construction* 70 (Oct. 2016), pp. 143–155.
- [62] Marianna Kopsida and Ioannis Brilakis. "Real-Time Volume-to-Plane Comparison for Mixed Reality-Based Progress Monitoring". In: *Journal of Computing in Civil Engineering* 34 (4 July 2020).
- [63] Liju Joshua and Koshy Varghese. "Accelerometer-Based Activity Recognition in Construction". In: *Journal of Computing in Civil Engineering* 25 (5 Sept. 2011), pp. 370–379.

- [64] Moustafa I. Ibrahim et al. "The association between pentraxin 3 in maternal circulation and pathological intrauterine fetal growth restriction". In: *European Journal of Obstetrics Gynecology and Reproductive Biology* 185 (Feb. 2015).
- [65] Stephen Hawking. *A Brief History of Time*. New York: Bantam Books, 1998.
- [66] Samir El-Omari and Osama Moselhi. "Integrating automated data acquisition technologies for progress reporting of construction projects". In: *Automation in Construction* 20 (6 Oct. 2011).
- [67] Frédéric Bosché et al. "The value of integrating Scan-to-BIM and Scan-vs-BIM techniques for construction monitoring using laser scanning and BIM: The case of cylindrical MEP components". In: *Automation in Construction* 49 (Jan. 2015), pp. 201–213.
- [68] Fei Dai et al. "Comparison of Image-Based and Time-of-Flight-Based Technologies for Three-Dimensional Reconstruction of Infrastructure". In: *Journal of Construction Engineering and Management* 139 (1 Jan. 2013), pp. 69–79.
- [69] Yi Chen et al. "RF-IDH: An intelligent fall detection system for hemodialysis patients via COTS RFID". In: *Future Generation Computer Systems* 113 (Dec. 2020), pp. 13–24.
- [70] Konstantinos Domdouzis, Bimal Kumar, and Chimay Anumba. "Radio-Frequency Identification (RFID) applications: A brief introduction". In: *Advanced Engineering Informatics* 21 (Oct. 2007), pp. 350–355.
- [71] Islam Ashour et al. "Performance of global navigation satellite systems (GNSS) in absence of GPS observations". In: *Ain Shams Engineering Journal* 13 (2 Mar. 2022).
- [72] Chenyu Xue and Panos A. Psimoulis. "Monitoring the dynamic response of a pedestrian bridge by using low-cost GNSS receivers". In: *Engineering Structures* 284 (June 2023).
- [73] Almat Raskaliyev, Sarosh Patel, and Tarek Sobh. "A dynamic model for GPS based attitude determination and testing using a serial robotic manipulator". In: *Journal of Advanced Research* 8 (2017), pp. 333–341.
- [74] Hisashi Osumi, Akinari Miura, and Shungo Eiraku. *Positioning of Wire Suspension System Using CCD Cameras*. 2005.
- [75] Ryan A Mckenzie and Rishad A Irani. "Motion compensation for maritime cranes during time-varying operations at the pendulum's natural frequency". In: *Mechanism and Machine Theory* 168 (2022).
- [76] Maokai Sun et al. "Multi-cable anti-swing system for cranes subject to ship excitation and wind disturbance: Dynamic analysis and application in engineering". In: *Ocean Engineering* 281 (2023).
- [77] Konrad Johan Jensen, Morten Kjeld Ebbesen, and Michael Rygaard Hansen. "Anti-swing control of a hydraulic loader crane with a hanging load". In: *Mechatronics* 77 (Aug. 2021).
- [78] Mohammad Saghafi Zanjani and Saleh Mobayen. "Event-triggered global sliding mode controller design for anti-sway control of offshore container cranes". In: *Ocean Engineering* 268 (Jan. 2023).
- [79] Hamed Moradi and Gholamreza Vossoughi. "State estimation, positioning and anti-swing robust control of traveling crane-lifter system". In: *Applied Mathematical Modelling* 39 (22 Nov. 2015).
- [80] Tianlei Wang et al. "Based on the two-dimensional air resistance bridge crane anti-swing control research". In: *Procedia Computer Science* 183 (Jan. 2021), pp. 175–181.
- [81] Iain A Martin and Rishad A Irani. "A generalized approach to anti-sway control for shipboard cranes". In: *Mechanical Systems and Signal Processing* (2021).
- [82] Qingxiang Wu et al. "Dynamic analysis and time optimal anti-swing control of double pendulum bridge crane with distributed mass beams". In: *Mechanical Systems and Signal Processing* 144 (2020).
- [83] Mariantonieta Gutierrez Soto and Hojjat Adeli. "Tuned Mass Dampers". In: *Arch Comput Methods Eng* 20 (2013), pp. 419–431.

- [84] Unal Aldemir, Arcan Yanik, and Mehmet Bakioglu. "Control of Structural Response Under Earthquake Excitation". In: *Computer-Aided Civil and Infrastructure Engineering* 27 (8 Sept. 2012), pp. 620–638.
- [85] Makita. *Principle of a Tuned Mass Damper*. 2023.
- [86] Julien Carlot. *Effects of a Tuned Mass Damper on Wind-Induced Motions in Tall Buildings*. 2012.
- [87] Zhenchuan Li et al. "A novel lever-arm tuned mass damper inerter (LTMDI) for vibration control of long-span bridges". In: *Engineering Structures* 293 (Oct. 2023).
- [88] Xiongjun Yang et al. "Physics-enhanced machine learning-based optimization of tuned mass damper parameters for seismically-excited buildings". In: *Engineering Structures* 292 (Oct. 2023).
- [89] Wolfgang Hintze, Marco Hinrichs, and Oliver Rosenthal. "Model based design of tuned mass dampers for boring bars of small diameter". In: *Procedia CIRP* 117 (2023).
- [90] Jiajun Zhang et al. "Design of parallel multiple tuned mass dampers for the vibration suppression of a parallel machining robot". In: *Mechanical Systems and Signal Processing* 200 (Oct. 2023).
- [91] Haonan Tian, Mohsen N Soltani, and Morten Eggert Nielsen. "Review of floating wind turbine damping technology". In: *Ocean Engineering* 278 (2023).
- [92] Tadashi Nagase. "Earthquake records observed in tall buildings with tuned pendulum mass damper". In: (2000).
- [93] Krzysztof Kecik and Andrzej Mitura. "Energy recovery from a pendulum tuned mass damper with two independent harvesting sources". In: *International Journal of Mechanical Sciences* 174 (May 2020).
- [94] Panagiota Atzampou et al. *Motion Control of a Pendulum via Magnetic Interaction*.
- [95] J K Woodacre, R J Bauer, and R A Irani. "A review of vertical motion heave compensation systems". In: *Ocean Engineering* 104 (2015).
- [96] Tim Ouwehand. "Earth-Fixed Heave Compensation". MA thesis. Delft University of Technology, 2020.
- [97] Serkan Beller and Hakan Yavuz. "Crane automation and mechanical damping methods". In: *Alexandria Engineering Journal* 60 (3 June 2021).
- [98] Puyang Zhang et al. "Hydrodynamic characteristics of the crane vessel-three-bucket jacket foundation coupling hoisting system during the process of lowering". In: *Ocean Engineering* 250 (2022).
- [99] D.J. Morin. *Introduction to Classical Mechanics*. Cambridge University Press, 2008.
- [100] How and Deyst. *Lecture 10: Friction in Lagrange's Formulation*. Lecture Notes. Massachusetts Institute of Technology. 2003.
- [101] Daan Jutten. *Coupled Dynamics of a Dual Lift Monopile Installation*. 2019.
- [102] Yuzhe Qian, Yongchun Fang, and Biao Lu. "Adaptive robust tracking control for an offshore ship-mounted crane subject to unmatched sea wave disturbances". In: *Mechanical Systems and Signal Processing* 114 (2018).
- [103] Geert Meskers. *Crane stiffness*. Heerema Marine Contractors. July 2019.
- [104] Yuzhe Qian and Yongchun Fang. "Switching Logic-Based Nonlinear Feedback Control of Offshore Ship-Mounted Tower Cranes: A Disturbance Observer-Based Approach". In: *IEEE Transactions on Automation Science and Engineering* 16 (2019).
- [105] Erika Abraham. *A Toolbox for the Reachability Analysis of Hybrid Systems using Geometric Approximations (HyPro): Spring Pendulum*. 2023.
- [106] Vladimir Dobrushkin. *Mathematica tutorial for the Second Course. Part III: Spring Pendulum*. Brown University.
- [107] MIT OpenCourseWare. *Classical Mechanics: Physical Pendulum*. Massachusetts Institute of Technology, 2022.
- [108] *Advanced Dynamics of Machines: Lagrange Equation*. Lecture Notes. University of Nottingham; Department of Mechanical, Materials and Manufacturing Engineering. 2008.

-
- [109] Heerema Marine Contractors. *Sleipnir, HMC Equipment*. Brochure. 2020. URL: <https://f.hubspotusercontent40.net/hubfs/8565747/HMC%20Equipment%20Folder%20-%20Sleipnir.pdf>.



Detailed model

This appendix corresponds to the detailed model described in Chapter 4. It provides explanations of standard parameters and outlines the verification cases for the detailed model. Additionally, information about the ODE solver in Simulink is provided. The EOMs for the detailed model can be found in appendix D.

A.1. Standard parameters

In this section, the standardized parameter values are explained that are used within the detailed model. The gravitational constant g is set to the standard value of 9.81 m/s^2 . Within Heerema MC, both the stiffness and damping constants for the crane cable are standard used values of $k_{tm} = 4.85 \text{ MN/m}$ and $c_{tm} = 10 \text{ kNs/m}$, respectively [103]. These constants are also used for the stiffness and damping constant of the crane cable within this thesis. It has been observed that, in practice, the cable stiffness is often larger than this value. However, the underlying reasons for this phenomenon is not well understood. Nonetheless, for the purposes of this project, the value of 4.85 MN/m is an acceptable approximation of the cable stiffness. The weight of the load is configured at 50 mT , a value consistent with an offshore wind turbine foundation.

The initial length of the tugger cable is defined as 60 m , subject to alteration by winch rotation. Within the parameters of Heerema MC, the tugger cable's stiffness k_c is given as 2.0 kN/m [3]. As for the damping coefficient of the tugger cable c_c , no established value exists within Heerema MC. Consequently, it is assumed to match the crane cable's damping constant of 10 kNs/m . The mass per unit length of the tugger cable stands at 73 kg/m , and the winch radius r_w measures 1.5 m [3]. Lastly, the crane tip and winch coordinates are chosen such that it represent realistic dimensions.

A.2. Verification cases of the detailed model

In this section, the outcomes of the free lifting system, the damping tugger system, and the controlled lifting system are evaluated through various verification cases. Certain standard parameters have been modified for the sake of clarity.

A.2.1. Vessel motions and tip motions

Wave elevation and current influence vessel motion. Due to a rigid connection between the vessel center and the crane tip, motion from the vessel transfers directly to the tip. This transfer is demonstrated through this through basic translation and rotation equations:

$$x_t = x_s(t) + l_x \cdot \cos(\theta_s(t)) - l_y \cdot \sin(\theta_s(t)) \quad (\text{A.1})$$

$$y_t = y_s(t) + l_x \cdot \sin(\theta_s(t)) + l_y \cdot \cos(\theta_s(t)) \quad (\text{A.2})$$

The horizontal distance l_x and vertical distance l_y of the rigid connection measure 40 m and 100 m , respectively. First, the impact of horizontal vessel motion x_s and vertical vessel motion y_s on tip motion

are investigated. Figure 4.3 presents the input vessel motions, and Figure A.2 displays the consequential tip motion. Both motions manifest identical amplitude and period, confirming direct transmission of vessel motion to tip motion when rotation is absent.

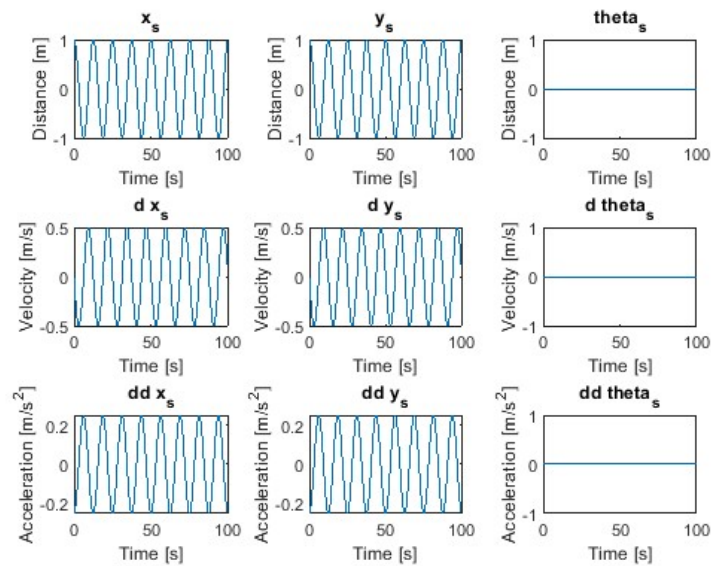


Figure A.1: The input vessel motions in x - and y -direction

Secondly, the impact of vessel rotation θ_s on tip motion undergoes examination. Figure A.3 depicts input vessel rotation θ_s , ranging between maximum values of 1 and -1 . Upon substituting these maximum θ_s values into Equations A.1 and A.2, the resultant maximum tip motion values are defined. These maximums align with the peaks shown in Figure A.4.

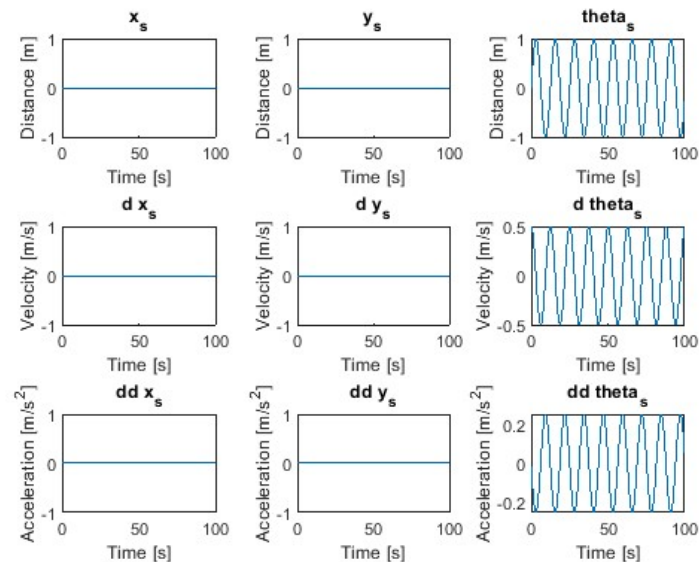


Figure A.3: The input vessel rotation in θ_s -direction

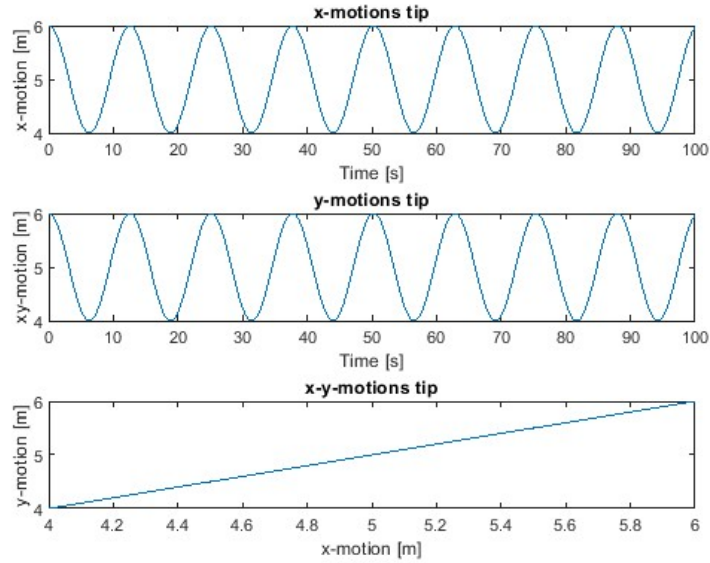


Figure A.2: The resulting motion of the crane tip, caused by both the horizontal vessel motion x_s and the vertical vessel motion y_s

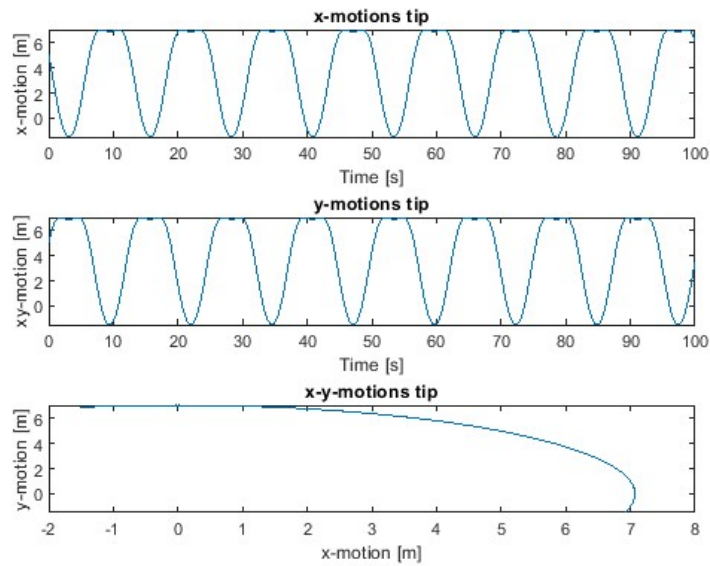


Figure A.4: The resulting motion of the crane tip, caused by both the horizontal vessel rotation θ_s

A.2.2. Free lifting system

First, the amplitude and period of the crane cable are tested. The pendulum motion is eliminated, leaving only vertical axial vibrations. The computed values for amplitude and period are then compared to the outcomes generated by the model. The calculated amplitude and period of the crane cable are:

$$r = \frac{m_o \cdot g}{k_{tm}} = 51.2 \text{ m} \quad (\text{A.3})$$

$$T_p = 2\pi \cdot \sqrt{\frac{m_o}{k_{tm}}} = 14.3 \text{ s} \quad (\text{A.4})$$

where m_o denotes the mass of the load which is 500 mT and k_{tm} displays the stiffness of the cable which is 100 kN/m in this case. Figure A.5 illustrates the elongation of the crane cable over time compared the calculated amplitude and period. Twice the calculated amplitude of 51.2 m leads to a maximum elongation of 102.4 m. It can be observed that the calculation align with the model outcomes.

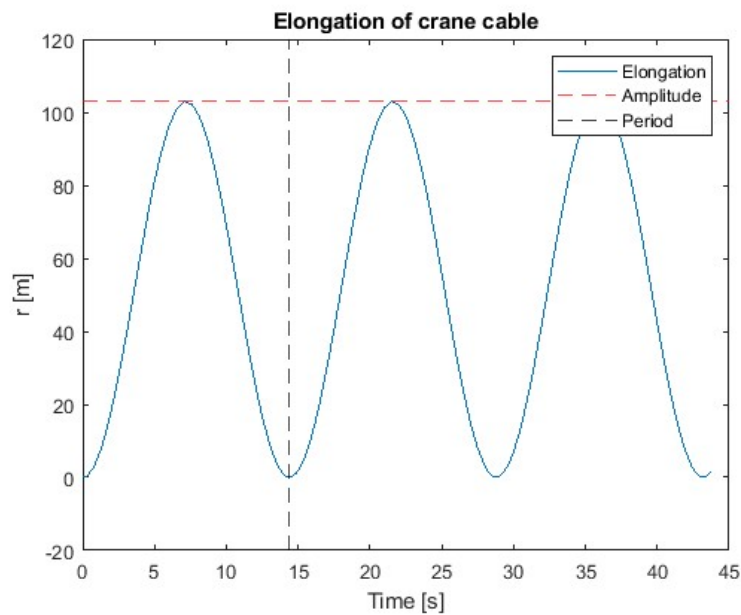


Figure A.5: The amplitude and period of the vibrating mass compared to the calculated values

To verify the motion of the elastic pendulum, two distinct experiments were conducted: one with relatively high stiffness and another with relatively low stiffness. In each experiment, the initial angle remained at $\theta_c = \frac{\pi}{4}$ rad. In the scenario with relatively high stiffness ($k = 200$ MN/m), elongation of the crane cable remained minimal. Therefore, the pendulum functions as a rigid cable pendulum, as illustrated in Figure A.6. Conversely, in the experiment with relatively low stiffness ($k = 2$ kN/m), significant elongation occurred in the crane cable. Consequently, the pendulum behaves as an elastic pendulum, as corroborated by Figure A.7.

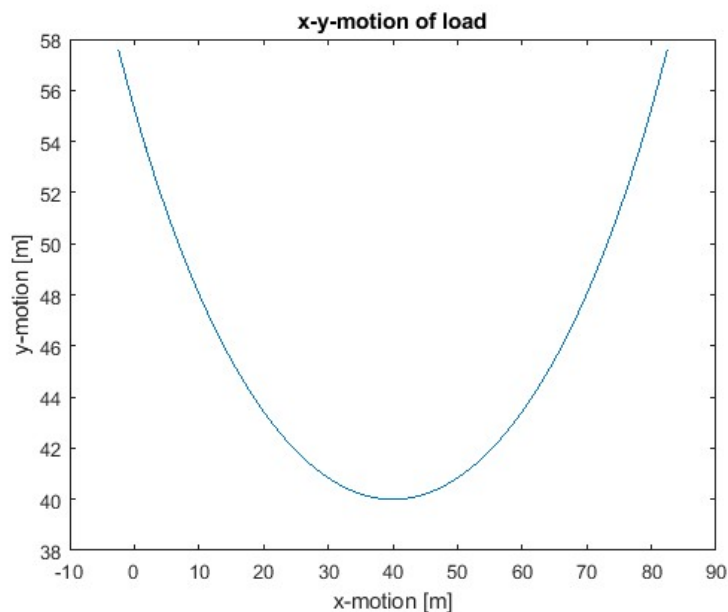


Figure A.6: The behaviour of the pendulum with increased stiffness

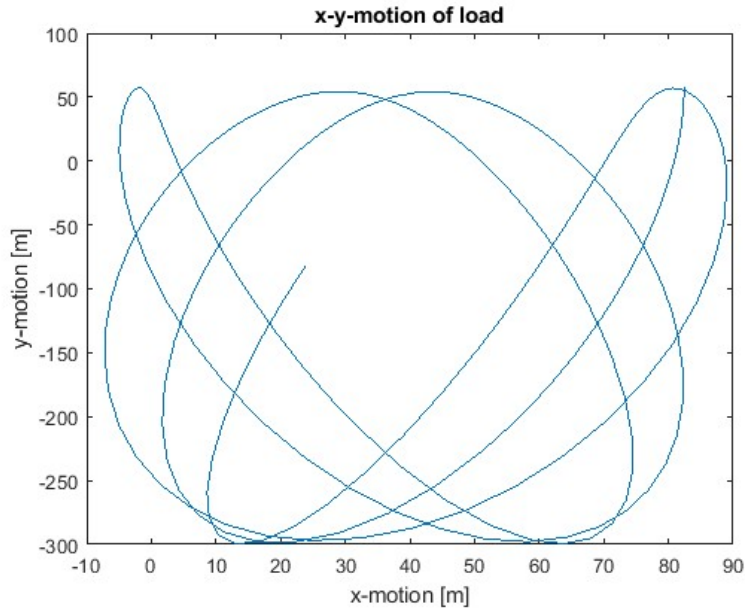


Figure A.7: The behaviour of the pendulum with decreased stiffness

Furthermore, the initial elongation of the crane cable is established at the equilibrium state, which is given by $r_c = \frac{m \cdot g}{k}$. Consequently, the mass remains motionless, with no vibration being observed. This phenomenon occurs because the system contains no potential or kinetic energy in the initial state, and no energy is added to the system.

A.2.3. The damping tugger system

Both the elongation of the two springs, represented by r_c and r_{s2} , as well as the angular displacement θ_k of the first spring, are investigated. Initially, the Y-coordinates for the winch and the load are equal. The initial conditions ensure that the cable mass starts at this vertical position. Due to the influence of potential energy, vertical oscillations in the cable mass take place, as depicted in Figure A.8. Both springs are equal resulting in equal elongations for both springs. Contrary to a simple sinusoidal motion, the elongation of the springs and the angular displacement of the first spring are complex. This complexity occurs due to lateral forces generated by both springs, which initiate the vertical velocity of the cable mass. These lateral forces continuously change, leading to non-sinusoidal motions for the springs' elongation and rotation.

In the second scenario, the steady-state conditions are tested. Gravity is restored to its original value, and the initial shift in horizontal position is undone and the springs are replaced by dissipating springs, exhibiting damping effects. Due to this damping effect, the system gradually approaches an equilibrium state, where spring 1 attains a specific elongation and angular orientation. Figure A.10 illustrates the system as it moves toward this equilibrium condition.

The steady-state values of the elongation and rotation of the springs are calculated as:

$$F_g = F_{n1} + F_{n2} = m_c \cdot g \quad (\text{A.5})$$

$$F_{n1} = \sin(\theta_{k-eq}) \cdot F_{k1} \quad (\text{A.6})$$

$$F_{k1} = k_1 \cdot x_1 \quad (\text{A.7})$$

$$r_{c-eq} = \frac{l_{s01}}{\cos(\theta_{k-eq})} - l_{s01} \quad (\text{A.8})$$

$$F_g = 2 \cdot \sin(\theta_{k-eq}) \cdot k_1 \cdot \left(\frac{l_{s01}}{\cos(\theta_{k-eq})} - l_{s01} \right) = m_c \cdot g \quad (\text{A.9})$$

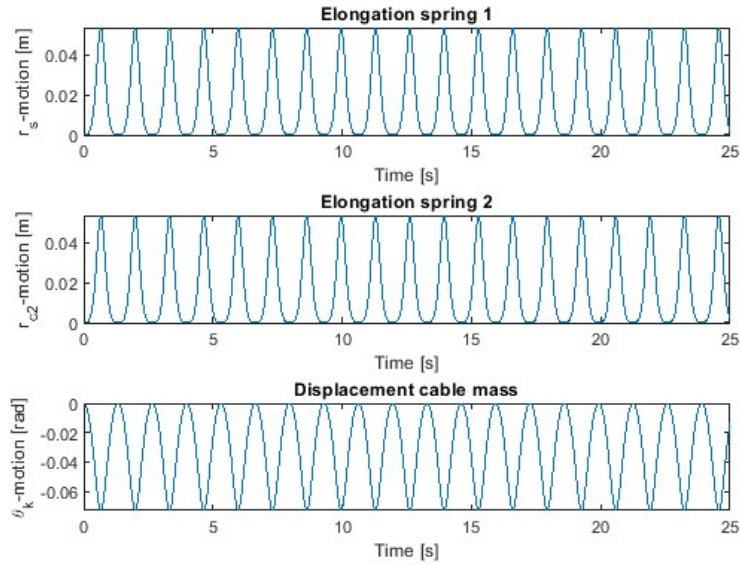


Figure A.8: The extension of springs 1 and 2 and the angle spring 1

where F_{nx} symbolizes the normal force, F_{kx} denotes the spring force, and l_{s0x} represents the initial length of either spring 1 or spring 2, which is 20 m in this case. The mass of the cable tugger m_c is 50 kg/m, leading to an initial mass of 2000 kg. Figure A.9 provides a visual representation of the spring geometry, incorporating the variables mentioned above. Solving equation A.9 leads to $\theta_k = 0.046$ rad. This is then incorporated into equation A.8, yielding $r_{c-eq} = 0.021$ meters. The red lines in Figure A.10 represent these outcomes. The motion damps out to the calculated values confirming the accuracy of the model.

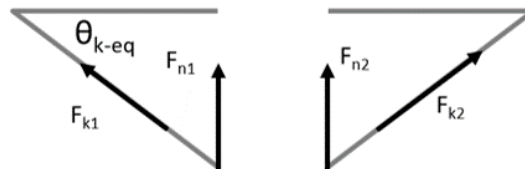


Figure A.9: The geometry of the springs

A.2.4. Controlled lifting system

The controlled lifting system is a combination of the free lifting system and the damping tugger system, which have been verified in sections A.2.2 and A.2.3, respectively.

In the first verification case of the controller lifting system, the load and the cable mass are treated as uncoupled elements by setting the spring 2 stiffness, denoted as k_{s2} , to zero e.i. eliminating spring 2. This results in two distinct pendulum systems. The initial conditions are set such that the load experiences only vertical vibrations due to gravitational forces and no pendulum-like swings. The amplitude and period of these vibrations should align with the results from the first case in Section A.2.2, as outlined by equations A.3 and A.4.

First, the behaviour of the crane cable and load is checked. Figure A.11 illustrates the motion of the load. The observations aligns with the calculated period and amplitude. Comparing this figure to Figure A.5, leads to the conclusion that both observed motions are equal, therefore the elimination of the

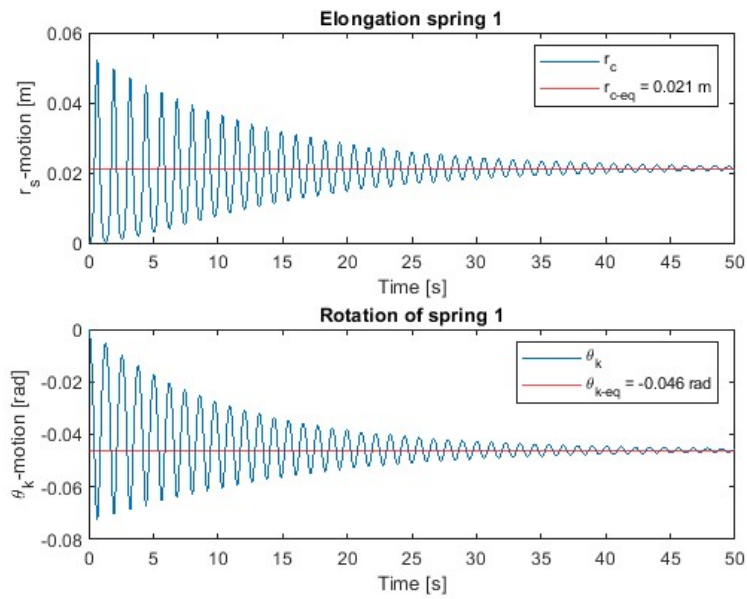


Figure A.10: Damped motion of the system

spring 2 is successful. Importantly, the motion of the load is exclusively vibrational, with no observed swinging.

Now the behaviour of the cable mass and spring 1 is tested. The above described initial conditions are set such that the mass of the cable operates as a pendulum. The period of this cable mass is described by:

$$T_p = 2\pi \cdot \sqrt{\frac{l_{0s1}}{g}} = 9.0 \text{ s} \quad (\text{A.10})$$

where l denotes the initial length of spring 1, which is 20 m in this case. Figure A.12 presents the observed period, which is in line with the value predicted by the model. Furthermore, the performance of the pendulum is in line with the behavior of a rigid pendulum. It should be noted that the mass of the cable is relatively small in comparison to the stiffness of Spring 1.

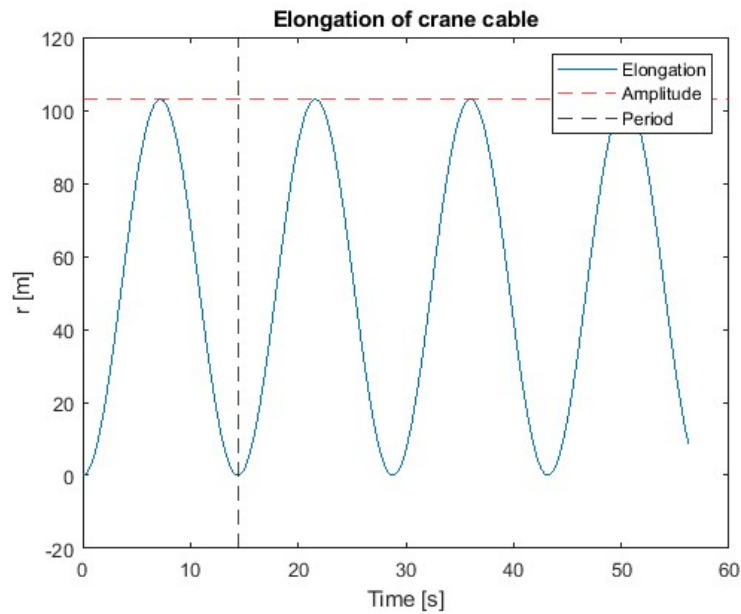


Figure A.11: The motion of the lifted load

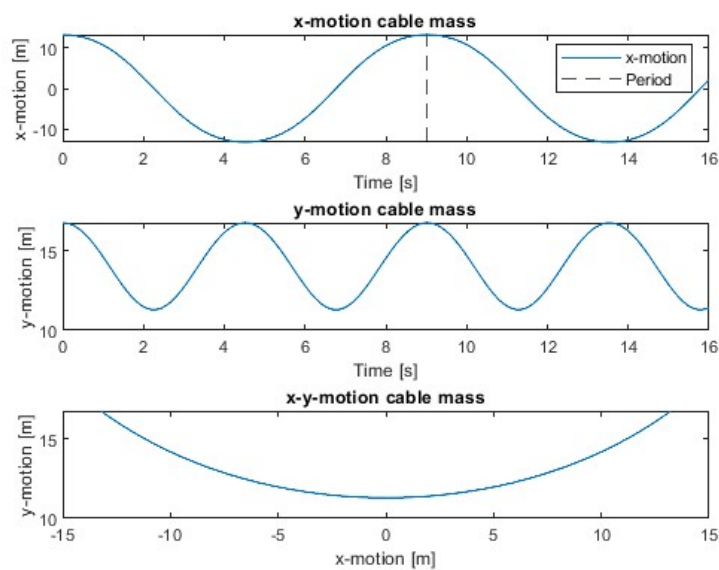


Figure A.12: The motion of the cable mass obtained from the model compared to the calculated period

A.3. Simulink ODE solver

In a Simulink model, the ODE solver operates differently compared to a regular MATLAB model. The Simulink model incorporates a MATLAB function containing the EOMs and implements them accordingly. The MATLAB function represents the EOMs in terms of one or more variables defining the DOFs and their respective first derivatives. Subsequently, the function provides the second derivatives as its output. These second derivatives are then integrated over time to determine the first derivatives, and further integration yields the corresponding state variables. Consequently, the complete state vector is obtained, comprising both the first derivatives and the state variables. These first derivatives and state variables become the inputs for the subsequent time step in the simulation process.

Figure A.13 depicts the visual representation of the ODE solving process in Simulink. In this represen-

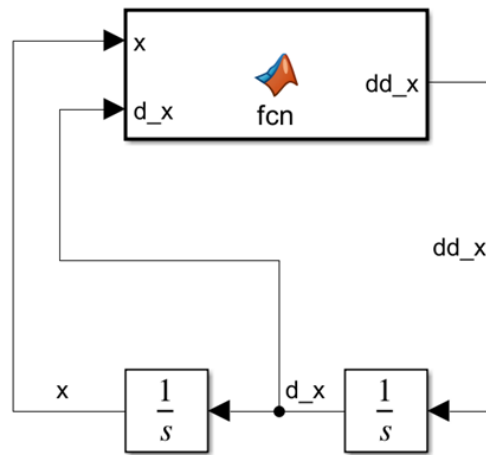


Figure A.13: ODE solver in simulink

tation, the state variable x and its first derivative d_x are the inputs to the EOMs contained within the MATLAB function. As a result, the EOMs generate the second derivative dd_x as the output. Subsequently, the second derivative dd_x is integrated to get the first derivative d_x , and further integration of the first derivative provides the state variable x .

In this thesis, the used ODE solver is ODE45. Simulink incorporates its own algorithm for selecting the most suitable ODE solver method, and in the majority of cases, this is ODE45. However, should Simulink select a different ODE solver, the reason for this choice will be assessed before determining whether an alternative ODE solver is indeed warranted. As mentioned before, ODE45 serves as the default ODE solver employed in this thesis, unless explicitly specified.

B

Analysis model

This appendix corresponds to the analysis model described in Chapter 5. It contains the explanations of modeling the winch as translating mass, the deadband and the limit values of the motion control setpoint. Furthermore, the verification cases for the outcomes of the analysis models are provided.

B.1. Modeling the winch as translating mass

This section provides the mathematical relationship between a rotating and a translating mass, which could both be used to model the winch. The aim is to derive the relation between a rotating mass and a translating mass that have the same effect on the motion of the tugger cable. Initially, the equation of motion for the rotating mass is provided as:

$$M_\theta = I\ddot{\theta} \quad (\text{B.1})$$

In this equation, M_θ represents the torque exerted on the rotating winch, I signifies the inertia of the winch, and $\ddot{\theta}$ denotes the rotational acceleration of the winch. Expanding the terms for inertia and rotational acceleration yields:

$$I = m_\theta r^2 \quad (\text{B.2})$$

$$\ddot{\theta} = \ddot{x}_\theta r \quad (\text{B.3})$$

Where m_θ is the mass of the rotating winch, r is the radius of the winch and \ddot{x}_θ is the effective transnational acceleration of the tugger cable due to the rotation of the winch. Substituting and rewriting these equation leads to:

$$\ddot{x}_\theta = \frac{M_\theta}{m_\theta r^3} \quad (\text{B.4})$$

The equation of motion for the translating mass is now provided as follows:

$$F_\theta = m_x \ddot{x}_x \quad (\text{B.5})$$

Where F_θ is the force acting on the translating mass, m_x denotes the mass of the translating winch and \ddot{x}_x represents the acceleration of the translating winch, which is equal to the effective transnational acceleration of the tugger cable. This equation could be rewritten to:

$$\ddot{x}_x = \frac{F_x}{m_x} \quad (\text{B.6})$$

Since both masses are influenced equally by the tugger cable, we set $\ddot{\theta}$ and \ddot{x} equal to each other. This results in the following equation:

$$\frac{M_\theta}{m_\theta r^3} = \frac{F_x}{m_x} \quad (\text{B.7})$$

Refactoring this equation yields the relationship between the rotational mass and the translational mass, assuming the impact on the motion of the tugger cable is held constant.

$$m_\theta = m_x \frac{M}{F_x r^3} \quad (\text{B.8})$$

This describes the relationship between rotational mass and translational mass, both of which can be used to model the winch. Further evaluation of this relationship is possible when an additional assumption is made. Specifically, if the force applied to the translational winch is equal to the force that generates the moment in the rotational winch at the radius of r , then the following equation holds true:

$$M_\theta = F_x r \quad (\text{B.9})$$

Substituting B.9 into equation B.8 leads to:

$$m_\theta = m_x \frac{F_x r}{F_x r^3} = \frac{m_x}{r^2} \quad (\text{B.10})$$

This is the relation between the rotational mass and translational mass under the assumptions that they produce the same effect on the tigger cable as well as that the force applied to the translational winch is equal to the force that generates the moment in the rotational winch at the radius of r .

B.2. Deadband

An accepted x-displacement of the load is established as $x_{o-max} = 0.1$ m. The maximum x-velocity is derived using kinetic and potential energy equations. This leads to the following expression for the x-velocity:

$$\dot{x}_o = \sqrt{\frac{2 \cdot T_p}{m}} - \dot{y}_o \quad (\text{B.11})$$

The kinetic energy reaches its maximum when the load crosses the cycle's center point, where the vertical velocity \dot{y}_o is zero. To find the relationship between the load's maximum x-displacement and maximum x-velocity, we substitute the kinetic energy with the potential energy. Here, the motion of the suspension x_t is omitted, as it concerns damping out the load's motion. Therefore, in this case, the relationship $x_{o-max} = \theta \cdot l$ holds, resulting in:

$$\dot{x}_{o-max} = \sqrt{\frac{g \cdot x_{o-max}^2}{l}} \quad (\text{B.12})$$

Given an accepted x-displacement of $x_{o-max} = 0.1$ m, the corresponding maximum x-velocity is approximately $\dot{x}_{o-max} \approx 0.05$ m/s. This value is set as the deadband for the system.

B.3. Limit values of motion control setpoint

The velocity error of the load serves as the input for the motion control setpoint. The proportional gain of the controller, denoted as k_p , multiplies the velocity error. Likewise, the derivative gain, denoted as k_d , multiplies the acceleration error. The displacement error has a maximum limit of $e_{o-max} = 0.5$ m. Using equation B.11, this corresponds to a maximum velocity value of $\dot{e}_{o-max} = 0.22$ m/s. The pre-tension is given as $F_k = -150$ kN, and the maximum force deviation from this pre-tension is $|F_{max-dev}| = 100$ kN. Consequently, the equation for calculating the limit of the proportional controller gain is as follows:

$$\lim(\bar{k}_p) = \frac{|F_{max-dev}|}{\dot{e}_{o-max}} = \frac{100e3}{0.22} \approx 450,000 \quad (\text{B.13})$$

The maximum acceleration error is unknown, so the limit for the proportional gain is used as the limit for the derivative gain as well. So the limit of the controller gain is set to 450,000.

B.4. Verification of the analysis model

To validate the models, various test cases are performed, starting with the verification of the force model. For this case, the load's mass is set to 1 kg, and the crane cable's length is 1 m. The initial conditions for the motion are $\theta = 0$ rad and $\dot{\theta} = 0$ rad/s. The force acting on the load is a constant $F_k = 2$ N. Now, the period of the motion and the angle of the static state can be calculated as follows:

$$T_p = 2\pi\sqrt{\frac{l}{g}} = 2.0 \text{ s} \tag{B.14}$$

$$\theta = \frac{F_k}{mg} = 0.2 \text{ rad} \tag{B.15}$$

Figure B.1 shows the response of the load when the force of 2 N is applied. As observed, the angle θ starts at the initial angle $\theta = 0$ and increases to the maximum angle $\theta = 0.4$. The static state corresponds to the equilibrium between these minimum and maximum angles, resulting in $\theta = 0.2$ rad, which aligns with the calculated angle. Additionally, Figure B.1 demonstrates that the period of the load is 2.0 seconds, consistent with the calculated period.

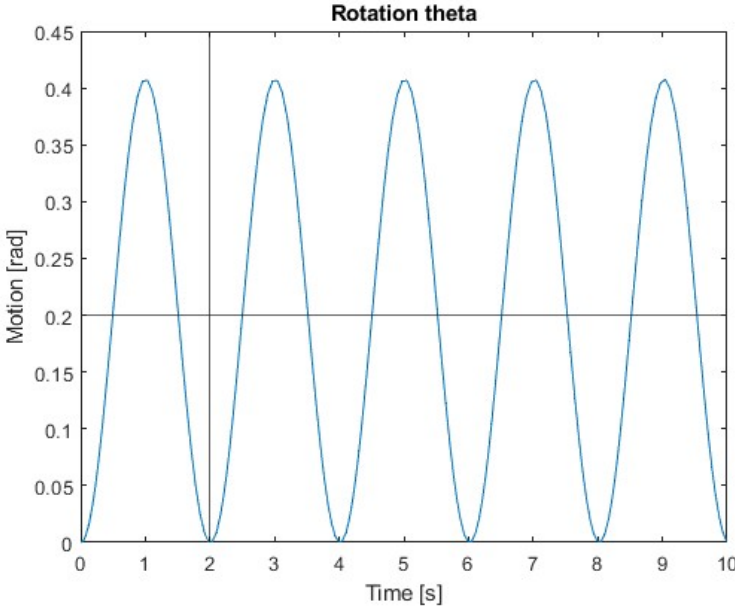


Figure B.1: Verification model of force system, case 1

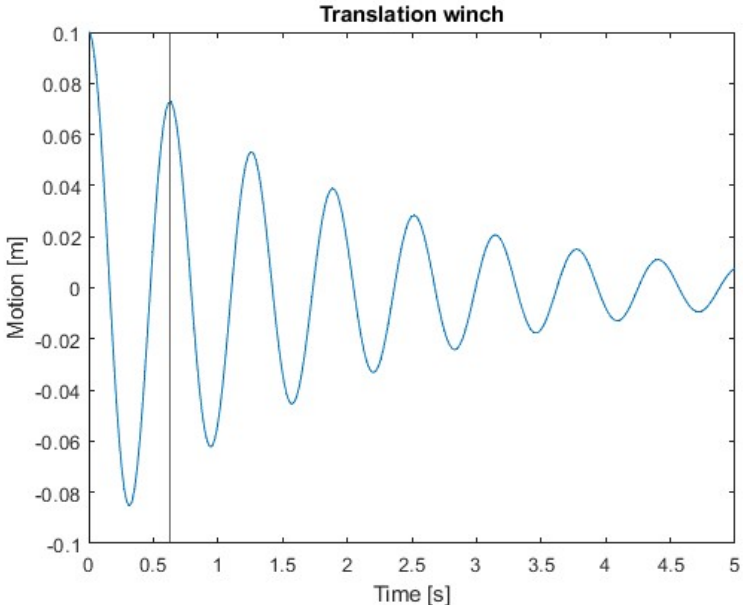


Figure B.2: Verification model of force system, case 1

Now the second model is verified through two distinct cases. In the first case, the focus is on the period of the motion of the winch. For this case, the load's mass is set to 10 kg to keep its motion negligible. The winch mass is set to 1 kg, the spring coefficient is set to 100 N/m, and the damping coefficient is set to 1 N/ms. Considering the mass of the load as fixed, the period of the motion of the winch can be calculated as:

$$T_p = 2\pi\sqrt{\frac{m_w}{k}} = 0.62 \text{ s} \quad (\text{B.16})$$

The initial displacement of the winch is set to $x_w = 1 \text{ m}$, and the initial velocity is $\dot{x}_w = 0 \text{ m/s}$. Figure B.2 shows the motion of the winch in this case, and as observed, the period of the winch is equal to 0.62 seconds, consistent with the calculated value.

The second case involves the period of the motion of the load, accounting for the presence of the spring and winch. For this case, the winch mass is set to 10 mT to maintain the winch's motion negligible. The load mass is set to 1 kg, the spring coefficient is set to 1 N/m, and the damping coefficient is set to 1 N/ms. Considering the mass of the winch as fixed, the period of the motion of the load can be calculated as done in equation B.14.

It should be noted that the period should be slightly smaller than 2.0 seconds due to the presence of the spring. The initial displacement of the load is set to $\theta = 1 \text{ rad}$, and the initial velocity is $\dot{\theta} = 0 \text{ m/s}$. Figure B.3 shows the motion of the load in this case, and as observed, the period of the load is slightly smaller than 2.0 seconds, corroborating the theoretical expectations.

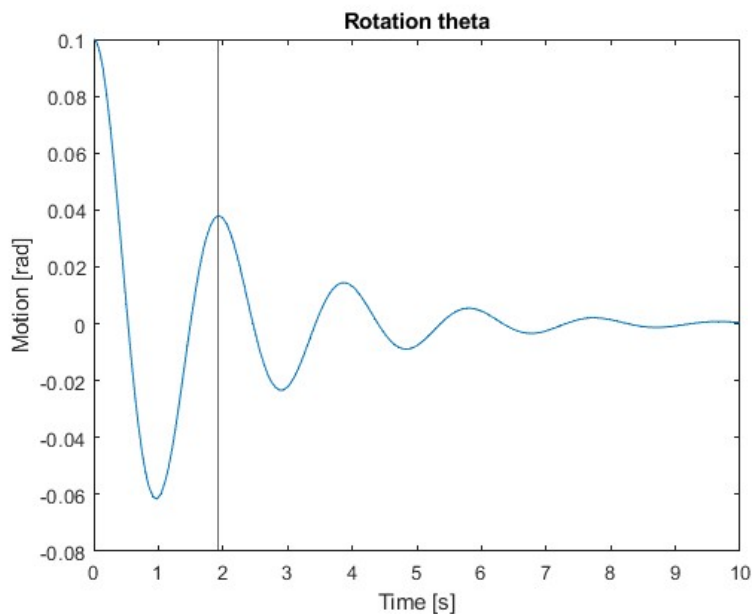


Figure B.3: Verification model of lifting system, case 2

C

Results

Table C.1 (next page) contains the results of the analysis done in chapter 6.2. These results are discussed in chapter 7.

Reference system \Rightarrow		On-deck			Global		
m_o [mT] \downarrow	m_w [mT] \Rightarrow	1	5	25	1	5	25
Maximum force setpoint							
10	No control	0.073	0.050	0.045	0.053	0.027	0.017
	Load control	0.051	0.049	0.049	0.037	0.021	0.015
	Winch control	0.043	0.048	0.050	0.035	0.022	0.015
100	No control	0.098	0.079	0.062	0.105	0.058	0.049
	Load control	0.051	0.050	0.049	0.045	0.042	0.035
	Winch control	0.062	0.060	0.057	0.046	0.042	0.036
1000	No control	0.126	0.150	0.111	0.118	0.133	0.101
	Load control	0.074	0.073	0.072	0.048	0.048	0.048
	Winch control	0.083	0.081	0.079	0.065	0.061	0.056
10000	No control	0.132	0.133	0.155	0.118	0.133	0.101
	Load control	0.089	0.088	0.087	0.048	0.048	0.048
	Winch control	0.102	0.098	0.094	0.065	0.061	0.056
Motion control setpoint							
10	No control	0.070	0.047	0.042	0.054	0.026	0.018
	Load control	0.007	0.007	0.007	0.004	0.004	0.004
	Winch control	0.037	0.038	0.037	0.003	0.003	0.003
100	No control	0.121	0.076	0.061	0.103	0.062	0.044
	Load control	0.004	0.004	0.003	0.005	0.005	0.005
	Winch control	0.060	0.060	0.060	0.015	0.015	0.014
1000	No control	0.126	0.142	0.102	0.109	0.130	0.088
	Load control	0.032	0.030	0.029	0.020	0.020	0.019
	Winch control	0.191	0.192	0.191	0.125	0.126	0.125
10000	No control	0.128	0.117	0.125	0.109	0.130	0.088
	Load control	0.075	0.073	0.073	0.020	0.020	0.019
	Winch control	0.126	0.127	0.126	0.125	0.126	0.125
Combined controller							
10	No control	0.072	0.047	0.042	0.053	0.027	0.019
	Load control	0.012	0.031	0.039	0.004	0.003	0.003
	Winch control	0.014	0.034	0.040	0.004	0.004	0.003
100	No control	0.119	0.079	0.062	0.104	0.062	0.043
	Load control	0.053	0.051	0.081	0.024	0.016	0.257
	Winch control	0.070	0.061	0.052	0.030	0.020	0.012
1000	No control	0.125	0.142	0.106	0.112	0.130	0.091
	Load control	0.076	0.072	0.067	0.044	0.039	0.033
	Winch control	0.081	0.077	0.072	0.047	0.042	0.036
10000	No control	0.130	0.120	0.129	0.112	0.104	0.115
	Load control	0.096	0.091	0.087	0.075	0.069	0.064
	Winch control	0.102	0.096	0.090	0.080	0.072	0.066

Table C.1: RMS of the velocity of the load for all scenarios

D

Equations of motion of detailed model

In this appendix, the EOMs derived in Chapter 4 are provided.

D.1. Free lifting system

$$\begin{aligned}
 \ddot{\theta}_t(t) = & (m_o \cdot (\cos(\theta_t(t)) \cdot (l_y \cdot \cos(\theta_s(t)) + \\
 & l_x \cdot \sin(\theta_s(t))) - \sin(\theta_t(t)) \cdot (l_x \cdot \cos(\theta_s(t)) - \\
 & l_y \cdot \sin(\theta_s(t)))) \cdot \ddot{\theta}_s(t) - \cos(\theta_t(t)) \cdot \ddot{x}_s(t) \cdot m_o - \\
 & \sin(\theta_t(t)) \cdot \ddot{y}_s(t) \cdot m_o + m_o \cdot ((l_y \cdot \cos(\theta_s(t)) + \\
 & l_x \cdot \sin(\theta_s(t))) \cdot \sin(\theta_t(t)) + \cos(\theta_t(t)) \cdot (l_x \cdot \cos(\theta_s(t)) - \\
 & l_y \cdot \sin(\theta_s(t)))) \cdot \dot{\theta}_s(t)^2 + \sin(\theta_t(t)) \cdot g \cdot m_o - \\
 & 2 \cdot \dot{r}_t(t) \cdot \dot{\theta}_t(t) \cdot m_o - \cos(\theta_t(t)) \cdot F_w / ((l_0 + r_t(t)) \cdot m_o)
 \end{aligned} \tag{D.1}$$

$$\begin{aligned}
 \ddot{r}_t(t) = & (-\sin(\theta_t(t)) \cdot F_w + ((l_y \cdot \cos(\theta_s(t)) + \\
 & l_x \cdot \sin(\theta_s(t))) \cdot \sin(\theta_t(t)) + \cos(\theta_t(t)) \cdot (l_x \cdot \cos(\theta_s(t)) - \\
 & l_y \cdot \sin(\theta_s(t)))) \cdot m_o \cdot \ddot{\theta}_s(t) - \sin(\theta_t(t)) \cdot \ddot{x}_s(t) \cdot m_o + \\
 & \cos(\theta_t(t)) \cdot \ddot{y}_s(t) \cdot m_o - (\cos(\theta_t(t)) \cdot (l_y \cdot \cos(\theta_s(t)) + \\
 & l_x \cdot \sin(\theta_s(t))) - \sin(\theta_t(t)) \cdot (l_x \cdot \cos(\theta_s(t)) - \\
 & l_y \cdot \sin(\theta_s(t)))) \cdot m_o \cdot \dot{\theta}_s(t)^2 + m_o \cdot (l_0 + r_t(t)) \cdot \dot{\theta}_t(t)^2 - \\
 & m_o \cdot g \cdot \cos(\theta_t(t)) - c_{tm} \cdot \dot{r}_t(t) - k_{tm} \cdot r_t(t)) / m_o
 \end{aligned} \tag{D.2}$$

D.2. Damping tugger system

$$\begin{aligned}
 \ddot{\theta}_k(t) = & (2 \cdot (\dot{\theta}_w(t) \cdot r_w \cdot c_s + k_s \cdot (\theta_w(t) \cdot r_w - \\
 & 2 \cdot l_0 s^2)) \cdot ((-y_o(t) + y_w(t)) \cdot \cos(\theta_k(t)) + \sin(\theta_k(t)) \cdot (x_o(t) - \\
 & x_w(t))) \cdot \text{sqr}t(4 \cdot (x_o(t) - x_w(t)) \cdot (\theta_w(t) \cdot r_w - 2 \cdot r_c(t) - 2 \cdot l_0 s^1) \cdot \cos(\theta_k(t)) + \\
 & 4 \cdot (y_o(t) - y_w(t)) \cdot (\theta_w(t) \cdot r_w - 2 \cdot r_c(t) - 2 \cdot l_0 s^1) \cdot \sin(\theta_k(t)) + \\
 & \theta_w(t)^2 \cdot r_w^2 - 4 \cdot r_w \cdot (l_0 s^1 + r_c(t)) \cdot \theta_w(t) + 4 \cdot l_0 s^1^2 + 8 \cdot l_0 s^1 \cdot r_c(t) + \\
 & 4 \cdot r_c(t)^2 + 4 \cdot x_o(t)^2 - 8 \cdot x_o(t) \cdot x_w(t) + 4 \cdot x_w(t)^2 + 4 \cdot y_o(t)^2 - 8 \cdot y_o(t) \cdot y_w(t) + \\
 & 4 \cdot y_w(t)^2 - 8 \cdot (-\theta_w(t) \cdot r_w - 2 \cdot r_c(t) - 2 \cdot l_0 s^1) \cdot (y_o(t) - \\
 & y_w(t)) \cdot \cos(\theta_k(t))^2 + \sin(\theta_k(t)) \cdot (\theta_w(t) \cdot r_w - 2 \cdot r_c(t) - \\
 & 2 \cdot l_0 s^1) \cdot (x_o(t) - x_w(t)) \cdot \cos(\theta_k(t)) + (x_o(t)^2 - 2 \cdot x_o(t) \cdot x_w(t) + x_w(t)^2 +
 \end{aligned} \tag{D.3}$$

$$\begin{aligned}
& y_o(t)^2 - 2 \cdot y_o(t) \cdot y_w(t) + y_w(t)^2 + (\theta_w(t) \cdot r_w - 2 \cdot r_c(t) - \\
& 2 \cdot l_0 s1)^2 / 4) \cdot \sin(\theta_k(t)) + (\theta_w(t) \cdot r_w - 2 \cdot r_c(t) - 2 \cdot l_0 s1) \cdot (y_o(t) - \\
& y_w(t)) \cdot m_c \cdot \ddot{x}_w(t) + 8 \cdot ((x_o(t) - x_w(t)) \cdot (\theta_w(t) \cdot r_w - 2 \cdot r_c(t) - \\
& 2 \cdot l_0 s1) \cdot \cos(\theta_k(t)) + (y_o(t) - y_w(t)) \cdot (\theta_w(t) \cdot r_w - 2 \cdot r_c(t) - \\
& 2 \cdot l_0 s1) \cdot \sin(\theta_k(t)) + x_o(t)^2 - 2 \cdot x_o(t) \cdot x_w(t) + x_w(t)^2 + y_o(t)^2 - \\
& 2 \cdot y_o(t) \cdot y_w(t) + y_w(t)^2 + (\theta_w(t) \cdot r_w - 2 \cdot r_c(t) - \\
& 2 \cdot l_0 s1)^2 / 4) \cdot m_c \cdot \cos(\theta_k(t)) \cdot \ddot{y}_w(t) + (-8 \cdot ((x_o(t) - x_w(t)) \cdot (\theta_w(t) \cdot r_w \\
& - 2 \cdot r_c(t) - 2 \cdot l_0 s1) \cdot \cos(\theta_k(t)) + (y_o(t) - y_w(t)) \cdot (\theta_w(t) \cdot r_w - 2 \cdot r_c(t) - \\
& 2 \cdot l_0 s1) \cdot \sin(\theta_k(t)) + x_o(t)^2 - 2 \cdot x_o(t) \cdot x_w(t) + x_w(t)^2 + y_o(t)^2 - \\
& 2 \cdot y_o(t) \cdot y_w(t) + y_w(t)^2 + (\theta_w(t) \cdot r_w - 2 \cdot r_c(t) - \\
& 2 \cdot l_0 s1)^2 / 4) \cdot m_c \cdot r_w \cdot \dot{\theta}_w(t) + 16 \cdot ((x_o(t) - x_w(t)) \cdot (\theta_w(t) \cdot r_w - 2 \cdot r_c(t) \\
& - 2 \cdot l_0 s1) \cdot \cos(\theta_k(t)) + (y_o(t) - y_w(t)) \cdot (\theta_w(t) \cdot r_w - 2 \cdot r_c(t) - \\
& 2 \cdot l_0 s1) \cdot \sin(\theta_k(t)) + x_o(t)^2 - 2 \cdot x_o(t) \cdot x_w(t) + x_w(t)^2 + y_o(t)^2 - \\
& 2 \cdot y_o(t) \cdot y_w(t) + y_w(t)^2 + (\theta_w(t) \cdot r_w - 2 \cdot r_c(t) - 2 \cdot l_0 s1)^2 / 4) \cdot m_c \cdot \dot{r}_c(t) + \\
& 4 \cdot ((x_o(t) - x_w(t) + y_o(t) - y_w(t)) \cdot (x_o(t) - x_w(t) - y_o(t) + \\
& y_w(t)) \cdot \cos(\theta_k(t))^2 + 2 \cdot \sin(\theta_k(t)) \cdot (y_o(t) - y_w(t)) \cdot (x_o(t) - \\
& x_w(t)) \cdot \cos(\theta_k(t)) - (x_o(t) - x_w(t))^2) \cdot c_s 2 \cdot (\theta_w(t) \cdot r_w - 2 \cdot r_c(t) - \\
& 2 \cdot l_0 s1) \cdot \dot{\theta}_k(t) + 4 \cdot (-2 \cdot (y_o(t) - y_w(t)) \cdot (x_o(t) - x_w(t)) \cdot \cos(\theta_k(t))^2 \\
& + ((x_o(t) - x_w(t) + y_o(t) - y_w(t)) \cdot (x_o(t) - x_w(t) - y_o(t) + \\
& y_w(t)) \cdot \sin(\theta_k(t)) - ((\theta_w(t) \cdot r_w - 2 \cdot r_c(t) - 2 \cdot l_0 s1) \cdot (y_o(t) - \\
& y_w(t))) / 2) \cdot \cos(\theta_k(t)) + (x_o(t) - x_w(t)) \cdot ((\theta_w(t) \cdot r_w / 2 - l_0 s1 - \\
& r_c(t)) \cdot \sin(\theta_k(t)) + y_o(t) - y_w(t))) \cdot c_s 2 \cdot r_w \cdot \dot{\theta}_w(t) - 8 \cdot (-2 \cdot (y_o(t) - \\
& y_w(t)) \cdot (x_o(t) - x_w(t)) \cdot \cos(\theta_k(t))^2 + ((x_o(t) - x_w(t) + y_o(t) - \\
& y_w(t)) \cdot (x_o(t) - x_w(t) - y_o(t) + y_w(t)) \cdot \sin(\theta_k(t)) - ((\theta_w(t) \cdot r_w - 2 \cdot r_c(t) \\
& - 2 \cdot l_0 s1) \cdot (y_o(t) - y_w(t))) / 2) \cdot \cos(\theta_k(t)) + (x_o(t) - x_w(t)) \cdot ((\theta_w(t) \cdot r_w / 2 - \\
& l_0 s1 - r_c(t)) \cdot \sin(\theta_k(t)) + y_o(t) - y_w(t))) \cdot c_s 2 \cdot \dot{r}_c(t) + \\
& 8 \cdot c_s 2 \cdot (-((\theta_w(t) \cdot r_w - 2 \cdot r_c(t) - 2 \cdot l_0 s1) \cdot (x_o(t) - x_w(t)) \cdot \cos(\theta_k(t))^2) / 2 - \\
& ((\theta_w(t) \cdot r_w / 2 - l_0 s1 - r_c(t)) \cdot \sin(\theta_k(t)) + y_o(t) - y_w(t)) \cdot (y_o(t) - \\
& y_w(t)) \cdot \cos(\theta_k(t)) + (x_o(t) - x_w(t)) \cdot ((y_o(t) - y_w(t)) \cdot \sin(\theta_k(t)) + \\
& \theta_w(t) \cdot r_w / 2 - l_0 s1 - r_c(t)) \cdot \dot{y}_o(t) - 8 \cdot c_s 2 \cdot (-((\theta_w(t) \cdot r_w - 2 \cdot r_c(t) - \\
& 2 \cdot l_0 s1) \cdot (x_o(t) - x_w(t)) \cdot \cos(\theta_k(t))^2) / 2 - ((\theta_w(t) \cdot r_w / 2 - l_0 s1 - \\
& r_c(t)) \cdot \sin(\theta_k(t)) + y_o(t) - y_w(t)) \cdot (y_o(t) - y_w(t)) \cdot \cos(\theta_k(t)) + (x_o(t) \\
& - x_w(t)) \cdot ((y_o(t) - y_w(t)) \cdot \sin(\theta_k(t)) + \theta_w(t) \cdot r_w / 2 - l_0 s1 - \\
& r_c(t))) \cdot \dot{y}_w(t) + 8 \cdot ((-y_o(t) + y_w(t)) \cdot \cos(\theta_k(t)) + \sin(\theta_k(t)) \cdot (x_o(t) \\
& - x_w(t))) \cdot c_s 2 \cdot ((\theta_w(t) \cdot r_w / 2 - l_0 s1 - r_c(t)) \cdot \cos(\theta_k(t)) + x_o(t) - \\
& x_w(t)) \cdot \dot{x}_o(t) - 8 \cdot ((-y_o(t) + y_w(t)) \cdot \cos(\theta_k(t)) + \sin(\theta_k(t)) \cdot (x_o(t) \\
& - x_w(t))) \cdot c_s 2 \cdot ((\theta_w(t) \cdot r_w / 2 - l_0 s1 - r_c(t)) \cdot \cos(\theta_k(t)) + x_o(t) - \\
& x_w(t)) \cdot \dot{x}_w(t) - 8 \cdot (\theta_w(t) \cdot r_w - 2 \cdot r_c(t) - 2 \cdot l_0 s1) \cdot (x_o(t) - x_w(t)) \cdot (g \cdot m_c + \\
& 2 \cdot k_s 2 \cdot y_o(t) - 2 \cdot y_w(t) \cdot k_s 2) \cdot \cos(\theta_k(t))^2 + (-8 \cdot (-k_s 2 \cdot x_o(t))^2 + \\
& 2 \cdot x_w(t) \cdot k_s 2 \cdot x_o(t) - x_w(t)^2 \cdot k_s 2 + (y_o(t) - y_w(t)) \cdot (g \cdot m_c + k_s 2 \cdot y_o(t) - \\
& y_w(t) \cdot k_s 2) \cdot (\theta_w(t) \cdot r_w - 2 \cdot r_c(t) - 2 \cdot l_0 s1) \cdot \sin(\theta_k(t)) - 8 \cdot (g \cdot m_c + \\
& k_s 2 \cdot y_o(t) - y_w(t) \cdot k_s 2) \cdot (x_o(t)^2 - 2 \cdot x_o(t) \cdot x_w(t) + x_w(t)^2 + y_o(t)^2 - \\
& 2 \cdot y_o(t) \cdot y_w(t) + y_w(t)^2 + (\theta_w(t) \cdot r_w - 2 \cdot r_c(t) - 2 \cdot l_0 s1)^2 / 4) \cdot \cos(\theta_k(t))
\end{aligned}$$

$$\begin{aligned}
& + 8 \cdot (x_o(t) - x_w(t)) \cdot k_s 2 \cdot ((x_o(t))^2 - 2 \cdot x_o(t) \cdot x_w(t) + x_w(t)^2 + y_o(t)^2 - \\
& 2 \cdot y_o(t) \cdot y_w(t) + y_w(t)^2 + (\theta_w(t) \cdot r_w - 2 \cdot r_c(t) - 2 \cdot l_0 s 1)^2 / 4) \cdot \sin(\theta_k(t)) + \\
& (\theta_w(t) \cdot r_w - 2 \cdot r_c(t) - 2 \cdot l_0 s 1) \cdot (y_o(t) - y_w(t))) / (4 \cdot ((x_o(t) - \\
& x_w(t)) \cdot (\theta_w(t) \cdot r_w - 2 \cdot r_c(t) - 2 \cdot l_0 s 1) \cdot \cos(\theta_k(t)) + (y_o(t) - \\
& y_w(t)) \cdot (\theta_w(t) \cdot r_w - 2 \cdot r_c(t) - 2 \cdot l_0 s 1) \cdot \sin(\theta_k(t)) + x_o(t)^2 - \\
& 2 \cdot x_o(t) \cdot x_w(t) + x_w(t)^2 + y_o(t)^2 - 2 \cdot y_o(t) \cdot y_w(t) + y_w(t)^2 + (\theta_w(t) \cdot r_w - \\
& 2 \cdot r_c(t) - 2 \cdot l_0 s 1)^2 / 4) \cdot m_c \cdot (\theta_w(t) \cdot r_w - 2 \cdot r_c(t) - 2 \cdot l_0 s 1)
\end{aligned}$$

$$\begin{aligned}
\ddot{r}_c(t) = & (4 \cdot ((-x_o(t) + x_w(t)) \cdot \cos(\theta_k(t)) + (-y_o(t) + \\
& y_w(t)) \cdot \sin(\theta_k(t)) - \theta_w(t) \cdot r_w / 2 + r_c(t) + \\
& l_0 s 1) \cdot (-\dot{\theta}_w(t) \cdot r_w \cdot c_s 2 / 2 + k_s 2 \cdot (-\theta_w(t) \cdot r_w / 2 + l_0 s 2)) \cdot \text{sqrt}(4 \cdot (x_o(t) - \\
& x_w(t)) \cdot (\theta_w(t) \cdot r_w - 2 \cdot r_c(t) - 2 \cdot l_0 s 1) \cdot \cos(\theta_k(t)) + 4 \cdot (y_o(t) - \\
& y_w(t)) \cdot (\theta_w(t) \cdot r_w - 2 \cdot r_c(t) - 2 \cdot l_0 s 1) \cdot \sin(\theta_k(t)) + \theta_w(t)^2 \cdot r_w^2 - \\
& 4 \cdot r_w \cdot (l_0 s 1 + r_c(t)) \cdot \theta_w(t) + 4 \cdot l_0 s 1^2 + 8 \cdot l_0 s 1 \cdot r_c(t) + 4 \cdot r_c(t)^2 + 4 \cdot x_o(t)^2 - \\
& 8 \cdot x_o(t) \cdot x_w(t) + 4 \cdot x_w(t)^2 + 4 \cdot y_o(t)^2 - 8 \cdot y_o(t) \cdot y_w(t) + 4 \cdot y_w(t)^2) - 8 \cdot m_c \cdot (2 \cdot (l_0 s 1 \\
& - \theta_w(t) \cdot r_w / 2 + r_c(t)) \cdot (y_o(t) - y_w(t)) \cdot \cos(\theta_k(t))^2 - 2 \cdot (l_0 s 1 - \\
& \theta_w(t) \cdot r_w / 2 + r_c(t)) \cdot (x_o(t) - x_w(t)) \cdot \sin(\theta_k(t)) \cdot \cos(\theta_k(t)) + \\
& (r_c(t))^2 + (-\theta_w(t) \cdot r_w + 2 \cdot l_0 s 1) \cdot r_c(t) + \theta_w(t)^2 \cdot r_w^2 / 4 - 2 \cdot x_o(t) \cdot x_w(t) - \\
& 2 \cdot y_o(t) \cdot y_w(t) + x_o(t)^2 + x_w(t)^2 + y_o(t)^2 + y_w(t)^2 + l_0 s 1^2 - \\
& l_0 s 1 \cdot \theta_w(t) \cdot r_w) \cdot \sin(\theta_k(t)) - 2 \cdot (l_0 s 1 - \theta_w(t) \cdot r_w / 2 + r_c(t)) \cdot (y_o(t) - \\
& y_w(t))) \cdot \ddot{y}_w(t) + 4 \cdot (-2 \cdot (l_0 s 1 - \theta_w(t) \cdot r_w / 2 + r_c(t)) \cdot (x_o(t) - \\
& x_w(t)) \cdot \cos(\theta_k(t)) - 2 \cdot (l_0 s 1 - \theta_w(t) \cdot r_w / 2 + r_c(t)) \cdot (y_o(t) - \\
& y_w(t)) \cdot \sin(\theta_k(t)) + r_c(t)^2 + (-\theta_w(t) \cdot r_w + 2 \cdot l_0 s 1) \cdot r_c(t) + \\
& \theta_w(t)^2 \cdot r_w^2 / 4 - 2 \cdot x_o(t) \cdot x_w(t) - 2 \cdot y_o(t) \cdot y_w(t) + x_o(t)^2 + x_w(t)^2 + y_o(t)^2 + \\
& y_w(t)^2 + l_0 s 1^2 - l_0 s 1 \cdot \theta_w(t) \cdot r_w) \cdot m_c \cdot r_w \cdot \ddot{\theta}_w(t) - 8 \cdot (-2 \cdot (l_0 s 1 - \\
& \theta_w(t) \cdot r_w / 2 + r_c(t)) \cdot (x_o(t) - x_w(t)) \cdot \cos(\theta_k(t)) - 2 \cdot (l_0 s 1 - \\
& \theta_w(t) \cdot r_w / 2 + r_c(t)) \cdot (y_o(t) - y_w(t)) \cdot \sin(\theta_k(t)) + r_c(t)^2 + \\
& (-\theta_w(t) \cdot r_w + 2 \cdot l_0 s 1) \cdot r_c(t) + \theta_w(t)^2 \cdot r_w^2 / 4 - 2 \cdot x_o(t) \cdot x_w(t) - \\
& 2 \cdot y_o(t) \cdot y_w(t) + x_o(t)^2 + x_w(t)^2 + y_o(t)^2 + y_w(t)^2 + l_0 s 1^2 - \\
& l_0 s 1 \cdot \theta_w(t) \cdot r_w) \cdot m_c \cdot \cos(\theta_k(t)) \cdot \ddot{x}_w(t) + 8 \cdot (-2 \cdot (l_0 s 1 - \theta_w(t) \cdot r_w / 2 \\
& + r_c(t)) \cdot (x_o(t) - x_w(t)) \cdot \cos(\theta_k(t)) - 2 \cdot (l_0 s 1 - \theta_w(t) \cdot r_w / 2 + \\
& r_c(t)) \cdot (y_o(t) - y_w(t)) \cdot \sin(\theta_k(t)) + r_c(t)^2 + (-\theta_w(t) \cdot r_w + 2 \cdot l_0 s 1) \cdot r_c(t) \\
& + \theta_w(t)^2 \cdot r_w^2 / 4 - 2 \cdot x_o(t) \cdot x_w(t) - 2 \cdot y_o(t) \cdot y_w(t) + x_o(t)^2 + x_w(t)^2 + y_o(t)^2 \\
& + y_w(t)^2 + l_0 s 1^2 - l_0 s 1 \cdot \theta_w(t) \cdot r_w) \cdot (l_0 s 1 - \theta_w(t) \cdot r_w / 2 + \\
& r_c(t)) \cdot m_c \cdot \dot{\theta}_k(t)^2 - 8 \cdot (l_0 s 1 - \theta_w(t) \cdot r_w / 2 + r_c(t)) \cdot c_s 2 \cdot (2 \cdot (y_o(t) - \\
& y_w(t)) \cdot (x_o(t) - x_w(t)) \cdot \cos(\theta_k(t))^2 + (-x_o(t) - x_w(t) + y_o(t) - \\
& y_w(t)) \cdot (x_o(t) - x_w(t) - y_o(t) + y_w(t)) \cdot \sin(\theta_k(t)) - (l_0 s 1 - \theta_w(t) \cdot r_w / 2 + \\
& r_c(t)) \cdot (y_o(t) - y_w(t))) \cdot \cos(\theta_k(t)) + (\sin(\theta_k(t)) \cdot (l_0 s 1 - \theta_w(t) \cdot r_w / 2 \\
& + r_c(t)) - y_o(t) + y_w(t)) \cdot (x_o(t) - x_w(t))) \cdot \dot{\theta}_k(t) + (-8 \cdot c_s 2 \cdot (x_o(t) - \\
& x_w(t) + y_o(t) - y_w(t)) \cdot (x_o(t) - x_w(t) - y_o(t) + y_w(t)) \cdot \cos(\theta_k(t))^2 + \\
& 16 \cdot (-c_s 2 \cdot (y_o(t) - y_w(t)) \cdot \sin(\theta_k(t)) + (c_s 1 + c_s 2) \cdot (l_0 s 1 - \theta_w(t) \cdot r_w / 2 + \\
& r_c(t))) \cdot (x_o(t) - x_w(t)) \cdot \cos(\theta_k(t)) + 16 \cdot (c_s 1 + c_s 2) \cdot (l_0 s 1 - \theta_w(t) \cdot r_w / 2 +
\end{aligned}$$

$$\begin{aligned}
& r_c(t) \cdot (y_o(t) - y_w(t)) \cdot \sin(\theta_k(t)) + (-8 \cdot c_s1 - 8 \cdot c_s2) \cdot r_c(t)^2 + 8 \cdot (c_s1 + \\
& c_s2) \cdot (\theta_w(t) \cdot r_w - 2 \cdot l_0s1) \cdot r_c(t) - 2 \cdot r_w^2 \cdot (c_s1 + c_s2) \cdot \theta_w(t)^2 + \\
& 8 \cdot l_0s1 \cdot r_w \cdot (c_s1 + c_s2) \cdot \theta_w(t) + (-8 \cdot c_s1 - 8 \cdot c_s2) \cdot y_o(t)^2 + 16 \cdot y_w(t) \cdot (c_s1 + \\
& c_s2) \cdot y_o(t) + (-8 \cdot c_s1 - 8 \cdot c_s2) \cdot y_w(t)^2 - 8 \cdot x_o(t)^2 \cdot c_s1 + 16 \cdot x_o(t) \cdot x_w(t) \cdot c_s1 - \\
& 8 \cdot x_w(t)^2 \cdot c_s1 - 8 \cdot l_0s1^2 \cdot (c_s1 + c_s2) \cdot \dot{r}_c(t) + 4 \cdot c_s2 \cdot ((x_o(t) - x_w(t) + y_o(t) \\
& - y_w(t)) \cdot (x_o(t) - x_w(t) - y_o(t) + y_w(t)) \cdot \cos(\theta_k(t))^2 - 2 \cdot ((-y_o(t) + \\
& y_w(t)) \cdot \sin(\theta_k(t)) - \theta_w(t) \cdot r_w/2 + r_c(t) + l_0s1) \cdot (x_o(t) - \\
& x_w(t)) \cdot \cos(\theta_k(t)) - 2 \cdot (l_0s1 - \theta_w(t) \cdot r_w/2 + r_c(t)) \cdot (y_o(t) - \\
& y_w(t)) \cdot \sin(\theta_k(t)) + r_c(t)^2 + (-\theta_w(t) \cdot r_w + 2 \cdot l_0s1) \cdot r_c(t) - \\
& l_0s1 \cdot \theta_w(t) \cdot r_w + l_0s1^2 - 2 \cdot y_o(t) \cdot y_w(t) + \theta_w(t)^2 \cdot r_w^2/4 + y_o(t)^2 + \\
& y_w(t)^2 \cdot r_w \cdot \dot{\theta}_w(t) + 8 \cdot (\cos(\theta_k(t)) \cdot (l_0s1 - \theta_w(t) \cdot r_w/2 + r_c(t)) \\
& - x_o(t) + x_w(t)) \cdot c_s2 \cdot ((-x_o(t) + x_w(t)) \cdot \cos(\theta_k(t)) + (-y_o(t) + \\
& y_w(t)) \cdot \sin(\theta_k(t)) - \theta_w(t) \cdot r_w/2 + r_c(t) + l_0s1) \cdot \dot{x}_o(t) - \\
& 8 \cdot (\cos(\theta_k(t)) \cdot (l_0s1 - \theta_w(t) \cdot r_w/2 + r_c(t)) - x_o(t) + x_w(t)) \cdot c_s2 \cdot ((-x_o(t) \\
& + x_w(t)) \cdot \cos(\theta_k(t)) + (-y_o(t) + y_w(t)) \cdot \sin(\theta_k(t)) - \theta_w(t) \cdot r_w/2 + \\
& r_c(t) + l_0s1) \cdot \dot{x}_w(t) + 8 \cdot c_s2 \cdot ((l_0s1 - \theta_w(t) \cdot r_w/2 + r_c(t)) \cdot (y_o(t) - \\
& y_w(t)) \cdot \cos(\theta_k(t))^2 - (\sin(\theta_k(t)) \cdot (l_0s1 - \theta_w(t) \cdot r_w/2 + r_c(t)) - \\
& y_o(t) + y_w(t)) \cdot (x_o(t) - x_w(t)) \cdot \cos(\theta_k(t)) + (r_c(t)^2 + (-\theta_w(t) \cdot r_w + \\
& 2 \cdot l_0s1) \cdot r_c(t) - l_0s1 \cdot \theta_w(t) \cdot r_w + l_0s1^2 - 2 \cdot y_o(t) \cdot y_w(t) + \theta_w(t)^2 \cdot r_w^2/4 + \\
& y_o(t)^2 + y_w(t)^2) \cdot \sin(\theta_k(t)) - 2 \cdot (l_0s1 - \theta_w(t) \cdot r_w/2 + r_c(t)) \cdot (y_o(t) - \\
& y_w(t)) \cdot \dot{y}_o(t) - 8 \cdot c_s2 \cdot ((l_0s1 - \theta_w(t) \cdot r_w/2 + r_c(t)) \cdot (y_o(t) - \\
& y_w(t)) \cdot \cos(\theta_k(t))^2 - (\sin(\theta_k(t)) \cdot (l_0s1 - \theta_w(t) \cdot r_w/2 + r_c(t)) - \\
& y_o(t) + y_w(t)) \cdot (x_o(t) - x_w(t)) \cdot \cos(\theta_k(t)) + (r_c(t)^2 + (-\theta_w(t) \cdot r_w + \\
& 2 \cdot l_0s1) \cdot r_c(t) - l_0s1 \cdot \theta_w(t) \cdot r_w + l_0s1^2 - 2 \cdot y_o(t) \cdot y_w(t) + \theta_w(t)^2 \cdot r_w^2/4 + \\
& y_o(t)^2 + y_w(t)^2) \cdot \sin(\theta_k(t)) - 2 \cdot (l_0s1 - \theta_w(t) \cdot r_w/2 + r_c(t)) \cdot (y_o(t) - \\
& y_w(t)) \cdot \dot{y}_w(t) + 16 \cdot (k_s2 \cdot y_o(t)^2 + (g \cdot m_c - 2 \cdot y_w(t) \cdot k_s2) \cdot y_o(t) + y_w(t)^2 \cdot k_s2 \\
& - g \cdot y_w(t) \cdot m_c - k_s2 \cdot (x_o(t) - x_w(t))^2) \cdot (l_0s1 - \theta_w(t) \cdot r_w/2 + \\
& r_c(t)) \cdot \cos(\theta_k(t))^2 - 16 \cdot ((l_0s1 - \theta_w(t) \cdot r_w/2 + r_c(t)) \cdot (g \cdot m_c + \\
& 2 \cdot k_s2 \cdot y_o(t) - 2 \cdot y_w(t) \cdot k_s2) \cdot \sin(\theta_k(t)) + (-k_s1 - (3 \cdot k_s2)/2) \cdot r_c(t)^2 + ((k_s1 + \\
& 3 \cdot k_s2) \cdot (\theta_w(t) \cdot r_w - 2 \cdot l_0s1) \cdot r_c(t))/2 - k_s2 \cdot ((3 \cdot \theta_w(t)^2 \cdot r_w^2)/4 - \\
& 3 \cdot l_0s1 \cdot \theta_w(t) \cdot r_w + x_o(t)^2 - 2 \cdot x_o(t) \cdot x_w(t) + x_w(t)^2 + y_o(t)^2 - 2 \cdot y_o(t) \cdot y_w(t) \\
& + y_w(t)^2 + 3 \cdot l_0s1^2)/2) \cdot (x_o(t) - x_w(t)) \cdot \cos(\theta_k(t)) + (((16 \cdot k_s1 + \\
& 24 \cdot k_s2) \cdot y_o(t) + (-16 \cdot k_s1 - 24 \cdot k_s2) \cdot y_w(t) + 8 \cdot g \cdot m_c) \cdot r_c(t)^2 - 8 \cdot ((k_s1 + \\
& 3 \cdot k_s2) \cdot y_o(t) + (-k_s1 - 3 \cdot k_s2) \cdot y_w(t) + g \cdot m_c) \cdot (\theta_w(t) \cdot r_w - 2 \cdot l_0s1) \cdot r_c(t) + \\
& 2 \cdot r_w^2 \cdot (g \cdot m_c + 3 \cdot k_s2 \cdot y_o(t) - 3 \cdot y_w(t) \cdot k_s2) \cdot \theta_w(t)^2 - 8 \cdot l_0s1 \cdot r_w \cdot (g \cdot m_c + \\
& 3 \cdot k_s2 \cdot y_o(t) - 3 \cdot y_w(t) \cdot k_s2) \cdot \theta_w(t) + 8 \cdot y_o(t)^3 \cdot k_s2 + (8 \cdot g \cdot m_c - \\
& 24 \cdot y_w(t) \cdot k_s2) \cdot y_o(t)^2 + (24 \cdot y_w(t)^2 \cdot k_s2 - 16 \cdot g \cdot y_w(t) \cdot m_c + 8 \cdot k_s2 \cdot (x_o(t)^2 - \\
& 2 \cdot x_o(t) \cdot x_w(t) + x_w(t)^2 + 3 \cdot l_0s1^2)) \cdot y_o(t) - 8 \cdot y_w(t)^3 \cdot k_s2 + 8 \cdot g \cdot y_w(t)^2 \cdot m_c - \\
& 8 \cdot k_s2 \cdot (x_o(t)^2 - 2 \cdot x_o(t) \cdot x_w(t) + x_w(t)^2 + 3 \cdot l_0s1^2) \cdot y_w(t) + 8 \cdot g \cdot m_c \cdot (x_o(t)^2 - \\
& 2 \cdot x_o(t) \cdot x_w(t) + x_w(t)^2 + l_0s1^2)) \cdot \sin(\theta_k(t)) + (-8 \cdot k_s1 - 8 \cdot k_s2) \cdot r_c(t)^3 + \\
& 8 \cdot (\theta_w(t) \cdot r_w - 2 \cdot l_0s1) \cdot (k_s1 + (3 \cdot k_s2)/2) \cdot r_c(t)^2 + (-2 \cdot r_w^2 \cdot (k_s1 + \\
& 3 \cdot k_s2) \cdot \theta_w(t)^2 + 8 \cdot l_0s1 \cdot r_w \cdot (k_s1 + 3 \cdot k_s2) \cdot \theta_w(t) + (-8 \cdot k_s1 -
\end{aligned}$$

$$\begin{aligned}
& 24 \cdot k_s 2) \cdot y_o(t)^2 + ((16 \cdot k_s 1 + 48 \cdot k_s 2) \cdot y_w(t) - 16 \cdot g \cdot m_c) \cdot y_o(t) + (-8 \cdot k_s 1 - \\
& 24 \cdot k_s 2) \cdot y_w(t)^2 + 16 \cdot g \cdot y_w(t) \cdot m_c + (-8 \cdot k_s 1 - 8 \cdot k_s 2) \cdot x_o(t)^2 + 16 \cdot x_w(t) \cdot (k_s 1 + \\
& k_s 2) \cdot x_o(t) + (-8 \cdot k_s 1 - 8 \cdot k_s 2) \cdot x_w(t)^2 - 8 \cdot l_0 s 1^2 \cdot (k_s 1 + 3 \cdot k_s 2)) \cdot r_c(t) + \\
& 8 \cdot (\theta_w(t) \cdot r_w - 2 \cdot l_0 s 1) \cdot (\theta_w(t)^2 \cdot k_s 2 \cdot r_w^2 / 8 - \theta_w(t) \cdot k_s 2 \cdot l_0 s 1 \cdot r_w / 2 + \\
& (3 \cdot k_s 2 \cdot y_o(t)^2) / 2 + (g \cdot m_c - 3 \cdot y_w(t) \cdot k_s 2) \cdot y_o(t) + (3 \cdot y_w(t)^2 \cdot k_s 2) / 2 - g \cdot y_w(t) \cdot m_c + \\
& k_s 2 \cdot (x_o(t)^2 - 2 \cdot x_o(t) \cdot x_w(t) + x_w(t)^2 + l_0 s 1^2) / 2) / (8 \cdot (-2 \cdot (l_0 s 1 - \theta_w(t) \cdot r_w / 2 \\
& + r_c(t)) \cdot (x_o(t) - x_w(t)) \cdot \cos(\theta_k(t)) - 2 \cdot (l_0 s 1 - \theta_w(t) \cdot r_w / 2 + \\
& r_c(t)) \cdot (y_o(t) - y_w(t)) \cdot \sin(\theta_k(t)) + r_c(t)^2 + (-\theta_w(t) \cdot r_w + 2 \cdot l_0 s 1) \cdot r_c(t) \\
& + \theta_w(t)^2 \cdot r_w^2 / 4 - 2 \cdot x_o(t) \cdot x_w(t) - 2 \cdot y_o(t) \cdot y_w(t) + x_o(t)^2 + x_w(t)^2 + y_o(t)^2 \\
& + y_w(t)^2 + l_0 s 1^2 - l_0 s 1 \cdot \theta_w(t) \cdot r_w) \cdot m_c)
\end{aligned}$$

D.3. Controller lifting system

$$\begin{aligned}
\ddot{r}_t(t) = & (2 \cdot (-s_{\theta t}(t) \cdot F_w + m_o \cdot (2 \cdot (\dot{x}_s(t) - l_t x \cdot \dot{\theta}_s(t)) \cdot s_{\theta} - \\
& l_t y \cdot \dot{\theta}_s(t) \cdot c_{\theta} + \dot{r}_t(t) \cdot s_{\theta t}(t) + (l_0 + \\
& r_t(t)) \cdot \dot{\theta}_t(t) \cdot c_{\theta t}(t)) \cdot \dot{\theta}_t(t) \cdot c_{\theta t}(t) + 2 \cdot (\dot{y}_s(t) + \\
& l_t x \cdot \dot{\theta}_s(t) \cdot c_{\theta} - l_t y \cdot \dot{\theta}_s(t) \cdot s_{\theta} - \dot{r}_t(t) \cdot c_{\theta t}(t) \\
& + (l_0 + r_t(t)) \cdot \dot{\theta}_t(t) \cdot s_{\theta t}(t)) \cdot \dot{\theta}_t(t) \cdot s_{\theta t}(t)) / 2 - \\
& m_o \cdot g \cdot c_{\theta t}(t) - k_{tm} \cdot r_t(t) - k_s 2 \cdot (\text{sqrt}((l_t x \cdot c_{\theta} - l_t y \cdot s_{\theta} + (l_0 + \\
& r_t(t)) \cdot s_{\theta t}(t) - l_w x \cdot c_{\theta} + l_w y \cdot s_{\theta} - \cos(\theta_t(t)) \cdot (l_0 s 1 - \\
& \theta_w(t) \cdot r_w / 2 + r_c(t)))^2 + (l_t x \cdot s_{\theta} + l_t y \cdot c_{\theta} - (l_0 + r_t(t)) \cdot c_{\theta t}(t) \\
& - l_w x \cdot s_{\theta} - l_w y \cdot c_{\theta} - \sin(r_c(t)) \cdot (l_0 s 1 - \theta_w(t) \cdot r_w / 2 + r_c(t)))^2) - \\
& l_0 s 2 + \theta_w(t) \cdot r_w / 2) \cdot (2 \cdot (l_t x \cdot c_{\theta} - l_t y \cdot s_{\theta} + (l_0 + r_t(t)) \cdot s_{\theta t}(t) - \\
& l_w x \cdot c_{\theta} + l_w y \cdot s_{\theta} - \cos(\theta_t(t)) \cdot (l_0 s 1 - \theta_w(t) \cdot r_w / 2 + \\
& r_c(t))) \cdot s_{\theta t}(t) - 2 \cdot (l_t x \cdot s_{\theta} + l_t y \cdot c_{\theta} - (l_0 + r_t(t)) \cdot c_{\theta t}(t) - \\
& l_w x \cdot s_{\theta} - l_w y \cdot c_{\theta} - \sin(r_c(t)) \cdot (l_0 s 1 - \theta_w(t) \cdot r_w / 2 + \\
& r_c(t))) \cdot c_{\theta t}(t)) / (2 \cdot \text{sqrt}((l_t x \cdot c_{\theta} - l_t y \cdot s_{\theta} + (l_0 + r_t(t)) \cdot s_{\theta t}(t) - \\
& l_w x \cdot c_{\theta} + l_w y \cdot s_{\theta} - \cos(\theta_t(t)) \cdot (l_0 s 1 - \theta_w(t) \cdot r_w / 2 + r_c(t)))^2 + \\
& (l_t x \cdot s_{\theta} + l_t y \cdot c_{\theta} - (l_0 + r_t(t)) \cdot c_{\theta t}(t) - l_w x \cdot s_{\theta} - l_w y \cdot c_{\theta} - \\
& \sin(r_c(t)) \cdot (l_0 s 1 - \theta_w(t) \cdot r_w / 2 + r_c(t)))^2) - c_{tm} \cdot \dot{r}_t(t) - \\
& c_s 2 \cdot ((2 \cdot (l_t x \cdot c_{\theta} - l_t y \cdot s_{\theta} + (l_0 + r_t(t)) \cdot s_{\theta t}(t) - l_w x \cdot c_{\theta} + \\
& l_w y \cdot s_{\theta} - \cos(\theta_t(t)) \cdot (l_0 s 1 - \theta_w(t) \cdot r_w / 2 + \\
& r_c(t))) \cdot (-l_t x \cdot \dot{\theta}_s(t) \cdot s_{\theta} - l_t y \cdot \dot{\theta}_s(t) \cdot c_{\theta} + \\
& \dot{r}_t(t) \cdot s_{\theta t}(t) + (l_0 + r_t(t)) \cdot \dot{\theta}_t(t) \cdot c_{\theta t}(t) + \\
& l_w x \cdot \dot{\theta}_s(t) \cdot s_{\theta} + l_w y \cdot \dot{\theta}_s(t) \cdot c_{\theta} + \\
& \theta_k(t) \cdot \sin(r_c(t)) \cdot (l_0 s 1 - \theta_w(t) \cdot r_w / 2 + r_c(t)) - \\
& \cos(\theta_t(t)) \cdot (-\dot{\theta}_w(t) \cdot r_w / 2 + \dot{r}_c(t))) + 2 \cdot (l_t x \cdot s_{\theta} + \\
& l_t y \cdot c_{\theta} - (l_0 + r_t(t)) \cdot c_{\theta t}(t) - l_w x \cdot s_{\theta} - l_w y \cdot c_{\theta} - \\
& \sin(r_c(t)) \cdot (l_0 s 1 - \theta_w(t) \cdot r_w / 2 + r_c(t))) \cdot (l_t x \cdot \dot{\theta}_s(t) \cdot c_{\theta} - \\
& l_t y \cdot \dot{\theta}_s(t) \cdot s_{\theta} - \dot{r}_t(t) \cdot c_{\theta t}(t) + (l_0 + \\
& r_t(t)) \cdot \dot{\theta}_t(t) \cdot s_{\theta t}(t) - l_w x \cdot \dot{\theta}_s(t) \cdot c_{\theta} + \\
& l_w y \cdot \dot{\theta}_s(t) \cdot s_{\theta} - \theta_k(t) \cdot \cos(\theta_t(t)) \cdot (l_0 s 1 - \theta_w(t) \cdot r_w / 2 + \\
& r_c(t)) - \sin(r_c(t)) \cdot (-\dot{\theta}_w(t) \cdot r_w / 2 +
\end{aligned}$$

$$\begin{aligned}
& \dot{r}_c(t))) / (2 \cdot \text{sqrt}((l_t x \cdot c_\theta - l_t y \cdot s_\theta + (l_0 + r_t(t)) \cdot s_{\theta_t}(t) - \\
& l_w x \cdot c_\theta + l_w y \cdot s_\theta - \cos(\theta_t(t)) \cdot (l_0 s_1 - \theta_w(t) \cdot r_w/2 + r_c(t)))^2 + \\
& (l_t x \cdot s_\theta + l_t y \cdot c_\theta - (l_0 + r_t(t)) \cdot c_{\theta_t}(t) - l_w x \cdot s_\theta - l_w y \cdot c_\theta - \\
& \sin(r_c(t)) \cdot (l_0 s_1 - \theta_w(t) \cdot r_w/2 + r_c(t)))^2)) + \theta_w(t) \\
& t) \cdot r_w/2) \cdot (2 \cdot (l_t x \cdot c_\theta - l_t y \cdot s_\theta + (l_0 + r_t(t)) \cdot s_{\theta_t}(t) - l_w x \cdot c_\theta + \\
& l_w y \cdot s_\theta - \cos(\theta_t(t)) \cdot (l_0 s_1 - \theta_w(t) \cdot r_w/2 + r_c(t))) \cdot s_{\theta_t}(t) - \\
& 2 \cdot (l_t x \cdot s_\theta + l_t y \cdot c_\theta - (l_0 + r_t(t)) \cdot c_{\theta_t}(t) - l_w x \cdot s_\theta - l_w y \cdot c_\theta \\
& - \sin(r_c(t)) \cdot (l_0 s_1 - \theta_w(t) \cdot r_w/2 + r_c(t))) \cdot c_{\theta_t}(t)) / (2 \cdot \text{sqrt}((l_t x \cdot c_\theta - \\
& l_t y \cdot s_\theta + (l_0 + r_t(t)) \cdot s_{\theta_t}(t) - l_w x \cdot c_\theta + l_w y \cdot s_\theta - \\
& \cos(\theta_t(t)) \cdot (l_0 s_1 - \theta_w(t) \cdot r_w/2 + r_c(t)))^2 + (l_t x \cdot s_\theta + l_t y \cdot c_\theta - \\
& (l_0 + r_t(t)) \cdot c_{\theta_t}(t) - l_w x \cdot s_\theta - l_w y \cdot c_\theta - \sin(r_c(t)) \cdot (l_0 s_1 - \\
& \theta_w(t) \cdot r_w/2 + r_c(t)))^2))) \cdot 1/m_o - 2 \cdot (\dot{x}_s(t) - l_t x \cdot \dot{\theta}_s(t) \cdot s_\theta \\
& - l_t y \cdot \dot{\theta}_s(t) \cdot c_\theta + \dot{r}_t(t) \cdot s_{\theta_t}(t) + (l_0 + \\
& r_t(t)) \cdot \dot{\theta}_t(t) \cdot c_{\theta_t}(t) \cdot \dot{\theta}_t(t) \cdot c_{\theta_t}(t) - 2 \cdot (\dot{y}_s(t) + \\
& l_t x \cdot \dot{\theta}_s(t) \cdot c_\theta - l_t y \cdot \dot{\theta}_s(t) \cdot s_\theta - \dot{r}_t(t) \cdot c_{\theta_t}(t) \\
& + (l_0 + r_t(t)) \cdot \dot{\theta}_t(t) \cdot s_{\theta_t}(t) \cdot \dot{\theta}_t(t) \cdot s_{\theta_t}(t) - \\
& (2 \cdot s_\theta) \cdot s_{\theta_t}(t) \cdot l_t y \cdot \dot{\theta}_s(t)^2 - (2 \cdot s_\theta) \cdot c_{\theta_t}(t) \cdot l_t x \cdot \dot{\theta}_s(t)^2 + \\
& (2 \cdot c_\theta) \cdot s_{\theta_t}(t) \cdot l_t x \cdot \dot{\theta}_s(t)^2 - (2 \cdot c_\theta) \cdot c_{\theta_t}(t) \cdot l_t y \cdot \dot{\theta}_s(t)^2 + \\
& (2 \cdot s_{\theta_t}(t)^2) \cdot r_t(t) \cdot \dot{\theta}_t(t)^2 + (2 \cdot s_{\theta_t}(t)^2) \cdot l_0 \cdot \dot{\theta}_t(t)^2 + (2 \cdot c_{\theta_t}(t)^2) \cdot r_t(t) \cdot \dot{\theta}_t(t)^2 + \\
& (2 \cdot c_{\theta_t}(t)^2) \cdot l_0 \cdot \dot{\theta}_t(t)^2 + (2 \cdot s_\theta) \cdot s_{\theta_t}(t) \cdot l_t x \cdot \ddot{\theta}_s(t) - \\
& (2 \cdot s_\theta) \cdot c_{\theta_t}(t) \cdot l_t y \cdot \ddot{\theta}_s(t) + (2 \cdot c_\theta) \cdot s_{\theta_t}(t) \cdot l_t y \cdot \ddot{\theta}_s(t) + \\
& (2 \cdot c_\theta) \cdot c_{\theta_t}(t) \cdot l_t x \cdot \ddot{\theta}_s(t) - (2 \cdot s_{\theta_t}(t)) \cdot \ddot{x}_s(t) + \\
& (2 \cdot c_{\theta_t}(t)) \cdot \ddot{y}_s(t) \cdot 1/(2 \cdot s_{\theta_t}(t)^2 + 2 \cdot c_{\theta_t}(t)^2);
\end{aligned}$$

$$\begin{aligned}
\ddot{\theta}_t(t) = & (-2 \cdot c_{\theta_t}(t)) \cdot l_0 \cdot \ddot{x}_s(t) - & \text{(D.6)} \\
& (4 \cdot s_{\theta_t}(t)^2) \cdot r_t(t) \cdot \dot{r}_t(t) \cdot \dot{\theta}_t(t) - (4 \cdot s_{\theta_t}(t)^2) \cdot l_0 \cdot \dot{r}_t(t) \cdot \dot{\theta}_t(t) - \\
& (4 \cdot c_{\theta_t}(t)^2) \cdot r_t(t) \cdot \dot{r}_t(t) \cdot \dot{\theta}_t(t) - (4 \cdot c_{\theta_t}(t)^2) \cdot l_0 \cdot \dot{r}_t(t) \cdot \dot{\theta}_t(t) + \\
& (2 \cdot s_\theta) \cdot s_{\theta_t}(t) \cdot r_t(t) \cdot l_t x \cdot \dot{\theta}_s(t)^2 + (2 \cdot s_\theta) \cdot s_{\theta_t}(t) \cdot l_0 \cdot l_t x \cdot \dot{\theta}_s(t)^2 - \\
& (2 \cdot s_\theta) \cdot c_{\theta_t}(t) \cdot r_t(t) \cdot l_t y \cdot \dot{\theta}_s(t)^2 - (2 \cdot s_\theta) \cdot c_{\theta_t}(t) \cdot l_0 \cdot l_t y \cdot \dot{\theta}_s(t)^2 + \\
& (2 \cdot c_\theta) \cdot s_{\theta_t}(t) \cdot r_t(t) \cdot l_t y \cdot \dot{\theta}_s(t)^2 + (2 \cdot c_\theta) \cdot s_{\theta_t}(t) \cdot l_0 \cdot l_t y \cdot \dot{\theta}_s(t)^2 + \\
& (2 \cdot c_\theta) \cdot c_{\theta_t}(t) \cdot r_t(t) \cdot l_t x \cdot \dot{\theta}_s(t)^2 + (2 \cdot c_\theta) \cdot c_{\theta_t}(t) \cdot l_0 \cdot l_t x \cdot \dot{\theta}_s(t)^2 - 2 \cdot (\dot{x}_s(t) - \\
& l_t x \cdot \dot{\theta}_s(t) \cdot s_\theta - l_t y \cdot \dot{\theta}_s(t) \cdot c_\theta + \dot{r}_t(t) \cdot s_{\theta_t}(t) \\
& + (l_0 + r_t(t)) \cdot \dot{\theta}_t(t) \cdot c_{\theta_t}(t) \cdot \dot{r}_t(t) \cdot c_{\theta_t}(t) - \\
& 2 \cdot (\dot{y}_s(t) + l_t x \cdot \dot{\theta}_s(t) \cdot c_\theta - l_t y \cdot \dot{\theta}_s(t) \cdot s_\theta - \\
& \dot{r}_t(t) \cdot c_{\theta_t}(t) + (l_0 + \\
& r_t(t)) \cdot \dot{\theta}_t(t) \cdot s_{\theta_t}(t) \cdot \dot{r}_t(t) \cdot s_{\theta_t}(t) - \\
& (2 \cdot s_{\theta_t}(t)) \cdot r_t(t) \cdot \ddot{y}_s(t) - (2 \cdot s_{\theta_t}(t)) \cdot l_0 \cdot \ddot{y}_s(t) + \\
& 2 \cdot (\dot{x}_s(t) - l_t x \cdot \dot{\theta}_s(t) \cdot s_\theta - l_t y \cdot \dot{\theta}_s(t) \cdot c_\theta + \\
& \dot{r}_t(t) \cdot s_{\theta_t}(t) + (l_0 + r_t(t)) \cdot \dot{\theta}_t(t) \cdot c_{\theta_t}(t)) \cdot (l_0 + \\
& r_t(t)) \cdot \dot{\theta}_t(t) \cdot s_{\theta_t}(t) - 2 \cdot (\dot{y}_s(t) + l_t x \cdot \dot{\theta}_s(t) \cdot c_\theta - \\
& l_t y \cdot \dot{\theta}_s(t) \cdot s_\theta - \dot{r}_t(t) \cdot c_{\theta_t}(t) + (l_0 +
\end{aligned}$$

$$\begin{aligned}
& r_t(t) \cdot \dot{\theta}_t(t) \cdot s_{\theta t}(t) \cdot (l_0 + r_t(t)) \cdot \dot{\theta}_t(t) \cdot c_{\theta t}(t) + \\
& 2 \cdot (-c_{\theta t}(t) \cdot F_w \cdot (l_0 + r_t(t)) + m_o \cdot (2 \cdot (\dot{x}_s(t) - l_t x \cdot \dot{\theta}_s(t) \cdot s_{\theta} \\
& - l_t y \cdot \dot{\theta}_s(t) \cdot c_{\theta} + \dot{r}_t(t) \cdot s_{\theta t}(t) + (l_0 + \\
& r_t(t)) \cdot \dot{\theta}_t(t) \cdot c_{\theta t}(t)) \cdot (\dot{r}_t(t) \cdot c_{\theta t}(t) - (l_0 + \\
& r_t(t)) \cdot \dot{\theta}_t(t) \cdot s_{\theta t}(t)) + 2 \cdot (\dot{y}_s(t) + l_t x \cdot \dot{\theta}_s(t) \cdot c_{\theta} \\
& - l_t y \cdot \dot{\theta}_s(t) \cdot s_{\theta} - \dot{r}_t(t) \cdot c_{\theta t}(t) + (l_0 + \\
& r_t(t)) \cdot \dot{\theta}_t(t) \cdot s_{\theta t}(t)) \cdot (\dot{r}_t(t) \cdot s_{\theta t}(t) + (l_0 + \\
& r_t(t)) \cdot \dot{\theta}_t(t) \cdot c_{\theta t}(t)))/2 + m_o \cdot g \cdot (l_0 + r_t(t)) \cdot s_{\theta t}(t) - \\
& k_s 2 \cdot (\text{sqrt}((l_t x \cdot c_{\theta} - l_t y \cdot s_{\theta} + (l_0 + r_t(t)) \cdot s_{\theta t}(t) - l_w x \cdot c_{\theta} + \\
& l_w y \cdot s_{\theta} - \cos(\theta_t(t)) \cdot (l_0 s_1 - \theta_w(t) \cdot r_w/2 + r_c(t)))^2 + (l_t x \cdot s_{\theta} + \\
& l_t y \cdot c_{\theta} - (l_0 + r_t(t)) \cdot c_{\theta t}(t) - l_w x \cdot s_{\theta} - l_w y \cdot c_{\theta} - \\
& \sin(r_c(t)) \cdot (l_0 s_1 - \theta_w(t) \cdot r_w/2 + r_c(t)))^2) - l_0 s_2 + \\
& \theta_w(t) \cdot r_w/2) \cdot (2 \cdot (l_t x \cdot c_{\theta} - l_t y \cdot s_{\theta} + (l_0 + r_t(t)) \cdot s_{\theta t}(t) - \\
& l_w x \cdot c_{\theta} + l_w y \cdot s_{\theta} - \cos(\theta_t(t)) \cdot (l_0 s_1 - \theta_w(t) \cdot r_w/2 + r_c(t))) \cdot (l_0 + \\
& r_t(t)) \cdot c_{\theta t}(t) + 2 \cdot (l_t x \cdot s_{\theta} + l_t y \cdot c_{\theta} - (l_0 + r_t(t)) \cdot c_{\theta t}(t) - \\
& l_w x \cdot s_{\theta} - l_w y \cdot c_{\theta} - \sin(r_c(t)) \cdot (l_0 s_1 - \theta_w(t) \cdot r_w/2 + r_c(t))) \cdot (l_0 + \\
& r_t(t)) \cdot s_{\theta t}(t))/2 \cdot \text{sqrt}((l_t x \cdot c_{\theta} - l_t y \cdot s_{\theta} + (l_0 + r_t(t)) \cdot s_{\theta t}(t) - \\
& l_w x \cdot c_{\theta} + l_w y \cdot s_{\theta} - \cos(\theta_t(t)) \cdot (l_0 s_1 - \theta_w(t) \cdot r_w/2 + r_c(t)))^2 + \\
& (l_t x \cdot s_{\theta} + l_t y \cdot c_{\theta} - (l_0 + r_t(t)) \cdot c_{\theta t}(t) - l_w x \cdot s_{\theta} - l_w y \cdot c_{\theta} - \\
& \sin(r_c(t)) \cdot (l_0 s_1 - \theta_w(t) \cdot r_w/2 + r_c(t)))^2) - c_s 2 \cdot ((2 \cdot (l_t x \cdot c_{\theta} - \\
& l_t y \cdot s_{\theta} + (l_0 + r_t(t)) \cdot s_{\theta t}(t) - l_w x \cdot c_{\theta} + l_w y \cdot s_{\theta} - \\
& \cos(\theta_t(t)) \cdot (l_0 s_1 - \theta_w(t) \cdot r_w/2 + r_c(t))) \cdot (-l_t x \cdot \dot{\theta}_s(t) \cdot s_{\theta} - \\
& l_t y \cdot \dot{\theta}_s(t) \cdot c_{\theta} + \dot{r}_t(t) \cdot s_{\theta t}(t) + (l_0 + \\
& r_t(t)) \cdot \dot{\theta}_t(t) \cdot c_{\theta t}(t) + l_w x \cdot \dot{\theta}_s(t) \cdot s_{\theta} + \\
& l_w y \cdot \dot{\theta}_s(t) \cdot c_{\theta} + \theta_k(t) \cdot \sin(r_c(t)) \cdot (l_0 s_1 - \theta_w(t) \cdot r_w/2 + \\
& r_c(t)) - \cos(\theta_t(t)) \cdot (-\dot{\theta}_w(t) \cdot r_w/2 + \dot{r}_c(t))) + \\
& 2 \cdot (l_t x \cdot s_{\theta} + l_t y \cdot c_{\theta} - (l_0 + r_t(t)) \cdot c_{\theta t}(t) - l_w x \cdot s_{\theta} - l_w y \cdot c_{\theta} \\
& - \sin(r_c(t)) \cdot (l_0 s_1 - \theta_w(t) \cdot r_w/2 + r_c(t))) \cdot (l_t x \cdot \dot{\theta}_s(t) \cdot c_{\theta} - \\
& l_t y \cdot \dot{\theta}_s(t) \cdot s_{\theta} - \dot{r}_t(t) \cdot c_{\theta t}(t) + (l_0 + \\
& r_t(t)) \cdot \dot{\theta}_t(t) \cdot s_{\theta t}(t) - l_w x \cdot \dot{\theta}_s(t) \cdot c_{\theta} + \\
& l_w y \cdot \dot{\theta}_s(t) \cdot s_{\theta} - \theta_k(t) \cdot \cos(\theta_t(t)) \cdot (l_0 s_1 - \theta_w(t) \cdot r_w/2 + \\
& r_c(t)) - \sin(r_c(t)) \cdot (-\dot{\theta}_w(t) \cdot r_w/2 + \\
& \dot{r}_c(t)))/2 \cdot \text{sqrt}((l_t x \cdot c_{\theta} - l_t y \cdot s_{\theta} + (l_0 + r_t(t)) \cdot s_{\theta t}(t) - \\
& l_w x \cdot c_{\theta} + l_w y \cdot s_{\theta} - \cos(\theta_t(t)) \cdot (l_0 s_1 - \theta_w(t) \cdot r_w/2 + r_c(t)))^2 + \\
& (l_t x \cdot s_{\theta} + l_t y \cdot c_{\theta} - (l_0 + r_t(t)) \cdot c_{\theta t}(t) - l_w x \cdot s_{\theta} - l_w y \cdot c_{\theta} - \\
& \sin(r_c(t)) \cdot (l_0 s_1 - \theta_w(t) \cdot r_w/2 + r_c(t)))^2) + \theta_w(t) \\
& t) \cdot r_w/2) \cdot (2 \cdot (l_t x \cdot c_{\theta} - l_t y \cdot s_{\theta} + (l_0 + r_t(t)) \cdot s_{\theta t}(t) - l_w x \cdot c_{\theta} + \\
& l_w y \cdot s_{\theta} - \cos(\theta_t(t)) \cdot (l_0 s_1 - \theta_w(t) \cdot r_w/2 + r_c(t))) \cdot (l_0 + \\
& r_t(t)) \cdot c_{\theta t}(t) + 2 \cdot (l_t x \cdot s_{\theta} + l_t y \cdot c_{\theta} - (l_0 + r_t(t)) \cdot c_{\theta t}(t) - \\
& l_w x \cdot s_{\theta} - l_w y \cdot c_{\theta} - \sin(r_c(t)) \cdot (l_0 s_1 - \theta_w(t) \cdot r_w/2 + r_c(t))) \cdot (l_0 + \\
& r_t(t)) \cdot s_{\theta t}(t))/2 \cdot \text{sqrt}((l_t x \cdot c_{\theta} - l_t y \cdot s_{\theta} + (l_0 + r_t(t)) \cdot s_{\theta t}(t) - \\
& l_w x \cdot c_{\theta} + l_w y \cdot s_{\theta} - \cos(\theta_t(t)) \cdot (l_0 s_1 - \theta_w(t) \cdot r_w/2 + r_c(t)))^2 +
\end{aligned}$$

$$\begin{aligned}
& (l_t x \cdot s_\theta + l_t y \cdot c_\theta - (l_0 + r_t(t)) \cdot c_{\theta_t}(t) - l_w x \cdot s_\theta - l_w y \cdot c_\theta - \\
& \mathbf{sin}(r_c(t)) \cdot (l_0 s_1 - \theta_w(t) \cdot r_w/2 + r_c(t)))^2)) \cdot 1/m_o + \\
& (2 \cdot s_\theta) \cdot s_{\theta_t}(t) \cdot r_t(t) \cdot l_t y \cdot \ddot{\theta}_s(t) + (2 \cdot s_\theta) \cdot s_{\theta_t}(t) \cdot l_0 \cdot l_t y \cdot \ddot{\theta}_s(t) + \\
& (2 \cdot s_\theta) \cdot c_{\theta_t}(t) \cdot r_t(t) \cdot l_t x \cdot \ddot{\theta}_s(t) + (2 \cdot s_\theta) \cdot c_{\theta_t}(t) \cdot l_0 \cdot l_t x \cdot \ddot{\theta}_s(t) - \\
& (2 \cdot c_\theta) \cdot s_{\theta_t}(t) \cdot r_t(t) \cdot l_t x \cdot \ddot{\theta}_s(t) - (2 \cdot c_\theta) \cdot s_{\theta_t}(t) \cdot l_0 \cdot l_t x \cdot \ddot{\theta}_s(t) + \\
& (2 \cdot c_\theta) \cdot c_{\theta_t}(t) \cdot r_t(t) \cdot l_t y \cdot \ddot{\theta}_s(t) + (2 \cdot c_\theta) \cdot c_{\theta_t}(t) \cdot l_0 \cdot l_t y \cdot \ddot{\theta}_s(t) - \\
& (2 \cdot c_{\theta_t}(t)) \cdot r_t(t) \cdot \ddot{x}_s(t)) \cdot 1/((2 \cdot s_{\theta_t}(t))^2 \cdot r_t(t)^2 + \\
& (2 \cdot s_{\theta_t}(t)^2) \cdot l_0^2 + (2 \cdot c_{\theta_t}(t)^2) \cdot r_t(t)^2 + (2 \cdot c_{\theta_t}(t)^2) \cdot l_0^2 + \\
& (4 \cdot s_{\theta_t}(t)^2) \cdot r_t(t) \cdot l_0 + (4 \cdot c_{\theta_t}(t)^2) \cdot r_t(t) \cdot l_0);
\end{aligned}$$

$$\begin{aligned}
\ddot{r}_c(t) = & (2 \cdot (m_c \cdot (-2 \cdot (\dot{x}_s(t) - l_w x \cdot \dot{\theta}_s(t)) \cdot s_\theta - \\
& l_w y \cdot \dot{\theta}_s(t) \cdot c_\theta - \theta_k(t) \cdot \mathbf{sin}(r_c(t)) \cdot (l_0 s_1 - \theta_w(t) \cdot r_w/2 + \\
& r_c(t)) + \mathbf{cos}(\theta_t(t)) \cdot (-\dot{\theta}_w(t) \cdot r_w/2 + \\
& \dot{r}_c(t))) \cdot \theta_k(t) \cdot \mathbf{sin}(r_c(t)) + 2 \cdot (\dot{y}_s(t) + l_w x \cdot \dot{\theta}_s(t) \cdot c_\theta - \\
& l_w y \cdot \dot{\theta}_s(t) \cdot s_\theta + \theta_k(t) \cdot \mathbf{cos}(\theta_t(t)) \cdot (l_0 s_1 - \theta_w(t) \cdot r_w/2 + \\
& r_c(t)) + \mathbf{sin}(r_c(t)) \cdot (-\dot{\theta}_w(t) \cdot r_w/2 + \\
& \dot{r}_c(t))) \cdot \theta_k(t) \cdot \mathbf{cos}(\theta_t(t)))/2 + m_c \cdot g \cdot \mathbf{sin}(r_c(t)) - k_s 1 \cdot r_c(t) - \\
& k_s 2 \cdot (\text{sqrt}((l_t x \cdot c_\theta - l_t y \cdot s_\theta + (l_0 + r_t(t)) \cdot s_{\theta_t}(t) - l_w x \cdot c_\theta + \\
& l_w y \cdot s_\theta - \mathbf{cos}(\theta_t(t)) \cdot (l_0 s_1 - \theta_w(t) \cdot r_w/2 + r_c(t)))^2 + (l_t x \cdot s_\theta + \\
& l_t y \cdot c_\theta - (l_0 + r_t(t)) \cdot c_{\theta_t}(t) - l_w x \cdot s_\theta - l_w y \cdot c_\theta - \\
& \mathbf{sin}(r_c(t)) \cdot (l_0 s_1 - \theta_w(t) \cdot r_w/2 + r_c(t)))^2) - l_0 s_2 + \\
& \theta_w(t) \cdot r_w/2) \cdot (-2 \cdot (l_t x \cdot c_\theta - l_t y \cdot s_\theta + (l_0 + r_t(t)) \cdot s_{\theta_t}(t) - \\
& l_w x \cdot c_\theta + l_w y \cdot s_\theta - \mathbf{cos}(\theta_t(t)) \cdot (l_0 s_1 - \theta_w(t) \cdot r_w/2 + \\
& r_c(t))) \cdot \mathbf{cos}(\theta_t(t)) - 2 \cdot (l_t x \cdot s_\theta + l_t y \cdot c_\theta - (l_0 + r_t(t)) \cdot c_{\theta_t}(t) - \\
& l_w x \cdot s_\theta - l_w y \cdot c_\theta - \mathbf{sin}(r_c(t)) \cdot (l_0 s_1 - \theta_w(t) \cdot r_w/2 + \\
& r_c(t))) \cdot \mathbf{sin}(r_c(t)))/(2 \cdot \text{sqrt}((l_t x \cdot c_\theta - l_t y \cdot s_\theta + (l_0 + r_t(t)) \cdot s_{\theta_t}(t) - \\
& l_w x \cdot c_\theta + l_w y \cdot s_\theta - \mathbf{cos}(\theta_t(t)) \cdot (l_0 s_1 - \theta_w(t) \cdot r_w/2 + r_c(t)))^2 + \\
& (l_t x \cdot s_\theta + l_t y \cdot c_\theta - (l_0 + r_t(t)) \cdot c_{\theta_t}(t) - l_w x \cdot s_\theta - l_w y \cdot c_\theta - \\
& \mathbf{sin}(r_c(t)) \cdot (l_0 s_1 - \theta_w(t) \cdot r_w/2 + r_c(t)))^2) - c_s 1 \cdot \dot{r}_c(t) - \\
& c_s 2 \cdot ((2 \cdot (l_t x \cdot c_\theta - l_t y \cdot s_\theta + (l_0 + r_t(t)) \cdot s_{\theta_t}(t) - l_w x \cdot c_\theta + \\
& l_w y \cdot s_\theta - \mathbf{cos}(\theta_t(t)) \cdot (l_0 s_1 - \theta_w(t) \cdot r_w/2 + \\
& r_c(t))) \cdot (-l_t x \cdot \dot{\theta}_s(t) \cdot s_\theta - l_t y \cdot \dot{\theta}_s(t) \cdot c_\theta + \\
& \dot{r}_t(t) \cdot s_{\theta_t}(t) + (l_0 + r_t(t)) \cdot \dot{\theta}_t(t) \cdot c_{\theta_t}(t) + \\
& l_w x \cdot \dot{\theta}_s(t) \cdot s_\theta + l_w y \cdot \dot{\theta}_s(t) \cdot c_\theta + \\
& \theta_k(t) \cdot \mathbf{sin}(r_c(t)) \cdot (l_0 s_1 - \theta_w(t) \cdot r_w/2 + r_c(t)) - \\
& \mathbf{cos}(\theta_t(t)) \cdot (-\dot{\theta}_w(t) \cdot r_w/2 + \dot{r}_c(t))) + 2 \cdot (l_t x \cdot s_\theta + \\
& l_t y \cdot c_\theta - (l_0 + r_t(t)) \cdot c_{\theta_t}(t) - l_w x \cdot s_\theta - l_w y \cdot c_\theta - \\
& \mathbf{sin}(r_c(t)) \cdot (l_0 s_1 - \theta_w(t) \cdot r_w/2 + r_c(t))) \cdot (l_t x \cdot \dot{\theta}_s(t) \cdot c_\theta - \\
& l_t y \cdot \dot{\theta}_s(t) \cdot s_\theta - \dot{r}_t(t) \cdot c_{\theta_t}(t) + (l_0 + \\
& r_t(t)) \cdot \dot{\theta}_t(t) \cdot s_{\theta_t}(t) - l_w x \cdot \dot{\theta}_s(t) \cdot c_\theta + \\
& l_w y \cdot \dot{\theta}_s(t) \cdot s_\theta - \theta_k(t) \cdot \mathbf{cos}(\theta_t(t)) \cdot (l_0 s_1 - \theta_w(t) \cdot r_w/2 + \\
& r_c(t)) - \mathbf{sin}(r_c(t)) \cdot (-\dot{\theta}_w(t) \cdot r_w/2 +
\end{aligned}$$

$$\begin{aligned}
& \dot{r}_c(t))) / (2 \cdot \text{sqrt}((l_t x \cdot c_\theta - l_t y \cdot s_\theta + (l_0 + r_t(t)) \cdot s_{\theta_t}(t) - \\
& l_w x \cdot c_\theta + l_w y \cdot s_\theta - \cos(\theta_t(t)) \cdot (l_0 s_1 - \theta_w(t) \cdot r_w/2 + r_c(t)))^2 + \\
& (l_t x \cdot s_\theta + l_t y \cdot c_\theta - (l_0 + r_t(t)) \cdot c_{\theta_t}(t) - l_w x \cdot s_\theta - l_w y \cdot c_\theta - \\
& \sin(r_c(t)) \cdot (l_0 s_1 - \theta_w(t) \cdot r_w/2 + r_c(t)))^2)) + \theta_w(t) \\
& t) \cdot r_w/2) \cdot (-2 \cdot (l_t x \cdot c_\theta - l_t y \cdot s_\theta + (l_0 + r_t(t)) \cdot s_{\theta_t}(t) - l_w x \cdot c_\theta + \\
& l_w y \cdot s_\theta - \cos(\theta_t(t)) \cdot (l_0 s_1 - \theta_w(t) \cdot r_w/2 + r_c(t))) \cdot \cos(\theta_t(t)) - \\
& 2 \cdot (l_t x \cdot s_\theta + l_t y \cdot c_\theta - (l_0 + r_t(t)) \cdot c_{\theta_t}(t) - l_w x \cdot s_\theta - l_w y \cdot c_\theta \\
& - \sin(r_c(t)) \cdot (l_0 s_1 - \theta_w(t) \cdot r_w/2 + r_c(t))) \cdot \sin(r_c(t))) / (2 \cdot \text{sqrt}((l_t x \cdot c_\theta - \\
& l_t y \cdot s_\theta + (l_0 + r_t(t)) \cdot s_{\theta_t}(t) - l_w x \cdot c_\theta + l_w y \cdot s_\theta - \\
& \cos(\theta_t(t)) \cdot (l_0 s_1 - \theta_w(t) \cdot r_w/2 + r_c(t)))^2 + (l_t x \cdot s_\theta + l_t y \cdot c_\theta - \\
& (l_0 + r_t(t)) \cdot c_{\theta_t}(t) - l_w x \cdot s_\theta - l_w y \cdot c_\theta - \sin(r_c(t)) \cdot (l_0 s_1 - \\
& \theta_w(t) \cdot r_w/2 + r_c(t)))^2))) \cdot 1/m_c + 2 \cdot (\dot{x}_s(t) - l_w x \cdot \dot{\theta}_s(t) \cdot s_\theta \\
& - l_w y \cdot \dot{\theta}_s(t) \cdot c_\theta - \theta_k(t) \cdot \sin(r_c(t)) \cdot (l_0 s_1 - \theta_w(t) \cdot r_w/2 + \\
& r_c(t)) + \cos(\theta_t(t)) \cdot (-\dot{\theta}_w(t) \cdot r_w/2 + \\
& \dot{r}_c(t))) \cdot \theta_k(t) \cdot \sin(r_c(t)) - 2 \cdot (\dot{y}_s(t) + l_w x \cdot \dot{\theta}_s(t) \cdot c_\theta - \\
& l_w y \cdot \dot{\theta}_s(t) \cdot s_\theta + \theta_k(t) \cdot \cos(\theta_t(t)) \cdot (l_0 s_1 - \theta_w(t) \cdot r_w/2 + \\
& r_c(t)) + \sin(r_c(t)) \cdot (-\dot{\theta}_w(t) \cdot r_w/2 + \\
& \dot{r}_c(t))) \cdot \theta_k(t) \cdot \cos(\theta_t(t)) - \theta_k(t)^2 \cdot \sin(r_c(t))^2 \cdot \theta_w(t) \cdot r_w - \\
& \theta_k(t)^2 \cdot \cos(\theta_t(t))^2 \cdot \theta_w(t) \cdot r_w + \\
& (2 \cdot \sin(r_c(t))) \cdot l_w x \cdot \dot{\theta}_s(t)^2 \cdot s_\theta - (2 \cdot \cos(\theta_t(t))) \cdot l_w y \cdot \dot{\theta}_s(t)^2 \cdot s_\theta + \\
& (2 \cdot \sin(r_c(t))) \cdot l_w y \cdot \dot{\theta}_s(t)^2 \cdot c_\theta + (2 \cdot \cos(\theta_t(t))) \cdot l_w x \cdot \dot{\theta}_s(t)^2 \cdot c_\theta + \\
& (2 \cdot \theta_k(t)^2) \cdot \sin(r_c(t))^2 \cdot r_c(t) + (2 \cdot \theta_k(t)^2) \cdot \sin(r_c(t))^2 \cdot l_0 s_1 + \\
& (2 \cdot \theta_k(t)^2) \cdot \cos(\theta_t(t))^2 \cdot r_c(t) + (2 \cdot \theta_k(t)^2) \cdot \cos(\theta_t(t))^2 \cdot l_0 s_1 + \\
& (2 \cdot \sin(r_c(t))) \cdot l_w y \cdot \ddot{\theta}_s(t) \cdot s_\theta + \\
& (2 \cdot \cos(\theta_t(t))) \cdot l_w x \cdot \ddot{\theta}_s(t) \cdot s_\theta - (2 \cdot \sin(r_c(t))) \cdot l_w x \cdot \ddot{\theta}_s(t) \cdot c_\theta + \\
& (2 \cdot \cos(\theta_t(t))) \cdot l_w y \cdot \ddot{\theta}_s(t) \cdot c_\theta + \sin(r_c(t))^2 \cdot \theta_w(t) t, \\
& t) \cdot r_w + \cos(\theta_t(t))^2 \cdot \ddot{\theta}_w(t) \cdot r_w - (2 \cdot \sin(r_c(t))) \cdot \ddot{y}_s(t) - \\
& (2 \cdot \cos(\theta_t(t))) \cdot \ddot{x}_s(t)) \cdot 1/(2 \cdot \sin(r_c(t))^2 + 2 \cdot \cos(\theta_t(t))^2);
\end{aligned}$$

$$\begin{aligned}
\ddot{\theta}_k(t) = & ((2 \cdot \sin(r_c(t))) \cdot l_w y \cdot \dot{\theta}_s(t)^2 \cdot s_\theta \cdot r_c(t) + \\
& (2 \cdot \theta_k(t)) \cdot \cos(\theta_t(t))^2 \cdot \dot{\theta}_w(t) \cdot r_w \cdot l_0 s_1 - \\
& \theta_k(t) \cdot \cos(\theta_t(t))^2 \cdot \dot{\theta}_w(t) \cdot r_w^2 \cdot \theta_w(t) + \\
& (2 \cdot \theta_k(t)) \cdot \cos(\theta_t(t))^2 \cdot \dot{\theta}_w(t) \cdot r_w \cdot r_c(t) + \\
& (2 \cdot \theta_k(t)) \cdot \cos(\theta_t(t))^2 \cdot \dot{r}_c(t) \cdot \theta_w(t) \cdot r_w + \\
& (2 \cdot \sin(r_c(t))) \cdot \ddot{x}_s(t) \cdot l_0 s_1 + (2 \cdot \sin(r_c(t))) \cdot \ddot{x}_s(t) \cdot r_c(t) - \\
& (2 \cdot \cos(\theta_t(t))) \cdot \ddot{y}_s(t) \cdot l_0 s_1 - (2 \cdot \cos(\theta_t(t))) \cdot \ddot{y}_s(t) \cdot r_c(t) + \\
& 2 \cdot (m_c \cdot (2 \cdot (\dot{x}_s(t) - l_w x \cdot \dot{\theta}_s(t) \cdot s_\theta - l_w y \cdot \dot{\theta}_s(t) \cdot c_\theta - \\
& \theta_k(t) \cdot \sin(r_c(t)) \cdot (l_0 s_1 - \theta_w(t) \cdot r_w/2 + r_c(t))) + \\
& \cos(\theta_t(t)) \cdot (-\dot{\theta}_w(t) \cdot r_w/2 + \\
& \dot{r}_c(t))) \cdot (-\theta_k(t) \cdot \cos(\theta_t(t)) \cdot (l_0 s_1 - \theta_w(t) \cdot r_w/2 + r_c(t)) - \\
& \sin(r_c(t)) \cdot (-\dot{\theta}_w(t) \cdot r_w/2 + \dot{r}_c(t))) + 2 \cdot (\dot{y}_s(t) +
\end{aligned} \tag{D.8}$$

$$\begin{aligned}
& l_w x \cdot \dot{\theta}_s(t) \cdot c_\theta - l_w y \cdot \dot{\theta}_s(t) \cdot s_\theta + \\
& \theta_k(t) \cdot \cos(\theta_t(t)) \cdot (l_0 s_1 - \theta_w(t) \cdot r_w/2 + r_c(t)) + \\
& \sin(r_c(t)) \cdot (-\dot{\theta}_w(t) \cdot r_w/2 + \\
& \dot{r}_c(t)) \cdot (-\theta_k(t) \cdot \sin(r_c(t)) \cdot (l_0 s_1 - \theta_w(t) \cdot r_w/2 + r_c(t)) + \\
& \cos(\theta_t(t)) \cdot (-\dot{\theta}_w(t) \cdot r_w/2 + \dot{r}_c(t))) / 2 + \\
& m_c \cdot g \cdot \cos(\theta_t(t)) \cdot (l_0 s_1 - \theta_w(t) \cdot r_w/2 + r_c(t)) - k_s 2 \cdot (\text{sqrt}((l_t x \cdot c_\theta - \\
& l_t y \cdot s_\theta + (l_0 + r_t(t)) \cdot s_{\theta_t}(t) - l_w x \cdot c_\theta + l_w y \cdot s_\theta - \\
& \cos(\theta_t(t)) \cdot (l_0 s_1 - \theta_w(t) \cdot r_w/2 + r_c(t)))^2 + (l_t x \cdot s_\theta + l_t y \cdot c_\theta - \\
& (l_0 + r_t(t)) \cdot c_{\theta_t}(t) - l_w x \cdot s_\theta - l_w y \cdot c_\theta - \sin(r_c(t)) \cdot (l_0 s_1 - \\
& \theta_w(t) \cdot r_w/2 + r_c(t)))^2) - l_0 s_2 + \theta_w(t) \cdot r_w/2) \cdot (2 \cdot (l_t x \cdot c_\theta - \\
& l_t y \cdot s_\theta + (l_0 + r_t(t)) \cdot s_{\theta_t}(t) - l_w x \cdot c_\theta + l_w y \cdot s_\theta - \\
& \cos(\theta_t(t)) \cdot (l_0 s_1 - \theta_w(t) \cdot r_w/2 + r_c(t))) \cdot \sin(r_c(t)) \cdot (l_0 s_1 - \\
& \theta_w(t) \cdot r_w/2 + r_c(t)) - 2 \cdot (l_t x \cdot s_\theta + l_t y \cdot c_\theta - (l_0 + r_t(t)) \cdot c_{\theta_t}(t) \\
& - l_w x \cdot s_\theta - l_w y \cdot c_\theta - \sin(r_c(t)) \cdot (l_0 s_1 - \theta_w(t) \cdot r_w/2 + \\
& r_c(t))) \cdot \cos(\theta_t(t)) \cdot (l_0 s_1 - \theta_w(t) \cdot r_w/2 + r_c(t))) / (2 \cdot \text{sqrt}((l_t x \cdot c_\theta - \\
& l_t y \cdot s_\theta + (l_0 + r_t(t)) \cdot s_{\theta_t}(t) - l_w x \cdot c_\theta + l_w y \cdot s_\theta - \\
& \cos(\theta_t(t)) \cdot (l_0 s_1 - \theta_w(t) \cdot r_w/2 + r_c(t)))^2 + (l_t x \cdot s_\theta + l_t y \cdot c_\theta - \\
& (l_0 + r_t(t)) \cdot c_{\theta_t}(t) - l_w x \cdot s_\theta - l_w y \cdot c_\theta - \sin(r_c(t)) \cdot (l_0 s_1 - \\
& \theta_w(t) \cdot r_w/2 + r_c(t)))^2) - c_s 2 \cdot ((2 \cdot (l_t x \cdot c_\theta - l_t y \cdot s_\theta + (l_0 + \\
& r_t(t)) \cdot s_{\theta_t}(t) - l_w x \cdot c_\theta + l_w y \cdot s_\theta - \cos(\theta_t(t)) \cdot (l_0 s_1 - \\
& \theta_w(t) \cdot r_w/2 + r_c(t))) \cdot (-l_t x \cdot \dot{\theta}_s(t) \cdot s_\theta - \\
& l_t y \cdot \dot{\theta}_s(t) \cdot c_\theta + \dot{r}_t(t) \cdot s_{\theta_t}(t) + (l_0 + \\
& r_t(t)) \cdot \dot{\theta}_t(t) \cdot c_{\theta_t}(t) + l_w x \cdot \dot{\theta}_s(t) \cdot s_\theta + \\
& l_w y \cdot \dot{\theta}_s(t) \cdot c_\theta + \theta_k(t) \cdot \sin(r_c(t)) \cdot (l_0 s_1 - \theta_w(t) \cdot r_w/2 + \\
& r_c(t)) - \cos(\theta_t(t)) \cdot (-\dot{\theta}_w(t) \cdot r_w/2 + \dot{r}_c(t))) + \\
& 2 \cdot (l_t x \cdot s_\theta + l_t y \cdot c_\theta - (l_0 + r_t(t)) \cdot c_{\theta_t}(t) - l_w x \cdot s_\theta - l_w y \cdot c_\theta \\
& - \sin(r_c(t)) \cdot (l_0 s_1 - \theta_w(t) \cdot r_w/2 + r_c(t))) \cdot (l_t x \cdot \dot{\theta}_s(t) \cdot c_\theta - \\
& l_t y \cdot \dot{\theta}_s(t) \cdot s_\theta - \dot{r}_t(t) \cdot c_{\theta_t}(t) + (l_0 + \\
& r_t(t)) \cdot \dot{\theta}_t(t) \cdot s_{\theta_t}(t) - l_w x \cdot \dot{\theta}_s(t) \cdot c_\theta + \\
& l_w y \cdot \dot{\theta}_s(t) \cdot s_\theta - \theta_k(t) \cdot \cos(\theta_t(t)) \cdot (l_0 s_1 - \theta_w(t) \cdot r_w/2 + \\
& r_c(t)) - \sin(r_c(t)) \cdot (-\dot{\theta}_w(t) \cdot r_w/2 + \\
& \dot{r}_c(t))) / (2 \cdot \text{sqrt}((l_t x \cdot c_\theta - l_t y \cdot s_\theta + (l_0 + r_t(t)) \cdot s_{\theta_t}(t) - \\
& l_w x \cdot c_\theta + l_w y \cdot s_\theta - \cos(\theta_t(t)) \cdot (l_0 s_1 - \theta_w(t) \cdot r_w/2 + r_c(t)))^2 + \\
& (l_t x \cdot s_\theta + l_t y \cdot c_\theta - (l_0 + r_t(t)) \cdot c_{\theta_t}(t) - l_w x \cdot s_\theta - l_w y \cdot c_\theta - \\
& \sin(r_c(t)) \cdot (l_0 s_1 - \theta_w(t) \cdot r_w/2 + r_c(t)))^2) + \theta_w(t) \\
& t) \cdot r_w/2) \cdot (2 \cdot (l_t x \cdot c_\theta - l_t y \cdot s_\theta + (l_0 + r_t(t)) \cdot s_{\theta_t}(t) - l_w x \cdot c_\theta + \\
& l_w y \cdot s_\theta - \cos(\theta_t(t)) \cdot (l_0 s_1 - \theta_w(t) \cdot r_w/2 + r_c(t))) \cdot \sin(r_c(t)) \cdot (l_0 s_1 - \\
& \theta_w(t) \cdot r_w/2 + r_c(t)) - 2 \cdot (l_t x \cdot s_\theta + l_t y \cdot c_\theta - (l_0 + r_t(t)) \cdot c_{\theta_t}(t) \\
& - l_w x \cdot s_\theta - l_w y \cdot c_\theta - \sin(r_c(t)) \cdot (l_0 s_1 - \theta_w(t) \cdot r_w/2 + \\
& r_c(t))) \cdot \cos(\theta_t(t)) \cdot (l_0 s_1 - \theta_w(t) \cdot r_w/2 + r_c(t))) / (2 \cdot \text{sqrt}((l_t x \cdot c_\theta - \\
& l_t y \cdot s_\theta + (l_0 + r_t(t)) \cdot s_{\theta_t}(t) - l_w x \cdot c_\theta + l_w y \cdot s_\theta - \\
& \cos(\theta_t(t)) \cdot (l_0 s_1 - \theta_w(t) \cdot r_w/2 + r_c(t)))^2 + (l_t x \cdot s_\theta + l_t y \cdot c_\theta - \\
& (l_0 + r_t(t)) \cdot c_{\theta_t}(t) - l_w x \cdot s_\theta - l_w y \cdot c_\theta - \sin(r_c(t)) \cdot (l_0 s_1 -
\end{aligned}$$

$$\begin{aligned}
& \theta_w(t) \cdot r_w/2 + r_c(t)))^2))) \cdot 1/m_c + 2 \cdot (\dot{x}_s(t) - l_w x \cdot \dot{\theta}_s(t) \cdot s_\theta \\
& - l_w y \cdot \dot{\theta}_s(t) \cdot c_\theta - \theta_k(t) \cdot \sin(r_c(t)) \cdot (l_0 s1 - \theta_w(t) \cdot r_w/2 + \\
& r_c(t)) + \cos(\theta_t(t)) \cdot (-\dot{\theta}_w(t) \cdot r_w/2 + \\
& \dot{r}_c(t)) \cdot \theta_k(t) \cdot \cos(\theta_t(t)) \cdot (l_0 s1 - \theta_w(t) \cdot r_w/2 + r_c(t)) + \\
& 2 \cdot (\dot{y}_s(t) + l_w x \cdot \dot{\theta}_s(t) \cdot c_\theta - l_w y \cdot \dot{\theta}_s(t) \cdot s_\theta + \\
& \theta_k(t) \cdot \cos(\theta_t(t)) \cdot (l_0 s1 - \theta_w(t) \cdot r_w/2 + r_c(t)) + \\
& \sin(r_c(t)) \cdot (-\dot{\theta}_w(t) \cdot r_w/2 + \dot{r}_c(t))) \cdot \theta_k(t) \cdot \sin(r_c(t)) \cdot (l_0 s1 \\
& - \theta_w(t) \cdot r_w/2 + r_c(t)) - (4 \cdot \theta_k(t)) \cdot \sin(r_c(t))^2 \cdot \dot{r}_c(t) \cdot l_0 s1 - \\
& (4 \cdot \theta_k(t)) \cdot \sin(r_c(t))^2 \cdot \dot{r}_c(t) \cdot r_c(t) - \\
& (4 \cdot \theta_k(t)) \cdot \cos(\theta_t(t))^2 \cdot \dot{r}_c(t) \cdot l_0 s1 - \\
& (4 \cdot \theta_k(t)) \cdot \cos(\theta_t(t))^2 \cdot \dot{r}_c(t) \cdot r_c(t) - \\
& \sin(r_c(t)) \cdot \ddot{x}_s(t) \cdot \theta_w(t) \cdot r_w + \cos(\theta_t(t)) \cdot \ddot{y}_s(t) \cdot \theta_w(t) \cdot r_w + \\
& 2 \cdot (\dot{x}_s(t) - l_w x \cdot \dot{\theta}_s(t) \cdot s_\theta - l_w y \cdot \dot{\theta}_s(t) \cdot c_\theta - \\
& \theta_k(t) \cdot \sin(r_c(t)) \cdot (l_0 s1 - \theta_w(t) \cdot r_w/2 + r_c(t)) + \\
& \cos(\theta_t(t)) \cdot (-\dot{\theta}_w(t) \cdot r_w/2 + \\
& \dot{r}_c(t)) \cdot \sin(r_c(t)) \cdot (-\dot{\theta}_w(t) \cdot r_w/2 + \dot{r}_c(t)) - \\
& 2 \cdot (\dot{y}_s(t) + l_w x \cdot \dot{\theta}_s(t) \cdot c_\theta - l_w y \cdot \dot{\theta}_s(t) \cdot s_\theta + \\
& \theta_k(t) \cdot \cos(\theta_t(t)) \cdot (l_0 s1 - \theta_w(t) \cdot r_w/2 + r_c(t)) + \\
& \sin(r_c(t)) \cdot (-\dot{\theta}_w(t) \cdot r_w/2 + \\
& \dot{r}_c(t)) \cdot \cos(\theta_t(t)) \cdot (-\dot{\theta}_w(t) \cdot r_w/2 + \dot{r}_c(t)) + \\
& \sin(r_c(t)) \cdot l_w x \cdot \ddot{\theta}_s(t) \cdot s_\theta \cdot \theta_w(t) \cdot r_w + \sin(r_c(t)) \cdot l_w y \cdot \ddot{\theta}_s(t) \cdot c_\theta \cdot \theta_w(t) \cdot r_w + \\
& \cos(\theta_t(t)) \cdot l_w x \cdot \ddot{\theta}_s(t) \cdot c_\theta \cdot \theta_w(t) \cdot r_w - \cos(\theta_t(t)) \cdot l_w y \cdot \ddot{\theta}_s(t) \cdot s_\theta \cdot \theta_w(t) \cdot r_w + \\
& \sin(r_c(t)) \cdot l_w x \cdot \dot{\theta}_s(t)^2 \cdot c_\theta \cdot \theta_w(t) \cdot r_w - \sin(r_c(t)) \cdot l_w y \cdot \dot{\theta}_s(t)^2 \cdot s_\theta \cdot \theta_w(t) \cdot r_w - \\
& \cos(\theta_t(t)) \cdot l_w x \cdot \dot{\theta}_s(t)^2 \cdot s_\theta \cdot \theta_w(t) \cdot r_w - \cos(\theta_t(t)) \cdot l_w y \cdot \dot{\theta}_s(t)^2 \cdot c_\theta \cdot \theta_w(t) \cdot r_w - \\
& (2 \cdot \cos(\theta_t(t))) \cdot l_w x \cdot \ddot{\theta}_s(t) \cdot c_\theta \cdot r_c(t) + (2 \cdot \cos(\theta_t(t))) \cdot l_w y \cdot \ddot{\theta}_s(t) \cdot s_\theta \cdot l_0 s1 + \\
& (2 \cdot \cos(\theta_t(t))) \cdot l_w y \cdot \ddot{\theta}_s(t) \cdot s_\theta \cdot r_c(t) - (2 \cdot \sin(r_c(t))) \cdot l_w x \cdot \ddot{\theta}_s(t) \cdot s_\theta \cdot l_0 s1 - \\
& (2 \cdot \sin(r_c(t))) \cdot l_w x \cdot \ddot{\theta}_s(t) \cdot s_\theta \cdot r_c(t) - (2 \cdot \sin(r_c(t))) \cdot l_w y \cdot \ddot{\theta}_s(t) \cdot c_\theta \cdot l_0 s1 - \\
& (2 \cdot \sin(r_c(t))) \cdot l_w y \cdot \ddot{\theta}_s(t) \cdot c_\theta \cdot r_c(t) - (2 \cdot \cos(\theta_t(t))) \cdot l_w x \cdot \ddot{\theta}_s(t) \cdot c_\theta \cdot l_0 s1 + \\
& (2 \cdot \cos(\theta_t(t))) \cdot l_w x \cdot \dot{\theta}_s(t)^2 \cdot s_\theta \cdot l_0 s1 + (2 \cdot \cos(\theta_t(t))) \cdot l_w x \cdot \dot{\theta}_s(t)^2 \cdot s_\theta \cdot r_c(t) + \\
& (2 \cdot \cos(\theta_t(t))) \cdot l_w y \cdot \dot{\theta}_s(t)^2 \cdot c_\theta \cdot l_0 s1 + (2 \cdot \cos(\theta_t(t))) \cdot l_w y \cdot \dot{\theta}_s(t)^2 \cdot c_\theta \cdot r_c(t) - \\
& \theta_k(t) \cdot \sin(r_c(t))^2 \cdot \dot{\theta}_w(t) \cdot r_w^2 \cdot \theta_w(t) + (2 \cdot \theta_k(t)) \cdot \sin(r_c(t))^2 \cdot \dot{\theta}_w(t) \cdot r_w \cdot r_c(t) + \\
& (2 \cdot \theta_k(t)) \cdot \sin(r_c(t))^2 \cdot \dot{r}_c(t) \cdot \theta_w(t) \cdot r_w + (2 \cdot \theta_k(t)) \cdot \sin(r_c(t))^2 \cdot \dot{\theta}_w(t) \cdot r_w \cdot l_0 s1 - \\
& (2 \cdot \sin(r_c(t))) \cdot l_w x \cdot \dot{\theta}_s(t)^2 \cdot c_\theta \cdot l_0 s1 - (2 \cdot \sin(r_c(t))) \cdot l_w x \cdot \dot{\theta}_s(t)^2 \cdot c_\theta \cdot r_c(t) + (2 \cdot \sin(r_c(t))) \cdot l_w y \cdot \dot{\theta}_s(t)^2 \cdot s_\theta \cdot l_0 s1 \\
& - 1/(-(2 \cdot \sin(r_c(t))^2) \cdot l_0 s1 \cdot \theta_w(t) \cdot r_w - \\
& (2 \cdot \sin(r_c(t))^2) \cdot \theta_w(t) \cdot r_w \cdot r_c(t) - (2 \cdot \cos(\theta_t(t))^2) \cdot l_0 s1 \cdot \theta_w(t) \cdot r_w - \\
& (2 \cdot \cos(\theta_t(t))^2) \cdot \theta_w(t) \cdot r_w \cdot r_c(t) + (2 \cdot \sin(r_c(t))^2) \cdot l_0 s1^2 + \\
& (2 \cdot \sin(r_c(t))^2) \cdot r_c(t)^2 + (2 \cdot \cos(\theta_t(t))^2) \cdot l_0 s1^2 + (2 \cdot \cos(\theta_t(t))^2) \cdot r_c(t)^2 \\
& + (4 \cdot \sin(r_c(t))^2) \cdot l_0 s1 \cdot r_c(t) + \sin(r_c(t))^2 \cdot \theta_w(t)^2 \cdot r_w^2/2 + \\
& (4 \cdot \cos(\theta_t(t))^2) \cdot l_0 s1 \cdot r_c(t) + \cos(\theta_t(t))^2 \cdot \theta_w(t)^2 \cdot r_w^2/2);
\end{aligned}$$